

Advanced Blind Signal Processing for MIMO Communications

Vom Fachbereich Elektrotechnik und Informationstechnik
der Technischen Universität Darmstadt
zur Erlangung des akademischen Grades eines
Doktor-Ingenieurs (Dr.-Ing.)
genehmigte Dissertation

von

Nima Sarmadi, M.Sc.

Geboren am 8 August 1975 in Khomein, Iran.

| | |
|----------------------------|---------------------------------|
| Referent: | Prof. Dr.-Ing. Marius Pesavento |
| Korreferent: | Prof. Dr. Shahram Shahbazpanahi |
| Tag der Einreichung: | 2. Februar, 2012 |
| Tag der mündlichen Prüfung | 31. Mai, 2012 |

D17

Darmstädter Dissertation

2012

To my parents,

Alimohammad Sarmadi and Khadijeh Shahabi

for their love.

Acknowledgments

This thesis is the result of years of research that included turbulent times, but also times of happiness and success. I would like to express my special gratitude to my inspiring mentor Prof. Marius Pesavento for his supervision and guidance. His motivation, questions, suggestions and discussions were always productive and have significantly influenced the contents of this thesis. I was also very lucky that I got the chance to work partly under supervision of Prof. Alex Gershman. His vision and trust have helped me to develop the self-confidence required for any Ph.D. student who endeavors to become an independent researcher. I was delighted to have such a renowned researcher as my supervisor. Unfortunately, he suddenly passed away on August 12, 2011 after a long illness. May God rest his soul in peace.

I also thank Prof. Shahram Shahbazpanahi from university of Ontario for his interest in my work and for taking the time to be the second reviewer of my thesis. I benefited greatly from our interactions.

Many thanks to all of my colleagues for building lovely working environments and also to our very helpful secretary Mrs. Marlis Gorecki. I am happy for the supervision of some students whose efforts motivated me to study more. My sincere thanks go to my master students: Julia Vinogradova, Jiawei Xie, Qi Mu, Muhammad Waseem and my bachelor students: Parvaneh Davarmanesh, Stefan Schmidt, Christophe Girardey, Bruno Keuni and Toby Christian Lawin-Ore.

I would also like to thank Hana for her understanding, encouragement, and support. Last, but certainly far from the least, I send my purest love to my parents whom the words are humbled to thank for their unconditional love and support throughout my life. I would

also like to thank the rest of my family, especially my lovely sisters Sima and Sareh.

Nima Sarmadi
Darmstadt, Germany
February 2012

Zusammenfassung

Die stetig wachsende Nachfrage nach höherer Bandbreiten-Effizienz, Reichweite und Zuverlässigkeit sowie höheren Übertragungsraten in der dritten Generation (3G) und in zukünftigen Generationen von drahtlosen Kommunikationssystemen hat zu intensiver Forschung auf dem Gebiet der Mehr-Antennen-Kommunikation geführt. Des Weiteren hat sich kürzlich Orthogonal Frequency-Division Multiplexing (OFDM) als vorteilhafter Kandidat für zukünftige Mobilfunksysteme herauskristallisiert. Grund hierfür sind vorteilhafte Eigenschaften von OFDM, wie z.B., eine effiziente Nutzung der Bandbreite, eine Kanalentzerrung, sowie Robustheit gegenüber Mehrwegeausbreitung. Aufgrund dieser Tatsachen sind Multiple-Input-Multiple-Output (MIMO) Systeme in Verbindung mit OFDM viel versprechende Verfahren, die bereits in viele neue Mobilfunkstandards wie Long Term Evolution (LTE) und Worldwide interoperability for Microwave Access (WiMAX) aufgenommen wurden.

Space-Time Coding (STC) Verfahren sind in der Lage, die räumliche Diversität auszunutzen, die Mehr-Antennen-Systemen mit sich bringen. STC-Verfahren wurden außerdem mit MIMO-OFDM-Mobilfunksystemen kombiniert, um die Zuverlässigkeit und die Übertragungsrate gegenüber Einzel-Antennen-Systemen zu erhöhen. Insbesondere stellen die sogenannten Orthogonal Space-Time Block Codes (OSTBCs) eine beliebte Klasse von STC-Verfahren dar. Sie sind dafür bekannt, nicht nur den räumlichen Diversitäts-Gewinn zu maximieren, sondern auch einfache Dekodier-Verfahren zuzulassen. In den Genuss der von der Theorie versprochenen Vorzüge von orthogonal kodierten MIMO-OFDM-Systemen

kommt man jedoch nur, wenn akkurate Kanalzustandsinformation (CSI) am Empfänger vorausgesetzt werden können. Ein Mangel an CSI am Empfänger geht mit erheblichen Einbußen der Leistungsfähigkeit der MIMO-OFDM Systeme einher.

In der Praxis werden die Kenntnisse über den Übertragungskanal gewöhnlicherweise mit Hilfe übertragener Pilotsymbole erlangt, welche auf Kosten einer reduzierten Bandbreiteneffizienz und einer höheren Leistungsaufnahme der Nachrichtenübertragung beigefügt werden. Blinde Kanalschätzmethoden sind insbesondere deshalb von großem Interesse, da sie die zuvor genannten Nachteile vermeiden.

Der Schwerpunkt dieser Arbeit liegt auf der Entwicklung von Algorithmen zur blinden Kanalschätzung für orthogonal kodierte MIMO- und MIMO-OFDM Systeme.

Zunächst stellen wir ein neues Modell für orthogonal kodierte Einträger-MIMO-Systeme vor. Auf diesem Modell basierend beweisen wir eine spezielle Unterraumeigenschaft der vektorisierten Übertragungsfunktion des Kanals für Einträger-Systeme. Wir begründen damit eine blinde Kanalschätzmethode mit analytisch geschlossener Darstellung, welche sich direkt auf die einzelnen Subträger eines MIMO-OFDM Systems anwenden lässt. Zudem schlagen wir zwei Methode vor, mit der sich Mehrdeutigkeiten bei der Kanalschätzung vermeiden lassen.

Als nächstes verallgemeinern wir die spezielle Unterraumeigenschaft der vektorisierten Übertragungsfunktion für Einträger-Systeme auf Mehrträger-Systeme und schlagen für orthogonal raum-zeit-kodierte MIMO-OFDM Systeme einen blinden Kanalschätzer vor, der eine analytisch geschlossene Darstellung besitzt. Zudem leiten wir Bedingungen her, unter denen eine eindeutige Kanalschätzung möglich ist.

Danach entwickeln wir einen neuartigen Algorithmus für MIMO-OFDM Systeme mit OSTBCs, basierend auf semi-definiten Relaxierung (SDR). Wir zeigen, dass sich das nicht-konvexe Kanalschätzungsproblem als ein konvexes semi-definites Programm (SDP) approximieren lässt. Hierdurch kann das Kanalschätzungsproblem mit den modernen Methoden

der konvexen Optimierung gelöst werden.

Schließlich entwickeln wir Algorithmen mit analytisch geschlossener Darstellung für die blinde Kanalschätzung, die auf den relaxierten Maximum Likelihood Empfänger und den Capon Empfänger basieren. Im Vergleich zu dem Algorithmus der auf der SDR-Technik basiert, weisen die beiden Algorithmen einen unterschiedlichen Kompromiss zwischen Leistungsfähigkeit und Komplexität auf.

Unter der Annahme einer zeitlichen Aufspreizung des Funkkanals unterhalb der Dauer eines OSTBC-OFDM Symbols ist es im Zeitbereich möglich, die Parameter aller Subträger zusammen zu schätzen. Dies erleichtert eine kohärente Datenverarbeitung über alle Subträger hinweg im Vergleich zu traditionellen Schätzmethoden, in denen die Subträger getrennt voneinander verarbeitet werden. Die vorgeschlagenen Kanalschätzmethoden bieten nicht nur einen erheblich reduzierten Rechenaufwand, sondern verbessern zudem auch noch die Genauigkeit der Schätzung.

Abstract

The ever growing interest for higher transmission rates, bandwidth efficiency, coverage, and reliability in the third generation (3G) of wireless communication systems and beyond, has initiated an intensive research in the field of multi-antenna communications. Moreover, orthogonal frequency-division multiplexing (OFDM) has recently emerged as a favorable candidate for future generation of wireless communication systems due to its efficient utilization of bandwidth, simplicity of equalization, and robustness to multipath fading. Motivated by these facts, multiple-input multiple-output (MIMO) systems in association with the OFDM transmission are promising schemes widely adopted in recent wireless network standards such as Long Term Evolution (LTE) and Worldwide interoperability for Microwave Access (WiMAX).

Space-time coding (STC) techniques are capable of exploiting the spatial diversity offered by multi-antenna systems. STC techniques have also been combined with MIMO-OFDM wireless communication systems to both improve reliability and to increase higher transmission rates compared to single-antenna systems. In particular, the so-called orthogonal space-time block codes (OSTBCs) represent a popular class of STC techniques which are known to not only maximize the spatial diversity gain, but also offer simple decoding schemes. However, to obtain the theoretical promises of orthogonally coded MIMO-OFDM systems, accurate channel state information (CSI) is required at the receiver. The lack of CSI at the receiver is associated with a severe performance degradation of the MIMO-OFDM

system.

In practice, the CSI is commonly acquired from known pilot symbols inserted in the transmission at the expense of a reduced bandwidth efficiency and power consumption. Therefore, *blind* channel estimation methods are of great interest as they avoid the aforementioned penalties. In this thesis, we focus on developing blind channel estimation algorithms for orthogonally coded MIMO and MIMO-OFDM systems.

First, we introduce a novel model for orthogonally coded single-carrier MIMO systems. Based on this model, we derive a special subspace property of the channel frequency response (CFR) vector. We then justify a closed-form blind channel estimation method that is also directly applicable to each individual subcarrier of a MIMO-OFDM system. Moreover, we propose two strategies to eliminate channel estimation ambiguities.

Next, we generalize the special subspace property of the CFR vector derived for single-carrier systems to the multi-carrier case and propose a new closed-form blind channel estimator for orthogonally space-time coded MIMO-OFDM systems. Moreover, we derive the condition under which unique channel estimates can be obtained.

Then, we develop a novel blind channel estimation algorithm for MIMO-OFDM systems under OSTBCs based on the semi-definite relaxation (SDR) technique. We show that the non-convex channel estimation problem can be approximated by a convex semi-definite programming (SDP) problem. Therefore, the channel estimation problem can be solved using modern convex optimization methods.

Finally, based on the Relaxed Maximum Likelihood (RML) and the Capon receiver, respectively, we develop blind channel estimators which have closed-form solutions. Both of these algorithms exhibit different performance-complexity trade-offs compared to the SDR-based approach.

Assuming a finite delay spread over the wireless channel that falls below the duration of the OSTBC-OFDM symbol in MIMO-OFDM systems allows us to estimate the channel

parameters in the time-domain jointly for all subcarriers. This facilitates coherent data processing across all the subcarriers compared to the traditional subcarrier-wise channel estimation methods. The proposed channel estimation methods not only offer a considerable reduced computational complexity, but also result in improved estimation accuracy.

Table of Contents

| | |
|---|------------|
| Acknowledgments | iii |
| Zusammenfassung | v |
| Abstract | ix |
| List of Figures | xv |
| Notations | xix |
| Abbreviations | xxi |
| Commonly used symbols | xxv |
| 1 Introduction | 1 |
| 1.1 Multi-antenna and multi-carrier communication systems | 1 |
| 1.2 Channel estimation | 3 |
| 1.3 Thesis overview and contributions | 8 |
| 2 Background | 11 |
| 2.1 Wireless channel | 11 |
| 2.1.1 Time dispersive fading | 12 |
| 2.1.2 Frequency dispersive fading | 13 |
| 2.2 MIMO and MIMO-OFDM system models | 15 |
| 2.2.1 MIMO system model | 15 |
| 2.2.2 MIMO-OFDM system model | 18 |
| 2.3 The OSTBCs properties | 20 |
| 2.3.1 Rotatable OSTBCs | 25 |
| 2.4 Blind ML estimation or detection | 28 |
| 2.4.1 Blind identifiability | 29 |
| 2.5 Optimal receiver | 32 |

| | | |
|----------|--|------------|
| 3 | Blind channel estimation in orthogonally coded MIMO-OFDM systems: | |
| | Single-carrier analysis | 33 |
| 3.1 | Introduction | 33 |
| 3.2 | Virtual snapshot model | 34 |
| 3.3 | Weighting strategy | 38 |
| | 3.3.1 The Euclidean correlation matching criterion | 45 |
| | 3.3.2 The Kullback correlation matching criterion | 47 |
| 3.4 | Simulations | 49 |
| 3.5 | Chapter summary | 57 |
| 4 | Blind channel estimation in orthogonally coded MIMO-OFDM systems: | |
| | Multi-carrier analysis | 59 |
| 4.1 | Introduction | 59 |
| 4.2 | Coherent processing | 60 |
| 4.3 | Uniqueness condition | 64 |
| 4.4 | Normalization schemes comparison | 68 |
| 4.5 | Simulations | 70 |
| 4.6 | Chapter summary | 85 |
| 5 | Blind channel estimation in orthogonally coded MIMO-OFDM systems: | |
| | Alternative approaches for multi-carrier analysis | 87 |
| 5.1 | Introduction | 87 |
| 5.2 | Semi-definite relaxation-based approach | 88 |
| 5.3 | Relaxed ML-based approach | 93 |
| 5.4 | Capon-based approach | 96 |
| 5.5 | Simulations | 99 |
| 5.6 | Chapter summary | 115 |
| 6 | Conclusions and future works | 117 |
| 6.1 | Conclusions | 117 |
| 6.2 | Future works | 120 |
| 7 | Appendices | 123 |
| | Appendix A | 123 |
| | Appendix B | 124 |
| | Appendix C | 125 |
| | Appendix D | 126 |
| | Appendix E | 126 |
| | Appendix F | 131 |
| | Bibliography | 134 |

List of Figures

| | | |
|------|--|----|
| 3.1 | Bias versus SNR, first example, Alamouti code. | 51 |
| 3.2 | RMSE versus SNR, first example, Alamouti code. | 52 |
| 3.3 | SER versus SNR, first example, Alamouti code. | 53 |
| 3.4 | Bias versus SNR, second example, $M = 1$ | 54 |
| 3.5 | RMSE versus SNR, second example, $M = 1$ | 54 |
| 3.6 | SER versus SNR, second example, $M = 1$ | 55 |
| 3.7 | Bias versus SNR, second example, $M = 2$ | 55 |
| 3.8 | RMSE versus SNR, second example, $M = 2$ | 56 |
| 3.9 | SER versus SNR, second example, $M = 2$ | 57 |
| 4.1 | Bias versus SNR, first example. | 72 |
| 4.2 | RMSE versus SNR, first example. | 73 |
| 4.3 | BER versus SNR, first example. | 73 |
| 4.4 | Bias versus SNR, second example. | 76 |
| 4.5 | RMSE versus SNR, second example. | 76 |
| 4.6 | BER versus SNR, second example. | 77 |
| 4.7 | Bias versus SNR, third example. | 78 |
| 4.8 | RMSE versus SNR, third example. | 78 |
| 4.9 | SER versus SNR, third example. | 79 |
| 4.10 | Bias versus L' , fourth example, $L = 5$ | 79 |
| 4.11 | RMSE versus L' , fourth example, $L = 5$ | 80 |
| 4.12 | BER versus L' , fourth example, $L = 5$ | 80 |
| 4.13 | Bias versus L' , fifth example, $L = L'$ | 82 |
| 4.14 | RMSE versus L' , fifth example, $L = L'$ | 82 |

| | | |
|------|--|-----|
| 4.15 | BER versus L' , fifth example, $L = L'$. | 83 |
| 4.16 | Bias versus SNR, sixth example. | 83 |
| 4.17 | RMSE versus SNR, sixth example. | 84 |
| 4.18 | BER versus SNR, sixth example. | 84 |
| 5.1 | Bias versus SNR, first example, $P = 2$. | 100 |
| 5.2 | RMSE versus SNR, first example, $P = 2$. | 101 |
| 5.3 | BER versus SNR, first example, $P = 2$. | 101 |
| 5.4 | Bias versus SNR, first example, $P = 1$. | 103 |
| 5.5 | RMSE versus SNR, first example, $P = 1$. | 104 |
| 5.6 | BER versus SNR, first example, $P = 1$. | 104 |
| 5.7 | Bias versus SNR, second example. | 105 |
| 5.8 | RMSE versus SNR, second example. | 106 |
| 5.9 | BER versus SNR, second example. | 106 |
| 5.10 | Bias versus SNR, third example. | 108 |
| 5.11 | RMSE versus SNR, third example. | 108 |
| 5.12 | SER versus SNR, third example. | 109 |
| 5.13 | Bias versus L' , fourth example, $L = 5$. | 110 |
| 5.14 | RMSE versus L' , fourth example, $L = 5$. | 110 |
| 5.15 | BER versus L' , fourth example, $L = 5$. | 111 |
| 5.16 | Bias versus L' , fifth example, $L = L'$. | 111 |
| 5.17 | RMSE versus L' , fifth example, $L = L'$. | 112 |
| 5.18 | BER versus L' , fifth example, $L = L'$. | 112 |
| 5.19 | Bias versus SNR, sixth example. | 114 |
| 5.20 | RMSE versus SNR, sixth example. | 114 |
| 5.21 | BER versus SNR, sixth example. | 115 |

Notations

| | |
|--|---|
| a | the scalar a |
| \mathbf{a} | the vector \mathbf{a} |
| \mathbf{A} | the matrix \mathbf{A} |
| $[\mathbf{a}]_i$ | the i th entry of \mathbf{a} |
| $[\mathbf{A}]_{ij}$ | the (i, j) th entry of \mathbf{A} |
| $\mathbf{A} \succeq 0$ | \mathbf{A} is positive semi-definite |
| $\Pi_{\mathbf{A}}$ | the orthogonal projector onto the column space of matrix \mathbf{A} |
| $\mathbf{a} \sim N_C(\boldsymbol{\mu}, \boldsymbol{\Sigma})$ | \mathbf{a} is circular complex Gaussian distribution random vector with mean $\boldsymbol{\mu}$ and covariance matrix $\boldsymbol{\Sigma}$ |
| $\text{diag}(\mathbf{a})$ | the diagonal matrix composed of the entries of vector \mathbf{a} |
| $E\{\cdot\}$ | the statistical expectation operation |
| $\text{rank}\{\cdot\}$ | the rank of a matrix |
| $\text{range}\{\cdot\}$ | the range (or column space) of a matrix |
| $\lambda_{\min}(\cdot)$ | the smallest eigenvalue of a matrix |
| $\lambda_{\max}(\cdot)$ | the largest eigenvalue of a matrix |
| $\mathcal{P}\{\cdot\}$ | the normalized principal eigenvector |
| $\ \cdot\ $ | the L_2 norm of a vector or Frobenius norm of a matrix |
| $ \cdot $ | the absolute value of a complex variable |
| \mathbf{I}_n | the $n \times n$ identity matrix |

| | |
|---------------------|---|
| $\text{tr}(\cdot)$ | the trace of a matrix |
| $\mathbf{0}_n$ | the $n \times n$ matrix containing zeros in all entries |
| \mathbf{e}_i | a vector whose i th entry is one and the rest are zero |
| \otimes | the Kronecker matrix product |
| $(\cdot)^T$ | the transpose operator |
| $(\cdot)^*$ | the complex conjugate operator |
| $(\cdot)^H$ | the transpose complex conjugate (Hermitian) operator |
| $\text{Re}(\cdot)$ | the real part of a complex value |
| $\text{Im}(\cdot)$ | the imaginary part of a complex value |
| j | the imaginary unit ($j = \sqrt{-1}$) |
| \in | membership in a set |
| $\text{vec}(\cdot)$ | the vectorization operator which stacks the columns of a matrix on top of each other |
| $\log(\cdot)$ | the natural logarithm |
| $\det(\cdot)$ | the determinant of a matrix |
| $\hat{(\cdot)}$ | the estimated value |
| ∞ | infinity |
| $\delta_{t,t'}$ | the Kronecker delta function ($\delta_{t,t'} = 1$ if $t = t'$ and $\delta_{t,t'} = 0$ if $t \neq t'$) |
| \mathbb{R} | the set of real numbers |
| \mathbb{C} | the set of complex numbers |

Abbreviations

| | |
|------|---|
| 3G | third generation of mobile systems |
| 4G | fourth generation of mobile systems |
| A/D | analog to digital |
| AWGN | additive white Gaussian noise |
| BER | bit error rate |
| BPSK | binary phase-shift keying |
| BS | base station |
| CFR | channel frequency response |
| CIR | channel impulse response |
| CP | cyclic prefix |
| CSI | channel state information |
| D/A | digital to analog |
| DFT | Discrete Fourier Transform |
| ECM | Euclidean covariance matching |
| FFT | Fast Fourier Transform |
| FIR | finite impulse response |
| GSM | Global System for Mobile communications |

| | |
|-------|--|
| IBI | inter-block-interference |
| IF | intermediate frequency |
| IFFT | Inverse Fast Fourier Transform |
| ISI | inter-symbol-interference |
| KCM | Kullback covariance matching |
| LOS | line-of-sight |
| LTE | Long Term Evolution |
| MF | matched filter |
| MIMO | multiple-input multiple-output |
| MISO | multiple-input single-output |
| ML | Maximum Likelihood |
| OFDM | orthogonal frequency-division multiplexing |
| OSTBC | orthogonal space-time block code/coding |
| pdf | probability density function |
| PSK | phase-shift keying |
| QCQP | quadratic constraint quadratic problem |
| QPSK | quadrature phase-shift keying |
| RF | radio frequency |
| RML | Relaxed Maximum Likelihood |
| RMSE | root mean square error |
| SDP | semi-definite programming |
| SDR | semi-definite relaxation |
| SER | symbol error rate |

| | |
|-------|---|
| SISO | single-input single-output |
| SNR | signal-to-noise ratio |
| SOCP | second-order cone programming |
| s.t. | subject to |
| STBC | space-time block code/coding |
| STC | space-time code/coding |
| WiMAX | Worldwide interoperability for Microwave Access |

Commonly used symbols

| | |
|--------------------------------|---|
| A | code-channel matrix |
| B_C | wireless channel coherence bandwidth |
| B_D | wireless channel Doppler spread |
| B_S | transmitted symbol bandwidth |
| C | OSTBC's basis matrix |
| F | Discrete Fourier Transform matrix |
| g | channel impulse response vector ($\mathbf{g} = \text{vec}(\mathbf{G})$) |
| G | channel impulse response matrix |
| $\gamma_u, \gamma_n, \gamma_b$ | weighting vectors |
| h | channel frequency response vector ($\mathbf{h} = \text{vec}(\mathbf{H})$) |
| H | channel frequency response matrix |
| i | subcarrier index |
| J | selection matrix |
| K | number of complex symbols per STBC matrix |
| l | channel tap index |
| L | effective channel length in the time-domain |
| L' | upper bound for effective channel length in the time-domain |
| λ | eigenvalue of a matrix |
| Λ | transmitted data covariance matrix |

| | |
|---|---|
| M | number of receive antennas |
| N | number of transmit antennas |
| N_0 | number of subcarriers |
| P | number of snapshots |
| \mathbf{P} | permutation matrix |
| \mathbf{Q} | OSTBC's rotation matrix |
| \mathbf{R} | received data covariance matrix |
| $\hat{\mathbf{R}}$ | sample received data covariance matrix |
| s | complex symbol |
| \mathbf{s} | vector of complex symbols |
| σ^2 | received noise variance |
| σ_τ | wireless channel delay spread |
| T | block length of the STBC |
| T_C | wireless channel coherence time |
| T_S | transmitted symbol duration |
| \mathbf{v} | received noise vector ($\mathbf{v} = \text{vec}(\mathbf{V})$) |
| \mathbf{V} | received noise matrix |
| \mathbf{X} | transmitted STBC matrix |
| \mathcal{X} | virtual snapshot covariance matrix |
| $\hat{\mathcal{X}}$ | sample virtual snapshot covariance matrix |
| $\xi_{\mathbf{u}}, \xi_{\ \cdot\ }, \xi_{\lambda_{\max}}$ | normalization vectors |
| \mathbf{y} | received data vector ($\mathbf{y} = \text{vec}(\mathbf{Y})$) |
| \mathbf{Y} | received data matrix |
| $\tilde{\mathbf{y}}$ | virtual snapshot vector |

Chapter 1

Introduction

Both multi-antenna and multi-carrier communication systems have been an intensive topic of recent research. This thesis aims at developing advanced blind channel estimation algorithms for single- and multi-carrier orthogonally coded MIMO systems and at studying various aspects to exploit potential promises of these systems. In this introductory chapter, we formulate the context and the motivation of the presented work, provide a literature survey on the channel estimation in wireless communication systems, and outline the contributions of the thesis.

1.1 Multi-antenna and multi-carrier communication systems

Multi-antenna communication systems attract significant interest of both academic researchers and practitioners as these systems enable high capacities, and also dramatically increase range and reliability of wireless communication systems without additional consumption of the available radio spectrum; see e.g., references [AH04], [DASC04], [FG98], [GS05], [LS03], [PGNB04], [PNG03], [PP97], [STTEP02], and [Tel99]. For instance, multiple antennas have been already deployed at the receiver side of wireless communication systems to improve signal reception at base stations (BSs) in the Global System for Mobile communications (GSM) since early 1990's. Also, multiple antennas have been considered both at the transmitters (multiple-input) and at the receivers (multiple-output) in third

generation (3G) wireless communication systems and beyond to benefit from spatial filtering and diversity.

Space-time coding (STC) techniques used in multiple-input multiple-output (MIMO) wireless communication systems are known to offer significantly improved transmission rates and immunity to channel fading effects, compared to single-antenna systems; see [GS05], [GSSSN03], [LS03], [PNG03], and [TSC98]. To mitigate the effects of fading, different types of diversity techniques are widely proposed and applied in wireless communications. The key concept of diversity is to transmit a same signal through different independent diversity branches to receive independent signal replicas [TV05]. These diversity branches can be time, frequency, space, and polarization. For instance, the frequency diversity can be exploited in multi-carrier communications where the same information is transmitted in different frequency bands. Also in MIMO systems, spatial diversity, which employs multi-antennas, can be used specifically to combat fading as different received signals corresponding to different antennas may undergo independent fading [GS05], [Jaf05], [LS03], and [PNG03]. Among different STC schemes developed to the date, orthogonal space-time block codes (OSTBCs) [Ala98], [Jaf05], [TJC99] represent an attractive choice because these codes achieve full spatial diversity gain while maintaining a low decoding complexity. It should be noted that full spatial diversity gain is defined by the number of transmit antennas times the number of receive antennas [TV05].

Space-time coded MIMO systems can also be combined with the orthogonal frequency-division multiplexing (OFDM) scheme [GSSSN03], [STTEP02]. This enables integrating the advantages of the multi-carrier and multi-antenna schemes such as high data rate, transmit and receive diversity, high spectral efficiency, and reduced system complexity [BGP02], [Li02], [LSA98]. Particularly, this combination facilitates the use of space-time codes in the frequency-selective fading channels as use of the OFDM converts the frequency-selective fading channel into a number of parallel flat fading channels [LS03], [WG00]. Also, since the number of equalizers increases proportionally with the number of receive antennas, implementation of the OFDM considerably simplifies equalization at the receiver. Motivated by these facts, MIMO-OFDM schemes are widely adopted in recent wireless network standards

such as Long Term Evolution (LTE), IEEE802.16a (WiMAX) and in the upcoming future fourth generation (4G) wireless communication systems [CS00]. Further, MIMO-OFDM schemes have been created tremendous surge of research related to their various aspects; see [AD07], [BGP02], [BHP02], [BLM03], [CB11], [CMC08], [CT07b], [DASC02], [GN07], [GZNN08], [LGBS01], [Li05], [LSA98], [LSA99], [LSL03], [Ma07], [MVDC06], [MYG05], [SGM05], [SHP07], [SHP08], [SL02], [SRHFGB11], [STTEP02], [TC10], [UAG01], [VS08a], [VTP97], [WZS08], [WZS11], [Yan05], [ZLN06], [ZM05], [ZMG02] and references therein.

1.2 Channel estimation

The performance of *coherent* MIMO communication systems, in which it can be safely assumed that channel state information (CSI) being known at the receiver, severely rely upon the quality of CSI available at the receiver [Yan05]. Even though pilot-based schemes are practically used for channel estimation in multi-antenna systems in modern cellular communication standards; see [ABL09], [BG06], [BLM03], [BT02], [CB08], [CT07a], [HH03], [Li02], [MYG05], [SDWL06], [SLL04], and [SRHFGB11], these schemes are associated with power consumption overhead and bandwidth inefficiency. This fact is particularly challenging in scenarios when severe power constraints apply at the transmitter or when the channel coefficients need to be updated more frequently due to fast fading. The former scenario applies, e.g., in the uplink transmission of mobile handsets, and the latter one occurs, e.g., in high mobility scenarios. Hence, in fading environments with channels that are time-, frequency-, and even space-selective, the pilot symbols power and bandwidth overheads can be substantial because of a relatively large number of pilots required in the time, frequency, and space planes, respectively. In such scenarios, *noncoherent* detection approaches represent a class of attractive solutions in which either the CSI is bypassed in the detection procedure or can be estimated by the aid of the received data.

Within the former category of noncoherent detection schemes for MIMO systems, differential space-time coding techniques can be considered as appropriate solutions to circumvent pilot symbols overheads; see [DASC02], [GS02], [HS00], [Hug00], [JT01], [Li05], [MTL05],

and [TJ00] for more details. In general, differential techniques encode the transmitted information based on differences between two consecutive transmitted symbols blocks. However, for differential techniques, a 3 dB signal-to-noise ratio (SNR) penalty in performance compared to their coherent counterparts is inevitable. This SNR penalty can be explained by the fact that in the detection process, the noise power of the current symbol adds to the noise power in the previous symbol. Similarly, the unitary space-time modulation technique proposed in [HM00] and [HMRSU00], refers to noncoherent detection scheme for MIMO systems which can be used in the absence of CSI at the receiver. However, the computational complexity of corresponding Maximum Likelihood (ML) receiver increases exponentially with size of the multi-dimensional space-time constellation. Moreover, there is a 2-4 dB SNR performance penalty compared to the coherent ML receiver [HM00].

To avoid the aforementioned penalties, another promising alternative is to estimate the wireless channel only based on the received data payload using *blind* or *semi-blind* techniques; see e.g., references [AD06], [AD07], [BHJZ02], [BHP02], [CHMC10], [CMC08], [CMHC09], [CT07b], [GN07], [GN08], [GZNN08], [LGBS01], [Li05], [LSA99], [LSL03], [Ma07], [MVDC06], [PK10], [SGM05], [SHP07], [SHP08], [SL02], [TC10], [UAG01], [VS08a], [VS08b], [VSPV09], [VTP97], [WZS08], [WZS11], [ZD10], [ZLN06], [ZM05], and [ZMG02].

Several blind MIMO channel estimation or symbol detection methods have been developed exclusively for frequency flat fading wireless channels; see, e.g., [AD06], [AD07], [BA07], [CHMC10], [CT07b], [LPMY07], [LSL03], [Ma07], [MVDC06], [PK10], [SG03], [SGM05], [VS08a], [VS08b], [ZD10] and references therein. In [CHMC10], [LPMY07] and [MVDC06], different blind symbol detectors specifically devised for OSTBCs have been proposed. However, these approaches are applicable only to the particular case of symbol constellations, e.g., binary phase-shift keying (BPSK) or quadrature phase-shift keying (QPSK) constellations in [MVDC06]. Also, the computational complexity of these methods is rather high as each new received data block requires a new detection process. Moreover, since the proposed approaches in [CHMC10] and [MVDC06] are based on a convex approximation technique known as semi-definite relaxation (SDR), their performance can be far from that of the optimal matched filter (MF) receiver. Note that the SDR technique

is a computationally efficient approximation of a non-convex optimization problem by a convex problem, that is easier to solve, through replacing the non-convex constraints by semi-definite constraints [LMSYZ10].

In [LSL03] and [SG03], two blind space-time decoding approaches based on joint channel estimation and symbol detection have been proposed. To solve the blind estimation problem, an iterative minimization of the ML function with respect to the channel matrix and the data symbols has been proposed. As a result, these approaches do not provide any closed-form solution for the channel estimates. Also, since these approaches require proper initialization of either the channel estimate or the symbol decisions, their respective global convergence can not be guaranteed.

The issue of blind channel identifiability under OSTBCs is investigated in [AD06], [AD07], [Ma07], and [VS08a]. The notion of blind channel identifiability is closely related to the fact that whether the CSI can be recovered, up to an arbitrary real scalar, only based on the second order statistics (SOSs) of the received data or not; see [VS08a] for more details. The numerical and analytical results provided in these works illustrate that most of the existing OSTBCs suffer from channel non-identifiability in two practical cases. These cases comprise the systems using the rotatable OSTBCs [Ma07]; see Section 2.3.1, that are also incorporated in the LTE standard and systems with multiple-input single-output (MISO) configuration like in downlink transmission to single-antenna users. Hence, most of the already existing blind channel estimation methods for orthogonally coded MIMO systems experience such non-identifiability problem. Although in [SGM05] and [VS08b], specific methods have been proposed to eliminate such non-identifiability problem, still the necessary and sufficient conditions under which this issue can be resolved remains unclear. Most of the cited approaches exhibit acceptable estimation performance particularly under the assumption that the wireless channel remains invariant over many transmitted data blocks. However, this assumption can be violated in certain wireless environments in which the channel coherence time is smaller than or comparable to the length of transmitted data block.

It should be noted that in frequency-selective fading wireless channels, all the previously

mentioned blind methods developed for frequency flat fading channels can be straightforwardly implemented in MIMO-OFDM systems in a so-called *subcarrier-wise* fashion. In the subcarrier-wise approaches, the problem of estimating the frequency-selective fading channel is transformed to that of independently estimating the frequency flat channels of multiple subcarriers [UAG01], [ZM05]. In these approaches, the subcarriers are not processed coherently. In this sense, the subcarrier-wise approaches neglect the fact that the wireless channel gains at each subcarrier are given by the Fourier transform of a smaller set of MIMO channel impulse response (CIR) coefficients in the time-domain. According to the parsimony principle [SS89], it is more advantageous from performance viewpoint to estimate CIR coefficients first and thereafter transform them to the frequency-domain, instead of estimating the frequency-domain propagation coefficients directly for each subcarrier [LSA99]. Furthermore, the subcarrier-wise approaches suffer from an excessively high computational complexity when the number of subcarriers is large [CB11].

There are also several blind and semi-blind methods for estimating frequency-selective fading MIMO channels; see e.g., [BHP02], [GN07], [GZNN08], [LGBS01], [SHP07], [SHP08], [SL02], [TC10], [VTP97], [WZS08], [WZS11], [ZMG02] and references therein. In a significant part of these methods, no assumption on space-time coded transmissions is used as in [BHP02], [GN07], [GZNN08], [SHP07], [SHP08], [TC10], [VTP97], [WZS08], and [WZS11]. Hence, these methods are not able to take advantage of the specific structure of the space-time code. The approach of [GN07] estimates the channel parameters in the frequency-domain. It does not take advantage of subcarriers correlations and is associated with a high computational complexity. The techniques of [BHP02], [GZNN08], [SHP07], [SHP08], [VTP97], [WZS08], and [ZMG02] make use of extra information, such as the cyclic prefix (CP), channel precoding at the transmitter, or virtual subcarriers, to warrant the identifiability of the resulting channel estimates. However, these methods impose specific requirements, e.g., on the CP length or on the precoding matrix, and, therefore, require additional resources that may dramatically limit the bandwidth efficiency. Further, a drawback associated with these methods is that the use of side information increases the overall system complexity.

In [LGBS01], [SL02], and [ZMG02], the structural properties of the space-time block codes (STBC) have been exploited to identify the channel. However, these approaches can not be extended to the scenarios with arbitrary numbers of receive and transmit antennas. Moreover, all these techniques require relatively long data records which translates to rather restrictive conditions on the coherence time of the wireless channel and makes these techniques inapplicable in fast fading scenarios.

Recently, two novel approaches for blind symbol detection and channel estimation in OSTBC-based MIMO-OFDM systems have been developed in [CMC08] and [VSPV09], respectively, that require only a small number of measurements to achieve acceptable accuracy. These approaches exploit inter-subcarrier relationships among channel coefficients and utilize the OSTBC structure. However, the applicability of the approach of [CMC08] is limited to the high computational complexity associated with this scheme. To reduce the complexity, the subchannel grouping technique of [CHMC10] has been deployed in combination with the approach of [CMC08]. This technique however degrades the quality of signal detection, and, therefore, the cyclic ML approach of [LSL03] has been proposed in [CMC08] to enhance the overall performance of the modified method. Nevertheless, the computational cost of the modified method still remains significantly high in the cases when either the number of subcarriers or the size of data block is large. Furthermore, the algorithm of [CMC08] requires block-wise processing and does not benefit from averaging over successive blocks of received OSTBC-OFDM data that can improve the estimation performance in case of slowly fading channels. Moreover, this algorithm is only applicable to the case of BPSK and QPSK constellations.

The approach proposed in [VSPV09] uses relaxation idea to convert the original complex blind ML channel estimation problem into a simple eigenvalue problem. This approach generally results in biased channel estimates for the finite sample case and under which unique channel estimates are obtained have not been provided in this work. Moreover, this approach fails to eliminate the ambiguities associated with the channel estimation as, e.g., in the case of rotatable OSTBCs [Ma07] including the popular Alamouti code [Ala98] or particular codes in the MISO system configurations [VS08a].

1.3 Thesis overview and contributions

In this thesis, we develop advanced techniques for blind channel estimation in orthogonally coded MIMO and MIMO-OFDM systems. The proposed techniques are free of most of the aforementioned shortcomings of the existing blind receivers. The outline and contributions of the thesis are as follows:

Chapter 2: Background

In this chapter, a brief overview of the wireless channel characteristics, the system model under consideration, the concepts of STBC and OSTBCs are provided. Also, the properties of rotatable OSTBCs are discussed. Further, the blind ML channel estimator is introduced and the structure of the optimal receiver is derived. In this context, we discuss in detail the issue of problem non-identifiability and ambiguities in the channel estimates that mark a major challenge in blind channel estimation.

Chapter 3: Blind channel estimation in orthogonally coded MIMO-OFDM systems: Single-carrier analysis

We propose a novel virtual snapshot model for orthogonally coded single-carrier MIMO systems in this chapter. We prove that the true channel frequency response (CFR) vector is the scaled version of the principal eigenvector of the received data covariance matrix. Two new weighting strategies are devised to eliminate the ambiguities associated with the blind channel estimates in two cases: the systems exploiting rotatable OSTBCs and the systems involving a single-receive antenna. This chapter is based on the following publications:

- N. Sarmadi and M. Pesavento, “Closed-form blind MIMO channel estimation for OSTBCs: Resolving ambiguities in rotatable codes,” in *Proc. European Signal Processing Conference (EUSIPCO)*, Barcelona, Spain, 2011, pp. 644-648.
- N. Sarmadi and M. Pesavento, “Closed-form blind channel estimation in orthogonally coded MIMO-OFDM systems: A simple strategy to resolve non-scalar ambiguities,” in *Proc. IEEE International Workshop on Signal Processing Advances in Wireless Communications (SPAWC)*, San Francisco, California, USA, 2011, pp. 301-305.

Chapter 4: Blind channel estimation in orthogonally coded MIMO-OFDM systems: Multi-carrier analysis

In this chapter a novel closed-form subspace-based blind channel estimation method for MIMO-OFDM systems based on the virtual snapshot model, devised in the previous chapter, is proposed. Taking into account subcarriers correlations in the case of finite delay spread of the wireless channel, we estimate a small number of channel parameters in the time-domain. Moreover, uniqueness conditions for unambiguous channel estimation are derived. This chapter is based on the following publications:

- N. Sarmadi, M. Pesavento, and A. B. Gershman, “Closed-form blind channel estimation in orthogonally coded MIMO-OFDM systems,” in preparation.
- N. Sarmadi, M. Pesavento, and A. B. Gershman, “Closed-form blind channel estimation for orthogonally coded MIMO-OFDM systems: An algorithm and uniqueness study,” in *Proc. International ITG Workshop on Smart Antennas (WSA)*, Aachen, Germany, 2011, pp. 1-6.

Chapter 5: Blind channel estimation in orthogonally coded MIMO-OFDM systems: Alternative approaches

First, based on per-subcarrier channel norm constraint together with SDR technique, a new blind channel estimation approach for orthogonally coded MIMO-OFDM systems is proposed in this chapter. Next, based on aggregate channel norm constraint over all subcarriers along with the Relaxed ML (RML) criterion, we derive a blind channel estimator which benefits from lower computational complexity compared to the SDR-based estimator. Then, Capon criterion is adopted to develop another channel estimator with improved accuracy compared to the RML-based approach. The results of this chapter have been published in the following papers:

- N. Sarmadi, S. Shahbazpanahi, and A. B. Gershman, “Blind channel estimation in orthogonally coded MIMO-OFDM systems: A semidefinite relaxation approach,” *IEEE Trans. Signal Process.*, vol. 57, pp. 2354-2364, June 2009.

- N. Sarmadi, A. B. Gershman, and S. Shahbazpanahi, “Blind channel estimation in MIMO-OFDM systems using semi-definite relaxation,” in *Proc. IEEE International Conference on Acoustics, Speech, and Signal Processing (ICASSP)*, Las Vegas, Nevada, USA, 2008, pp. 2381-2384.
- N. Sarmadi, A. B. Gershman, and S. Shahbazpanahi, “Closed-form blind channel estimation in orthogonally coded MIMO-OFDM systems,” in *Proc. IEEE International Conference on Acoustics, Speech, and Signal Processing (ICASSP)*, Dallas, Texas, USA, 2010, pp. 3306-3309.

Chapter 6: Conclusions and future work

Concluding remarks are summarized in this chapter. We also propose some future works to further improve or extend the results of this thesis. Some of these ideas associated with the proposed methods and the model developed in this thesis have been addressed in the following papers:

- F. Römer, N. Sarmadi, B. Song, M. Haardt, M. Pesavento, and A. B. Gershman, “Tensor-based semi-blind channel estimation for MIMO OSTBC-coded systems,” in *Proc. Asilomar Conference on Signals, Systems and Computers*, Pacific Grove, California, USA, 2011.
- J. Vinogradova, N. Sarmadi, and M. Pesavento, “Subspace-based semiblind channel estimation method for fast fading orthogonally coded MIMO-OFDM systems,” in *Proc. International Workshop on Computational Advances in Multi-Sensor Adaptive Processing (CAMSAP)*, San Juan, Puerto Rico, 2011, pp. 149-152.
- J. Vinogradova, N. Sarmadi, and M. Pesavento, “Iterative semiblind channel estimation method for fast fading orthogonally coded MIMO-OFDM systems,” to be submitted.

Chapter 2

Background

In the first section of this chapter, the characteristics of the wireless channel are briefly reviewed. The MIMO and MIMO-OFDM system models under consideration are described in the second section. Then, we provide the background on the OSTBCs and introduce the rotatable OSTBCs and their properties in the third section. Next, we discuss the blind ML channel estimator. In this context, we address the issue of problem identifiability that is important for designing unique estimation procedures. Finally, we conclude the chapter with the optimal receiver structure for OSTBCs.

2.1 Wireless channel

The performance of wireless communication systems and associated fundamental limitations for data transmission heavily depend on the characteristics of the wireless channel. In general, wireless channels are random in nature which do not offer simple analysis as compared to the wired channels that are relatively deterministic and predictable. Modeling the wireless channels has been one of the most demanding parts of the wireless communication systems analysis and typically done in a statistical manner based on measurements. Depending on the surrounding environment, a transmitted signal usually propagates in the wireless channel through several different paths before it reaches the received antenna. This phenomenon is often referred to as *multipath* propagation. Hence, the transmitted signal received by the receiver antenna consists of the superposition of the various multipaths.

In the wireless channels, the received signal strength variations are generally described by both the large-scale and the small-scale propagation models. The former model describes the average received signal strength for an arbitrary large distance between transmitter and receiver and explains the path loss effects. The latter model characterizes the rapid fluctuations of the received signal strength over remarkable short distances or time intervals due to channel *fading*, i.e., the constructive or destructive combination of multipath signal components in the received signal. Actually, fading is a phenomenon corresponding to the wireless channel that results from multipath propagation due to scattering and from relative motion of transmitter, receiver, and scatterers. Next, we discuss fading in the multipath wireless channels from the physical perspective before we introduce a statistical model description for fading wireless channels. The delay spread due to the difference among the arrival times of different copies of the transmitted signal over different propagation paths results in and is proportional to the *time-dispersiveness* or the *frequency-selectivity* of the wireless channel. The Doppler spread, which is independent from delay spread, results from different Doppler shifts that are induced by the relative motion. Doppler spread results in and is proportional to the *frequency-dispersiveness* or the *time-selectivity* of the wireless channel [Rap02]. Similarly, the angular spread of the antenna elements in combination with multipath propagation results in *spatial-selectivity* of the wireless channel. Different types of fading can be distinguished that depend both on the transmitted signal nature and the wireless channel features. In other words, the characteristics of the signals and the choice of signal parameters only define the implications that fading channels have on the communication system. In the following, we explain in more detail four different types of fading and their corresponding circumstances related to frequency- or time-selectivity of the wireless channel [Rap02].

2.1.1 Time dispersive fading

If the transmitted symbol bandwidth is much smaller than the coherence bandwidth of the wireless channel, that is inversely proportional to the wireless channel delay spread, channel

can be modeled as constant gain over the entire frequency band. This case is referred to *frequency flat* fading. Defining T_S as the symbol duration, that is inversely proportional to the transmitted symbol bandwidth B_S , and B_C and σ_τ as the wireless channel coherence bandwidth and the wireless channel delay spread, respectively, condition for frequency flat fading can be summarized as

$$T_S \gg \sigma_\tau \quad \text{or} \quad B_S \ll B_C.$$

In flat fading scenarios, the wireless channel has a constant gain with linear phase response over the transmitted symbol bandwidth which preserves the spectral characteristics of the transmitted symbol at the receiver. However, due to the multipath propagations in combination with relative motion of transmitter, receiver and scatterers, the received signal strength generally varies with time. If the transmitted symbol duration is smaller than or comparable to the delay spread of channel, the transmitted symbol experiences frequency-selective fading, i.e., when

$$T_S < \sigma_\tau \quad \text{or} \quad B_S > B_C.$$

In this case, the wireless channel acts as a finite impulse response (FIR) filter and the received symbol comprises multiple attenuated and time-delayed versions of the transmitted symbol. This, in turn, causes the time dispersion of the received signal due to the inter-symbol interference (ISI). In other words, different frequency components in the transmitted symbol spectrum experience different gains in the frequency-domain. As a result, costly received symbol equalization is required in frequency-selective channels.

2.1.2 Frequency dispersive fading

The rate of variations of the transmitted baseband symbols in comparison with the rate of change of the wireless channel determines whether the channel is time-selective, i.e., *fast*, or time non-selective, i.e., *slow*, fading. The rate of change of the wireless channel depends on the velocity of scattering objects presented in the channel and the relative velocity of the transmitter and receiver to each other and to the scatterers. If the channel coherence time

is smaller than or comparable to the transmitted symbol duration, the transmitted symbol undergoes fast fading. Hence, in fast fading wireless channel we have

$$T_S > T_C \quad \text{or} \quad B_S < B_D,$$

where T_C stands for the channel coherence time and B_D represents the Doppler spread. Note that T_C is proportional to the inverse of the wireless channel Doppler spread. Fast fading results in frequency dispersion and increases with increasing Doppler spread in comparison with the bandwidth of the transmitted symbol. If the channel coherence time is much larger than the transmitted symbol duration or the Doppler spread of the wireless channel is much smaller than the transmitted symbol bandwidth, i.e.,

$$T_S \ll T_C \quad \text{or} \quad B_S \gg B_D,$$

the transmitted symbol undergoes slow fading. In this case, the CIR changes at a rate much lower than the transmitted symbol rate. Therefore, it can be assumed to be invariant over one symbol duration or even several symbol durations that make a transmission block. In the latter case, the wireless channel is quasi-static and is called *block-fading* channel as it remains invariant during the transmission of a block of symbols and varies independently in the next block.

It is noteworthy to mention that throughout this thesis, unless otherwise stated, the wireless channel is assumed to be block-fading. It should be also stressed that, an equivalent baseband model of a communication system is considered to simplify the analysis. This means that the modulated signal is represented by a complex-valued equivalent baseband signal and an equivalent baseband channel model is taken the place of radio frequency (RF) channel model in which the frequency response of channel is shifted to the baseband frequencies. This implies that the RF processing at the transmitter and at the receiver which in general comprises digital to analog (D/A) and analog to digital (A/D) conversion, up and down conversion to intermediate frequency (IF), pulse shaping, filtering, RF modulation and demodulation is not reflected in our modeling. Moreover, the discrete-time representation has been adopted throughout the thesis because it is assumed that all signals are band-limited and Nyquist-Shannon sampling criterion has been satisfied.

2.2 MIMO and MIMO-OFDM system models

It is known that the behavior of the wireless channel can be fully characterized by the channel impulse response [TV05]. Consequently, the wireless channel can be modeled as a time varying impulse response linear filter [Rap02]. The input-output relationship for a single-input single-output (SISO) wireless system with quasi-static or block-fading channel can be modeled as the discrete-time complex-valued baseband representation. For this representation, we recognize two different cases of frequency flat and frequency-selective fading. For the case of frequency-selective wireless channels, the input-output relation can be written as

$$y(t) = \sum_{l=0}^L h_l x(t-l) + v(t), \quad (2.1)$$

where $y(t)$ denotes the received signal, h_l stands for the l th tap of the complex baseband CIR with L as the effective channel length (hence, the total number of channel taps is $L+1$), $x(t)$ is the transmitted signal, $v(t)$ represents the additive noise, and t is the discrete time index. For the case of frequency flat wireless channel, the relation (2.1) can be simplified as

$$y(t) = h x(t) + v(t). \quad (2.2)$$

2.2.1 MIMO system model

Taking into account (2.2) for SISO systems, the input-output relationship corresponding to the frequency flat MIMO system using the standard complex-valued baseband representation for narrow-band signals can be written in matrix-algebraic form. To this aim, consider a point-to-point MIMO system with N transmit and M receive antennas. Assume that the complex-valued encoded signals $\{x_1(t), \dots, x_N(t)\}$ are transmitted by the N transmit antennas at a certain time instant t . Then, the received signal at the m th antenna can be expressed as [LS03]

$$y_m(t) = \sum_{n=1}^N h_{n,m} x_n(t) + v_m(t), \quad m = 1, \dots, M \quad (2.3)$$

where $h_{n,m}$ is the complex baseband channel gain between the n th transmit and the m th receive antennas and $v_m(t)$ models the receiver noise. Let us stack individual received

signals at different antennas in a $1 \times M$ row vector as

$$\mathbf{y}(t) \triangleq [y_1(t), \dots, y_M(t)]. \quad (2.4)$$

Taking into account (2.4) equation (2.3) can be expressed as [LS03]

$$\mathbf{y}(t) = \mathbf{x}(t)\mathbf{H} + \mathbf{v}(t), \quad (2.5)$$

where $\mathbf{x}(t) \triangleq [x_1(t), \dots, x_N(t)]$, $\mathbf{v}(t) \triangleq [v_1(t), \dots, v_M(t)]$ and \mathbf{H} is the following complex channel gain matrix [LS03]

$$\mathbf{H} \triangleq \begin{bmatrix} h_{1,1} & \dots & h_{1,M} \\ \vdots & \ddots & \vdots \\ h_{N,1} & \dots & h_{N,M} \end{bmatrix} \in \mathbb{C}^{N \times M}. \quad (2.6)$$

If we assume that the wireless channel is block-faded which is invariant during the transmission of T consecutive vectors $\{\mathbf{x}(1), \dots, \mathbf{x}(T)\}$, the corresponding received signal vectors in (2.5), the transmit signal vectors, and the noise vectors can be arranged in matrices, respectively, as follows:

$$\mathbf{Y} \triangleq \begin{bmatrix} \mathbf{y}(1) \\ \vdots \\ \mathbf{y}(T) \end{bmatrix} \in \mathbb{C}^{T \times M}, \quad \mathbf{X} \triangleq \begin{bmatrix} \mathbf{x}(1) \\ \vdots \\ \mathbf{x}(T) \end{bmatrix} \in \mathbb{C}^{T \times N}, \quad \mathbf{V} \triangleq \begin{bmatrix} \mathbf{v}(1) \\ \vdots \\ \mathbf{v}(T) \end{bmatrix} \in \mathbb{C}^{T \times M}. \quad (2.7)$$

Then, the input-output relation using (2.6) and (2.7) can be expressed in a compact matrix form as [LS03]

$$\mathbf{Y} = \mathbf{X} \mathbf{H} + \mathbf{V}, \quad (2.8)$$

in which \mathbf{X} represents the so-called STBC matrix containing the information symbols. Generally, STBC can be seen as a unique way of mapping a set of K information symbols $\{s_1, \dots, s_K\}$ onto a matrix \mathbf{X} which may in principle take on any form, e.g., linear or nonlinear. The focus in this thesis is on subclass of linear STBCs which exhibits appealing properties from both performance and implementation point of view. In linear STBCs, the transmitted code matrix is linear in the real and imaginary parts of the data symbols, or equivalently, in the symbols and their complex conjugates. The rate of an STBC measures

on average how many symbols per time slot it transmits, hence, using mapping \mathbf{X} in (2.7) is equal to $r = K/T$. According to (2.7), each column of matrix \mathbf{X} represents transmission over different time slots from specific transmit antenna, i.e., space dimension, and each row represents transmission of symbols from different transmit antennas at specific time slot, i.e., time dimension. Therefore, the matrix \mathbf{X} is capable to exploit space, i.e., multiple transmit antenna, and time dimensions as two independent diversity branches to transmit different signal replicas which may undergo independent fading. Although it should be emphasized that in construction of an STBC, three conflicting goals of maximizing diversity, i.e., maximizing the error performance, maximizing the transmission rate, and minimizing decoding complexity should be considered simultaneously.

In this thesis, the vectors $\{\mathbf{v}(t)\}_{t=1}^T$ in (2.7) are modeled as additive white circular Gaussian noise (AWGN), i.e.,

$$\mathbf{v}(t) \sim N_C(\mathbf{0}, \sigma^2 \mathbf{I}_M). \quad (2.9)$$

A Gaussian distribution of the noise term is quite common as it can be justified often by the central limit theorem [LS03]. Also, note that choosing Gaussian distribution usually results in enhanced mathematical tractability of the model and its corresponding derivations. We further assume that the noise is temporally white, hence, the noise realizations at different time instances are independent. As a conclusion, we assume that the set of complex Gaussian vectors $\{\mathbf{v}(t)\}_{t=1}^T$ has the following statistical properties:

$$\mathbb{E}\{\mathbf{v}(t)^H \mathbf{v}(t')\} = \delta_{t,t'} \sigma^2 \mathbf{I}_M, \quad (2.10)$$

$$\mathbb{E}\{\mathbf{v}(t)^T \mathbf{v}(t')\} = \mathbf{0}, \quad \forall t, t', \quad (2.11)$$

where (2.10) reflects spatially and temporally white assumption and (2.11) shows circularity property.

So far, we have characterized the fading channel through a linear impulse response model by the aid of physical parameters such as the delay spread and the Doppler spread. In the case of frequency flat or frequency-selective fading, the channel can be approximated by one tap or multiple taps CIRs, respectively. The statistical models of the wireless channel are such that the amplitudes of these channel taps are random. In this sense, coherence

time, i.e., T_C , is a statistical measure of the time duration over which the CIR is essentially invariant, and quantifies the similarity of the channel response at different times. In other words, coherence time is the time duration over which two received signals have a strong potential for amplitude correlation. Also, coherence bandwidth, i.e., B_C , is actually a statistical measure of the range of frequencies over which two frequency components of the received signal have a strong potential for amplitude correlation [Rap02]. Further, to characterize the random time and frequency varying nature of the received signal, some statistical distributions are commonly used. These statistical characterizations of the fading channels are based on the assumptions that multiple independent scattered paths with random magnitudes are present and the phases of these paths are independent and uniformly distributed [TV05]. The latter hypothesis results from another assumption that the carrier wavelength is much smaller than the distance traveled by the paths. Based on the aforementioned assumptions, the channel can be modeled as, e.g., *Rayleigh* or *Rician* fading. In the former one, we assume that the entries of MIMO channel matrix at each tap are complex zero mean Gaussian random variables. Equivalently, their corresponding magnitudes have a Rayleigh distribution, hence, it is referred to by Rayleigh fading. Rayleigh fading assumption models fading induced by the local scatterers in the absence of a line-of-sight (LOS). The latter one is applicable in the presence of a LOS in which channel matrix entries in (2.6) can be modeled by a Gaussian distribution with a non-zero mean. Also, several other models have been suggested to explain the statistical behavior of a fading channel [Cla68], [Oss64], [SA00], [SOZ11], [Stü01]. These models are of eminent importance for the purpose of evaluating and predicting the performance of a wireless communication system.

2.2.2 MIMO-OFDM system model

It is known [LS03], [WG00] that inverse Fourier transformation at the transmitter together with Fourier transformation of the received data make the frequency-selective channel act as several flat fading channels. This property has been exploited via implementation of the inverse Fourier Transform at the transmitter and the Fast Fourier Transform (FFT) at

the receiver in the OFDM schemes to obtain multiple flat fading subchannels as so-called subcarriers. According to the expression (2.8), the input-output relation for a point-to-point MIMO-OFDM system with the aforementioned number of transmit and receive antennas introduced in Subsection 2.2.1 and N_0 subcarriers can be expressed in the frequency-domain as [LS03]

$$\mathbf{Y}_i(p) = \mathbf{X}_i(p) \mathbf{H}_i + \mathbf{V}_i(p), \quad i = 0, \dots, N_0 - 1 \quad (2.12)$$

where p denotes data block index and i represents subcarrier index. Note that for fixed subcarrier index i , the frequency-domain input-output relationship of (2.12) translates to the input-output relationship of (2.8). Referring to the matrix model presented in (2.8) for flat fading MIMO systems and using definitions in (2.6) and (2.7), we conclude that $\mathbf{Y}_i(p) \in \mathbb{C}^{T \times M}$ and $\mathbf{X}_i(p) \in \mathbb{C}^{T \times N}$ are the p th received data matrix and the p th transmitted code matrix, respectively. The matrix $\mathbf{H}_i \in \mathbb{C}^{N \times M}$ contains the complex-valued MIMO channel coefficients corresponding to the i th flat block-fading subchannel and $\mathbf{V}_i(p) \in \mathbb{C}^{T \times M}$ is the matrix containing the additive receiver noise at the i th subcarrier. The noise matrix at each subcarrier assumed to have the same characteristics as the noise matrix in (2.8). In (2.12), it is also assumed that the inter-block-interference (IBI) is eliminated due to the use of CP and the data received during the CP interval of OFDM scheme are discarded at each receiver antenna. This can be achieved by proper selection of CP length which must exceed the channel length. It is noteworthy to stress that besides using as guard interval, the main interesting feature of the CP is that the linear convolution induced by the propagation channel is transformed into a circular convolution which corresponds exactly to a multiplication in the frequency-domain [LS03]. Further, in (2.12), the channel is assumed to be constant during at least one OSTBC-OFDM block, i.e., the channel coherence time is assumed to be significantly larger than the OSTBC-OFDM data block length. Extending the time-domain input-output relationship in (2.1) for the SISO case to the MIMO channel case, we obtain the following time-domain model corresponding to (2.12) as [LS03]

$$\mathbf{Z}(n) = \sum_{l=0}^L \Omega(n-l) \mathbf{G}_l + \mathbf{E}(n), \quad (2.13)$$

where $(L + 1)$ stands for the number of effective channel taps as in (2.1) and $\mathbf{Z}(n)$, $\mathbf{\Omega}(n)$, \mathbf{G}_l , and $\mathbf{E}(n)$ are the time-domain counterparts of $\mathbf{Y}_i(p)$, $\mathbf{X}_i(p)$, \mathbf{H}_i , and $\mathbf{V}_i(p)$ in (2.12), respectively, i.e.,

$$\mathbf{Y}_i(p) = \frac{1}{\sqrt{N_0}} \sum_{n=0}^{N_0-1} \mathbf{Z}(n) \exp\left(-j \frac{2\pi}{N_0} ni\right), \quad (2.14)$$

$$\mathbf{X}_i(p) = \frac{1}{\sqrt{N_0}} \sum_{n=0}^{N_0-1} \mathbf{\Omega}(n) \exp\left(-j \frac{2\pi}{N_0} ni\right), \quad (2.15)$$

$$\mathbf{H}_i = \sum_{l=0}^L \mathbf{G}_l \exp\left(-j \frac{2\pi}{N_0} li\right), \quad (2.16)$$

with $j \triangleq \sqrt{-1}$. Let us stack, respectively, all channel matrices for different taps and subcarriers on top of each other and define

$$\mathbf{G}' \triangleq [\mathbf{G}_0^T, \dots, \mathbf{G}_L^T, \mathbf{0}_{N \times M}^T, \dots, \mathbf{0}_{N \times M}^T]^T \in \mathbb{C}^{N_0 N \times M}, \quad (2.17)$$

$$\mathbf{H}' \triangleq [\mathbf{H}_0^T, \dots, \mathbf{H}_{N_0-1}^T]^T \in \mathbb{C}^{N_0 N \times M}. \quad (2.18)$$

Note that the finite delay spread assumption over the wireless channel in (2.13) is reflected in the definition (2.17). Using the N_0 -point normalized Discrete Fourier Transform (DFT) matrix $\mathbf{F} \in \mathbb{C}^{N_0 \times N_0}$ with the associated $(i + 1)$ -th row \mathbf{f}_i and the (k, l) -th entry equal to

$$[\mathbf{F}]_{k,l} = \frac{1}{\sqrt{N_0}} \exp\left(-j 2\pi \frac{(k-1)(l-1)}{N_0}\right),$$

along with (2.17) and (2.18), we obtain the following expression

$$\mathbf{H}' = \sqrt{N_0} (\mathbf{F} \otimes \mathbf{I}_N) \mathbf{G}', \quad (2.19)$$

which represents (2.16) and \otimes stands for the Kronecker matrix product. Expression (2.19) provides a compact linear relation between the CFR and the CIR matrices.

2.3 The OSTBCs properties

To explain the transmit encoding procedure in the aforementioned MIMO-OFDM system of (2.12), assume that the transmitted symbol sequence, $s(\cdot)$, has the length of KN_0 in the

p th frame of the data block where K stands for the number of symbols prior to encoding of each STBC. We obtain K parallel data streams, $\{s_{i1}(p)\}_{i=0}^{N_0-1}, \dots, \{s_{iK}(p)\}_{i=0}^{N_0-1}$, each of length N_0 , after the serial-to-parallel conversion at the transmitter side. Using the same block code for the sake of simplicity, these symbol streams are then encoded by mapping them onto a set of $T \times N$ matrices $\{\mathbf{X}_i(p)\}$ as

$$\{s_{i1}(p), \dots, s_{iK}(p)\} \rightarrow \{\mathbf{X}_i(p)\}, \quad i = 0, \dots, N_0 - 1. \quad (2.20)$$

Next, the sequence of code matrices $\{\mathbf{X}_i(p)\}_{i=0}^{N_0-1}$ are inverse Fourier-transformed to obtain N_0 code matrices $\{\mathbf{\Omega}(n)\}_{n=0}^{N_0-1}$, according to

$$\mathbf{\Omega}(n) = \frac{1}{\sqrt{N_0}} \sum_{m=0}^{N_0-1} \mathbf{X}_m(p) \exp\left(j \frac{2\pi}{N_0} nm\right), \quad n = 0, \dots, N_0 - 1$$

which reflects (2.15). Then, transmission can be done through successive bursts after inserting proper CP and performing pulse-shaping [LS03]. Note that the encoding procedure for the frequency flat MIMO system of (2.8) can be also explained in a same way by assuming $N_0 = 1$ in the previous transmit encoding procedure explained for the MIMO-OFDM system.

Consider the obtained K complex information symbols in (2.20) of the p th data block prior to encoding at the i th subcarrier and define the vector $\mathbf{s}_i(p) \triangleq [s_{i1}(p), \dots, s_{iK}(p)]^T$. Essentially, these symbols are transmitted in T consecutive OFDM symbols during which the channel is assumed to be invariant. Further, if we consider that in (2.12), each code matrix $\mathbf{X}_i(p) \triangleq \mathbf{X}(\mathbf{s}_i(p))$ is an OSTBC matrix we have [SGM05], [TJC99]

$$\mathbf{X}_i^H(p) \mathbf{X}_i(p) = \|\mathbf{s}_i(p)\|^2 \mathbf{I}_N. \quad (2.21)$$

It should be noted that OSTBCs are subclass of linear STBCs which satisfy (2.21) by definition. Hence, all entries of $\mathbf{X}(\mathbf{s}_i(p))$ are the linear functions of the K complex variables $\{s_{ik}(p)\}_{k=1}^K$ and their complex conjugates and the ratio K/T defines the rate of an OSTBC. Further, the OSTBC matrix $\mathbf{X}(\mathbf{s}_i(p))$ can be expressed as [GG05], [HH02], [SGM05]

$$\mathbf{X}_i(p) = \sum_{k=1}^K \left(\mathbf{C}_k \operatorname{Re}(s_{ik}(p)) + \mathbf{C}_{k+K} \operatorname{Im}(s_{ik}(p)) \right), \quad (2.22)$$

where \mathbf{C}_k , for $k = 1, \dots, 2K$, are defined as [SGG08]

$$\mathbf{C}_k \triangleq \begin{cases} \mathbf{X}(\mathbf{e}_k), & \text{for } 1 \leq k \leq K \\ \mathbf{X}(j\mathbf{e}_{k-K}), & \text{for } K+1 \leq k \leq 2K \end{cases}, \quad (2.23)$$

with \mathbf{e}_k stands for the $K \times 1$ vector equal to the k th column of the identity matrix \mathbf{I}_K . The $\{\mathbf{C}_k\}_{k=1}^{2K} \in \mathbb{C}^{T \times N}$ are the so-called OSTBC ‘‘basis’’ matrices and are entirely determined by the OSTBC matrix, hence, they are known at the receiver side. Moreover, the OSTBC basis matrices exhibit the following property [LS03], [SGM05]

$$\mathbf{C}_k^H \mathbf{C}_l = \begin{cases} \mathbf{I}_N, & \text{if } k = l \\ -\mathbf{C}_l^H \mathbf{C}_k, & \text{if } k \neq l \end{cases}. \quad (2.24)$$

Next we discuss about an important notion corresponding to the STBCs. We call an STBC *identifiable* or *observable* if, in noise free case of model (2.12), two distinct transmitted codewords

$$\mathbf{X}_i(p) = \mathbf{X}(\mathbf{s}_i(p)) \in \mathbb{C}^{T \times N}, \quad \check{\mathbf{X}}_i(p) = \mathbf{X}(\check{\mathbf{s}}_i(p)) \in \mathbb{C}^{T \times N},$$

result in two distinct received codewords as long as the channel matrix \mathbf{H}_i has at least one nonzero entry [LS03]. This implies that an STBC is identifiable if it is observable for all receive antennas, i.e., $\mathbf{X}_i(p)[\mathbf{H}_i]_m \neq \check{\mathbf{X}}_i(p)[\mathbf{H}_i]_m$ for $m = 1, \dots, M$ where $[\mathbf{H}_i]_m$ stands for the m th column of the matrix \mathbf{H}_i associated to the m th receiver. It is worth mentioning that an STBC is identifiable when it provides maximal diversity which means that its codeword differences should have maximum rank [LS03], i.e.,

$$\mathbf{X}_i(p)[\mathbf{H}_i]_m \neq \check{\mathbf{X}}_i(p)[\mathbf{H}_i]_m \quad \forall [\mathbf{H}_i]_m \neq \mathbf{0} \quad \Leftrightarrow \quad \det\left(\left(\mathbf{X}_i(p) - \check{\mathbf{X}}_i(p)\right)^H \left(\mathbf{X}_i(p) - \check{\mathbf{X}}_i(p)\right)\right) \neq 0. \quad (2.25)$$

To see this, note first that if $\left(\left(\mathbf{X}_i(p) - \check{\mathbf{X}}_i(p)\right)^H \left(\mathbf{X}_i(p) - \check{\mathbf{X}}_i(p)\right)\right)$ is nonsingular, then $\left(\mathbf{X}_i(p) - \check{\mathbf{X}}_i(p)\right)$ is full rank and $\mathbf{X}_i(p)[\mathbf{H}_i]_m \neq \check{\mathbf{X}}_i(p)[\mathbf{H}_i]_m$ for all $[\mathbf{H}_i]_m \neq \mathbf{0}$ and hence the code is identifiable. Conversely, if $\left(\left(\mathbf{X}_i(p) - \check{\mathbf{X}}_i(p)\right)^H \left(\mathbf{X}_i(p) - \check{\mathbf{X}}_i(p)\right)\right)$ is singular then for any vector $[\mathbf{H}_i]_m \neq \mathbf{0}$ in the null space of this matrix we have $\mathbf{X}_i(p)[\mathbf{H}_i]_m = \check{\mathbf{X}}_i(p)[\mathbf{H}_i]_m$ and the code is not identifiable. Due to the fact that all OSTBCs offer a maximum diversity

order of MN , we conclude that OSTBCs are identifiable. Blind identifiability issue will be discussed later in Section 2.4.

Expression (2.22) explicitly shows that OSTBCs are linear in the real and imaginary parts of the information symbols. In order to exploit this linearity property, we transform the complex-valued signal model to an equivalent real-valued one. This transformation enables us to analyze the effect of the real and imaginary parts of the symbol on the channel estimation, independently. This issue is clarified more when we present different weighting strategies in Section 3.3. Let us introduce the following operators for any complex-valued matrix \mathbf{B} [SSG09]

$$\bar{\mathbf{B}} \triangleq \text{Re}(\mathbf{B}) \otimes \begin{bmatrix} 1 & 0 \\ 0 & 1 \end{bmatrix} + \text{Im}(\mathbf{B}) \otimes \begin{bmatrix} 0 & -1 \\ 1 & 0 \end{bmatrix}, \quad (2.26)$$

$$\underline{\mathbf{B}} \triangleq \left[\text{vec}\{\text{Re}(\mathbf{B})\}^T, \text{vec}\{\text{Im}(\mathbf{B})\}^T \right]^T, \quad (2.27)$$

where $\text{Re}(\cdot)$, $\text{Im}(\cdot)$, and $\text{vec}\{\cdot\}$ represent the real part, the imaginary part, and the column-wise vectorization operator, respectively. Taking into account (2.27), we define the equivalent CIR vector for each channel tap and the equivalent CFR vector for each subcarrier as [SSG09]

$$\mathbf{g}_l \triangleq \underline{\mathbf{G}}_l \in \mathbb{R}^{2MN \times 1}, \quad l = 0, \dots, L \quad (2.28)$$

$$\mathbf{h}_i \triangleq \underline{\mathbf{H}}_i \in \mathbb{R}^{2MN \times 1}, \quad i = 0, \dots, N_0 - 1. \quad (2.29)$$

Taking into account (2.26)-(2.29), we can rewrite (2.19) to establish the following compact linear relationships among the channel parameters in the frequency and the time domains [SSG09]

$$\mathbf{h}_i = \sqrt{N_0} (\bar{\mathbf{f}}_i \otimes \mathbf{I}_{MN}) \mathbf{g}' = \mathcal{F}_i \mathbf{g}', \quad (2.30)$$

$$\mathbf{h}' = \sqrt{N_0} (\bar{\mathbf{F}} \otimes \mathbf{I}_{MN}) \mathbf{g}' = \mathcal{F} \mathbf{g}', \quad (2.31)$$

where

$$\mathbf{g}' \triangleq [\mathbf{g}_0^T, \dots, \mathbf{g}_L^T, \mathbf{0}_{2MN \times 1}^T, \dots, \mathbf{0}_{2MN \times 1}^T]^T \in \mathbb{R}^{2MNN_0 \times 1}, \quad (2.32)$$

$$\mathbf{h}' \triangleq [\mathbf{h}_0^T, \dots, \mathbf{h}_{N_0-1}^T]^T \in \mathbb{R}^{2MNN_0 \times 1}, \quad (2.33)$$

$$\mathcal{F}_i \triangleq \sqrt{N_0} (\bar{\mathbf{f}}_i \otimes \mathbf{I}_{MN}) \in \mathbb{R}^{2MN \times 2MNN_0}, \quad (2.34)$$

$$\mathcal{F} \triangleq \sqrt{N_0} (\bar{\mathbf{F}} \otimes \mathbf{I}_{MN}) \in \mathbb{R}^{2MNN_0 \times 2MNN_0}. \quad (2.35)$$

Using (2.22) and (2.27), we rewrite the model (2.12) in the following vectorized form [SGM05]

$$\mathbf{y}_i(p) = \mathbf{A}(\mathbf{h}_i) \underline{\mathbf{s}}_i(p) + \mathbf{v}_i(p), \quad i = 0, \dots, N_0 - 1 \quad (2.36)$$

where i denotes the subcarrier index, $\mathbf{y}_i(p) \triangleq \underline{\mathbf{Y}}_i(p)$, $\mathbf{v}_i(p) \triangleq \underline{\mathbf{V}}_i(p)$, and the $2MT \times 2K$ real matrix $\mathbf{A}(\mathbf{h}_i)$ is defined as [SGM05]

$$\mathbf{A}(\mathbf{h}_i) \triangleq [\mathbf{a}_1(\mathbf{h}_i), \dots, \mathbf{a}_{2K}(\mathbf{h}_i)] = [\underline{\mathbf{C}}_1 \mathbf{H}_i, \dots, \underline{\mathbf{C}}_{2K} \mathbf{H}_i]. \quad (2.37)$$

It should be emphasized that the matrix $\mathbf{A}(\mathbf{h}_i)$ in the model (2.36) captures both the effects of the wireless channel and the exploited OSTBC. It can be proved, see Appendix A, that the columns of $\mathbf{A}(\mathbf{h}_i)$ in (2.37) are orthogonal to each other and have the same norm regardless of the values of channel entries [GG05], [SGM05], i.e.,

$$\mathbf{A}(\mathbf{h}_i)^T \mathbf{A}(\mathbf{h}_i) = \|\mathbf{h}_i\|^2 \mathbf{I}_{2K}. \quad (2.38)$$

The relation (2.38) is the so-called ‘‘orthogonality’’ property of the matrix $\mathbf{A}(\mathbf{h}_i)$ which is extensively exploited to develop our blind MIMO channel estimators in the following chapters. Consider the following Kronecker matrix product property [Bre78]

$$\text{vec}\{\mathbf{MNP}\} = (\mathbf{P}^T \otimes \mathbf{M}) \text{vec}\{\mathbf{N}\}, \quad (2.39)$$

for any arbitrary conformable matrices \mathbf{M}, \mathbf{N} and \mathbf{P} and the definition (2.27), we obtain

$$\mathbf{Q} \triangleq \mathbf{MNP} \Rightarrow \underline{\mathbf{Q}} = \begin{bmatrix} \text{Re}(\mathbf{P}^T \otimes \mathbf{M}) & -\text{Im}(\mathbf{P}^T \otimes \mathbf{M}) \\ \text{Im}(\mathbf{P}^T \otimes \mathbf{M}) & \text{Re}(\mathbf{P}^T \otimes \mathbf{M}) \end{bmatrix} \underline{\mathbf{N}}. \quad (2.40)$$

Using (2.29) along with (2.37) and (2.40), we acquire [SGS10]

$$\mathbf{a}_k(\mathbf{h}_i) = \mathbf{\Phi}_k \mathbf{h}_i, \quad k = 1, \dots, 2K \quad (2.41)$$

with

$$\mathbf{\Phi}_k \triangleq \begin{bmatrix} \operatorname{Re}(\mathbf{I}_M \otimes \mathbf{C}_k) & -\operatorname{Im}(\mathbf{I}_M \otimes \mathbf{C}_k) \\ \operatorname{Im}(\mathbf{I}_M \otimes \mathbf{C}_k) & \operatorname{Re}(\mathbf{I}_M \otimes \mathbf{C}_k) \end{bmatrix}. \quad (2.42)$$

Taking into account (2.37) together with (2.41) shows that $\mathbf{A}(\mathbf{h}_i)$ is linear with respect to \mathbf{h}_i . Also, (2.42) shows that the real matrices $\mathbf{\Phi}_k \in \mathbb{R}^{2MT \times 2MN}$, $k = 1, \dots, 2K$, only depend on the code basis matrices $\{\mathbf{C}_k\}_{k=1}^{2K}$, therefore, they are OSTBC-specific and known to the receiver. Making use of (2.37) and (2.41), we obtain [SGM05]

$$\operatorname{vec}\{\mathbf{A}(\mathbf{h}_i)\} = \mathbf{\Phi} \mathbf{h}_i, \quad i = 0, \dots, N_0 - 1 \quad (2.43)$$

with the unique $4KMT \times 2MN$ matrix $\mathbf{\Phi}$ defined as

$$\mathbf{\Phi} \triangleq [\mathbf{\Phi}_1^T, \mathbf{\Phi}_2^T, \dots, \mathbf{\Phi}_{2K}^T]^T. \quad (2.44)$$

Moreover, the OSTBC-specific matrices $\{\mathbf{\Phi}_k\}_{k=1}^{2K}$, defined in (2.42), satisfy [BSK06]

$$\mathbf{\Phi}_k^T \mathbf{\Phi}_l = \begin{cases} \mathbf{I}_{2MN}, & \text{if } k = l \\ -\mathbf{\Phi}_l^T \mathbf{\Phi}_k, & \text{if } k \neq l \end{cases}. \quad (2.45)$$

See Appendix B for the proof of (2.45).

2.3.1 Rotatable OSTBCs

The OSTBC matrix $\mathbf{X}_i(p) = \mathbf{X}(\mathbf{s}_i(p))$ in (2.21) is called *rotatable*, if there exists a matrix $\mathbf{Q} \in \mathbb{C}^{N \times N}$ such that [Ma07]

$$\mathbf{X}(\mathbf{s}_i(p)) \mathbf{Q} = \mathbf{X}(\check{\mathbf{s}}_i(p)), \quad (2.46)$$

for any $\mathbf{s}_i(p) \in \mathbf{s}_i \triangleq \{\mathbf{s}_i^{(l)}(p)\}_{l=1}^I$ and some $\check{\mathbf{s}}_i(p) \in \mathbf{s}_i$ with $\check{\mathbf{s}}_i(p) \neq \pm \mathbf{s}_i(p)$ where I stands for the number of all possible symbol vectors within constellation set at each subcarrier.

Otherwise, the code matrix $\mathbf{X}(\mathbf{s}_i(p))$ is non-rotatable. Taking into account (2.21) and (2.46), it can be easily verified that the code rotation matrix \mathbf{Q} , if it exists, is unitary, i.e.,

$$\mathbf{Q}^H \mathbf{Q} = \mathbf{Q} \mathbf{Q}^H = \mathbf{I}_N. \quad (2.47)$$

A necessary and sufficient condition for the OSTBC to be rotatable is that the code rotation matrix \mathbf{Q} in (2.46) satisfies [Ma07]

$$\mathbf{C}_k \mathbf{Q} = d_k \mathbf{C}_{n_k}, \quad k = 1, \dots, 2K \quad (2.48)$$

with $d_k \in \{\pm 1\}$, and $n_k \in \{1, \dots, 2K\}$ is an index with $n_k \neq k$ and $n_k \neq n_l$ for $k \neq l$. \square

As a result, for a particular choice of \mathbf{Q} in (2.48), there exists a specific one-to-one mapping such that

$$[n_1, n_2, \dots, n_{2K}]^T = \mathbf{P}_1 [1, 2, \dots, 2K]^T, \quad (2.49)$$

where $\mathbf{P}_1 \in \{0, 1\}^{2K \times 2K}$ stands for the associated permutation matrix. Taking into account (2.24) and (2.48) we have

$$\mathbf{C}_k \mathbf{Q} = d_k \mathbf{C}_{n_k} \Rightarrow \mathbf{C}_k^H \mathbf{C}_k \mathbf{Q} = d_k \mathbf{C}_k^H \mathbf{C}_{n_k} \Rightarrow \mathbf{Q} = d_k \mathbf{C}_k^H \mathbf{C}_{n_k}, \quad (2.50)$$

hence,

$$\mathbf{Q}^H = d_k \mathbf{C}_{n_k}^H \mathbf{C}_k = -d_k \mathbf{C}_k^H \mathbf{C}_{n_k} = -\mathbf{Q}. \quad (2.51)$$

So, the code rotation matrix \mathbf{Q} , if it exists, is skew-hermitian. Consider both the skew-hermitian and the unitary properties of the code rotation matrix along with the relation (2.48), we have

$$\mathbf{C}_k \mathbf{Q} = d_k \mathbf{C}_{n_k} \Rightarrow \mathbf{C}_{n_k} \mathbf{Q} = -d_k \mathbf{C}_k, \quad (2.52)$$

which shows that by applying code rotation matrix \mathbf{Q} , not only \mathbf{C}_k transforms to \mathbf{C}_{n_k} , but also the reverse transformation is valid, i.e., \mathbf{C}_{n_k} transforms to \mathbf{C}_k . Therefore, relation (2.52) implies that the permutation matrix \mathbf{P}_1 in (2.49) is symmetric. Let us introduce

$$\check{\mathbf{Q}} \triangleq \begin{bmatrix} \text{Re}(\mathbf{I}_M \otimes \mathbf{Q}) & -\text{Im}(\mathbf{I}_M \otimes \mathbf{Q}) \\ \text{Im}(\mathbf{I}_M \otimes \mathbf{Q}) & \text{Re}(\mathbf{I}_M \otimes \mathbf{Q}) \end{bmatrix}, \quad (2.53)$$

where

$$\check{\mathbf{Q}}^T \check{\mathbf{Q}} = \check{\mathbf{Q}} \check{\mathbf{Q}}^T = \mathbf{I}_{2MN} \quad (2.54)$$

follows from the unitary property of \mathbf{Q} in (2.47). Taking into account (2.42), (2.48) and (2.53), we obtain

$$\begin{aligned} \Phi_k \check{\mathbf{Q}} &= \begin{bmatrix} \text{Re}(\mathbf{I}_M \otimes \mathbf{C}_k) & -\text{Im}(\mathbf{I}_M \otimes \mathbf{C}_k) \\ \text{Im}(\mathbf{I}_M \otimes \mathbf{C}_k) & \text{Re}(\mathbf{I}_M \otimes \mathbf{C}_k) \end{bmatrix} \begin{bmatrix} \text{Re}(\mathbf{I}_M \otimes \mathbf{Q}) & -\text{Im}(\mathbf{I}_M \otimes \mathbf{Q}) \\ \text{Im}(\mathbf{I}_M \otimes \mathbf{Q}) & \text{Re}(\mathbf{I}_M \otimes \mathbf{Q}) \end{bmatrix} \\ &= \begin{bmatrix} \text{Re}(\mathbf{I}_M \otimes \mathbf{C}_k \mathbf{Q}) & -\text{Im}(\mathbf{I}_M \otimes \mathbf{C}_k \mathbf{Q}) \\ \text{Im}(\mathbf{I}_M \otimes \mathbf{C}_k \mathbf{Q}) & \text{Re}(\mathbf{I}_M \otimes \mathbf{C}_k \mathbf{Q}) \end{bmatrix} = d_k \Phi_{n_k}, \quad k = 1, \dots, 2K \end{aligned} \quad (2.55)$$

where $d_k \in \{\pm 1\}$, and $n_k \in \{1, \dots, 2K\}$ is an index with $n_k \neq k$ and $n_k \neq n_l$ for $k \neq l$. The expression (2.55) shows that the rotation of the code basis matrices $\{\mathbf{C}_k\}_{k=1}^{2K}$ by the matrix \mathbf{Q} in (2.48) can be viewed as the permutation of indices among OSTBC-specific matrices $\{\Phi_k\}_{k=1}^{2K}$ combined with a possible sign change according to the value of d_k . Considering (2.37) and (2.41), this in turn results in changing the order of the columns of $\mathbf{A}(\mathbf{h}_i)$. This interpretation provides an insight towards a practically important ambiguity characteristic of the blind ML estimator in the case of rotatable OSTBCs presented in the next section.

If the code rotation matrix \mathbf{Q} exists, the properties (2.45) and (2.55) imply that

$$\Phi_k \check{\mathbf{Q}} = d_k \Phi_{n_k} \Rightarrow \Phi_k^T \Phi_k \check{\mathbf{Q}} = d_k \Phi_k^T \Phi_{n_k} \Rightarrow \check{\mathbf{Q}} = d_k \Phi_k^T \Phi_{n_k}, \quad (2.56)$$

for $k = 1, \dots, 2K$, $n_k \neq k$, $n_k \neq n_l$ for $k \neq l$. Hence, $\check{\mathbf{Q}}$ belongs to each of the following sets

$$\begin{aligned} \check{\mathbf{Q}} &\in \mathcal{C}_1 \triangleq \left\{ \pm \Phi_1^T \Phi_2, \pm \Phi_1^T \Phi_3, \dots, \pm \Phi_1^T \Phi_{2K} \right\}, \\ \check{\mathbf{Q}} &\in \mathcal{C}_2 \triangleq \left\{ \pm \Phi_2^T \Phi_1, \pm \Phi_2^T \Phi_3, \dots, \pm \Phi_2^T \Phi_{2K} \right\}, \\ &\vdots \\ \check{\mathbf{Q}} &\in \mathcal{C}_{2K} \triangleq \left\{ \pm \Phi_{2K}^T \Phi_1, \pm \Phi_{2K}^T \Phi_2, \dots, \pm \Phi_{2K}^T \Phi_{2K-1} \right\}. \end{aligned} \quad (2.57)$$

Also, from (2.45) and (2.56) we conclude that

$$\check{\mathbf{Q}}^T = -\check{\mathbf{Q}}, \quad (2.58)$$

which reflects skew-symmetric property of $\check{\mathbf{Q}}$.

2.4 Blind ML estimation or detection

Prior to devising blind MIMO channel estimators, it is noteworthy to investigate in more detail different probable types of ambiguities associated with channel estimates that may result from assumptions based on which we devise an estimator or from parameterization model under consideration. The former case is discussed in the present section and the latter case is analyzed in the next section. In the blind estimation or detection problem where neither the CSI at each subcarrier nor any pilot symbol is available at the receiver, the entries of channel matrix and the transmitted symbols should be estimated jointly. We consider the parametric model of (2.36) and assume a quasi-static MIMO channel which remains invariant during the transmission of P consecutive OSTBC-OFDM data blocks. Further, in ML approach we assume that the entries of CFR vector and the transmitted symbols at the i th subcarrier are unknown deterministic parameters. Then, the joint blind ML estimates of the CFR vector \mathbf{h}_i and the symbol vectors $\underline{\mathbf{s}}_i(p)$, for $p = 1, \dots, P$, are obtained as their values for which the log-likelihood function is maximized, i.e., [LSL02], [LSL03], [SGM05], [TVP96]

$$\left\{ \hat{\mathbf{h}}_{i,\text{ML}}, \hat{\underline{\mathbf{S}}}_{i,\text{ML}} \right\} = \arg \max_{\underline{\mathbf{S}}_i \in \mathcal{S}_i, \mathbf{h}_i} \log f(\mathbf{y}_i(1), \dots, \mathbf{y}_i(P) | \mathbf{h}_i, \underline{\mathbf{S}}_i), \quad (2.59)$$

where $\underline{\mathbf{S}}_i \triangleq [\underline{\mathbf{s}}_i(1), \underline{\mathbf{s}}_i(2), \dots, \underline{\mathbf{s}}_i(P)] \in \mathcal{S}_i$ stacks all the available information symbol vectors corresponding to the i th subcarrier and $\mathcal{S}_i \triangleq \{\underline{\mathbf{S}}_i^{(l)}\}_{l=1}^{IP}$ is the set of all possible values of $\underline{\mathbf{S}}_i$. It should be reminded that I stands for the number of all possible symbol vectors $\underline{\mathbf{s}}_i(p)$ within constellation set at each subcarrier. Since it is very difficult to solve (2.59) as its computational complexity grows exponentially in P , we simplify (2.59) by relaxing the finite alphabet constraint of $\underline{\mathbf{S}}_i \in \mathcal{S}_i$ and by replacing it with $\tilde{\underline{\mathbf{S}}}_i \in \mathbb{R}^{2K \times P}$. Therefore, we rewrite (2.59) as [SGM05]

$$\left\{ \hat{\mathbf{h}}_{i,\text{RML}}, \hat{\tilde{\underline{\mathbf{S}}}}_{i,\text{RML}} \right\} = \arg \max_{\tilde{\underline{\mathbf{S}}}_i, \mathbf{h}_i} \log f(\mathbf{y}_i(1), \dots, \mathbf{y}_i(P) | \mathbf{h}_i, \tilde{\underline{\mathbf{S}}}_i), \quad (2.60)$$

where RML stands for the relaxed ML. Assume that the characteristics of the noise vectors in the model (2.36), for $p = 1, \dots, P$, are according to (2.9)-(2.11). Then, the conditional

probability density function (pdf) of each $\mathbf{y}_i(p)$ can be written as [SGM05]

$$f(\mathbf{y}_i(p) | \mathbf{h}_i, \underline{\mathbf{s}}_i(p)) = \frac{1}{(\pi\sigma^2)^{MT}} \exp\left(-\frac{\|\mathbf{y}_i(p) - \mathbf{A}(\mathbf{h}_i)\underline{\mathbf{s}}_i(p)\|^2}{\sigma^2}\right), \quad p = 1, \dots, P. \quad (2.61)$$

As it is assumed that all received data vectors at the i th subcarrier $\mathbf{y}_i(p)$, for $p = 1, \dots, P$, are independent random vectors, we obtain [SGM05]

$$f(\mathbf{y}_i(1), \dots, \mathbf{y}_i(P) | \mathbf{h}_i, \underline{\mathbf{S}}_i) = \prod_{p=1}^P f(\mathbf{y}_i(p) | \mathbf{h}_i, \underline{\mathbf{s}}_i(p)). \quad (2.62)$$

Taking into account (2.61) together with (2.62), we reformulate (2.60) as [SGM05]

$$\{\hat{\mathbf{h}}_{i,\text{RML}}, \hat{\underline{\mathbf{S}}}_{i,\text{RML}}\} = \arg \min_{\underline{\hat{\mathbf{s}}}_i, \hat{\mathbf{h}}_i} \sum_{p=1}^P \|\mathbf{y}_i(p) - \mathbf{A}(\hat{\mathbf{h}}_i)\underline{\hat{\mathbf{s}}}_i(p)\|^2, \quad (2.63)$$

which represents the joint RML estimator for the CFR vector and the transmitted symbol vectors at the i th subcarrier. From the linearity property of $\mathbf{A}(\mathbf{h}_i)$ in (2.43), it can be concluded that if the pair $\{\hat{\mathbf{h}}_{i,\text{RML}}, \hat{\underline{\mathbf{S}}}_{i,\text{RML}}\}$ is the solution of (2.63), the pair $\{-\alpha \hat{\mathbf{h}}_{i,\text{RML}}, -1/\alpha \hat{\underline{\mathbf{S}}}_{i,\text{RML}}\}$ with arbitrary scalar α is also the solution of (2.63). Hence, the blind RML estimator (2.63) suffers from scalar ambiguity (including sign ambiguity) [CMC08], [SGM05], which is in fact resulted from relaxation of the finite alphabet constraint over the transmitted symbols in (2.60). The aforementioned ambiguity translates to *norm ambiguity* in CFR vector estimation and reflects the effect of assumption under which we develop an estimator. This norm ambiguity can be resolved using a few pilot symbols or by the aid of other methods mentioned in [CMC08], [SGM05], [TVP96]. The implementation simplicity of estimator (2.63) [LSL03], [MVDC06], [SG03], [SGM05] motivates us to study further corresponding blind identifiability aspects. Next, we discuss another kind of ambiguity associated with the estimator (2.63) that is inherited from parameterization model (2.36) when special type of codes are used.

2.4.1 Blind identifiability

For the sake of notational simplicity, suppose that the true channel vector \mathbf{h}_i and the data matrix $\underline{\mathbf{S}}_i$ are the solution of (2.63). The solution pair $\{\mathbf{h}_i, \underline{\mathbf{S}}_i\}$ is unique up to some scalar

only when another solution pair $\{\check{\mathbf{h}}_i, \check{\mathbf{S}}_i\}$ for (2.63) can not be obtained such that

$$\mathbf{A}(\mathbf{h}_i)\underline{\mathbf{s}}_i(p) = \mathbf{A}(\check{\mathbf{h}}_i)\check{\underline{\mathbf{s}}}_i(p), \quad p = 1, \dots, P \quad (2.64)$$

for some $\check{\mathbf{h}}_i \neq \pm\alpha \mathbf{h}_i$ and $\check{\underline{\mathbf{s}}}_i(p) \neq \pm 1/\alpha \underline{\mathbf{s}}_i(p)$ with arbitrary scalar α . Equivalently, the parameter set $\{\mathbf{h}_i, \underline{\mathbf{S}}_i\}$ for the model (2.36) is unique up to scalar when two parameter sets for (2.36) can not be found which satisfy

$$\mathbf{A}(\mathbf{h}_i)\underline{\mathbf{s}}_i(p) + \mathbf{v}_i(p) = \mathbf{A}(\check{\mathbf{h}}_i)\check{\underline{\mathbf{s}}}_i(p) + \mathbf{v}_i(p), \quad p = 1, \dots, P \quad (2.65)$$

for some $\check{\mathbf{h}}_i \neq \pm\alpha \mathbf{h}_i$ and $\check{\underline{\mathbf{s}}}_i(p) \neq \pm 1/\alpha \underline{\mathbf{s}}_i(p)$. In the case of rotatable OSTBCs, we prove that channel-code ambiguity equation (2.64) is satisfied for each code rotation matrix \mathbf{Q} , any $\mathbf{s}_i(p) \in \mathbf{s}_i$, and some $\check{\mathbf{s}}_i(p) \neq (\pm 1/\alpha \mathbf{s}_i(p)) \in \mathbf{s}_i$. In this case, it can be concluded that the rotatable OSTBCs are inherently susceptible to the non-scalar ambiguities in the blind estimation scenario. In fact, such ambiguities are resulted from the non-uniqueness of parameter set of model (2.36) and imply that equation (2.65) holds true. To prove (2.64) for the rotatable codes, the following equivalent statement to (2.48) [Ma07] needs to be proved first:

The code rotation matrix \mathbf{Q} satisfies

$$\mathbf{X}(\mathbf{s}_i(p)) \mathbf{Q} = \mathbf{X}(\mathbf{P}\mathbf{W}\mathbf{s}_i(p)), \quad (2.66)$$

where $\mathbf{P} \in \{0, 1\}^{K \times K}$ is a permutation matrix with $\text{diag}(\mathbf{P}) = \mathbf{0}$, and \mathbf{W} is a diagonal matrix with $\text{diag}(\mathbf{W}) \in \{\pm 1\}^K$. \square

To prove the equivalence of (2.48) and (2.66), first we assume that (2.48) holds true and conclude (2.66) and, then, we prove that assuming (2.66) results in (2.48). To show the first part, we have

$$\mathbf{X}(\mathbf{s}_i(p)) \mathbf{Q} = \sum_{k=1}^{2K} \mathbf{C}_k \mathbf{Q} s_{ik}(p) = \sum_{k=1}^{2K} d_k \mathbf{C}_{n_k} s_{ik}(p) = \mathbf{X}(\mathbf{P}\mathbf{W}\mathbf{s}_i(p)), \quad (2.67)$$

where the first equality comes from (2.22) and the second equality results from (2.48). To clarify the last equality in (2.67), note that $\sum_{k=1}^{2K} d_k \mathbf{C}_{n_k} s_{ik}(p)$ can be obtained from $\sum_{k=1}^{2K} \mathbf{C}_k s_{ik}(p) = \mathbf{X}(\mathbf{s}_i(p))$ by reordering the entries $s_{ik}(p)$ of $\mathbf{s}_i(p)$ and weighting them with

± 1 . The weighting with ± 1 is represented by the diagonal matrix \mathbf{W} and the reordering is expressed by the permutation matrix \mathbf{P} in (2.66). Since the statement (2.48) enforces $n_k \neq k$, for $k = 1, \dots, 2K$, it follows that the diagonal entries of \mathbf{P} have to be zero. To present the second part of the proof, notice that

$$\sum_{k=1}^{2K} \mathbf{C}_k \mathbf{Q} s_{ik}(p) = \mathbf{X}(\mathbf{s}_i(p)) \mathbf{Q} = \mathbf{X}(\mathbf{P} \mathbf{W} \mathbf{s}_i(p)) = \sum_{k=1}^{2K} d_k \mathbf{C}_{n_k} s_{ik}(p), \quad (2.68)$$

where again the first and the second equalities result from (2.22) and (2.66), respectively. Thus, we have $\sum_{k=1}^{2K} \mathbf{C}_k \mathbf{Q} s_{ik}(p) = \sum_{k=1}^{2K} d_k \mathbf{C}_{n_k} s_{ik}(p)$ for $n_k \neq k$, $k = 1, \dots, 2K$ as (2.66) enforces the diagonal entries of \mathbf{P} to be zero. Since this has to be valid for all the possible values of $\mathbf{s}_i(p)$, we obtain $\mathbf{C}_k \mathbf{Q} = d_k \mathbf{C}_{n_k}$, for $k = 1, \dots, 2K$, and, therefore, we conclude (2.48). Taking into account both (2.67) and (2.68), the equivalence of (2.48) and (2.66) can be deduced.

Consider the definitions of \mathbf{P} and \mathbf{W} in (2.66), we obtain

$$\mathbf{A}(\mathbf{h}_i) \underline{\mathbf{s}}_i(p) = \mathbf{A}(\mathbf{h}_i) (\mathbf{W}^T \mathbf{P}^T \otimes \mathbf{I}_2) (\mathbf{P} \mathbf{W} \otimes \mathbf{I}_2) \underline{\mathbf{s}}_i(p) = \check{\mathbf{A}}(\mathbf{h}_i) \check{\underline{\mathbf{s}}}_i(p), \quad (2.69)$$

where $\check{\underline{\mathbf{s}}}_i(p) = (\mathbf{P} \mathbf{W} \otimes \mathbf{I}_2) \underline{\mathbf{s}}_i(p)$ is deduced from the comparison of (2.46) with (2.66) and $\check{\mathbf{A}}(\mathbf{h}_i) \triangleq \mathbf{A}(\mathbf{h}_i) (\mathbf{W}^T \mathbf{P}^T \otimes \mathbf{I}_2)$. Actually, the matrix $\check{\mathbf{A}}(\mathbf{h}_i)$ can be formed by changing the order (and probably the sign) of columns of the matrix $\mathbf{A}(\mathbf{h}_i)$. Taking into account (2.53), we define

$$\check{\mathbf{h}} \triangleq \begin{bmatrix} \text{Re}(\mathbf{I}_M \otimes \mathbf{Q}^H) & -\text{Im}(\mathbf{I}_M \otimes \mathbf{Q}^H) \\ \text{Im}(\mathbf{I}_M \otimes \mathbf{Q}^H) & \text{Re}(\mathbf{I}_M \otimes \mathbf{Q}^H) \end{bmatrix} \mathbf{h} = \check{\mathbf{Q}}^T \mathbf{h}. \quad (2.70)$$

Using the definition of $\check{\mathbf{A}}(\mathbf{h}_i)$ together with (2.54), (2.55), (2.70), and the equivalence of (2.48) and (2.66), we have

$$\begin{aligned} \check{\mathbf{A}}(\mathbf{h}_i) &= [\check{\Phi}_{n_1} \mathbf{h}_i, \check{\Phi}_{n_2} \mathbf{h}_i, \dots, \check{\Phi}_{n_{2K}} \mathbf{h}_i] \\ &= [\check{\Phi}_{n_1} \check{\mathbf{Q}} \check{\mathbf{Q}}^T \mathbf{h}_i, \check{\Phi}_{n_2} \check{\mathbf{Q}} \check{\mathbf{Q}}^T \mathbf{h}_i, \dots, \check{\Phi}_{n_{2K}} \check{\mathbf{Q}} \check{\mathbf{Q}}^T \mathbf{h}_i] \\ &= [\check{\Phi}_1 \check{\mathbf{h}}_i, \check{\Phi}_2 \check{\mathbf{h}}_i, \dots, \check{\Phi}_{2K} \check{\mathbf{h}}_i] = \mathbf{A}(\check{\mathbf{h}}_i). \end{aligned} \quad (2.71)$$

Finally, by comparison of (2.69) and (2.71) we conclude channel-code ambiguity equation (2.64) which implies that a certain transformation of the symbol vector $\underline{\mathbf{s}}_i(p)$ and the equivalent CFR vector \mathbf{h}_i is blindly unresolvable. In other words, even if an arbitrary number of

noise-free observations corresponding to the model (2.36) are available at the receiver, blind joint estimation of the channel and the symbol vectors suffers from non-scalar ambiguity for the case of rotatable OSTBCs. To resolve such cases either few pilot symbols, if available, can be exploited or some prior knowledge or characteristics regarding transmitted symbols can be utilized. This issue is discussed in more detail in Section 3 from another viewpoint where we propose how to utilize prior knowledge about the transmitted symbols and devise a strategy to resolve such non-scalar ambiguities.

2.5 Optimal receiver

In this section we introduce the optimal receiver structure for the case when the channel matrix of each subcarrier is available at the receiver. The CSI may be obtained, e.g., from blind estimation methods introduced in the following chapters. In this case, the optimal, from ML sense, symbol decoder is a simple nearest neighbor detector. This decoder uses the obtained CSI to find the closest point to all the vectors belonging to the set $\mathcal{Y}_i \triangleq \{\mathbf{y}_i^{(l)}(p)\}_{l=1}^I$ [TJC99]. Hence, as derived in (2.59)-(2.63) under Gaussian noise assumption, it computes

$$l_{\text{opt}} = \arg \min_{l \in \{1, \dots, I\}} \|\mathbf{y}_i(p) - \mathbf{y}_i^{(l)}(p)\|, \quad (2.72)$$

where $\mathbf{y}_i^{(l)}(p)$ is the vectorized version of the noise-free received data matrix corresponding to the symbol vector $\mathbf{s}_i^{(l)}(p)$, and I stands for the number of all possible symbol vectors at each subcarrier. The so-obtained l_{opt} is then used to decode the data symbols.

In the OSTBC case, the ML decoder in (2.72) can also be viewed as the MF [LSL02] receiver whose output SNR is maximized [GS01]. Using such a receiver and the linear model (2.36) along with the orthogonality property (2.38), the ML estimate, which is also the least square estimate, of $\underline{\mathbf{s}}_i$ can be computed as [GG05], [SGM05]

$$\hat{\underline{\mathbf{s}}}_i(p) = \left(\mathbf{A}(\mathbf{h}_i)^T \mathbf{A}(\mathbf{h}_i) \right)^{-1} \mathbf{A}(\mathbf{h}_i)^T \mathbf{y}_i(p) = \frac{1}{\|\mathbf{h}_i\|^2} \mathbf{A}(\mathbf{h}_i)^T \mathbf{y}_i(p). \quad (2.73)$$

Then, the final estimate of $\mathbf{s}_i(p)$ is obtained from $\hat{\mathbf{s}}_i(p) = [\mathbf{I}_K, j\mathbf{I}_K] \hat{\underline{\mathbf{s}}}_i(p)$ followed by the symbol-by-symbol nearest neighbor detector. For all numerical results presented in this thesis, the optimal receiver (2.73) is implemented to decode the transmitted symbols.

Chapter 3

Blind channel estimation in orthogonally coded MIMO-OFDM systems: Single-carrier analysis

3.1 Introduction

In this chapter, first a novel virtual snapshot model for single-carrier of orthogonally coded MIMO-OFDM systems is introduced. The virtual snapshot model exploits redundancies contained in the OSTBC to augment the received data. This model is then used to develop a blind channel estimation method that is implemented in a subcarrier-wise manner. Based on the properties of the OSTBCs, we show that a low-rank subspace model applies to the weighted covariance matrix of the available virtual snapshots. Also, we prove that the vector of true CFR parameters is the principal eigenvector of the obtained covariance matrix at each subcarrier. Moreover, we propose two weighting strategies for the virtual snapshot model in the weighted covariance matrix and prove that the principal eigenvalue of this matrix is unique. We further show that with the proposed weighting strategies, all non-scalar ambiguities inherent to blind channel estimation techniques in specific cases can be eliminated. These cases include respectively the systems involving rotatable codes such as the popular Alamouti code that is, e.g., used in the LTE and the systems involving single-antenna receivers like in downlink transmission for mobile handsets. Based on

our analysis, we also show that the linear precoding method of [SGM05] and the correlation matching method of [VS08b] satisfy partly the proposed uniqueness conditions of the weighted covariance matrix principal eigenvalue. The necessary conditions to obtain unique channel estimates have not been introduced before and the methods of [SGM05] and [VS08b] just provide special cases of proper weighting coefficients. Finally, the performance of the proposed strategies is illustrated by means of extensive numerical examples.

3.2 Virtual snapshot model

It should be noted that the proposed model and the suggested weighting strategies in this chapter correspond to the case of frequency flat fading channels. However, we have adopted the subcarrier MIMO-OFDM model for the sake of notational consistency with the next chapters throughout our derivations. The main idea behind developing a new model is to exploit the structural properties of the OSTBCs presented in Section 2.3 to generate a set of *virtual snapshots*. Then, we form the respective weighted covariance matrix at each subcarrier which corresponds to a low-rank subspace model. This is of particular importance in fast fading scenarios, when the low number of available snapshots leads to severe degradation in the performance of subspace estimates. Making use of (2.45) along with the relations (2.36), (2.37) and (2.41), the $2K$ virtual snapshots can be defined as

$$\tilde{\mathbf{y}}_i(k, p) \triangleq \Phi_k^T \mathbf{y}_i(p) = \tilde{\mathbf{A}}_k(\mathbf{h}_i) \underline{\mathbf{s}}_i(p) + \Phi_k^T \mathbf{v}_i(p), \quad k = 1, \dots, 2K \quad (3.1)$$

where

$$\begin{aligned} \tilde{\mathbf{A}}_1(\mathbf{h}_i) &\triangleq \Phi_1^T \mathbf{A}(\mathbf{h}_i) = [\mathbf{h}_i, \Phi_1^T \Phi_2 \mathbf{h}_i, \dots, \Phi_1^T \Phi_{2K} \mathbf{h}_i], \\ \tilde{\mathbf{A}}_2(\mathbf{h}_i) &\triangleq \Phi_2^T \mathbf{A}(\mathbf{h}_i) = [\Phi_2^T \Phi_1 \mathbf{h}_i, \mathbf{h}_i, \dots, \Phi_2^T \Phi_{2K} \mathbf{h}_i], \\ &\vdots \\ \tilde{\mathbf{A}}_{2K}(\mathbf{h}_i) &\triangleq \Phi_{2K}^T \mathbf{A}(\mathbf{h}_i) = [\Phi_{2K}^T \Phi_1 \mathbf{h}_i, \Phi_{2K}^T \Phi_2 \mathbf{h}_i, \dots, \mathbf{h}_i], \end{aligned} \quad (3.2)$$

stand for the virtual signal matrices corresponding to the respective virtual snapshots. It can be observed from (3.2) that the signal component \mathbf{h}_i is contained in all virtual snapshots

of (3.1). Further, this signal component is orthogonal to the remaining signal components in each of the matrices $\tilde{\mathbf{A}}_k(\mathbf{h}_i)$ for $k = 1, \dots, 2K$, i.e., $\mathbf{h}_i \perp \Phi_k^T \Phi_l \mathbf{h}_i$ for $k \neq l$. To show this, consider the skew-symmetry property (2.45), we obtain

$$\mathbf{h}_i^T \Phi_k^T \Phi_l \mathbf{h}_i = (\mathbf{h}_i^T \Phi_k^T \Phi_l \mathbf{h}_i)^T = \mathbf{h}_i^T \Phi_l^T \Phi_k \mathbf{h}_i = -\mathbf{h}_i^T \Phi_k^T \Phi_l \mathbf{h}_i = 0, \quad k \neq l. \quad (3.3)$$

Consider that all transmitted symbols $s_{ik}(p)$ for $k = 1, \dots, 2K$, are mutually independent and independent of the sensor noise at the i th subcarrier. Next, we define the weighted covariance matrix at the i th subcarrier obtained from the respective $2K$ virtual snapshots in (3.1) by using (3.2) as

$$\begin{aligned} \mathcal{X}_i(\boldsymbol{\gamma}) &\triangleq \mathbb{E} \left\{ \sum_{k=1}^{2K} \gamma_k \tilde{\mathbf{y}}_i(k, p) \tilde{\mathbf{y}}_i(k, p)^T \right\} \\ &= \sum_{k=1}^{2K} \gamma_k \left(\tilde{\mathbf{A}}_k(\mathbf{h}_i) \mathbb{E} \{ \underline{\mathbf{s}}_i \underline{\mathbf{s}}_i^T \} \tilde{\mathbf{A}}_k(\mathbf{h}_i)^T \right) + \sum_{k=1}^{2K} \frac{\gamma_k \sigma^2}{2} \mathbf{I}_{2MN} \\ &= \underbrace{\sum_{k=1}^{2K} \gamma_k \mathbb{E} \{ |s_{ik}|^2 \} \mathbf{h}_i \mathbf{h}_i^T}_{\text{desired component}} + \underbrace{\sum_{k=1}^{2K} \frac{\gamma_k \sigma^2}{2} \mathbf{I}_{2MN}}_{\text{noise contribution}} + \underbrace{\sum_{k=1}^{2K} \sum_{l=1; l \neq k}^{2K} \gamma_k \mathbb{E} \{ |s_{il}|^2 \} \Phi_k^T \Phi_l \mathbf{h}_i \mathbf{h}_i^T \Phi_l^T \Phi_k}_{\text{orthogonal to the desired component}}, \end{aligned} \quad (3.4)$$

where the vector $\boldsymbol{\gamma} \triangleq [\gamma_1, \dots, \gamma_{2K}]^T$ includes the positive real weighting coefficients. Taking into account (3.3), it can be readily verified from (3.4) that

$$\mathbf{u}_i \triangleq \frac{\mathbf{h}_i}{\|\mathbf{h}_i\|}, \quad (3.5)$$

is the normalized eigenvector of $\mathcal{X}_i(\boldsymbol{\gamma})$ associated with the eigenvalue

$$\lambda_{\mathbf{u}_i} \triangleq \sum_{k=1}^{2K} \gamma_k \mathbb{E} \{ |s_{ik}|^2 \} \|\mathbf{h}_i\|^2 + \sum_{k=1}^{2K} \frac{\gamma_k \sigma^2}{2}. \quad (3.6)$$

Next, we prove that for uniform weighting $\boldsymbol{\gamma} = \gamma_{\mathbf{u}} \triangleq \gamma [1, \dots, 1]^T$ in (3.4) with arbitrary real $\gamma > 0$, \mathbf{u}_i is the principal eigenvector of $\mathcal{X}_i(\boldsymbol{\gamma})$. This property has also been derived in [SGM05], however, from a different perspective. Here, we perform the proof in an entirely novel way that sheds further light on how we eliminate the principal eigenvalue multiplicity

of $\mathcal{X}_i(\boldsymbol{\gamma}_u)$ in the weighted covariance approach of the next section. Towards this goal we reformulate (3.4) as

$$\begin{aligned}\mathcal{X}_i(\boldsymbol{\gamma}) &= \sum_{k=1}^{2K} \sum_{l=1}^{2K} \gamma_k \mathbb{E}\{|s_{il}|^2\} \boldsymbol{\Phi}_k^T \boldsymbol{\Phi}_l \mathbf{h}_i \mathbf{h}_i^T \boldsymbol{\Phi}_l^T \boldsymbol{\Phi}_k + \sum_{k=1}^{2K} \frac{\gamma_k \sigma^2}{2} \mathbf{I}_{2MN} \\ &= \sum_{l=1}^{2K} \mathbb{E}\{|s_{il}|^2\} \mathcal{U}_{il}(\boldsymbol{\gamma}) + \sum_{k=1}^{2K} \frac{\gamma_k \sigma^2}{2} \mathbf{I}_{2MN},\end{aligned}\quad (3.7)$$

where

$$\mathcal{U}_{il}(\boldsymbol{\gamma}) \triangleq \sum_{k=1}^{2K} \gamma_k \boldsymbol{\Phi}_k^T \boldsymbol{\Phi}_l \mathbf{h}_i \mathbf{h}_i^T \boldsymbol{\Phi}_l^T \boldsymbol{\Phi}_k. \quad (3.8)$$

Then, taking into account (3.7) together with the result of Appendix C, we obtain

$$\begin{aligned}\lambda_{\max}(\mathcal{X}_i(\boldsymbol{\gamma})) &= \lambda_{\max}\left(\sum_{l=1}^{2K} \mathbb{E}\{|s_{il}|^2\} \mathcal{U}_{il}(\boldsymbol{\gamma}) + \sum_{k=1}^{2K} \frac{\gamma_k \sigma^2}{2} \mathbf{I}_{2MN}\right) \\ &\leq \|\mathbf{h}_i\|^2 \sum_{l=1}^{2K} \mathbb{E}\{|s_{il}|^2\} \lambda_{\max}(\boldsymbol{\Gamma}) + \sum_{k=1}^{2K} \frac{\gamma_k \sigma^2}{2} \\ &= \max\{\boldsymbol{\gamma}\} \|\mathbf{h}_i\|^2 \sum_{l=1}^{2K} \mathbb{E}\{|s_{il}|^2\} + \sum_{k=1}^{2K} \frac{\gamma_k \sigma^2}{2},\end{aligned}\quad (3.9)$$

where $\lambda_{\max}(\cdot)$ stands for the principal eigenvalue of an arbitrary matrix and $\boldsymbol{\Gamma} \triangleq \text{diag}(\boldsymbol{\gamma})$. Comparing (3.6) and (3.9), it can be directly verified that for the uniform weighting $\boldsymbol{\gamma} = \boldsymbol{\gamma}_u$, $\lambda_{\max}(\mathcal{X}_i(\boldsymbol{\gamma})) = \lambda_{\mathbf{u}_i}$ and the single-carrier normalized true CFR vector \mathbf{u}_i is the principal eigenvector of $\mathcal{X}_i(\boldsymbol{\gamma}_u)$. Therefore, when the respective principal eigenvalue is unique, the i th single-carrier CFR vector can be estimated up to an arbitrary scalar ambiguity. Otherwise, there exist a set of linearly independent principal eigenvectors that span the subspace in which the true i th single-carrier CFR vector is located. In this case, blind channel estimation methods based on finding the principal eigenvector of $\mathcal{X}_i(\boldsymbol{\gamma}_u)$ are not capable to estimate the CFR vector at the i th subcarrier up to a scaling factor. Unfortunately, the latter case occurs in two practically interesting scenarios: the systems comprising single-antenna receivers and the systems deploying rotatable codes [Ma07] such as the celebrated Alamouti [Ala98] code. In particular, we show analytically that in the case of rotatable codes, the principal eigenvalue of $\mathcal{X}_i(\boldsymbol{\gamma}_u)$ exhibits multiplicity. Consider the definition of subcarrier

weighted covariance matrix in (3.4) and take into account (2.55) together with (3.1). We observe that multiplying $\mathcal{X}_i(\gamma_u)$ from left and right, respectively, by $\check{\mathbf{Q}}^T$ and $\check{\mathbf{Q}}$ defined in (2.53), only changes the order in which the summation in (3.4) is performed, i.e.,

$$\begin{aligned} \check{\mathbf{Q}}^T \mathcal{X}_i(\gamma_u) \check{\mathbf{Q}} &= \check{\mathbf{Q}}^T \mathbb{E} \left\{ \sum_{k=1}^{2K} \gamma \tilde{\mathbf{y}}_i(k, p) \tilde{\mathbf{y}}_i(k, p)^T \right\} \check{\mathbf{Q}} = \mathbb{E} \left\{ \sum_{k=1}^{2K} \gamma \check{\mathbf{Q}}^T \Phi_k^T \mathbf{y}_i(p) \mathbf{y}_i(p)^T \Phi_k \check{\mathbf{Q}} \right\} \\ &= \mathbb{E} \left\{ \sum_{k=1}^{2K} \gamma d_k^2 \Phi_{n_k}^T \mathbf{y}_i(p) \mathbf{y}_i(p)^T \Phi_{n_k} \right\} = \mathbb{E} \left\{ \sum_{k=1}^{2K} \gamma \tilde{\mathbf{y}}_i(n_k, p) \tilde{\mathbf{y}}_i(n_k, p)^T \right\}. \end{aligned} \quad (3.10)$$

Hence, this multiplication does not change the individual components of the summation in (3.4) and the result of the summation as well. Therefore, the following permutation invariance property for the rotatable OSTBCs holds

$$\check{\mathbf{Q}}^T \mathcal{X}_i(\gamma_u) \check{\mathbf{Q}} = \mathcal{X}_i(\gamma_u). \quad (3.11)$$

Using (2.54) and (3.11), we obtain

$$\begin{aligned} \mathcal{X}_i(\gamma_u) \mathbf{h}_i &= \lambda_{\max}(\mathcal{X}_i(\gamma_u)) \mathbf{h}_i \\ \Rightarrow \mathcal{X}_i(\gamma_u) \check{\mathbf{Q}} \check{\mathbf{Q}}^T \mathbf{h}_i &= \lambda_{\max}(\mathcal{X}_i(\gamma_u)) \mathbf{h}_i \\ \Rightarrow \check{\mathbf{Q}}^T \mathcal{X}_i(\gamma_u) \check{\mathbf{Q}} \check{\mathbf{Q}}^T \mathbf{h}_i &= \lambda_{\max}(\mathcal{X}_i(\gamma_u)) \check{\mathbf{Q}}^T \mathbf{h}_i \\ \Rightarrow \mathcal{X}_i(\gamma_u) \check{\mathbf{h}}_i &= \lambda_{\max}(\mathcal{X}_i(\gamma_u)) \check{\mathbf{h}}_i, \end{aligned} \quad (3.12)$$

where $\check{\mathbf{h}}_i \triangleq \check{\mathbf{Q}}^T \mathbf{h}_i$ is also the principal eigenvector of $\mathcal{X}_i(\gamma_u)$. As a conclusion, for each code rotation matrix \mathbf{Q} satisfying (2.46), or the associated real-valued rotation matrix $\check{\mathbf{Q}}$ in (2.53), both the normalized true CFR vector \mathbf{u}_i and its transformed version $\check{\mathbf{u}}_i \triangleq \check{\mathbf{h}}_i / \|\check{\mathbf{h}}_i\|$ are the principal eigenvectors of $\mathcal{X}_i(\gamma_u)$. This holds true even if different information symbols that form $\underline{\mathbf{s}}_i(p)$ in (3.4) have different powers. In this case, the blind channel estimation method based on finding the principal eigenvector of $\mathcal{X}_i(\gamma_u)$ suffers from non-scalar ambiguities which precludes unambiguous blind channel recovery. This has already been addressed in expression (2.64) of Subsection 2.4.1 where we discussed the issue of blind identifiability. It should also be noted that although having different symbol powers in (3.4) does not resolve non-scalar ambiguities by itself, but it provides the means to resolve such ambiguities which is discussed in the next section.

It is also reasonable to further investigate the principal eigenvalue multiplicity order of $\mathcal{X}_i(\gamma_u)$ for non-rotatable codes with different system configurations, and constellations. Table 3.1 [SGM05], [VS08a] in the next page, summarizes numerical inspection regarding the mentioned issue for different OSTBCs proposed based on the amicable designs [LS03] as well as generalized orthogonal designs [TJC99]. To check rotatability, the fast numerical inspection based on (2.50) is used while for checking principal eigenvalue multiplicity order, an exhaustive inspection is performed. In Table 3.1, it is assumed that all symbols are drawn from the same BPSK (QPSK) constellations in the real (complex) OSTBC case. As mentioned in Section 2.3.1, for rotatable OSTBCs, i.e., code indices 1-4, relation (2.46) holds true for *every* symbol vector $\mathbf{s}_i(p)$ in the constellation set. Among non-rotatable codes, there are some codes which are called strictly non-rotatable [Ma07] in which relation (2.46) does not satisfy even for *one* single symbol vector $\mathbf{s}_i(p)$ in the constellation set, e.g., code indices 5, 6, 8, 10, 13, and 14. Further, there are some non-rotatable codes in Table 3.1, e.g., code indices 7 and 9, for which relation (2.46) satisfies for *some* symbol vectors in the constellation set [Ma07]. It should be also noted that each particular value of multiplicity order in Table 3.1 is computed for multiple independently generated zero-mean Gaussian CFR vectors \mathbf{h}_i . However, this value is observed to be independent of the CFR vector realization and depends only on the type of OSTBC and the number of receive antennas, i.e., M [SGM05]. From Table 3.1, it can be observed that in the rotatable OSTBCs case or most of the MISO system configurations, principal eigenvalue multiplicity order of $\mathcal{X}_i(\gamma_u)$ is greater than one. In the next section, we propose two strategies in choosing the weighting coefficients γ_k , $k = 1, \dots, 2K$, in (3.4) to resolve non-scalar ambiguities.

3.3 Weighting strategy

First, we introduce a weighting strategy which exploits the rotatable OSTBCs specific properties presented in Subsection 2.3.1 to select the coefficients $\{\gamma_k\}_{k=1}^{2K}$ in (3.4) in order to eliminate the types of multiplicity satisfying (3.12). To develop this strategy, we rely on the assumption that the transmitted symbols have non-uniform powers such that

| Code index | Rate (K/T) | Constellation | Number of transmit antennas (N) | Number of symbols per block (K) | Design approach | Rotatable | Multiplicity order ($M = 1$) MISO | Multiplicity order ($M > 1$) MIMO |
|------------|----------------|---------------|-------------------------------------|-------------------------------------|-----------------|------------|---|---|
| 1 | 1 | real | 2 | 2 | Alamouti | Yes | ↓ <u>2</u> | ↓ <u>2</u> |
| 2 | 1 | real | 4 | 4 | Gen. ort. | Yes | <u>4</u> | <u>4</u> |
| 3 | 1 | complex | 2 | 2 | Alamouti | Yes | <u>4</u> | <u>4</u> |
| 4 | 1/2 | complex | 4 | 4 | Gen. ort. | Yes | <u>4</u> | <u>4</u> |
| 5 | 1 | real | 3 | 4 | Gen. ort. | No | ↓ <u>2</u> | 1 |
| 6 | 1 | real | 5 | 8 | Gen. ort. | No | <u>2</u> | 1 |
| 7 | 1 | real | 6 | 8 | Gen. ort. | No | <u>2</u> | 1 |
| 8 | 1 | real | 7 | 8 | Gen. ort. | No | <u>2</u> | 1 |
| 9 | 1 | real | 8 | 8 | Gen. ort. | No | <u>2</u> | 1 |
| 10 | 1 | real | 9 | 16 | Gen. ort. | No | <u>2</u> | 1 |
| 11 | 1 | real | 10 | 16 | Gen. ort. | No | <u>2</u> | 1 |
| 12 | 1/2 | complex | 3 | 4 | Gen. ort. | No | <u>2</u> | 1 |
| 13 | 1/2 | complex | 5 | 8 | Gen. ort. | No | <u>2</u> | 1 |
| 14 | 1/2 | complex | 6 | 8 | Gen. ort. | No | <u>2</u> | 1 |
| 15 | 1/2 | complex | 7 | 8 | Gen. ort. | No | <u>2</u> | 1 |
| 16 | 1/2 | complex | 8 | 8 | Gen. ort. | No | <u>2</u> | 1 |
| 17 | 3/4 | complex | 3 | 3 | Amicable | No | <u>2</u> | 1 |
| 18 | 3/4 | complex | 4 | 3 | Amicable | No | <u>2</u> | 1 |
| 19 | 1/2 | complex | 5 | 4 | Amicable | No | 1 | 1 |
| 20 | 1/2 | complex | 6 | 4 | Amicable | No | 1 | 1 |
| 21 | 1/2 | complex | 7 | 4 | Amicable | No | 1 | 1 |
| 22 | 1/2 | complex | 8 | 4 | Amicable | No | 1 | 1 |

Table 3.1: The principal eigenvalue multiplicity order of $\mathcal{X}_i(\gamma_u)$ for different OSTBCs [SGM05], [VS08a].

$E\{|s_{ik}|^2\} \neq E\{|s_{in_k}|^2\}$, for at least one $k \in \{1, \dots, 2K\}$ corresponding to the mapping (2.49). It is noteworthy to emphasize that this assumption embraces two important cases as its special example. First, when there is only one complex transmitted symbol that its real or imaginary part has unique power level among all the others and second, when the real and imaginary parts of all complex transmitted symbols have distinct power levels. The latter assumption is considered in the proposed precoding technique of [SGM05]. With no loss of generality, assume that the symbol powers are ordered in non-increasing manner as

$$E\{|s_{i1}|^2\} \geq E\{|s_{i2}|^2\} \geq \dots \geq E\{|s_{i2K}|^2\}; \quad E\{|s_{ik}|^2\} \neq E\{|s_{in_k}|^2\}, \quad (3.13)$$

for some $k \in \{1, \dots, 2K\}$. Also, the weight vector entries $\{\gamma_k\}_{k=1}^{2K}$ in (3.4) are selected in accordance with the symbol powers in (3.13), i.e.,

$$\gamma_1 \geq \gamma_2 \geq \dots \geq \gamma_{2K} > 0; \quad \gamma_k \neq \gamma_{n_k}, \quad (3.14)$$

for the same $k \in \{1, \dots, 2K\}$ where $E\{|s_{ik}|^2\} \neq E\{|s_{in_k}|^2\}$. The proposed weighting strategy is stated in the following lemma:

Lemma 3.1: At the i th subcarrier, the principal eigenvalue multiplicity of $\mathcal{X}_i(\boldsymbol{\gamma})$ shown in (3.12) for signal powers $E\{|s_{ik}|^2\}_{k=1}^{2K}$ arranged as in (3.13) and the weighting coefficients $\{\gamma_k\}_{k=1}^{2K}$ in (3.4) chosen according to (3.14), is equal to one. \square

The proof of the previous lemma relies on the properties of the rotatable OSTBC and the specific relation between (3.13) and (3.14). Considering the skew-symmetric property of $\check{\mathbf{Q}}$ in (2.58), we have that the vector $\check{\mathbf{h}}_i = \check{\mathbf{Q}}^T \mathbf{h}_i$ is orthogonal to the vector \mathbf{h}_i as

$$\check{\mathbf{h}}_i^T \mathbf{h}_i = \mathbf{h}_i^T \check{\mathbf{Q}} \mathbf{h}_i = (\mathbf{h}_i^T \check{\mathbf{Q}} \mathbf{h}_i)^T = \mathbf{h}_i^T \check{\mathbf{Q}}^T \mathbf{h}_i = \mathbf{h}_i^T (-\check{\mathbf{Q}}) \mathbf{h}_i = -\mathbf{h}_i^T \check{\mathbf{Q}} \mathbf{h}_i = 0. \quad (3.15)$$

Moreover, from comparison of (3.2) and (2.57), we also conclude that $\check{\mathbf{h}}_i$ is a column of each matrix $\tilde{\mathbf{A}}_k(\mathbf{h}_i)$, $k = 1, \dots, 2K$ in (3.2). Specifically, using (2.56) we obtain

$$\check{\mathbf{Q}} = \pm \boldsymbol{\Phi}_1^T \boldsymbol{\Phi}_{n_1} = \pm \boldsymbol{\Phi}_2^T \boldsymbol{\Phi}_{n_2} = \dots = \pm \boldsymbol{\Phi}_{2K}^T \boldsymbol{\Phi}_{n_{2K}}, \quad (3.16)$$

with $n_1 \neq n_2 \neq \dots \neq n_{2K}$. Therefore, $\check{\mathbf{h}}_i$ appears at a different column position in each of

the virtual signal matrices $\tilde{\mathbf{A}}_k(\mathbf{h}_i)$ in (3.2). In addition, using (2.58) we infer that

$$\check{\mathbf{h}}_i^T \Phi_k^T \Phi_l \mathbf{h}_i = \mathbf{h}_i^T \check{\mathbf{Q}} \Phi_k^T \Phi_l \mathbf{h}_i = \mathbf{h}_i^T (-\check{\mathbf{Q}}^T) \Phi_k^T \Phi_l \mathbf{h}_i = -\mathbf{h}_i^T (\Phi_k \check{\mathbf{Q}})^T \Phi_l \mathbf{h}_i = -\mathbf{h}_i^T \Phi_{n_k}^T \Phi_l \mathbf{h}_i = 0, \quad (3.17)$$

for $n_k \neq l$. In other words, taking into account (2.57) and (3.15)-(3.17), we conclude that the vector $\check{\mathbf{h}}_i$ is the n_k th column (up to a sign) of the matrix $\tilde{\mathbf{A}}_k(\mathbf{h}_i)$, $k = 1, \dots, 2K$, for some $n_k \neq k$ with $n_k \neq n_l$ when $k \neq l$ and is orthogonal to the remaining columns in $\tilde{\mathbf{A}}_k(\mathbf{h}_i)$. To reveal an important property of the vector $\check{\mathbf{h}}_i$, we reformulate (3.4) as

$$\mathcal{X}_i(\boldsymbol{\gamma}) = \sum_{k=1}^{2K} \gamma_k \mathbb{E}\{|s_{in_k}|^2\} \check{\mathbf{h}}_i \check{\mathbf{h}}_i^T + \sum_{k=1}^{2K} \frac{\gamma_k \sigma^2}{2} \mathbf{I}_{2MN} + \sum_{k=1}^{2K} \sum_{l=1; l \neq n_k}^{2K} \gamma_k \mathbb{E}\{|s_{il}|^2\} \Phi_k^T \Phi_l \mathbf{h}_i \mathbf{h}_i^T \Phi_l^T \Phi_k. \quad (3.18)$$

Taking into account (3.15) along with (3.17) and multiplying (3.18) from right by $\check{\mathbf{h}}_i$, we conclude that $\check{\mathbf{h}}_i$ is the eigenvector of $\mathcal{X}_i(\boldsymbol{\gamma})$ in (3.18) even in the case of non-uniform weighting and its respective eigenvalue is given by

$$\lambda_{\check{\mathbf{u}}_i} = \|\check{\mathbf{h}}_i\|^2 \sum_{k=1}^{2K} \gamma_k \mathbb{E}\{|s_{in_k}|^2\} + \sum_{k=1}^{2K} \gamma_k \frac{\sigma^2}{2}. \quad (3.19)$$

As a result, both vectors \mathbf{h}_i and $\check{\mathbf{h}}_i$ are the eigenvectors of $\mathcal{X}_i(\boldsymbol{\gamma})$ and the respective eigenvalues are given by (3.6) and (3.19), respectively. Let us have a closer look at the eigenvalue expressions corresponding to the vectors \mathbf{h}_i and $\check{\mathbf{h}}_i$ in (3.6) and (3.19), respectively. Next, we aim to prove that

$$\sum_{k=1}^{2K} \gamma_k \mathbb{E}\{|s_{ik}|^2\} > \sum_{k=1}^{2K} \gamma_k \mathbb{E}\{|s_{in_k}|^2\}, \quad (3.20)$$

provided that (3.13) and (3.14) are fulfilled.

Each pair term $\left(\gamma_k \mathbb{E}\{|s_{ik}|^2\} + \gamma_{n_k} \mathbb{E}\{|s_{in_k}|^2\} \right)$ in the left-hand side of the inequality (3.20) has respective counterpart term of $\left(\gamma_k \mathbb{E}\{|s_{in_k}|^2\} + \gamma_{n_k} \mathbb{E}\{|s_{ik}|^2\} \right)$ in the right-hand side of the inequality (3.20) since the permutation matrix \mathbf{P}_1 in (2.49) is symmetric. The latter term is obtained from exchanging the signal power components in the former term. We show that such an exchange, either does not change or does decrease the total value of the former term provided that different symbol powers satisfy (3.13) and weighting

coefficients are chosen in agreement with (3.14). To do this, let us present the following inequality

$$\left((\gamma_k - \gamma_{n_k}) \mathbb{E}\{|s_{ik}|^2\} \right) \geq \left((\gamma_k - \gamma_{n_k}) \mathbb{E}\{|s_{in_k}|^2\} \right). \quad (3.21)$$

The inequality in (3.21) is valid in all the possible cases of $\mathbb{E}\{|s_{ik}|^2\} > \mathbb{E}\{|s_{in_k}|^2\}$, or $\mathbb{E}\{|s_{ik}|^2\} < \mathbb{E}\{|s_{in_k}|^2\}$, or $\mathbb{E}\{|s_{ik}|^2\} = \mathbb{E}\{|s_{in_k}|^2\}$. This is due to the condition (3.14) as we have $\gamma_k > \gamma_{n_k} > 0$, or $0 < \gamma_k < \gamma_{n_k}$, or $\gamma_k = \gamma_{n_k}$, respectively, for all the previous cases. Therefore, taking into account (3.21) and performing a re-arrangement of the terms, we obtain

$$\left(\gamma_k \mathbb{E}\{|s_{ik}|^2\} + \gamma_{n_k} \mathbb{E}\{|s_{in_k}|^2\} \right) \geq \left(\gamma_k \mathbb{E}\{|s_{in_k}|^2\} + \gamma_{n_k} \mathbb{E}\{|s_{ik}|^2\} \right). \quad (3.22)$$

Hence, any exchange of the signal power components in the left-hand side of (3.22) which yields the right-hand side of (3.22) results in reduction or no change of the corresponding value, and, therefore, we conclude (3.20). Also, from the orthogonality property of the matrix $\check{\mathbf{Q}}$ in (2.54) and the definition of the vector $\check{\mathbf{h}}_i = \check{\mathbf{Q}}^T \mathbf{h}_i$ we have that

$$\|\check{\mathbf{h}}_i\|^2 = \check{\mathbf{h}}_i^T \check{\mathbf{h}}_i = \mathbf{h}_i^T \check{\mathbf{Q}} \check{\mathbf{Q}}^T \mathbf{h}_i = \mathbf{h}_i^T \mathbf{h}_i = \|\mathbf{h}_i\|^2. \quad (3.23)$$

Taking into account (3.23) along with (3.6), (3.19), and (3.20), we conclude that

$$\begin{aligned} \sum_{k=1}^{2K} \gamma_k \mathbb{E}\{|s_{ik}|^2\} > \sum_{k=1}^{2K} \gamma_k \mathbb{E}\{|s_{in_k}|^2\} &\Rightarrow \|\mathbf{h}_i\|^2 \sum_{k=1}^{2K} \gamma_k \mathbb{E}\{|s_{ik}|^2\} > \|\check{\mathbf{h}}_i\|^2 \sum_{k=1}^{2K} \gamma_k \mathbb{E}\{|s_{in_k}|^2\} \\ \Rightarrow \|\mathbf{h}_i\|^2 \sum_{k=1}^{2K} \gamma_k \mathbb{E}\{|s_{ik}|^2\} + \sum_{k=1}^{2K} \frac{\gamma_k \sigma^2}{2} &> \|\check{\mathbf{h}}_i\|^2 \sum_{k=1}^{2K} \gamma_k \mathbb{E}\{|s_{in_k}|^2\} + \sum_{k=1}^{2K} \frac{\gamma_k \sigma^2}{2} \Rightarrow \lambda_{\mathbf{u}_i} > \lambda_{\check{\mathbf{u}}_i}. \end{aligned} \quad (3.24)$$

Therefore, the principal eigenvalue multiplicity results from using the rotatable codes, e.g., corresponding to the code indices 1-4 in Table 3.1, can be resolved by the aid of proper weighting coefficients.

Next, we introduce another weighting strategy and prove its corresponding capability to resolve the weighted covariance matrix principal eigenvalue multiplicity of $\mathcal{X}_i(\boldsymbol{\gamma})$. This second weighting strategy resolves non-scalar ambiguity not only for the case of the rotatable

OSTBCs, but also for some non-rotatable OSTBCs in the MISO system configuration which according to the Table I in both [SGM05] and [VS08a], we confront such ambiguities, e.g., corresponding to the code indices 5-18 in Table 3.1. The proposed strategy is based on both, the assumption that there exists a particular real-valued symbol among $\{s_{ik}\}_{k=1}^{2K}$ with a higher power level than all other ones, and the equivalence of $\lambda_{\max}(\mathcal{X}_i(\boldsymbol{\gamma}))$ with $\lambda_{\mathbf{u}_i}$ obtained from (3.6) and (3.9) in the case of $\boldsymbol{\gamma} = \boldsymbol{\gamma}_u$. Without loss of generality, the aforementioned assumption over symbol powers can be presented as

$$\mathbb{E}\{|s_{i1}|^2\} > \mathbb{E}\{|s_{i2}|^2\} \geq \dots \geq \mathbb{E}\{|s_{i2K}|^2\}, \quad (3.25)$$

since labeling the transmitted symbols is immaterial. Based on (3.25), we suggest to choose non-uniform $\boldsymbol{\gamma}$ as

$$\boldsymbol{\gamma} = \boldsymbol{\gamma}_n \triangleq [\gamma + \Delta\gamma, \gamma, \dots, \gamma]^T. \quad (3.26)$$

Taking into account (3.26) and $\boldsymbol{\gamma}_u = [\gamma, \dots, \gamma]^T$, we obtain

$$\boldsymbol{\gamma}_n = \boldsymbol{\gamma}_u + \boldsymbol{\gamma}_b, \quad (3.27)$$

where $\boldsymbol{\gamma}_b \triangleq [\Delta\gamma, 0, \dots, 0]^T$ stands for the boosting weight vector. Using (3.27) and the fact that $\mathcal{X}_i(\boldsymbol{\gamma})$ is linear with respect to $\boldsymbol{\gamma}$ according to (3.4), it can be directly verified that the weighted covariance matrix $\mathcal{X}_i(\boldsymbol{\gamma}_n)$ partitions as

$$\mathcal{X}_i(\boldsymbol{\gamma}_n) = \mathcal{X}_i(\boldsymbol{\gamma}_u) + \mathcal{X}_i(\boldsymbol{\gamma}_b). \quad (3.28)$$

Further, according to (3.4) and the definition of $\boldsymbol{\gamma}_b$, we obtain

$$\begin{aligned} \mathcal{X}_i(\boldsymbol{\gamma}_b) &= \Delta\gamma \left(\tilde{\mathbf{A}}_1(\mathbf{h}_i) \mathbb{E}\{\underline{\mathbf{s}}_i \underline{\mathbf{s}}_i^T\} \tilde{\mathbf{A}}_1(\mathbf{h}_i)^T + \frac{\sigma^2}{2} \mathbf{I}_{2MN} \right) \\ &= \underbrace{\Delta\gamma \mathbb{E}\{|s_{i1}|^2\} \mathbf{h}_i \mathbf{h}_i^T}_{\text{desired component}} + \underbrace{\frac{\Delta\gamma \sigma^2}{2} \mathbf{I}_{2MN}}_{\text{noise contribution}} + \underbrace{\sum_{l=2}^{2K} \Delta\gamma \mathbb{E}\{|s_{il}|^2\} \boldsymbol{\Phi}_1^T \boldsymbol{\Phi}_l \mathbf{h}_i \mathbf{h}_i^T \boldsymbol{\Phi}_l^T \boldsymbol{\Phi}_1}_{\text{orthogonal to the desired component}}. \end{aligned} \quad (3.29)$$

Taking into account (3.3), it can be verified from (3.29) that $\mathbf{u}_i = \mathbf{h}_i / \|\mathbf{h}_i\|$ is the normalized eigenvector of $\mathcal{X}_i(\boldsymbol{\gamma}_b)$ associated with the eigenvalue $(\Delta\gamma \mathbb{E}\{|s_{i1}|^2\} \|\mathbf{h}_i\|^2 + (\Delta\gamma \sigma^2)/2)$.

Let $\boldsymbol{\theta} \triangleq [\mathbb{E}\{|s_{i1}|^2\}, \dots, \mathbb{E}\{|s_{i2K}|^2\}]^T$ be a vector containing powers of the real and imaginary parts of the transmitted symbols at the i th subcarrier and $\boldsymbol{\Theta} \triangleq \text{diag}(\boldsymbol{\theta})$. Next, we reformulate (3.29) by using (3.8) to obtain

$$\begin{aligned} \mathcal{X}_i(\gamma_b) &= \sum_{l=1}^{2K} \Delta\gamma \mathbb{E}\{|s_{il}|^2\} \boldsymbol{\Phi}_1^T \boldsymbol{\Phi}_l \mathbf{h}_i \mathbf{h}_i^T \boldsymbol{\Phi}_l^T \boldsymbol{\Phi}_1 + \frac{\Delta\gamma\sigma^2}{2} \mathbf{I}_{2MN} \\ &= \Delta\gamma \mathcal{U}_{i1}(\boldsymbol{\theta}) + \frac{\Delta\gamma\sigma^2}{2} \mathbf{I}_{2MN}. \end{aligned} \quad (3.30)$$

Then, taking into account (3.30) together with the result of Appendix C, we obtain

$$\begin{aligned} \lambda_{\max}(\mathcal{X}_i(\gamma_b)) &= \lambda_{\max}\left(\Delta\gamma \mathcal{U}_{i1}(\boldsymbol{\theta}) + \frac{\Delta\gamma\sigma^2}{2} \mathbf{I}_{2MN}\right) \\ &\leq \Delta\gamma \|\mathbf{h}_i\|^2 \lambda_{\max}(\boldsymbol{\Theta}) + \frac{\Delta\gamma\sigma^2}{2} \\ &= \Delta\gamma \|\mathbf{h}_i\|^2 \mathbb{E}\{|s_{i1}|^2\} + \frac{\Delta\gamma\sigma^2}{2}, \end{aligned} \quad (3.31)$$

where the last equality in (3.31) follows from (3.25). Comparing (3.31) and the eigenvalue associated to the vector \mathbf{u}_i , we conclude that the vector \mathbf{u}_i is the unique normalized principal eigenvector of $\mathcal{X}_i(\gamma_b)$ with associated eigenvalue

$$\lambda_{\max}(\mathcal{X}_i(\gamma_b)) = \Delta\gamma \mathbb{E}\{|s_{i1}|^2\} \|\mathbf{h}_i\|^2 + \frac{\Delta\gamma\sigma^2}{2}.$$

Consider (3.28), it can be deduced that \mathbf{u}_i is the unique normalized principal eigenvector of $\mathcal{X}_i(\gamma_n)$ as it is the unique normalized principal eigenvector of $\mathcal{X}_i(\gamma_b)$ and the principal eigenvector of $\mathcal{X}_i(\gamma_u)$. Therefore, the proposed weighting strategy of (3.26) eliminates any non-scalar ambiguity corresponding to the principal eigenvalue multiplicity of $\mathcal{X}_i(\gamma)$ by boosting the desired signal component \mathbf{h}_i provided that (3.25) holds.

It is noteworthy to mention that the necessary condition (3.13) over symbol powers and the respective weighting strategy introduced earlier in this section are more general than the assumption and the corresponding weighting method presented in (3.25) and (3.26), respectively. However, the associated proofs reveal that the latter weighting strategy is able to resolve more general cases of the non-scalar ambiguities including the ones which are guaranteed to be eliminated by the former strategy. In fact, we have proved that (3.13)

along with (3.14) can resolve the principal eigenvalue multiplicities reflected in Table 3.1 corresponding to the code indices 1-4 while (3.25) together with (3.26) are able to resolve all principal eigenvalue multiplicities illustrated in Table 3.1. It should be further emphasized that we have not optimized the selection of weighting coefficients for instance to minimize the SER or to improve other performance index and provided weighting strategies only guarantee elimination of the non-scalar ambiguities.

In the following, we show that the correlation matching approaches of [VS08b] can be considered as a particular choices of weight coefficients that satisfy the conditions of (3.14) and which are not sufficient to resolve non-scalar ambiguity without (3.13). Hence, as the necessary conditions of (3.13) for the non-scalar ambiguity elimination have not been provided in [VS08b], the corresponding methods may not be successful and the conditions under which we can get unique channel estimates are not presented in this work. We also observe that the same statement holds true for the precoding approach of [SGM05]. It should be noted that only a special case of (3.13), i.e., the case where the symbols exhibit distinct real and imaginary part powers, has been addressed in [SGM05]. Therefore, the proposed weighting strategy with the respective necessary condition over symbol powers explained in Lemma 3.1 provides theoretical basis for simulation results in [SGM05] and [VS08b].

3.3.1 The Euclidean correlation matching criterion

Taking into account that the symbol streams are mutually independent and independent of the sensor noise along with the model (2.36), we obtain the following covariance matrix of the received data vector at the i th subcarrier [SGM05]

$$\mathbf{R}_i \triangleq \mathbb{E}\{\mathbf{y}_i \mathbf{y}_i^T\} = \mathbf{A}(\mathbf{h}_i) \mathbf{\Lambda}_{\underline{\mathbf{s}}_i} \mathbf{A}(\mathbf{h}_i)^T + \frac{\sigma^2}{2} \mathbf{I}_{2MT}, \quad (3.32)$$

where $\mathbf{\Lambda}_{\underline{\mathbf{s}}_i} \triangleq \mathbb{E}\{\underline{\mathbf{s}}_i \underline{\mathbf{s}}_i^T\}$ is the covariance matrix of the transmitted real vector $\underline{\mathbf{s}}_i$. Each diagonal entry of $\mathbf{\Lambda}_{\underline{\mathbf{s}}_i}$ represents the average power of the real or imaginary parts of the corresponding data symbol and depends only on the shape of constellation of that particular symbol, hence, it is known at the receiver. Multiplying (3.32) from the right by $\mathbf{A}(\mathbf{h}_i)/\|\mathbf{h}_i\|$

and using (2.38), we have [SGM05]

$$\mathbf{R}_i \frac{\mathbf{A}(\mathbf{h}_i)}{\|\mathbf{h}_i\|} = \frac{\mathbf{A}(\mathbf{h}_i)}{\|\mathbf{h}_i\|} \left(\underline{\Lambda}_{\mathbf{s}_i} \|\mathbf{h}_i\|^2 + \frac{\sigma^2}{2} \mathbf{I}_{2K} \right). \quad (3.33)$$

Since $\mathbf{A}(\mathbf{h}_i)/\|\mathbf{h}_i\|$ has orthonormal columns, according to (2.38), and $\underline{\Lambda}_{\mathbf{s}_i}$ is diagonal in the case of mutually uncorrelated transmitted symbols, (3.33) can be viewed as the characteristic equation for \mathbf{R}_i and $\left(\underline{\Lambda}_{\mathbf{s}_i} \|\mathbf{h}_i\|^2 + (\sigma^2/2) \mathbf{I}_{2K} \right)$ contains the $2K$ largest eigenvalues of \mathbf{R}_i . Therefore, the signal subspace eigenvalues of \mathbf{R}_i depend only on the norm of CFR vector \mathbf{h}_i and not its spatial signature. It is shown that this statement is also valid even if $\underline{\Lambda}_{\mathbf{s}_i}$ is not a diagonal matrix; see Appendix D. In practice, \mathbf{R}_i can be estimated as [SGM05]

$$\hat{\mathbf{R}}_i = \frac{1}{P} \sum_{p=1}^P \mathbf{y}_i(p) \mathbf{y}_i(p)^T, \quad (3.34)$$

where P represents the total number of data blocks that are used to estimate \mathbf{R}_i . It is important to mention that the estimator in (3.34) is a consistent estimator of the received data covariance matrix \mathbf{R}_i [SGM05].

The key idea of the Euclidean correlation matching (ECM) approach is to estimate the CFR vector \mathbf{h}_i , by minimizing the norm of difference between the true and sample covariance matrices as [VS08b]

$$\hat{\mathbf{h}}_{i,\text{ECM}} = \arg \min_{\tilde{\mathbf{h}}_i} \|\hat{\mathbf{R}}_i - \mathbf{R}(\tilde{\mathbf{h}}_i)\|^2, \quad (3.35)$$

where the dependency of the true covariance matrix, according to (3.32), to the CFR is explicitly emphasized by adopting the notation $\mathbf{R}(\tilde{\mathbf{h}}_i)$. To further simplify (3.35), we drop the term in (3.35) that is independent of the optimization variable. Also, we take into account that both $\hat{\mathbf{R}}_i$ and $\mathbf{R}_i(\tilde{\mathbf{h}}_i)$ are symmetric matrices along with the matrix identity $\text{tr}(\mathbf{X}\mathbf{Y}) = \text{tr}(\mathbf{Y}\mathbf{X})$ for any arbitrary conformable matrices \mathbf{X} and \mathbf{Y} to obtain

$$\hat{\mathbf{h}}_{i,\text{ECM}} = \arg \min_{\tilde{\mathbf{h}}_i} \|\hat{\mathbf{R}}_i - \mathbf{R}(\tilde{\mathbf{h}}_i)\|^2 = \arg \max_{\tilde{\mathbf{h}}_i} \left\{ 2 \text{tr}(\hat{\mathbf{R}}_i \mathbf{R}(\tilde{\mathbf{h}}_i)) - \|\mathbf{R}(\tilde{\mathbf{h}}_i)\|^2 \right\}. \quad (3.36)$$

Using the orthogonality property (2.38) together with (3.32), we can rewrite the both terms in the right-hand side of (3.36) as

$$\begin{aligned} \text{tr}(\hat{\mathbf{R}}_i \mathbf{R}(\tilde{\mathbf{h}}_i)) &= \text{tr} \left(\mathbf{A}(\tilde{\mathbf{h}}_i)^T \hat{\mathbf{R}}_i \mathbf{A}(\tilde{\mathbf{h}}_i) \underline{\Lambda}_{\mathbf{s}_i} \right) + \frac{\sigma^2}{2} \text{tr}(\hat{\mathbf{R}}_i) \\ \|\mathbf{R}(\tilde{\mathbf{h}}_i)\|^2 &= \|\tilde{\mathbf{h}}_i\|^4 \|\underline{\Lambda}_{\mathbf{s}_i}\|^2 + \sigma^2 \|\tilde{\mathbf{h}}_i\|^2 \text{tr}(\underline{\Lambda}_{\mathbf{s}_i}) + \frac{MT\sigma^4}{2}. \end{aligned}$$

Using these two equations and dropping the terms which do not depend on $\tilde{\mathbf{h}}_i$, (3.36) can be expressed as

$$\hat{\mathbf{h}}_{i,\text{ECM}} = \arg \max_{\tilde{\mathbf{h}}_i} \left\{ 2 \operatorname{tr} \left(\mathbf{A}(\tilde{\mathbf{h}}_i)^T \hat{\mathbf{R}}_i \mathbf{A}(\tilde{\mathbf{h}}_i) \underline{\boldsymbol{\Lambda}}_{\mathbf{s}_i} \right) - \|\tilde{\mathbf{h}}_i\|^4 \|\underline{\boldsymbol{\Lambda}}_{\mathbf{s}_i}\|^2 - \sigma^2 \|\tilde{\mathbf{h}}_i\|^2 \operatorname{tr}(\underline{\boldsymbol{\Lambda}}_{\mathbf{s}_i}) \right\}. \quad (3.37)$$

It is noteworthy to stress that the main issue in the blind channel estimation algorithm is the estimation of the channel vector spatial signature while estimation of the channel norm corresponds to a proper scaling and can be performed, e.g., as in [SGM05]. Hence, by assuming the norm constraint on the optimization variable in (3.37) such as $\|\tilde{\mathbf{h}}_i\| = \|\mathbf{h}_i\|$, the terms $\left(\|\tilde{\mathbf{h}}_i\|^4 \|\underline{\boldsymbol{\Lambda}}_{\mathbf{s}_i}\|^2 \right)$ and $\left(\sigma^2 \|\tilde{\mathbf{h}}_i\|^2 \operatorname{tr}(\underline{\boldsymbol{\Lambda}}_{\mathbf{s}_i}) \right)$ become constants and, therefore, they can be dropped. It can be shown [SGM05] that using (2.43), the problem (3.37) becomes equivalent to

$$\hat{\mathbf{h}}_{i,\text{ECM}} = \arg \max_{\tilde{\mathbf{h}}_i} \tilde{\mathbf{h}}_i^T \boldsymbol{\Phi}^T (\underline{\boldsymbol{\Lambda}}_{\mathbf{s}_i} \otimes \hat{\mathbf{R}}_i) \boldsymbol{\Phi} \tilde{\mathbf{h}}_i, \quad (3.38)$$

together with $\|\tilde{\mathbf{h}}_i\| = \|\mathbf{h}_i\|$. Taking into account the definition (2.44) along with the equations (3.4), and (3.34), we define

$$\begin{aligned} \hat{\mathcal{X}}_i(\gamma_{\text{ECM}}) &\triangleq \boldsymbol{\Phi}^T (\underline{\boldsymbol{\Lambda}}_{\mathbf{s}_i} \otimes \hat{\mathbf{R}}_i) \boldsymbol{\Phi} \\ &= \sum_{k=1}^{2K} \mathbb{E}\{|s_{ik}|^2\} \boldsymbol{\Phi}_k^T \hat{\mathbf{R}}_i \boldsymbol{\Phi}_k = \frac{1}{P} \sum_{k=1}^{2K} \sum_{p=1}^P \mathbb{E}\{|s_{ik}|^2\} \tilde{\mathbf{y}}_i(k,p) \tilde{\mathbf{y}}_i(k,p)^T, \end{aligned} \quad (3.39)$$

$$\boldsymbol{\gamma}_{\text{ECM}} \triangleq \left[\mathbb{E}\{|s_{i1}|^2\}, \mathbb{E}\{|s_{i2}|^2\}, \dots, \mathbb{E}\{|s_{i2K}|^2\} \right]^T, \quad (3.40)$$

to obtain

$$\hat{\mathbf{h}}_{i,\text{ECM}} = \arg \max_{\tilde{\mathbf{h}}_i} \tilde{\mathbf{h}}_i^T \hat{\mathcal{X}}_i(\boldsymbol{\gamma}_{\text{ECM}}) \tilde{\mathbf{h}}_i. \quad (3.41)$$

If the proposed necessary condition (3.13) over the transmitted signal powers holds true, then the comparison of (3.40) and (3.14) reveals that the ECM approach of [VS08b] provides the particular selection for the proposed weighting strategy.

3.3.2 The Kullback correlation matching criterion

The main idea of the Kullback correlation matching (KCM) is to minimize the divergence between the true and sample covariance matrices of the received data based on the Kullback-Leibler divergence. Applying this measure to the model (2.36) along with corresponding

assumptions results in the following optimization problem to estimate the CFR vector at the i th subcarrier as [VS08b]

$$\begin{aligned}\hat{\mathbf{h}}_{i,\text{KCM}} &= \arg \min_{\tilde{\mathbf{h}}_i} \left\{ \text{tr} \left(\mathbf{R}^{-1}(\tilde{\mathbf{h}}_i) \hat{\mathbf{R}}_i - \mathbf{I}_{2MT} \right) - \log \det \left(\mathbf{R}^{-1}(\tilde{\mathbf{h}}_i) \hat{\mathbf{R}}_i \right) \right\} \\ &= \arg \min_{\tilde{\mathbf{h}}_i} \left\{ \text{tr} \left(\mathbf{R}^{-1}(\tilde{\mathbf{h}}_i) \hat{\mathbf{R}}_i \right) + \log \det \left(\mathbf{R}(\tilde{\mathbf{h}}_i) \right) \right\},\end{aligned}\quad (3.42)$$

where we have dropped the terms which do not depend on the optimization variable in the last equality of (3.42). It should be noted that the optimization problem (3.42) reduces to the joint ML estimator for channel parameters and symbols based on Gaussian source assumption [Jaf88]. To simplify the first term in (3.42), let us apply the Woodbury identity [Mey00] to the true covariance matrix in (3.32) to obtain

$$\mathbf{R}^{-1}(\tilde{\mathbf{h}}_i) = \frac{1}{\sigma^2/2} \mathbf{I}_{2MT} - \frac{1}{(\sigma^2/2)^2} \mathbf{A}(\tilde{\mathbf{h}}_i) \mathbf{\Lambda}_{\mathbf{s}_i} \left(\mathbf{I}_{2K} + \frac{\|\tilde{\mathbf{h}}_i\|^2}{(\sigma^2/2)} \mathbf{\Lambda}_{\mathbf{s}_i} \right)^{-1} \mathbf{A}(\tilde{\mathbf{h}}_i)^T. \quad (3.43)$$

Substituting (3.43) in (3.42) and dropping the term which does not depend on the vector $\tilde{\mathbf{h}}_i$, we obtain

$$\hat{\mathbf{h}}_{i,\text{KCM}} = \arg \max_{\tilde{\mathbf{h}}_i} \left\{ \text{tr} \left(\mathbf{A}(\tilde{\mathbf{h}}_i) \mathbf{\Lambda}_{\mathbf{s}_i} \left(\mathbf{I}_{2K} + \frac{\|\tilde{\mathbf{h}}_i\|^2}{(\sigma^2/2)} \mathbf{\Lambda}_{\mathbf{s}_i} \right)^{-1} \mathbf{A}(\tilde{\mathbf{h}}_i)^T \hat{\mathbf{R}} \right) - \log \det \left(\mathbf{R}(\tilde{\mathbf{h}}_i) \right) \right\}. \quad (3.44)$$

The $(\log \det (\mathbf{R}(\tilde{\mathbf{h}}_i)))$ term in (3.44) depends on the product of eigenvalues of the true covariance matrix which in turn depends on the norm of CFR vector and not its spatial signature. Hence, this term becomes constant and can be dropped if we again consider the norm constraint such as in (3.38). Hence, using (2.43), we have that (3.44) is equivalent to

$$\hat{\mathbf{h}}_{i,\text{KCM}} = \arg \max_{\tilde{\mathbf{h}}_i} \tilde{\mathbf{h}}_i^T \mathbf{\Phi}^T \left(\mathbf{\Lambda}_{\mathbf{s}_i} \left(\mathbf{I}_{2K} + \frac{\|\tilde{\mathbf{h}}_i\|^2}{(\sigma^2/2)} \mathbf{\Lambda}_{\mathbf{s}_i} \right)^{-1} \otimes \hat{\mathbf{R}}_i \right) \mathbf{\Phi} \tilde{\mathbf{h}}_i, \quad (3.45)$$

with $\|\tilde{\mathbf{h}}_i\| = \|\mathbf{h}_i\|$. Considering the Kronecker matrix product property, (2.44), (3.4) and (3.34), we define

$$\begin{aligned}\hat{\mathcal{X}}_i(\gamma_{\text{KCM}}) &\triangleq \mathbf{\Phi}^T \left(\mathbf{\Lambda}_{\mathbf{s}_i} \left(\mathbf{I}_{2K} + \frac{\|\tilde{\mathbf{h}}_i\|^2}{(\sigma^2/2)} \mathbf{\Lambda}_{\mathbf{s}_i} \right)^{-1} \otimes \hat{\mathbf{R}}_i \right) \mathbf{\Phi} \\ &= \frac{1}{P} \sum_{k=1}^{2K} \sum_{p=1}^P \frac{\text{E}\{|s_{ik}|^2\}}{1 + \text{E}\{|s_{ik}|^2\} \|\tilde{\mathbf{h}}_i\|^2 / (\sigma^2/2)} \tilde{\mathbf{y}}_i(k, p) \tilde{\mathbf{y}}_i(k, p)^T, \quad (3.46)\end{aligned}$$

$$[\gamma_{\text{KCM}}]_k \triangleq \frac{\text{E}\{|s_{ik}|^2\}}{1 + \text{E}\{|s_{ik}|^2\} \|\tilde{\mathbf{h}}_i\|^2 / (\sigma^2/2)}, \quad k = 1, \dots, 2K \quad (3.47)$$

to obtain

$$\hat{\mathbf{h}}_{i,\text{KCM}} = \arg \max_{\tilde{\mathbf{h}}_i} \tilde{\mathbf{h}}_i^T \hat{\mathcal{X}}_i(\gamma_{\text{KCM}}) \tilde{\mathbf{h}}_i. \quad (3.48)$$

Similarly as in (3.40), if the necessary condition (3.13) holds, the comparison of (3.47) and (3.14) shows that the specific selection for the proposed weighting strategy is offered by the KCM approach of [VS08b].

Remark 3.1: It is noteworthy to mention that the proposed channel estimation method based on finding the principal eigenvector of virtual snapshot weighted covariance matrix, e.g., (3.41) or (3.48), suffers from the sign ambiguity even if all non-scalar ambiguities are removed by the help of a proper weighting coefficients introduced in Section 3.3. Nevertheless, the former ambiguity is common in many blind detectors; see, e.g., [CMC08], [SGM05], [VSPV09], and can be resolved by appropriate decoding of each symbol sequence [TVP96]. Also, pilot symbols can be exploited to resolve the sign ambiguity.

3.4 Simulations

In this section, we compare the performance of the weighting strategies proposed in this chapter with that of the technique of [SGM05] both with and without the linear precoding and the ECM and the KCM methods of [VS08b] in the Rayleigh fading frequency flat MIMO

channel scenario. In fact, almost similar results can be expected for the frequency-selective fading channel scenario when the OFDM encoding is implemented and the aforementioned techniques are applied in the frequency-domain subcarrier-wise. In each simulation run, the entries of \mathbf{h}_i are independently drawn from a Gaussian distribution with zero mean and variance of $\sigma_{\mathbf{h}_i}^2$ and kept fixed for this run. In other words, the channel remains invariant over the number of data blocks, i.e., P , that are used to compute the sample covariance matrix. All curves are averaged over 200 Monte-Carlo channel realizations and the SNR is defined as $\sigma_{\mathbf{h}_i}^2/\sigma^2$ [SL02]. The bias of the estimates, computed for a fixed CFR vector \mathbf{h}_i as the norm of averaged channel estimation errors

$$\text{Bias} = \left\| \frac{1}{N_{\text{runs}}} \sum_{m=1}^{N_{\text{runs}}} \frac{\hat{\mathbf{h}}_i^{(m)}}{\|\hat{\mathbf{h}}_i^{(m)}\|} - \frac{\mathbf{h}_i}{\|\mathbf{h}_i\|} \right\|, \quad (3.49)$$

where N_{runs} is the number of Monte-Carlo runs and $\hat{\mathbf{h}}_i^{(m)}$ is the estimate of \mathbf{h}_i in the m th run for the methods tested versus SNRs is shown in figures. Also, for different channel realizations, the root mean square estimation error (RMSE), i.e.,

$$\text{RMSE} = \sqrt{\frac{1}{N_{\text{runs}}} \sum_{m=1}^{N_{\text{runs}}} \left\| \frac{\hat{\mathbf{h}}_i^{(m)}}{\|\hat{\mathbf{h}}_i^{(m)}\|} - \frac{\mathbf{h}_i^{(m)}}{\|\mathbf{h}_i^{(m)}\|} \right\|^2}, \quad (3.50)$$

where $\mathbf{h}_i^{(m)}$ is the channel realization in the m th run for the methods tested versus SNRs is also displayed in figures. Moreover, the symbol error rates (SERs) versus the SNR for the methods tested combined with the ML decoder of (2.73) are depicted in figures. Additionally, the results for the informed ML decoder are shown in figures which is assumed to know the channel exactly. This decoder is used just as a benchmark to illustrate performance losses of the blind techniques with respect to the informed receiver case.

In the first set of numerical results, the full rate Alamouti OSTBC [Ala98], i.e.,

$$\mathbf{X}(\mathbf{s}_i) = \begin{bmatrix} s_{i1} & s_{i2} \\ -s_{i2}^* & s_{i1}^* \end{bmatrix}, \quad (3.51)$$

with $N = K = T = 2$, and QPSK symbols are used for encoding. Note that this code is rotatable and its blind identifiability is not guaranteed in Rayleigh fading channels according

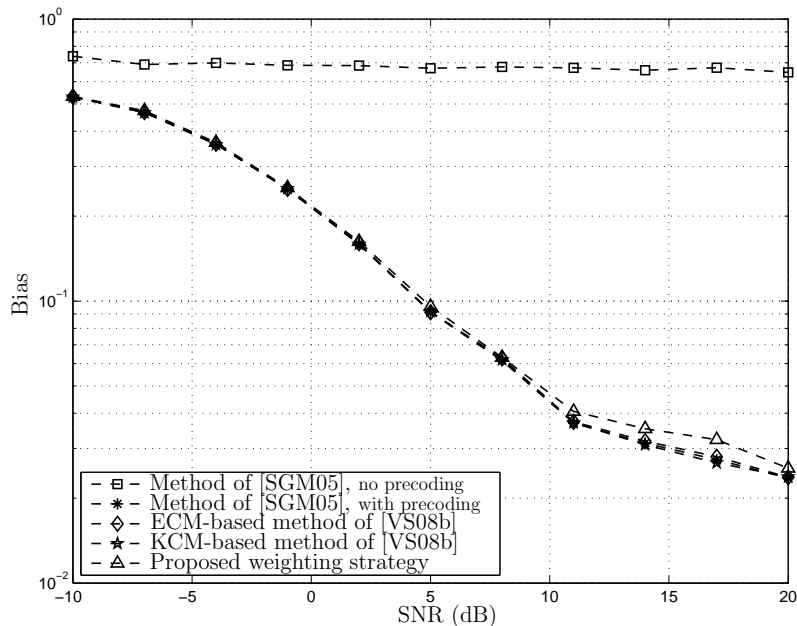


Figure 3.1: Bias versus SNR, first example, Alamouti code.

to [Ma07] and [VS08a], respectively. Further, the principal eigenvalue of $\mathcal{X}_i(\gamma_u)$ shows multiplicity of order four either in the case of $M = 1$ or for the cases when $M > 1$ according to Table 3.1, the code index 3. The number of data blocks that are used to estimate the covariance matrix according to (3.34) is set to $P = 50$. In the current numerical example, it is assumed that the transmit covariance matrix in (3.32) is selected as $\mathbf{\Lambda}_{\underline{s}_i} = \frac{2K}{15} \text{diag}([5, 5, 4, 1])$ that guarantees $\text{tr}(\mathbf{\Lambda}_{\underline{s}_i}) = 2K$, i.e., the average transmit power per symbol is equal to that with equi-power source. Further, this selection of $\mathbf{\Lambda}_{\underline{s}_i}$ satisfies the necessary condition provided in (3.13). The vector γ associated with the proposed weighting strategy in Lemma 3.1 is also selected as $\gamma = [4, 4, 3, 2]$ which is in accordance with (3.14). In addition, γ_{ECM} and γ_{KCM} are chosen according to (3.40) and (3.47), respectively, and the linear precoding matrix in [SGM05] is selected as a diagonal matrix with the square root of entries of $\mathbf{\Lambda}_{\underline{s}_i}$ on its main diagonal.

It can be seen from Fig.3.1-Fig.3.3 that for the aforementioned particular choice of the transmitted covariance matrix and the weight vector γ the approach of [SGM05] with

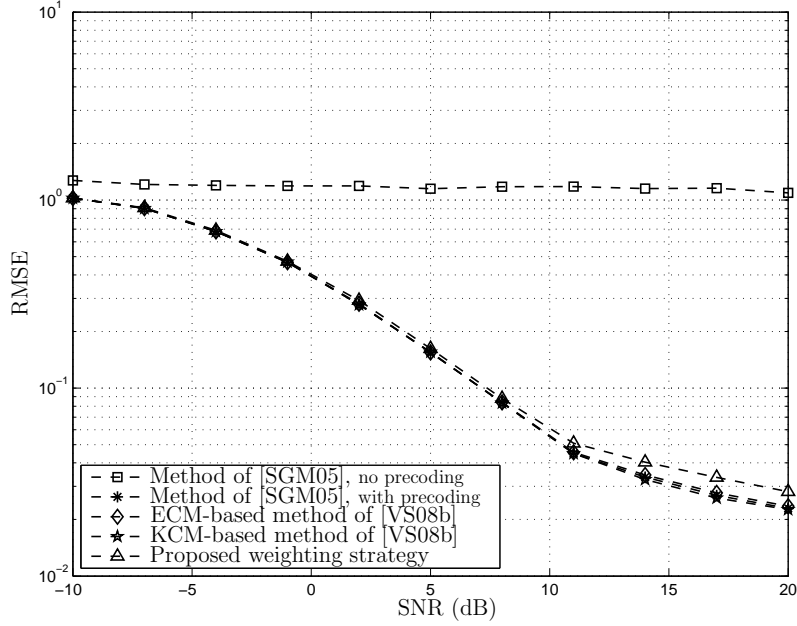


Figure 3.2: RMSE versus SNR, first example, Alamouti code.

uniform weighting is not able to resolve the ambiguity corresponding to use of the rotatable OSTBC while the other methods resolve the ambiguities. This is due to the fact that not only the necessary condition of (3.13) over the transmitted symbol powers holds true, but also the choices of weight vectors in all the methods tested satisfy the sufficient condition (3.14). Moreover, the performance of all methods that satisfy conditions of Lemma 3.1 is comparable and the corresponding SER performances closely achieve that of the informed ML detector.

In the second set of numerical results, the 3/4-rate OSTBC [LS03, Equation (7.4.10)] corresponding to the code index 18 in Table 3.1, i.e.,

$$\mathbf{X}(\mathbf{s}_i) = \begin{bmatrix} s_{i1} & 0 & -s_{i2}^* & s_{i3}^* \\ 0 & s_{i1} & -s_{i3} & -s_{i2} \\ s_{i2} & s_{i3}^* & s_{i1}^* & 0 \\ -s_{i3} & s_{i2}^* & 0 & s_{i1}^* \end{bmatrix}, \quad (3.52)$$

with $N = 4, K = 3, T = 4$, and QPSK symbols are used for encoding. It should be noted

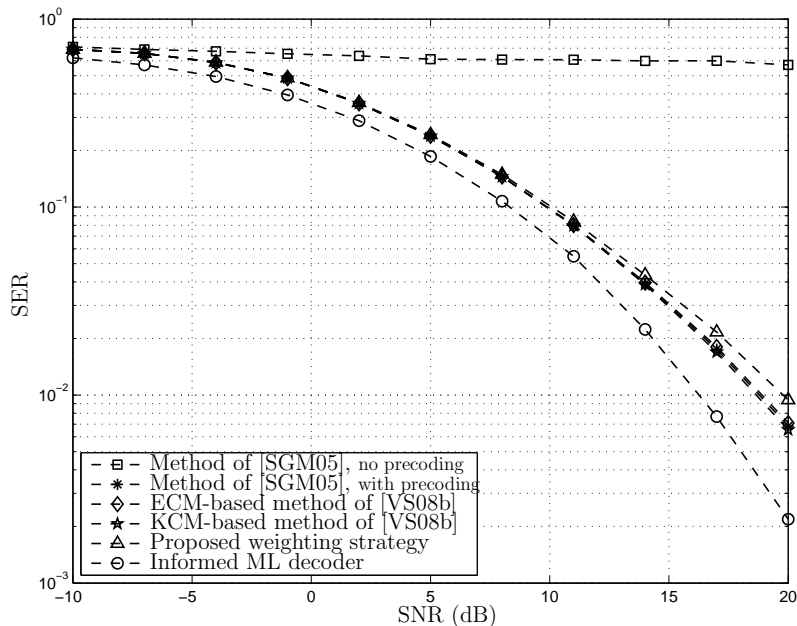
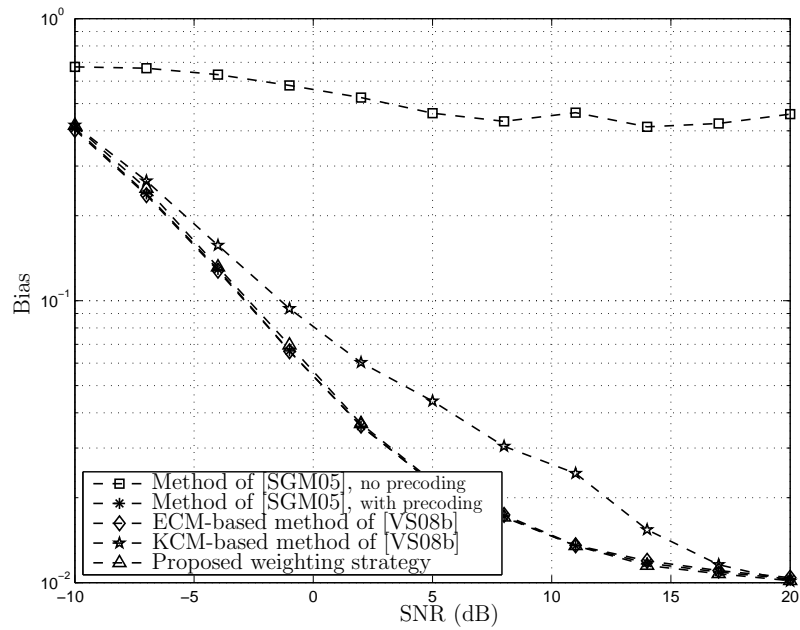
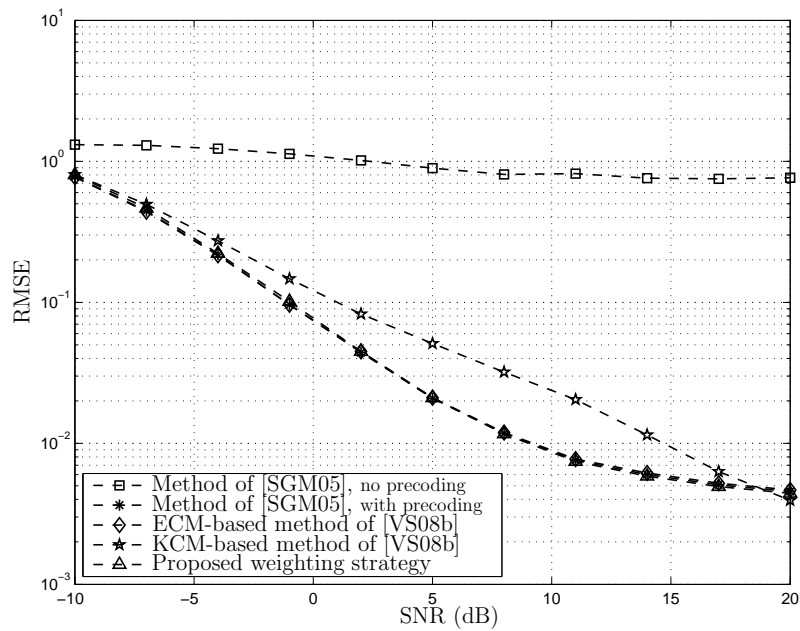


Figure 3.3: SER versus SNR, first example, Alamouti code.

that this code is not rotatable and the principal eigenvalue of $\mathcal{X}_i(\gamma_u)$ shows multiplicity of order two when $M = 1$ and one when $M > 1$ according to Table 3.1 for the code index 18. The transmit covariance matrix is selected as $\mathbf{\Lambda}_{\mathbf{s}_i} = \frac{2K}{8}\text{diag}([5, 1, 1, 1])$. This choice again guarantees $\text{tr}(\mathbf{\Lambda}_{\mathbf{s}_i}) = 2K$ and satisfies the necessary condition provided in (3.25). The vector γ associated with the proposed weighting strategy is also selected as $\gamma = [3, 1, 1, 1]$, which is in accordance with (3.26) and it is assumed that $P = 50$. Further, the selection of weight coefficients for ECM, KCM, and the precoding method of [SGM05] is same as the first simulation setup.

Fig.3.4-Fig.3.6 illustrate performance of the methods tested when $M = 1$. It can be observed from these figures that the method of [SGM05] with equal weighting can not resolve non-scalar ambiguity as expected before hand. Moreover, although the estimation bias and RMSE corresponding to the KCM method of [VS08b] are higher than that of all the other methods which are able to resolve non-scalar ambiguity, the SER performance of all blind methods are almost similar and very close to that of the informed receiver.

Figure 3.4: Bias versus SNR, second example, $M = 1$.Figure 3.5: RMSE versus SNR, second example, $M = 1$.

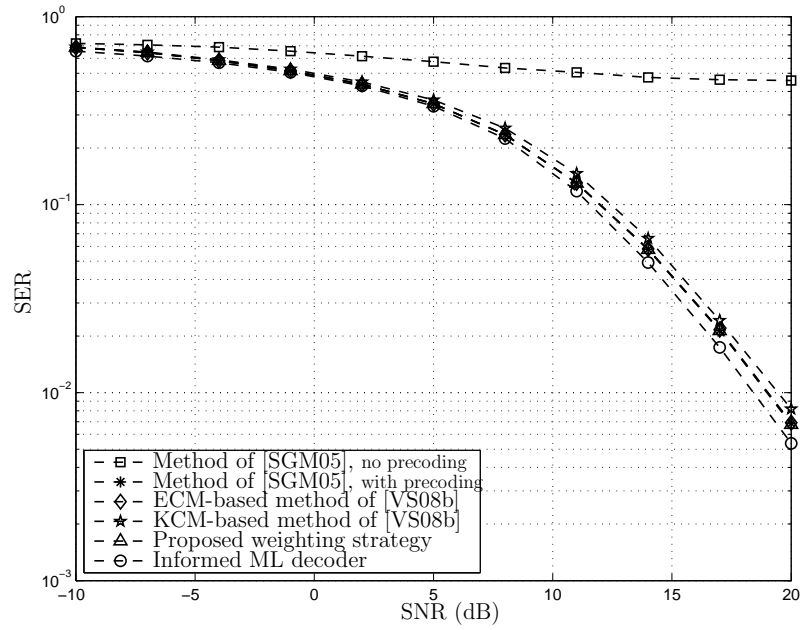


Figure 3.6: SER versus SNR, second example, $M = 1$.

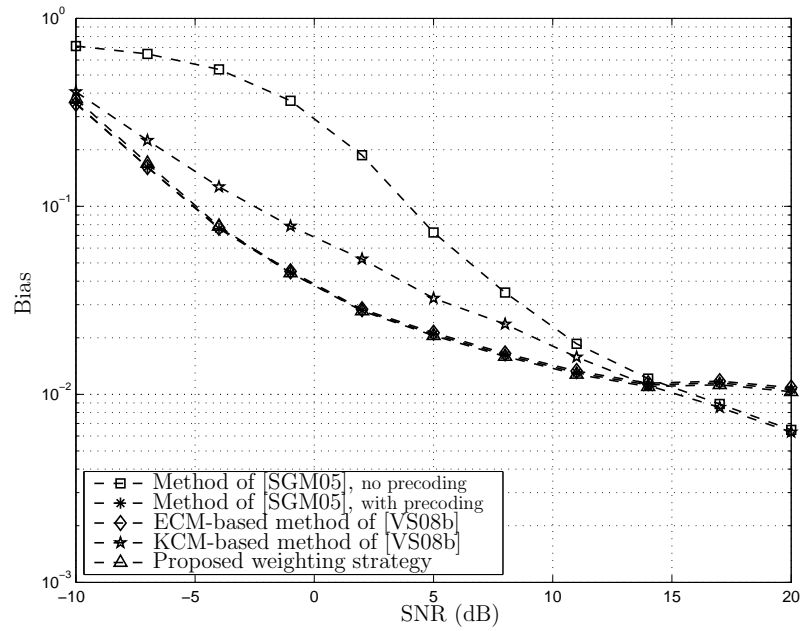


Figure 3.7: Bias versus SNR, second example, $M = 2$.

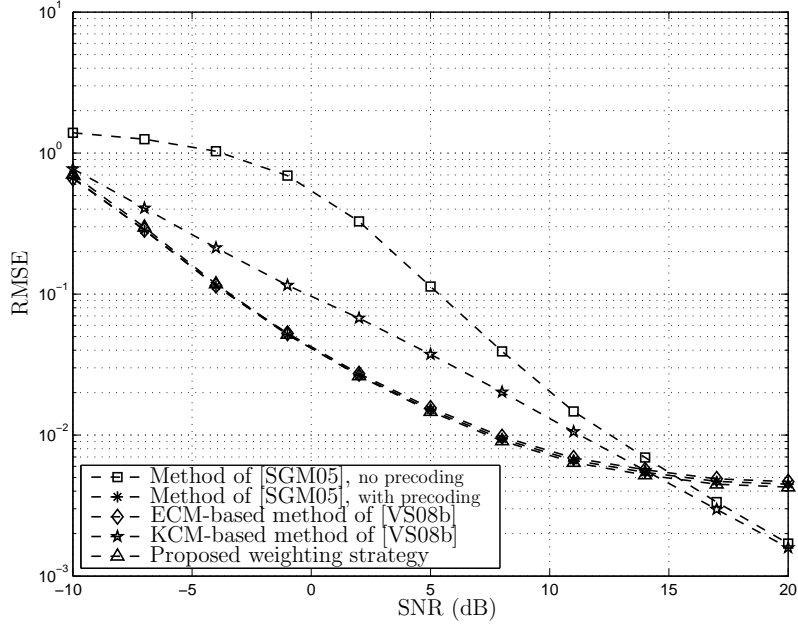
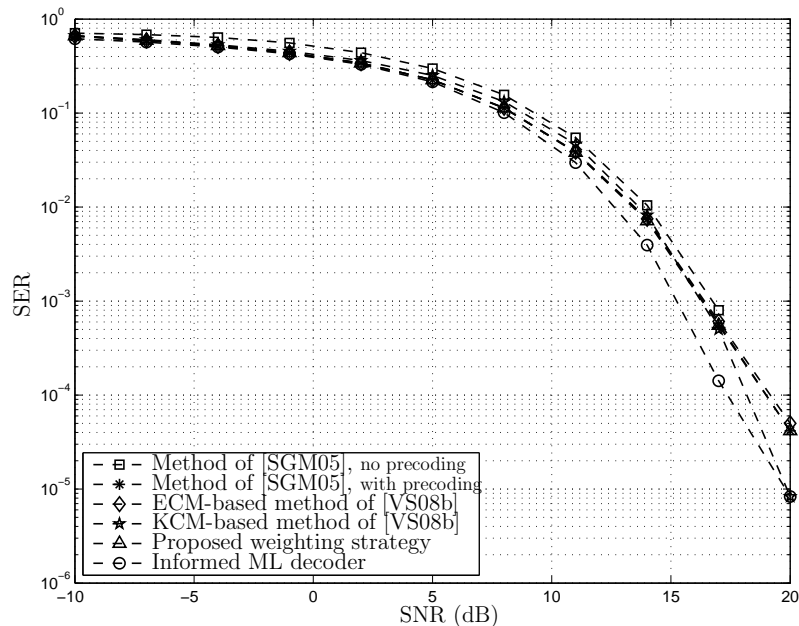
Figure 3.8: RMSE versus SNR, second example, $M = 2$.

Fig.3.7-Fig.3.9 depict the performance of the methods tested for $M = 2$ receive antennas. All the other parameters are same as the previous example. In this case according to Table 3.1 for the code index 18, the principal eigenvalue of $\mathcal{X}_i(\gamma_u)$ does not show multiplicity and essentially there is no need to assume that the covariance matrix of the transmitted symbols is not a scaled version of the identity matrix. This assumption is only considered to show the performance differences among different methods. It can be seen from Fig.3.7 and Fig.3.8 that as there is no non-scalar ambiguity, all methods are capable to estimate the true CFR. At low SNRs, the performance of the method of [SGM05] with equal weighting and the KCM method of [VS08b] is worse than that of the others while at high SNRs, it is the other way around. In Fig.3.9 the SER performance of all methods are shown to be comparable to that of the informed ML receiver. It is noteworthy to stress that the presented numerical results correspond to the particular choices of the transmitted covariance matrices and the weight vectors although nearly the same relative performances can be expected for a different set of choices as shown by our extensive simulations not displayed in this thesis.

Figure 3.9: SER versus SNR, second example, $M = 2$.

3.5 Chapter summary

We have introduced a novel virtual snapshot model in which the redundancies embedded in the OSTBCs are exploited. Specific properties of the OSTBCs have been used to compose the weighted covariance matrix of the received data vector for each single-carrier that exhibits the desired signal subspace characteristics. Further, we have proved that the vector of true CFR parameters is a scaled version of the normalized principal eigenvector of the obtained virtual snapshot covariance matrix. It has been shown both numerically and analytically that this matrix exhibits the principal eigenvalue multiplicity in two practically important cases: systems employing the rotatable OSTBCs like the popular Alamouti code as in the LTE and systems with single-antenna receivers as in the downlink transmission to mobile handsets. For these scenarios, two weighting strategies have been devised, respectively. Also, their ability in resolving the problem of non-scalar ambiguities of channel estimates associated with the aforementioned multiplicity of the principal eigenvalue,

provided that specific conditions on the weighting coefficients and the symbol powers are satisfied, have been proved. The proposed weighting strategies comprise the linear precoding scheme of [SGM05], and the correlation matching method of [VS08b] as their particular cases. Simulation results have demonstrated the ability of the proposed methods to eliminate non-scalar ambiguities inherent to existing blind MIMO channel estimation techniques.

Chapter 4

Blind channel estimation in orthogonally coded MIMO-OFDM systems: Multi-carrier analysis

4.1 Introduction

In this chapter, a new closed-form blind channel estimation approach for orthogonally space-time coded MIMO-OFDM systems is developed. We use the previously devised virtual snapshot model along with a novel normalization method to preserve the desired property of the subcarrier CFR vector introduced in Chapter 3 for all subcarriers. Then, we exploit the finite delay spread assumption of the wireless channel to estimate a lower number of channel parameters in the time-domain rather than in the frequency-domain. As a consequence, increased parsimony of the channel parametric model and coherent processing among different subcarriers compared to the conventional subcarrier-wise channel estimation methods is achieved.

These advantages not only offer a substantially reduced computational complexity, but also result in improved estimation accuracy. Moreover, they guarantee uniqueness of the

channel estimates under certain conditions. In contrast to the technique of [CMC08], the proposed method is applicable to more than one OSTBC-OFDM data block, and its associated complexity is independent of the symbol constellation size. At the same time, unlike many existing blind and semi-blind MIMO-OFDM symbol detection techniques (such as, e.g., [BHP02], [LGBS01], [LSL03], [MVDC06], [SGM05], [SL02], [VTP97], [WZS08], [ZMG02]), the proposed method does not require the channel to be static over many data blocks, i.e., it works sufficiently well with only a few blocks.

Moreover, the proposed technique has no limitations on the numbers of receive or transmit antennas observed in many other methods. Numerical examples demonstrate performance advantages of the proposed approach as compared to some state-of-the-art blind MIMO-OFDM channel estimation methods.

4.2 Coherent processing

In Chapter 3, it is proved that the true CFR vector lies in the subspace spanned by the principal eigenvector (or eigenvectors in the case of the principal eigenvalue multiplicity) of the virtual snapshots covariance matrix at each subcarrier. Since any probable principal eigenvalue multiplicity of $\mathcal{X}_i(\boldsymbol{\gamma})$ can be eliminated by applying weighting strategies proposed in the previous chapter, we assume that the true CFR vector at each subcarrier lies in the subspace spanned by the unique principal eigenvector of $\mathcal{X}_i(\boldsymbol{\gamma})$. The approach introduced in the previous chapter can be used to estimate the CFR vector for each subcarrier independently. However, independent processing of the subcarriers does not take into account any correlations among subcarriers that exists if the coherence bandwidth of the channel is larger than the subcarrier spacing.

To keep the aforementioned principal eigenvector properties of the single-carrier weighted covariance matrices and to exploit the correlation among subcarriers of the MIMO-OFDM system, we generalize the covariance model introduced in (3.4). To this aim, we define the block diagonal extended covariance matrix $\mathcal{X}'(\boldsymbol{\gamma}, \boldsymbol{\xi})$ as

$$\mathcal{X}'(\boldsymbol{\gamma}, \boldsymbol{\xi}) \triangleq \begin{bmatrix} \frac{\mathcal{X}_0(\boldsymbol{\gamma})}{\xi_0} & \mathbf{0} & \cdots & \mathbf{0} \\ \mathbf{0} & \frac{\mathcal{X}_1(\boldsymbol{\gamma})}{\xi_1} & & \mathbf{0} \\ \vdots & & \ddots & \vdots \\ \mathbf{0} & \cdots & \mathbf{0} & \frac{\mathcal{X}_{N_0-1}(\boldsymbol{\gamma})}{\xi_{N_0-1}} \end{bmatrix}, \quad (4.1)$$

where $\boldsymbol{\xi} \triangleq [\xi_0, \dots, \xi_{N_0-1}]^T$ and $\{\xi_i\}_{i=0}^{N_0-1}$ are arbitrary positive real scalars. It should be noted that in (4.1), the N_0 scalars $\{\xi_i\}_{i=0}^{N_0-1}$ are exploited as *normalization* coefficients for corresponding subcarrier covariance matrices. The effect of normalization coefficients choices on channel estimator will become more clear when we select different $\{\xi_i\}_{i=0}^{N_0-1}$ and discuss corresponding implications in the current and next chapters. First, let us choose

$$\boldsymbol{\xi} = \boldsymbol{\xi}_{\lambda_{\max}} \triangleq \left[\lambda_{\max}(\mathcal{X}_0(\boldsymbol{\gamma})), \dots, \lambda_{\max}(\mathcal{X}_{N_0-1}(\boldsymbol{\gamma})) \right]^T, \quad (4.2)$$

i.e., $\xi_i = \lambda_{\max}(\mathcal{X}_i(\boldsymbol{\gamma}))$ for $i = 0, \dots, N_0 - 1$. It can be readily verified that $\mathcal{X}'(\boldsymbol{\gamma}, \boldsymbol{\xi}_{\lambda_{\max}})$ has N_0 identical principal eigenvalues equal to one as each subcarrier covariance matrix in (4.1) is normalized by its respective principal eigenvalue. Moreover, its associated principal eigenvectors can be, e.g., represented as

$$\begin{aligned} \tilde{\mathbf{u}}_0 &\triangleq \left[\mathbf{u}_0^T, \mathbf{0}_{1 \times 2MN}, \dots, \mathbf{0}_{1 \times 2MN} \right]^T = \left[\frac{\mathbf{h}_0^T}{\|\mathbf{h}_0\|}, \mathbf{0}_{1 \times 2MN}, \dots, \mathbf{0}_{1 \times 2MN} \right]^T, \\ \tilde{\mathbf{u}}_1 &\triangleq \left[\mathbf{0}_{1 \times 2MN}, \mathbf{u}_1^T, \dots, \mathbf{0}_{1 \times 2MN} \right]^T = \left[\mathbf{0}_{1 \times 2MN}, \frac{\mathbf{h}_1^T}{\|\mathbf{h}_1\|}, \dots, \mathbf{0}_{1 \times 2MN} \right]^T, \\ &\vdots \\ \tilde{\mathbf{u}}_{N_0-1} &\triangleq \left[\mathbf{0}_{1 \times 2MN}, \dots, \mathbf{0}_{1 \times 2MN}, \mathbf{u}_{N_0-1}^T \right]^T = \left[\mathbf{0}_{1 \times 2MN}, \dots, \mathbf{0}_{1 \times 2MN}, \frac{\mathbf{h}_{N_0-1}^T}{\|\mathbf{h}_{N_0-1}\|} \right]^T. \end{aligned} \quad (4.3)$$

To show this, first we observe that all vectors $\{\tilde{\mathbf{u}}_i\}_{i=0}^{N_0-1}$ are orthogonal to each other and each of them satisfies the corresponding characteristic equation, i.e.,

$$\begin{aligned} \mathcal{X}'(\boldsymbol{\gamma}, \boldsymbol{\xi}_{\lambda_{\max}}) \tilde{\mathbf{u}}_i &= \left[\mathbf{0}_{1 \times 2MN}, \dots, \frac{\mathcal{X}_i(\boldsymbol{\gamma})}{\lambda_{\max}(\mathcal{X}_i(\boldsymbol{\gamma}))} \mathbf{u}_i, \dots, \mathbf{0}_{1 \times 2MN} \right]^T \\ &= \left[\mathbf{0}_{1 \times 2MN}, \dots, \mathbf{u}_i, \dots, \mathbf{0}_{1 \times 2MN} \right]^T = \lambda_{\max}(\mathcal{X}'(\boldsymbol{\gamma}, \boldsymbol{\xi}_{\lambda_{\max}})) \tilde{\mathbf{u}}_i = \tilde{\mathbf{u}}_i. \end{aligned} \quad (4.4)$$

As a result, any arbitrary linear combination of the principal eigenvectors in (4.3) as

$$\mathring{\mathbf{h}} \triangleq \alpha_0 \tilde{\mathbf{u}}_0 + \alpha_1 \tilde{\mathbf{u}}_1 + \cdots + \alpha_{N_0-1} \tilde{\mathbf{u}}_{N_0-1} = \tilde{\mathbf{U}} \boldsymbol{\alpha}, \quad (4.5)$$

in which $\boldsymbol{\alpha} \triangleq [\alpha_0, \dots, \alpha_{N_0-1}]^T$ and $\tilde{\mathbf{U}} \triangleq [\tilde{\mathbf{u}}_0, \dots, \tilde{\mathbf{u}}_{N_0-1}]$, is a principal eigenvector of $\mathcal{X}'(\boldsymbol{\gamma}, \boldsymbol{\xi}_{\lambda_{\max}})$ with respective eigenvalue $\lambda_{\max}(\mathcal{X}'(\boldsymbol{\gamma}, \boldsymbol{\xi}_{\lambda_{\max}})) = 1$, i.e.,

$$\mathcal{X}'(\boldsymbol{\gamma}, \boldsymbol{\xi}_{\lambda_{\max}}) \hat{\mathbf{h}} = \lambda_{\max}(\mathcal{X}'(\boldsymbol{\gamma}, \boldsymbol{\xi}_{\lambda_{\max}})) \hat{\mathbf{h}} = \hat{\mathbf{h}}. \quad (4.6)$$

As a special case of (4.5), the true overall CFR vector defined in (2.33), which can be written as

$$\mathbf{h}' = \|\mathbf{h}_0\| \tilde{\mathbf{u}}_0 + \|\mathbf{h}_1\| \tilde{\mathbf{u}}_1 + \dots + \|\mathbf{h}_{N_0-1}\| \tilde{\mathbf{u}}_{N_0-1},$$

is the principal eigenvector of the extended covariance matrix in (4.1) with the corresponding eigenvalue $\lambda_{\max}(\mathcal{X}'(\boldsymbol{\gamma}, \boldsymbol{\xi}_{\lambda_{\max}})) = 1$, i.e.,

$$\mathcal{X}'(\boldsymbol{\gamma}, \boldsymbol{\xi}_{\lambda_{\max}}) \mathbf{h}' = \lambda_{\max}(\mathcal{X}'(\boldsymbol{\gamma}, \boldsymbol{\xi}_{\lambda_{\max}})) \mathbf{h}' = \mathbf{h}'. \quad (4.7)$$

It can be directly observed from (4.3)-(4.6) that the principal eigenvectors of the extended covariance matrix $\mathcal{X}'(\boldsymbol{\gamma}, \boldsymbol{\xi}_{\lambda_{\max}})$ are formed from the principal eigenvectors of the subcarrier covariance matrices $\mathcal{X}_i(\boldsymbol{\gamma})$ which are the CFRs at each subcarrier, i.e., the vectors \mathbf{u}_i for $i = 0, \dots, N_0 - 1$ in (3.5). This important property results from the fact that subcarrier covariance matrices in (4.1) are normalized by their respective principal eigenvalues. This property is still valid when the true subcarrier covariance matrices in (4.1) are replaced by their corresponding finite sample estimates

$$\hat{\mathcal{X}}_i(\boldsymbol{\gamma}) \triangleq \frac{1}{P} \sum_{k=1}^{2K} \sum_{p=1}^P \gamma_k \tilde{\mathbf{y}}_i(k, p) \tilde{\mathbf{y}}_i(k, p)^T, \quad i = 0, \dots, N_0 - 1 \quad (4.8)$$

where P stands for the total number of available snapshots as in (3.34). It should be noted that due to the block diagonal structure of $\mathcal{X}'(\boldsymbol{\gamma}, \boldsymbol{\xi}_{\lambda_{\max}})$, there is no coherent processing among different subcarriers in estimation of \mathbf{h}' .

Taking into account the linear relation among the CFRs and the CIRs in (2.31) and also the orthogonality property of the DFT matrix \mathcal{F} defined in (2.35), equation (4.7) can be expressed as

$$\mathcal{F}^T \mathcal{X}'(\boldsymbol{\gamma}, \boldsymbol{\xi}_{\lambda_{\max}}) \mathcal{F} \mathbf{g}' = \lambda_{\max}(\mathcal{X}'(\boldsymbol{\gamma}, \boldsymbol{\xi}_{\lambda_{\max}})) \mathcal{F}^T \mathcal{F} \mathbf{g}' = \lambda_{\max}(\mathcal{X}'(\boldsymbol{\gamma}, \boldsymbol{\xi}_{\lambda_{\max}})) N_0 \mathbf{g}'. \quad (4.9)$$

Therefore, the true overall CIR vector \mathbf{g}' defined as (2.32) is proportional to the normalized principal eigenvector of $\mathcal{F}^T \mathcal{X}'(\gamma, \boldsymbol{\xi}_{\lambda_{\max}}) \mathcal{F}$ with the respective principal eigenvalue $\left(\lambda_{\max}(\mathcal{X}'(\gamma, \boldsymbol{\xi}_{\lambda_{\max}}))N_0\right)$ of multiplicity order N_0 . In fact, we have shown that making use of virtual snapshot model (3.1) and definition (4.1) along with the specific choice of normalization coefficients in (4.2), the true overall CIR vector \mathbf{g}' satisfies the following characteristic equation

$$\left(\mathcal{F}^T \mathcal{X}'(\gamma, \boldsymbol{\xi}_{\lambda_{\max}}) \mathcal{F}\right) \tilde{\mathbf{g}} = \left(\lambda_{\max}(\mathcal{X}'(\gamma, \boldsymbol{\xi}_{\lambda_{\max}}))N_0\right) \tilde{\mathbf{g}}, \quad (4.10)$$

with

$$\tilde{\mathbf{g}} \triangleq \left[\tilde{\mathbf{g}}_0^T, \dots, \tilde{\mathbf{g}}_{N_0-1}^T\right]^T, \quad (4.11)$$

as the $2MN_0 \times 1$ vector of the time-domain variables. To reduce the solution set of the principal eigenvectors in (4.10), we exploit correlations among subcarriers that exist if the coherence bandwidth of the channel is larger than the subcarrier spacing. To do this, we enforce the finite delay spread assumption in (2.32) by introducing the equations

$$\tilde{\mathbf{g}}_{N_0-(L'+1)} = \dots = \tilde{\mathbf{g}}_{N_0-1} = \mathbf{0}_{2MN \times 1}, \quad (4.12)$$

for $L' \geq L$ where L' denotes the assumed channel length upper bound at the receiver. To find the true overall CIR vector by solving the characteristic equation (4.10) together with equations (4.12), we can equivalently solve the following optimization problem

$$\begin{aligned} \hat{\mathbf{g}} &\triangleq \arg \max_{\tilde{\mathbf{g}}} \tilde{\mathbf{g}}^T \mathcal{F}^T \mathcal{X}'(\gamma, \boldsymbol{\xi}_{\lambda_{\max}}) \mathcal{F} \tilde{\mathbf{g}} \\ \text{s.t.} \quad &\tilde{\mathbf{g}}_{N_0-(L'+1)} = \dots = \tilde{\mathbf{g}}_{N_0-1} = \mathbf{0}_{2MN \times 1} \\ &\|\tilde{\mathbf{g}}\|^2 = \|\mathbf{g}'\|^2, \end{aligned} \quad (4.13)$$

since \mathbf{g}' also resides in the solution set of (4.13). It should be emphasized again that the solution of (4.13) is not unique since the principal eigenvalue of $\mathcal{F}^T \mathcal{X}'(\gamma, \boldsymbol{\xi}_{\lambda_{\max}}) \mathcal{F}$ has multiplicity order of N_0 . The corresponding conditions for uniqueness of the vector satisfying both (4.10) and (4.12) or for the solution uniqueness of their counterpart optimization problem (4.13) will be derived in the next section.

4.3 Uniqueness condition

To derive the uniqueness condition for the proposed blind channel estimation method of (4.13), we assume that the true CFR vector at each subcarrier lies in the subspace spanned by the unique principal eigenvector of $\mathcal{X}_i(\gamma)$ since any probable principal eigenvalue multiplicity of $\mathcal{X}_i(\gamma)$ can be resolved by applying weighting strategies proposed in Section 3.3. Using (2.31) along with (4.6) we obtain

$$\left(\mathcal{F}^T \mathcal{X}'(\gamma, \boldsymbol{\xi}_{\lambda_{\max}}) \mathcal{F}\right) \mathring{\mathbf{g}} = \left(\lambda_{\max} \left(\mathcal{X}'(\gamma, \boldsymbol{\xi}_{\lambda_{\max}})\right) N_0\right) \mathring{\mathbf{g}},$$

and, therefore, making use of (4.5), any vector satisfying (4.10) or any solution of (4.13) including the true overall CIR vector \mathbf{g}' can be expressed as

$$\mathring{\mathbf{g}} = \mathcal{F}^T \tilde{\mathbf{U}} \boldsymbol{\alpha}. \quad (4.14)$$

Let us define $2MN N_0 \times 2MN$ selection matrix \mathbf{J}_i as

$$\mathbf{J}_i \triangleq \left[\mathbf{0}_{2MN} \mid \cdots \mid \overbrace{\mathbf{I}_{2MN}}^{(i+1)\text{-th block}} \mid \cdots \mid \mathbf{0}_{2MN} \right]^T, \quad i = 0, \dots, N_0 - 1 \quad (4.15)$$

which is a block matrix made of N_0 blocks of dimensions $2MN \times 2MN$ whose $(i+1)$ -th block is identity matrix and the rest are zero. Also, using (4.15) we define the following $2MN N_0 \times 2MN(N_0 - (L' + 1))$ selection matrix as

$$\mathcal{J}_{L'+1} \triangleq \left[\mathbf{J}_{L'+1}, \dots, \mathbf{J}_{N_0-1} \right]. \quad (4.16)$$

Making use of (4.14) and (4.16), the equations in (4.12) can be rewritten as

$$\mathcal{J}_{L'+1}^T \mathring{\mathbf{g}} = \mathcal{J}_{L'+1}^T \mathcal{F}^T \tilde{\mathbf{U}} \boldsymbol{\alpha} = \mathbf{0}_{2MN(N_0 - (L'+1)) \times 1}, \quad (4.17)$$

in which $\mathcal{J}_{L'+1}^T$ selects the last $2MN(N_0 - (L' + 1))$ entries of $\mathring{\mathbf{g}}$ that are equal to zero. Due to the fact that the matrix $\mathcal{J}_{L'+1}^T \mathcal{F}^T \tilde{\mathbf{U}}$ in (4.17) has $2MN(N_0 - (L' + 1))$ rows and N_0 columns, it can be deduced that if $(L' + 1) > N_0(2MN - 1)/(2MN)$, the homogeneous system of linear equations (4.17) becomes underdetermined. As a result, there may exist

more than one vector $\boldsymbol{\alpha}$, that solves the characteristic equation for the principal eigenvalue and also satisfies the conditions. On the contrary, if

$$(L' + 1) \leq N_0(2MN - 1)/(2MN), \quad (4.18)$$

the matrix $\mathcal{J}_{L'+1}^T \mathcal{F}^T \tilde{\mathbf{U}}$ is full-rank with probability one in the case of randomly fading channels, hence, there exist a unique solution for $\boldsymbol{\alpha}$. Thus, under the condition (4.18), adding the constraints (4.17) to the principal eigenvalue problem (4.9) eliminates the aforementioned multiplicity of the principal eigenvector and makes the true overall CIR vector \mathbf{g}' corresponding unique principal eigenvector.

It should be added that considering the finite delay spread of the wireless channel by augmenting the equations (4.17) to (4.9) results in considerable problem dimension reduction. To show this, let us introduce the following $2MNN_0 \times 2MN(L' + 1)$ selection matrix

$$\tilde{\mathcal{J}}_{L'+1} \triangleq [\mathbf{J}_0, \dots, \mathbf{J}_{L'}], \quad (4.19)$$

and

$$\tilde{\mathbf{g}}_{L'+1} \triangleq \tilde{\mathcal{J}}_{L'+1}^T \tilde{\mathbf{g}}, \quad (4.20)$$

which is formed by elimination of the last $2MN(N_0 - (L' + 1))$ entries of $\tilde{\mathbf{g}}$ in (4.11). Using (4.12), (4.19), and (4.20), for $L' \geq L$, we obtain

$$\tilde{\mathbf{g}} = \left[\tilde{\mathbf{g}}_{L'+1}^T, \mathbf{0}_{2MN(N_0 - (L'+1)) \times 1}^T \right]^T = \tilde{\mathcal{J}}_{L'+1} \tilde{\mathbf{g}}_{L'+1}. \quad (4.21)$$

By inserting (4.21) into (4.13), we have the following eigenproblem

$$\begin{aligned} \hat{\mathbf{g}}'_{L'+1} = & \arg \max_{\tilde{\mathbf{g}}_{L'+1}} \tilde{\mathbf{g}}_{L'+1}^T \left(\tilde{\mathcal{J}}_{L'+1}^T \mathcal{F}^T \mathcal{X}'(\gamma, \boldsymbol{\xi}_{\lambda_{\max}}) \mathcal{F} \tilde{\mathcal{J}}_{L'+1} \right) \tilde{\mathbf{g}}_{L'+1} \\ \text{s.t. } & \|\tilde{\mathbf{g}}_{L'+1}\|^2 = \|\mathbf{g}'\|^2, \end{aligned} \quad (4.22)$$

in which the constraints of (4.12) are essentially considered. So, it can be concluded that under condition (4.18) and for $L' \geq L$, the reduced size true overall CIR vector, i.e., $\mathbf{g}'_{L'+1} \triangleq \tilde{\mathcal{J}}_{L'+1}^T \mathbf{g}'$, can be obtained by scaling the unique normalized principal eigenvector of $\left(\tilde{\mathcal{J}}_{L'+1}^T \mathcal{F}^T \mathcal{X}'(\gamma, \boldsymbol{\xi}_{\lambda_{\max}}) \mathcal{F} \tilde{\mathcal{J}}_{L'+1} \right)$. It should be highlighted that utilizing the finite

delay spread assumption over the wireless channel in problem formulation (4.22) not only warrants the uniqueness of the solution as shown before, but also results in reducing problem dimension and in turn the computational complexity of the proposed method. This also eliminates part of the noise in the time-domain which exceeds the assumed upper bound on the wireless channel delay spread L' at the receiver side.

Remark 4.3.1: It is noteworthy to stress that the need for implementation of a precise channel order estimation method prior to the channel estimation scheme is lessened in the proposed method. This is due to the fact that in the proposed method, only an upper bound on the effective channel length at the receiver, L' , instead of the respective true value, L , is required. However, there is a trade-off between performance and model mismatch, i.e., over- or under-estimation of the effective channel length degrades the performance and yields a bias; see Figs 4.10-4.15 in Section 4.5.

Remark 4.3.2: As mentioned in Remark 3.1, the proposed channel estimation method of (4.22) suffers from the sign ambiguity. To eliminate the sign ambiguity, a few pilot symbols can be exploited in some or even only one of subcarriers and the other subcarriers benefit from these pilots due to coherent processing ability of the proposed method. This is in contrast to the subcarrier-wise approach in which each subcarrier is unable to take advantage of the pilot symbols in other subcarriers. This feature can be exploited further to eliminate non-scalar ambiguities by the aid of the proposed weighting strategies of Section 3.3; see Figs 4.16-4.18 in Section 4.5. To do this, a proper weighting coefficients can be applied to some (even one) of the subcarriers and the other subcarriers benefit from them. Obviously, this is another favorable feature of the proposed method compared to the subcarrier-wise schemes in which such pilot symbols or weighting coefficients have to be applied at each subcarrier.

Remark 4.3.3: As the norm of the true overall CIR vector \mathbf{g}' is unknown, corresponding estimated version should be used in the proposed estimator (4.22). First, by using the property of the received data covariance matrix \mathbf{R}_i presented in (3.32), it follows that

$$\begin{aligned}\mathrm{tr}(\mathbf{R}_i) &= \mathrm{tr}\left(\|\mathbf{h}_i\|^2 \mathbf{\Lambda}_{\underline{s}_i}\right) + \mathrm{tr}\left(\frac{\sigma^2}{2} \mathbf{I}_{2MT}\right) \\ &= \|\mathbf{h}_i\|^2 \mathrm{tr}(\mathbf{\Lambda}_{\underline{s}_i}) + \sigma^2 MT,\end{aligned}\quad (4.23)$$

and, therefore, $\|\mathbf{h}_i\|$ for $i = 0, \dots, N_0 - 1$ can be obtained as

$$\|\mathbf{h}_i\| = \sqrt{(\mathrm{tr}(\mathbf{R}_i) - MT\sigma^2)/\mathrm{tr}(\mathbf{\Lambda}_{\underline{s}_i})}. \quad (4.24)$$

Again, it should be noted that $\mathbf{\Lambda}_{\underline{s}_i}$ in (4.24) is assumed to be known as the symbol constellations are assumed to be known at the receiver. Then, taking into account the linear relation of (2.31) and based on the subcarrier CFR vector norm (4.24), the norm of \mathbf{g}' can be directly computed as

$$\|\mathbf{g}'\| = \sqrt{\frac{1}{N_0} \sum_{i=0}^{N_0-1} \|\mathbf{h}_i\|^2}. \quad (4.25)$$

In practice, the following estimates of (4.24) and (4.25)

$$\|\widehat{\mathbf{h}}_i\| = \sqrt{(\mathrm{tr}(\widehat{\mathbf{R}}_i) - MT\hat{\sigma}^2)/\mathrm{tr}(\widehat{\mathbf{\Lambda}}_{\underline{s}_i})}, \quad (4.26)$$

$$\|\widehat{\mathbf{g}}'\| = \sqrt{\frac{1}{N_0} \sum_{i=0}^{N_0-1} \|\widehat{\mathbf{h}}_i\|^2}, \quad (4.27)$$

can be used, respectively. Then, the true overall CIR vector \mathbf{g}' can be estimated from (4.22) and (4.27). This procedure amounts to solving the principal eigenvector problem in (4.22) and to subsequent rescaling the obtained principal eigenvector to guarantee that the respective norm is equal to $\|\widehat{\mathbf{g}}'\|$ computed in (4.27).

Remark 4.3.4: It is worth noting that if the constant modulus constellations, like PSK, are used for each of the encoded symbols, the channel vector norm is immaterial for the signal detection. This fact follows from the structural property of the linear receiver (2.73) and linearity of $\mathbf{A}(\mathbf{h}_i)$ with respect to \mathbf{h}_i according to (2.41). Hence, the norm constraint can be dropped in (4.22) or in general from eigenvalue problem in this case.

Remark 4.3.5: To compute the channel vector norm according to (4.24), we have considered that the noise power is known at the receiver. If constant modulus constellations are used for symbol encoding, according to Remark 4.3.4, knowledge of the noise power is

not required. Otherwise, this knowledge is required and can be approximated by averaging over the $(2MT - 2K)$ smallest eigenvalues of the sample covariance matrix $\hat{\mathbf{R}}_i$ provided that the total number of the data blocks used to compute the sample covariance matrix is large enough. The obtained estimate of the noise power can be used in (4.24) instead of σ^2 as in (4.26).

Remark 4.3.6: In current wireless communication standards such as LTE and WiMAX, pilot symbols are inserted in the data frame structure for various reasons. Regarding the proposed method in (4.22), a question is how to exploit these already available pilot symbols systematically to further improve channel estimates quality. The maximum eigenvalue problem estimates blindly the subspace which contains the true channel vector, irrespective of whether pilot symbols exist in the received data blocks or not. The rank of this subspace is or can be made, in the case of rotatable codes and some codes in the MISO scenario according to Table 3.1, equal to one. This can be done, e.g., by the aid of weighting coefficients discussed in Section 3.3 or by utilizing pilot symbols already available in the data frame structure. In the latter case, a modified semi-blind version of the proposed method can be devised. This semi-blind modification can be performed in two ways. In the first way, pilot symbols can be used to obtain a preliminary estimate of the channel vector and then, using the idea similar to that used in robust beamforming [CY92], [FG94], the so-obtained preliminary channel estimate can be improved by projecting it onto the blind subspace estimate achieved by the maximum eigenvalue problem. In the second way, the whole received data symbols, either pilots or non-pilots, can be used to obtain subspace containing the channel vector in a blind fashion and then pilots can be exploited to extract CSI from the attained subspace; see [SGG06] for more detail.

4.4 Normalization schemes comparison

In this section, the proposed normalization of the individual subcarrier covariance matrices introduced in (4.2) and the normalization scheme devised in [VSPV09] are compared. In the former approach, each subcarrier covariance matrix is normalized by the corresponding

principal eigenvalue $\lambda_{max}(\mathcal{X}_i(\gamma))$, $i = 0, \dots, N_0 - 1$. Doing this guarantees that the principal eigenvectors of the extended covariance matrix $\mathcal{X}'(\gamma, \xi_{\lambda_{max}})$ are made of the subcarrier covariance matrices principal eigenvectors, i.e., the vectors \mathbf{u}_i , for $i = 0, \dots, N_0 - 1$, as can be observed from (4.3). The mentioned property still holds true even if the finite sample estimates of subcarrier covariance matrices are replaced in (4.1). This important property does not necessarily hold true for different normalization strategies which generally result in a bias of the channel estimates. In the estimation method of [VSPV09], the signal subspace energy of the received data covariance matrix at the i th subcarrier is used as the normalization factor to normalize corresponding subcarrier covariance matrix.

To illustrate the difference in the various normalization schemes, we consider the special case of $P = 1$, i.e., single-snapshot, and prove that the aforementioned normalization schemes are not necessarily identical. For the single-snapshot scenario in which only one received data sample is used to estimate the i th subcarrier covariance matrix, the normalization factor in the proposed method of (4.22) for uniform weighting coefficients $\{\gamma_k\}_{k=1}^{2K} = 1$ using (2.43) and (2.44) is given by

$$\begin{aligned}
\xi_i = \lambda_{max}(\hat{\mathcal{X}}_i(\gamma)) &= \mathcal{P}\{\hat{\mathcal{X}}_i(\gamma)\}^T \left(\sum_{k=1}^{2K} \Phi_k^T \mathbf{y}_i(1) \mathbf{y}_i(1)^T \Phi_k \right) \mathcal{P}\{\hat{\mathcal{X}}_i(\gamma)\} \\
&= \mathcal{P}\{\hat{\mathcal{X}}_i(\gamma)\}^T \left(\Phi^T (\mathbf{I}_{2K} \otimes \mathbf{y}_i(1) \mathbf{y}_i(1)^T) \Phi \right) \mathcal{P}\{\hat{\mathcal{X}}_i(\gamma)\} \\
&= \text{tr} \left(\mathbf{A}^T (\mathcal{P}\{\hat{\mathcal{X}}_i(\gamma)\}) \mathbf{y}_i(1) \mathbf{y}_i(1)^T \mathbf{A} (\mathcal{P}\{\hat{\mathcal{X}}_i(\gamma)\}) \right) \\
&= \text{tr} \left(\mathbf{\Pi}_{\mathbf{A}(\mathcal{P}\{\hat{\mathcal{X}}_i(\gamma)\})} \mathbf{y}_i(1) \mathbf{y}_i(1)^T \right) \\
&= (\mathbf{A}(\mathbf{h}_i) \underline{\mathbf{s}}_i(1))^T \mathbf{\Pi}_{\mathbf{A}(\mathcal{P}\{\hat{\mathcal{X}}_i(\gamma)\})} (\mathbf{A}(\mathbf{h}_i) \underline{\mathbf{s}}_i(1)) \\
&\quad + 2 (\mathbf{A}(\mathbf{h}_i) \underline{\mathbf{s}}_i(1))^T \mathbf{\Pi}_{\mathbf{A}(\mathcal{P}\{\hat{\mathcal{X}}_i(\gamma)\})} \mathbf{v}_i(1) + \mathbf{v}_i(1)^T \mathbf{\Pi}_{\mathbf{A}(\mathcal{P}\{\hat{\mathcal{X}}_i(\gamma)\})} \mathbf{v}_i(1). \quad (4.28)
\end{aligned}$$

The signal subspace energy of the received data covariance matrix at the i th subcarrier which is equal to summation over the corresponding eigenvalues is used as the normalization factor in [VSPV09]. For the single-snapshot scenario due to the fact that the rank-one covariance matrix in (3.34), i.e., $\hat{\mathbf{R}}_i = \mathbf{y}_i(1) \mathbf{y}_i(1)^T$, has only one non-zero eigenvalue equal to $\|\mathbf{y}_i(1)\|^2$,

the i th normalization factor, i.e., ξ_i in (4.1), for $i = 0, \dots, N_0 - 1$, is equal to

$$\begin{aligned}\xi_i &= \|\mathbf{y}_i(1)\|^2 = \mathbf{y}_i(1)^T \mathbf{y}_i(1), \quad i = 0, \dots, N_0 - 1 \\ &= (\mathbf{A}(\mathbf{h}_i) \underline{\mathbf{s}}_i(1))^T (\mathbf{A}(\mathbf{h}_i) \underline{\mathbf{s}}_i(1)) + 2 (\mathbf{A}(\mathbf{h}_i) \underline{\mathbf{s}}_i(1))^T \mathbf{v}_i(1) + \mathbf{v}_i(1)^T \mathbf{v}_i(1).\end{aligned}\quad (4.29)$$

This can be explained by considering the following characteristics equation

$$\hat{\mathbf{R}}_i \mathbf{y}_i(1) = \left(\mathbf{y}_i(1) \mathbf{y}_i(1)^T \right) \mathbf{y}_i(1) = \|\mathbf{y}_i(1)\|^2 \mathbf{y}_i(1), \quad (4.30)$$

which holds true in this case. Comparing the expressions (4.28) and (4.29) reveals that in general the corresponding normalization factors are not equal. Also, it can be deduced from our extensive numerical examples that the same statement remains valid in the case of multiple snapshots. It should be noted that only for the asymptotic cases of perfect covariance matrices estimates, when $\hat{\mathcal{X}}_i(\gamma) = \mathcal{X}_i(\gamma)$ or in the absence of noise, the normalization factors of the proposed method (4.22) and that of the method of [VSPV09] become identical.

4.5 Simulations

In this section, we present the performance of the proposed blind channel estimator (4.22) in both the identifiable and non-identifiable [VS08a] scenarios. We compare the performance of the proposed estimator to that of the blind symbol detection method of [CMC08], the subcarrier-wise method of [SGM05], and the generalized eigenvalue estimator of [VSPV09] for Rayleigh fading frequency-selective channels. In the simulations, the entries of the vectors $\{\mathbf{g}_l\}_{l=0}^L$ defined in (2.28) are assumed to be independent and identically distributed (i.i.d.) random variables that are drawn from a Gaussian distribution with zero mean and variance $\sigma_{\mathbf{g}_l}^2$, and are assumed to be invariant during each simulation run. The SNR is defined as $\sigma_{\mathbf{h}_i}^2 / \sigma^2$ [SL02] and all curves are averaged over 200 Monte Carlo realizations. The estimation bias and the RMSE, which are defined in (3.49) and (3.50), respectively, and the SERs (or the BERs) are selected as measures to evaluate the estimation performance.

These measures are averaged over all subcarriers, e.g., the relation in (3.49) is modified as

$$\text{Bias} = \frac{1}{N_0} \sum_{i=0}^{N_0-1} \left\| \frac{1}{N_{\text{runs}}} \sum_{m=1}^{N_{\text{runs}}} \frac{\hat{\mathbf{h}}_i^{(m)}}{\|\hat{\mathbf{h}}_i^{(m)}\|} - \frac{\mathbf{h}_i}{\|\mathbf{h}_i\|} \right\|.$$

For the first set of simulation results including the first and the second examples, the full rate OSTBC of [TJC99, Equation (27)], the code index 5 in Table 3.1, i.e.,

$$\mathbf{X}(\mathbf{s}_i) = \begin{bmatrix} s_{i1} & s_{i2} & s_{i3} \\ -s_{i2} & s_{i1} & -s_{i4} \\ -s_{i3} & s_{i4} & s_{i1} \\ -s_{i4} & -s_{i3} & s_{i2} \end{bmatrix}, \quad (4.31)$$

with $N = 3$, $K = T = 4$, and BPSK symbols are used for encoding.

In the first example, it is assumed that the number of receivers, the number of data blocks that are used to estimate covariance matrix according to (3.34), the effective channel length, and the number of subcarriers are set to $M = 2$, $P = 2$, $L = L' = 5$, and $N_0 = 64$, respectively. It should be noted that, the code (4.31) is not rotatable [Ma07] and its blind identifiability is guaranteed in Rayleigh fading channels [VS08a]. In other words, the principal eigenvalue of $\mathcal{X}_i(\gamma_u)$ does not exhibit multiplicity for the selected setup; see Table 3.1 the for code index 5. As a result, we use uniform weighting with $\gamma = \gamma_u$ in our simulations. It should also be noted that for all presented simulations in this thesis, the CP length is set properly, i.e., $\text{CP}_{\text{length}} \geq (L + 1)$, to avoid IBI.

Fig. 4.1 and Fig. 4.2 display the estimation bias and RMSE, respectively, for all the methods tested versus SNR. As the method of [CMC08] is applicable only to a single OSTBC-OFDM block, we average the respective channel estimates over $P = 2$ blocks before evaluating the performance. It can be observed from Fig. 4.1 that in this setup the subcarrier-wise approach of [SGM05] shows the highest estimation bias for all SNR values. Further, while the method of [VSPV09] shows a larger estimation bias, the method of [CMC08] exhibits lower estimation bias compared to the proposed estimator in (4.22). It should be mentioned that the aforementioned lower estimation bias is achieved at the cost of higher computational burden since the complexity of the method of [CMC08] is linear with respect to N_0 and P . We further emphasize that according to the extensive

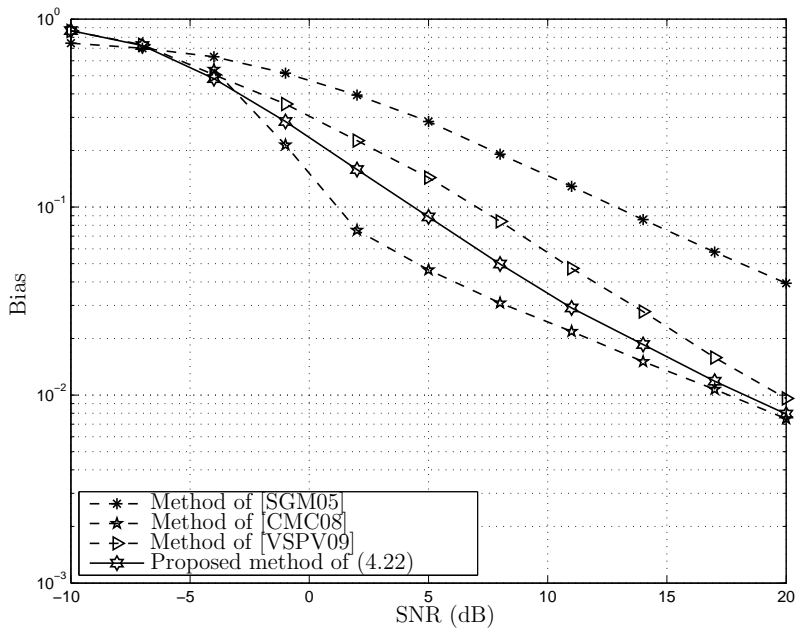


Figure 4.1: Bias versus SNR, first example.

simulation results for higher SNR values or by increasing P the difference between the biases of the proposed estimator in (4.22) and the method of [VSPV09] is less pronounced. This corresponds well to the fact mentioned earlier in Section 4.4 that in the asymptotic cases of large SNRs or a large number of available snapshots, i.e., for $\hat{\mathcal{X}}_i = \mathcal{X}_i$, both the latter methods become identical. Further, all methods outperform the subcarrier-wise approach of [SGM05].

Fig. 4.2 illustrates the estimation RMSE of all the methods tested versus the SNR. A similar relationship among these methods, as previously noted for the estimation bias can also be observed for the estimation RMSEs. However, the estimation RMSE difference between the proposed method in (4.22) and the method of [VSPV09] is less pronounced than for the estimation bias in Fig. 4.1. The same statement holds true for the proposed method and the method of [CMC08].

To detect the symbols in the proposed method, the technique of [SGM05], and the method of [VSPV09], the ML decoder of (2.73) is used in the presented simulations. For

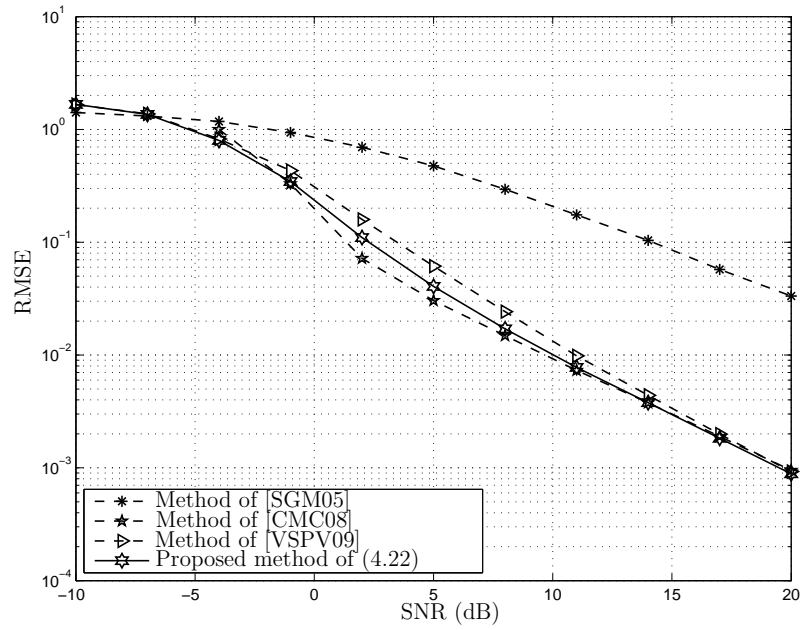


Figure 4.2: RMSE versus SNR, first example.

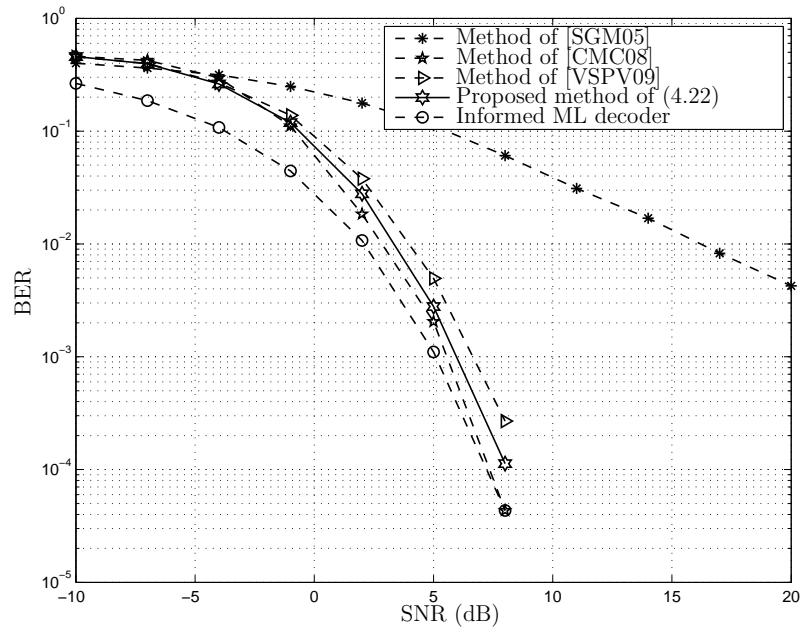


Figure 4.3: BER versus SNR, first example.

the method of [CMC08], when $P = 1$, the symbols should be estimated using Boolean quadratic programming, as recommended in [CMC08]. Hence, as the original method of [CMC08] can only exploit a single OSTBC-OFDM block for symbol detection, the case of $P = 2$ for this method corresponds to decoding the symbols by means of the ML detector (2.73) using the resulting channel estimates. It should be also noted that the full OSTBC-OFDM (FOO) version of the algorithm [CMC08] is implemented in the simulations which exhibits significantly improved performance as compared to its corresponding subchannel grouping OSTBC-OFDM (SGOO) version. The informed ML receiver is also included in Fig. 4.3. As mentioned in Section 3.4, this receiver is implemented here just as a benchmark to illustrate performance losses of the blind techniques with respect to the informed receiver case.

From Fig. 4.3, it can be seen that in terms of the BER, the proposed approach performs much better than the method of [SGM05], slightly better than the method of [VSPV09], and only a little worse than the method of [CMC08]. Moreover, all methods substantially outperform the subcarrier-wise approach of [SGM05]. This fact is the result of the coherent processing over all subcarriers as well as parsimonious channel parameterization used in the proposed method and in the methods of [CMC08] and [VSPV09].

Note that since the sample covariance matrix defined in (4.8) is a consistent estimate of the true covariance matrix, the proposed estimator in (4.22) is also consistent. Hence, when the channel can be assumed invariant over many OSTBC-OFDM blocks which is equal to increasing P in the simulation setup, we expect performance improvement for the proposed method. The same statement also holds true for the methods of [SGM05] and [VSPV09] due to the fact that both of these methods are based on the SOS of the received data. Further, as the method of [CMC08] originally is proposed in a block-wise manner, it can not benefit from averaging over successive blocks during which the channel is invariant. For the sake of brevity, we have not provide the simulation results associated with the different values of P . It is also noteworthy to mention that by increasing the number of subcarriers, all the methods tested, except the subcarrier-wise method of [SGM05], which benefit from coherent processing across the subcarriers experience performance improvement. In this case, nearly

the same relative conclusions as Figs. 4.1-4.3 can be expected, but the improvements of all methods over the method of [SGM05] become more pronounced. However, as mentioned above, the computational complexity of the approach of [CMC08] tends to grow dramatically by increasing the number of subcarriers or the number of OSTBC-OFDM blocks.

To investigate the effect of increasing N_0 , in the second example, the case of $N_0 = 256$ subcarriers is considered. All the other parameters are the same as in the first example. As the approach of [CMC08] has an enormously high complexity for $N_0 = 256$, we only compare the proposed approach with the technique of [SGM05] and [VSPV09]. Figs. 4.4, 4.5, and 4.6 display, respectively, the channel estimation bias, the estimation RMSE, and the BER performances of the methods tested versus SNR. It can be seen from these figures that the performance of the proposed method is substantially improved as compared to the first example (where $N_0 = 64$), and is much better than that of the method of [SGM05]. In particular, from Fig. 4.6 it can be seen that the performance of the proposed technique in (4.22) is very close to that of the informed ML decoder. It worth mentioning that the difference between the performance of the proposed technique in (4.22) and that of the informed ML decoder in Fig. 4.6 is notably less than that of differential schemes which in comparison typically suffer from 3 dB performance penalty.

To investigate the performance of the proposed method under different OSTBC, for the third example, the 3/4-rate OSTBC expressed in (3.52) [LS03, Equation (7.4.10)] with $N = 4, K = 3, T = 4$ and QPSK symbols are used for encoding. All the other parameters are the same as in the first example. Note that the principal eigenvalue of $\mathcal{X}_i(\gamma_u)$ does not exhibit multiplicity for the selected code and setup; see Table 3.1 for the code index 18, and its blind identifiability is guaranteed in Rayleigh fading channels [VS08a]. It can be seen from Fig. 4.7 that the subcarrier-wise approach of [SGM05] exhibits the highest estimation bias for all SNR values which is even worse than the corresponding performance displayed in Fig. 4.1. Moreover, while the method of [VSPV09] exhibits higher estimation bias, the method of [CMC08] shows lower estimation bias compared to the proposed estimator in (4.22). The difference among estimation biases of all methods tested, excluding the method of [SGM05], is less pronounced in high SNRs.

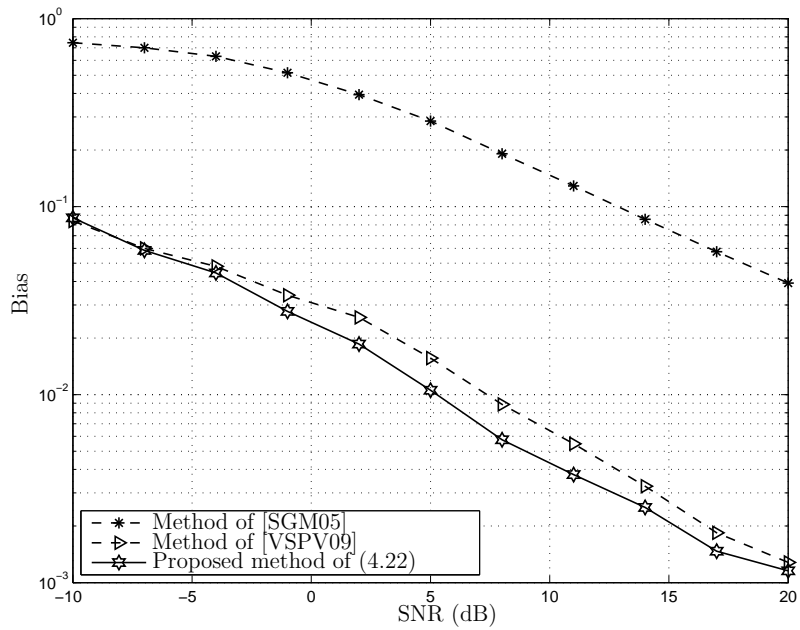


Figure 4.4: Bias versus SNR, second example.

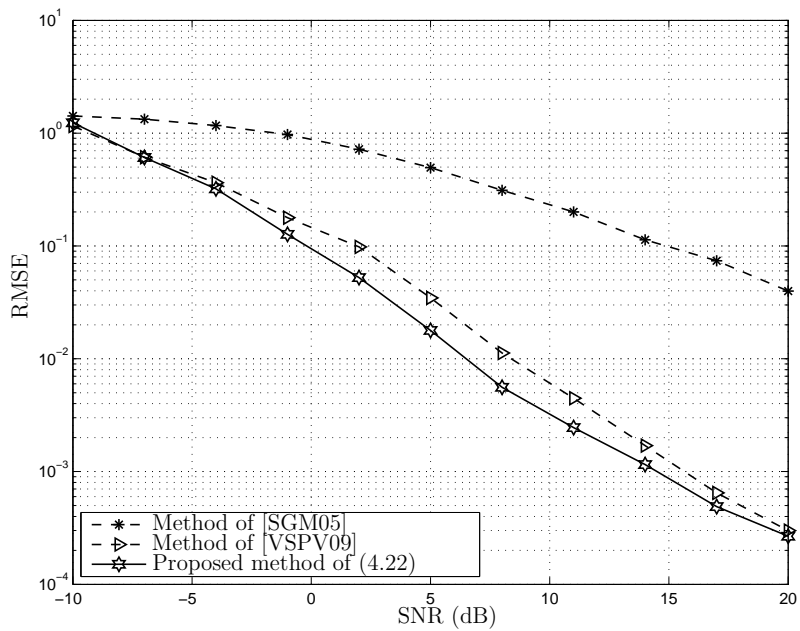


Figure 4.5: RMSE versus SNR, second example.

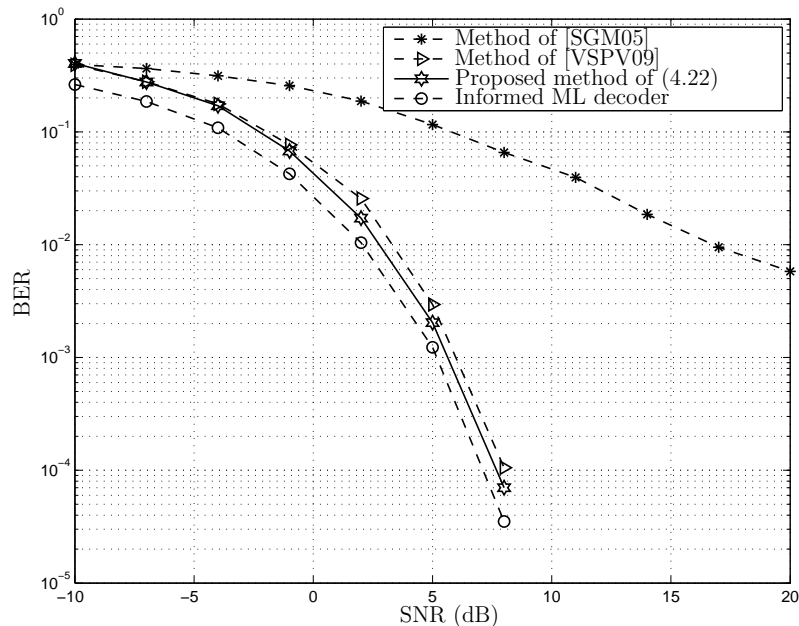


Figure 4.6: BER versus SNR, second example.

A quite similar relationship among the estimation RMSEs can be observed for the methods tested in Fig. 4.8 as the estimation biases in Fig. 4.7. However, the estimation RMSE performances of the proposed method and the method of [VSPV09] are nearly similar. Also, it can be deduced from Fig. 4.9 that the SER values of the proposed approach of (4.22) are much better than that of the method of [SGM05], slightly better than that of the method of [CMC08], and almost same as that of the method of [VSPV09]. It should be emphasized that according to our extensive numerical examples for different OSTBCs, channel conditions, and number of subcarriers, almost the same performances are observed which are not illustrated for the sake of brevity.

In the fourth and the fifth numerical example, the parameter P and the SNR are set to 2 and 0 dB, respectively, and the assumed upper limit for the channel length, i.e., L' , is varied. All the other parameters are the same as in the first example. In the fourth example, the true channel length is fixed at $L = 5$, and in the fifth example, $L = L'$ and both values are varied from 5 to 20.

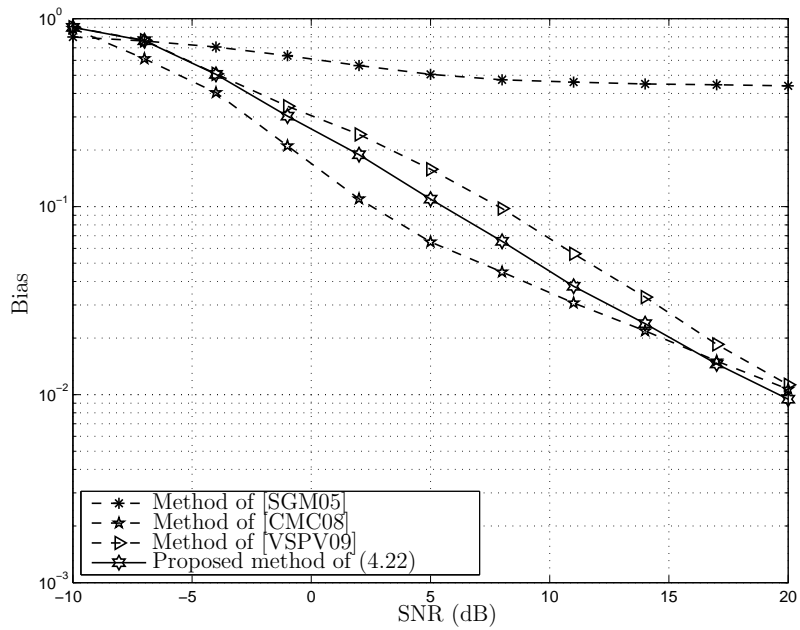


Figure 4.7: Bias versus SNR, third example.

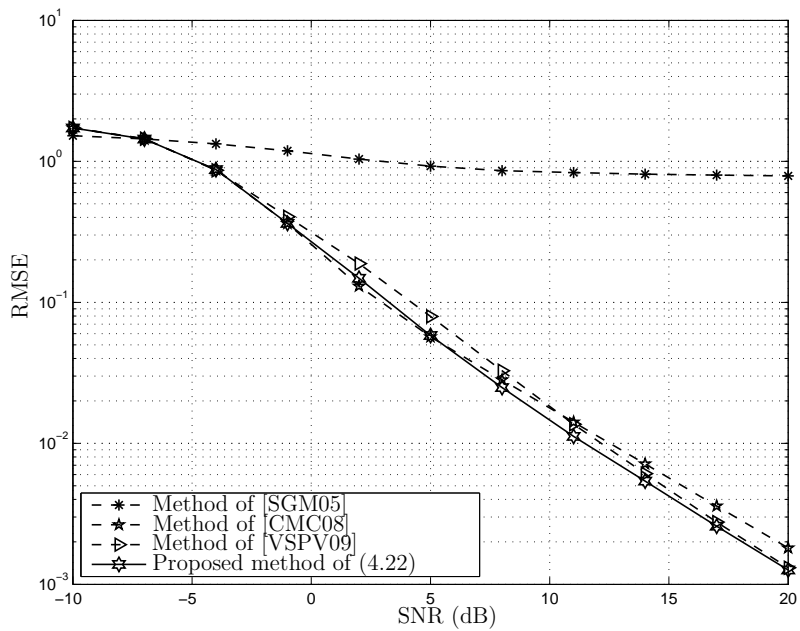


Figure 4.8: RMSE versus SNR, third example.

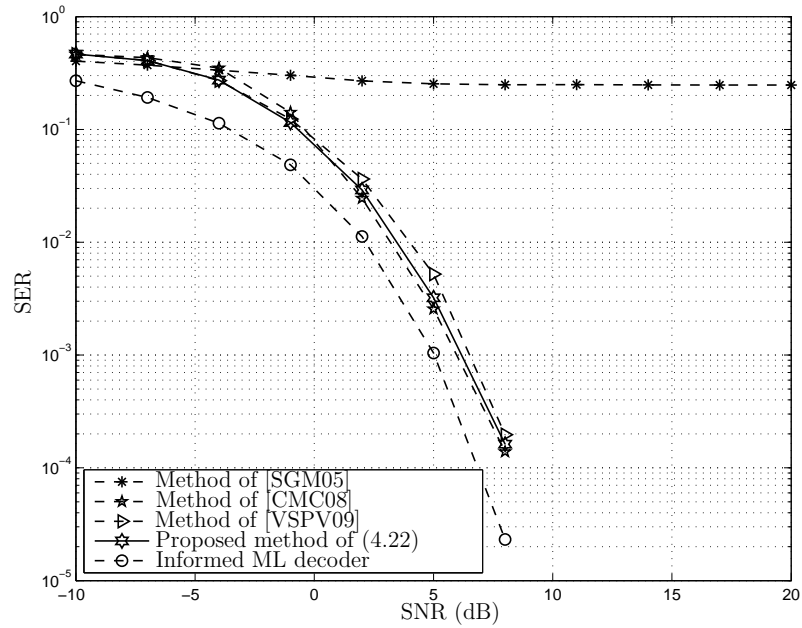


Figure 4.9: SER versus SNR, third example.

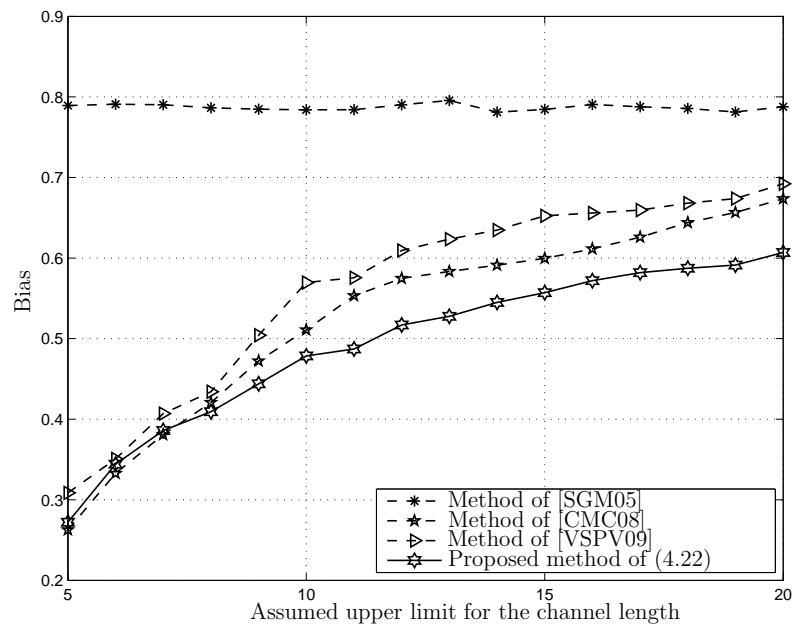


Figure 4.10: Bias versus L' , fourth example, $L = 5$.

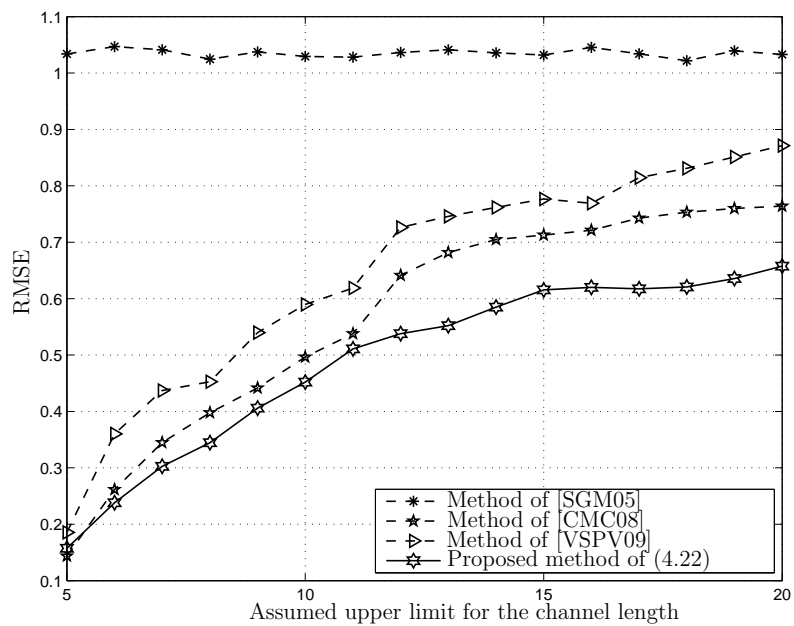
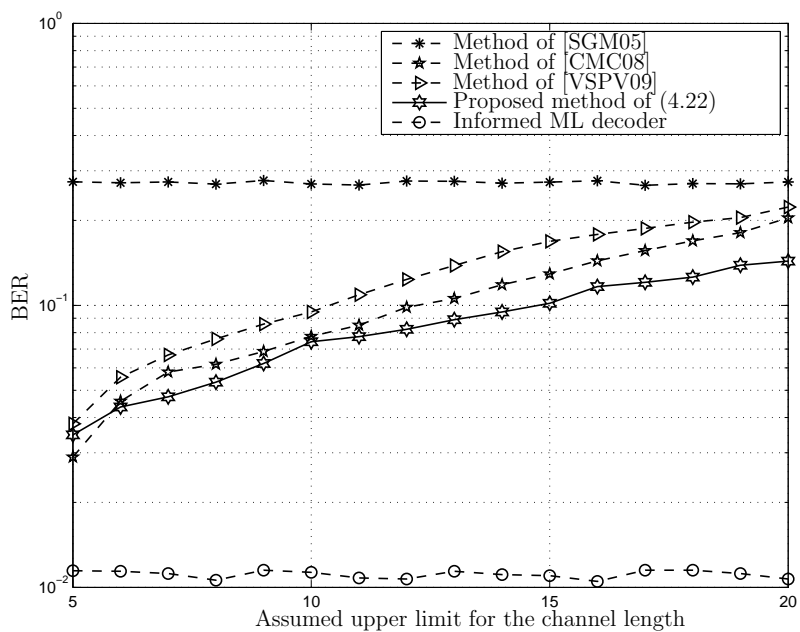
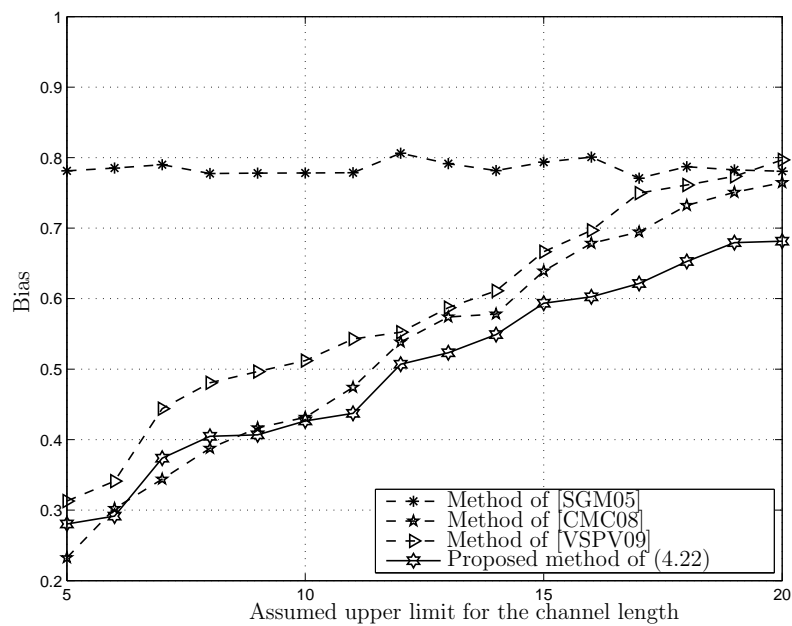
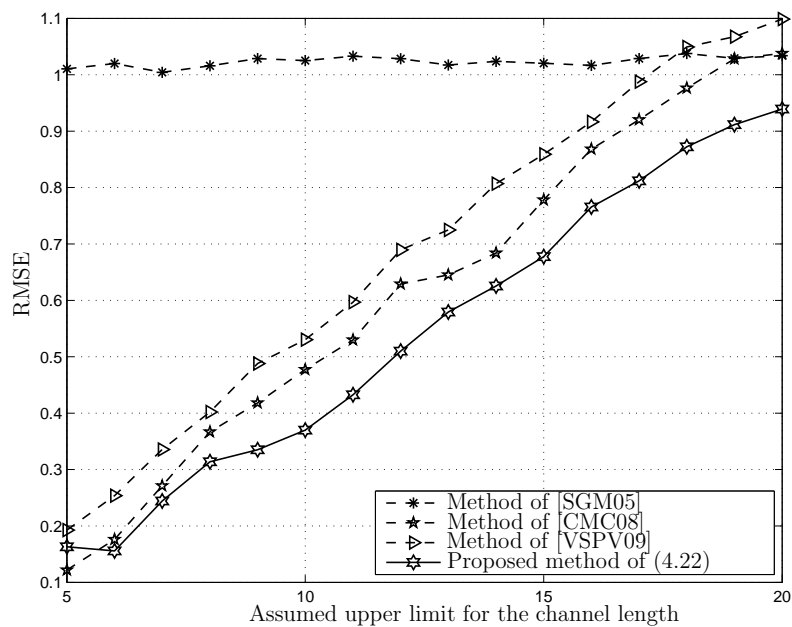
Figure 4.11: RMSE versus L' , fourth example, $L = 5$.Figure 4.12: BER versus L' , fourth example, $L = 5$.

Fig. 4.10 and Fig. 4.13 show the estimation bias for all the methods tested versus L' for the both latter numerical examples. It can be observed from Fig. 4.10 and Fig. 4.13 that the proposed approach of (4.22) results in a lowest estimation bias compared to the other methods tested. Further, it can be seen from Fig. 4.10 that in all methods, excluding the subcarrier-wise method of [SGM05], the best estimation performance is obtained for $L = L'$. This is due to the fact that according to the parsimony principle, the number of parameters, that should be estimated, increases with L' , and, hence, increasing L' results in a performance degradation. In addition, in Fig. 4.13, we see that the best performance for all the methods tested, excluding the method of [SGM05], corresponds to the case when the wireless channel is less frequency-selective or L is minimum. Increasing the delay spread while keeping the number of subcarriers fixed results in a performance degradation. In other words, the performance of all the methods tested, excluding the method of [SGM05], improves by increasing the numbers of subcarriers due to the coherent processing across the subcarriers as long as the true effective channel length is still smaller than its corresponding assumed one, i.e., L' .

Figs. 4.11 and 4.14 show the channel estimation RMSE performances of the methods tested versus L' . These figures lead to nearly the same conclusions as Figs. 4.10 and 4.13, but improvement of the proposed method over the other methods is become more pronounced. Further, the performance of the subcarrier-wise method of [SGM05] is insensitive to the true channel length or respective upper bound, i.e., L or L' , respectively.

Figs. 4.12 and 4.15 illustrate BERs of the methods tested versus L' . It can be seen from these figures that the proposed approach of (4.22) has the best symbol decoding performance compared to the other methods tested. Moreover, according to Fig. 4.12 and Fig. 4.15, all methods, excluding the method of [SGM05], have the best decoding performance for $L = L'$ or minimum L , respectively. Also, it can be observed that the symbol decoding performance of the subcarrier-wise method of [SGM05] and the informed ML receiver are invariant with respect to L' .

Next, to numerically verify the ability of the proposed method of (4.22) expressed in Remark 4.3.2 of Section 4.3, in the sixth example, we adopt the same simulation setup as

Figure 4.13: Bias versus L' , fifth example, $L = L'$.Figure 4.14: RMSE versus L' , fifth example, $L = L'$.

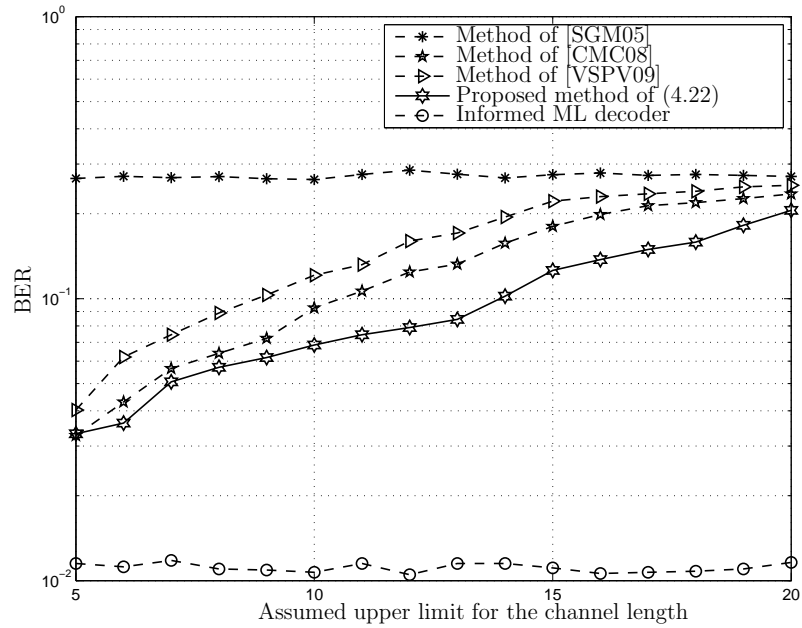


Figure 4.15: BER versus L' , fifth example, $L = L'$.

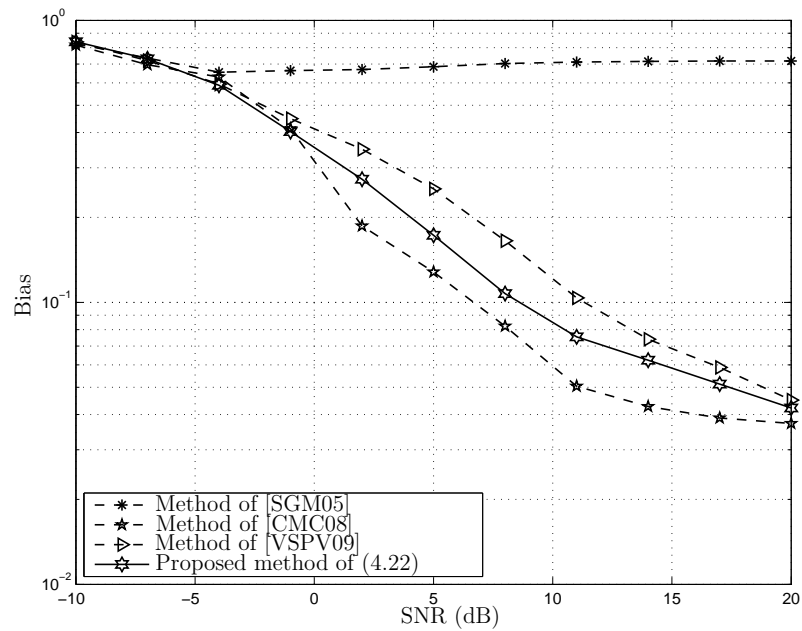


Figure 4.16: Bias versus SNR, sixth example.

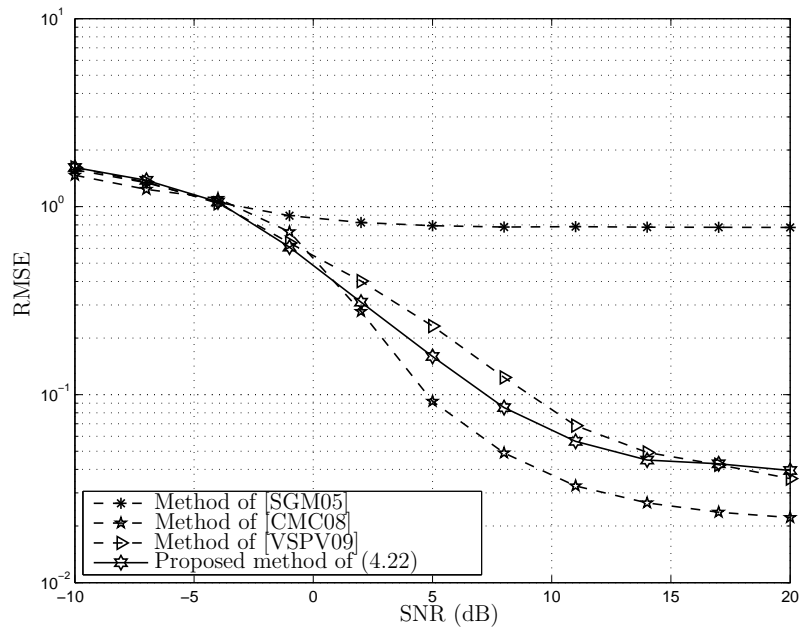


Figure 4.17: RMSE versus SNR, sixth example.

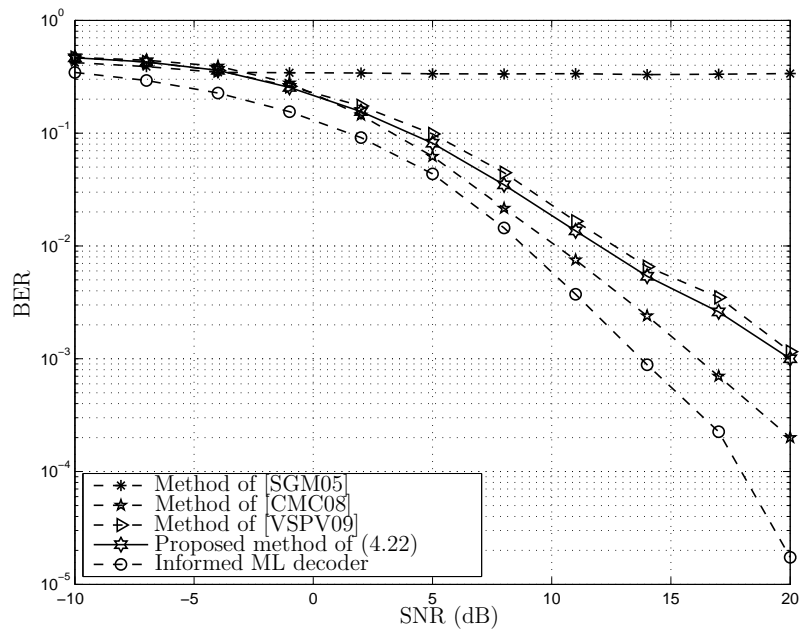


Figure 4.18: BER versus SNR, sixth example.

in the first example, but for single-antenna receiver, i.e., $M = 1$. According to Table 3.1 for the code index 5, the principal eigenvalue of $\mathcal{X}_i(\gamma_u)$ shows multiplicity of order two for the selected setup. Hence, we use non-uniform weighting strategy of (3.26), i.e., $\gamma = \gamma_n$, in the first ten subcarriers. The covariance matrices of the transmitted symbols in the first ten subcarriers are selected as $\{\mathbf{\Lambda}_{\underline{s}_i}\}_{i=0}^9 = \frac{K}{6}\text{diag}([3, 1, 1, 1])$ that guarantee $\text{tr}(\mathbf{\Lambda}_{\underline{s}_i}) = K$ and satisfy the necessary condition provided in (3.25). The weight vector γ corresponding to the proposed weighting strategy of (3.26) is selected as $\gamma = [2, 1, 1, 1]$ for the first ten subcarriers. For the remaining subcarriers, the covariance matrices of the transmitted symbols are proportional to the identity matrix and the uniform weight vectors, i.e., $\gamma = \gamma_u$, are used. It can be seen from Figs. 4.16-4.18 that the subcarrier-wise method of [SGM05] is not able to resolve non-scalar ambiguities while the other methods tested have resolved such ambiguities. This shows that implementing the proposed weighting strategies of Chapter 3 in a few subcarriers along with coherent processing across all subcarriers allows to resolve non-scalar ambiguities in the non-identifiable cases. Moreover, comparing the symbol decoding performance of all the methods tested in Fig. 4.3 and Fig. 4.18, excluding that of the subcarrier-wise method of [SGM05], reveals that applying such weighting strategy results in a lower decoding performance. This can be explained by the fact that the minimum Euclidean distance among constellation points is decreased by applying such linear precoding.

4.6 Chapter summary

A novel closed-form blind channel estimation approach for orthogonally coded MIMO-OFDM wireless communication systems has been proposed. We have exploited virtual snapshot model introduced in Chapter 3 and proposed a new normalization scheme to generalize the property of the received data covariance matrix principal eigenvector for multi-carriers. Furthermore, assuming a given delay spread over a wireless channel, we have estimated the FIR channel parameters in the time-domain jointly for all subcarriers.

This has been demonstrated to result in coherent processing across all subcarriers. Associated with this procedure is an inherent denoising effect and a lower computation complexity. Simulation results have demonstrated performance advantages of the proposed method as compared to other state-of-the-art blind MIMO-OFDM channel estimation techniques.

Chapter 5

Blind channel estimation in orthogonally coded MIMO-OFDM systems: Alternative approaches for multi-carrier analysis

5.1 Introduction

In this chapter, different approaches for blind channel estimation in orthogonally space-time coded MIMO-OFDM systems, that show different performance-complexity trade-offs in contrast to each other and to the proposed method in Chapter 4, are developed. Like the proposed method in (4.22), these approaches take advantage of the structural properties of the OSTBCs and of parsimonious channel parameterization in the time-domain and enjoy coherent processing across all subcarriers. First, we propose a new approach to formulate the blind channel estimation problem which results in different normalization coefficients compared to that of the method presented in Chapter 4 defined in (4.2). As a result, this method alleviates the need for finding the per subcarrier principal eigenvalue in the method presented in Chapter 4 and replaces them by corresponding individual CFR vector norm constraints. Then, in the context of semi-definite programming (SDP), a SDR technique is used to convert the underlying non-convex blind channel estimation problem to a convex form. Next, to further simplify the proposed technique and to reduce the computational

burden, we propose another blind channel estimation approach based on the finite alphabet constraint relaxation over the transmitted symbols and aggregate CFR vector norm constraint. This RML-based technique also uses a special case of extended covariance matrix in (4.1) with uniform normalization coefficients instead of the ones in (4.2). Then, we consider the channel estimation problem at hand from a different perspective and exploit the popular Capon technique to introduce a new approach for blind channel estimation. Corresponding performances are illustrated by means of extensive numerical examples which demonstrate performance of new approaches with respect to the one introduced in the previous chapter and several other state-of-the-art MIMO-OFDM channel estimation techniques.

5.2 Semi-definite relaxation-based approach

Exploiting the subspace structure of observations in different subcarriers of MIMO-OFDM systems and using a lemma in linear algebra, it is shown in Appendix E that the true overall CFR vector for all subcarriers, i.e., \mathbf{h}' , can be estimated from the following optimization problem as

$$\begin{aligned} \hat{\mathbf{h}}' &= \arg \max_{\tilde{\mathbf{h}}} \tilde{\mathbf{h}}^T \hat{\mathcal{X}}'(\gamma, \boldsymbol{\xi}_{\|\mathbf{h}\|}) \tilde{\mathbf{h}} \\ \text{s.t.} \quad & \tilde{\mathbf{h}}^T \mathbf{J}_i \mathbf{J}_i^T \tilde{\mathbf{h}} = \|\mathbf{h}_i\|^2, \quad i = 0, \dots, N_0 - 1, \end{aligned} \quad (5.1)$$

where $\hat{\mathcal{X}}'(\gamma, \boldsymbol{\xi}_{\|\mathbf{h}\|})$ is defined according to (4.1), $\boldsymbol{\xi}_{\|\mathbf{h}\|} \triangleq [\|\mathbf{h}_0\|^2, \dots, \|\mathbf{h}_{N_0-1}\|^2]$, and \mathbf{J}_i represents a selection matrix according to (4.15). Since the problem (5.1) is developed in the frequency-domain, the number of the optimization variables linearly grows in the number of subcarriers and, therefore, for a large number of subcarriers, it is extremely large as well. To reduce the problem dimension and in consequence the computational complexity of the proposed method, we exploit the finite delay spread assumption over the wireless channel presented in (2.32) in the same way of Section 4.3. As a result, we reformulate (5.1) in the time-domain where the number of variables is independent of the number of subcarriers and, hence, remains small even for remarkably large subcarrier numbers. To this aim, using the linear relationship among the frequency and time-domain variables in (2.30) along with

(4.11), (4.12), (4.19)-(4.21), we can rewrite (5.1) in the time-domain as

$$\begin{aligned} \hat{\mathbf{g}}'_{L'+1} &= \arg \max_{\tilde{\mathbf{g}}_{L'+1}} \tilde{\mathbf{g}}_{L'+1}^T \left(\tilde{\mathcal{J}}_{L'+1}^T \mathcal{F}^T \hat{\chi}'(\gamma, \boldsymbol{\xi}_{\|\mathbf{h}\|}) \mathcal{F} \tilde{\mathcal{J}}_{L'+1} \right) \tilde{\mathbf{g}}_{L'+1} \\ \text{s.t.} \quad & \tilde{\mathbf{g}}_{L'+1}^T \left(\tilde{\mathcal{J}}_{L'+1}^T \mathcal{F}^T \mathbf{J}_i \mathbf{J}_i^T \mathcal{F} \tilde{\mathcal{J}}_{L'+1} \right) \tilde{\mathbf{g}}_{L'+1} = \|\mathbf{h}_i\|^2, \quad i = 0, \dots, N_0 - 1. \end{aligned} \quad (5.2)$$

Equivalently, we rewrite (5.2) as

$$\begin{aligned} \hat{\mathbf{g}}'_{L'+1} &= \arg \min_{\tilde{\mathbf{g}}_{L'+1}} -\tilde{\mathbf{g}}_{L'+1}^T \mathbf{P}^t \tilde{\mathbf{g}}_{L'+1} \\ \text{s.t.} \quad & \tilde{\mathbf{g}}_{L'+1}^T \mathbf{T}_i^t \tilde{\mathbf{g}}_{L'+1} = \|\mathbf{h}_i\|^2, \quad i = 0, \dots, N_0 - 1 \end{aligned} \quad (5.3)$$

where

$$\begin{aligned} \mathbf{P}^t &\triangleq \left(\tilde{\mathcal{J}}_{L'+1}^T \mathcal{F}^T \hat{\chi}'(\gamma, \boldsymbol{\xi}_{\|\mathbf{h}\|}) \mathcal{F} \tilde{\mathcal{J}}_{L'+1} \right) \succeq 0 \in \mathbb{R}^{2MN(L'+1) \times 2MN(L'+1)}, \\ \mathbf{T}_i^t &\triangleq \left(\tilde{\mathcal{J}}_{L'+1}^T \mathcal{F}^T \mathbf{J}_i \mathbf{J}_i^T \mathcal{F} \tilde{\mathcal{J}}_{L'+1} \right) \succeq 0 \in \mathbb{R}^{2MN(L'+1) \times 2MN(L'+1)}, \end{aligned} \quad (5.4)$$

and the superscript “t” refers to the time-domain. Since the matrix $(-\mathbf{P}^t)$ in (5.3) is not positive semi-definite, this problem is not convex. Also, because the equality constraints in (5.3) are quadratic, this problem belongs to the set of problems which generally referred to as *non-convex quadratically constrained quadratic problems* (QCQPs) [BV04]. To transform the non-convex problem (5.3) to a convex one, we exploit the SDR approach [BV04]. Let us introduce a new matrix variable

$$\tilde{\mathbf{G}}_{L'+1} \triangleq \tilde{\mathbf{g}}_{L'+1} \tilde{\mathbf{g}}_{L'+1}^T \in \mathbb{R}^{2MN(L'+1) \times 2MN(L'+1)},$$

and consider the properties

$$\tilde{\mathbf{g}}_{L'+1}^T \mathbf{P}^t \tilde{\mathbf{g}}_{L'+1} = \text{tr} \left(\tilde{\mathbf{G}}_{L'+1} \mathbf{P}^t \right) \quad \text{and} \quad \tilde{\mathbf{g}}_{L'+1}^T \mathbf{T}_i^t \tilde{\mathbf{g}}_{L'+1} = \text{tr} \left(\tilde{\mathbf{G}}_{L'+1} \mathbf{T}_i^t \right).$$

Then, the equation (5.3) can be rewritten in terms of the new matrix variable $\tilde{\mathbf{G}}_{L'+1}$ as

$$\begin{aligned} \hat{\mathbf{G}}'_{L'+1} &= \arg \min_{\tilde{\mathbf{G}}_{L'+1}} -\text{tr} \left(\tilde{\mathbf{G}}_{L'+1} \mathbf{P}^t \right) \\ \text{s.t.} \quad & \text{tr} \left(\tilde{\mathbf{G}}_{L'+1} \mathbf{T}_i^t \right) = \|\mathbf{h}_i\|^2, \quad i = 0, \dots, N_0 - 1 \\ & \tilde{\mathbf{G}}_{L'+1}^T = \tilde{\mathbf{G}}_{L'+1}, \quad \text{rank}\{\tilde{\mathbf{G}}_{L'+1}\} = 1. \end{aligned} \quad (5.5)$$

To follow the idea of SDR technique, we drop the non-convex constraint in (5.5), i.e., $\text{rank}\{\tilde{\mathbf{G}}_{L'+1}\} = 1$, and replace it by its associated semi-definite counterpart $\tilde{\mathbf{G}}_{L'+1} \succeq 0$. As a result, we obtain the following *convex* SDP problem

$$\begin{aligned} \hat{\mathbf{G}}'_{L'+1} = \arg \min_{\tilde{\mathbf{G}}_{L'+1}} & -\text{tr}(\tilde{\mathbf{G}}_{L'+1} \mathbf{P}^t) \\ \text{s.t.} \quad & \text{tr}(\tilde{\mathbf{G}}_{L'+1} \mathbf{T}_i^t) = \|\mathbf{h}_i\|^2, \quad i = 0, \dots, N_0 - 1 \\ & \tilde{\mathbf{G}}_{L'+1}^T = \tilde{\mathbf{G}}_{L'+1}, \quad \tilde{\mathbf{G}}_{L'+1} \succeq 0, \end{aligned} \quad (5.6)$$

which can be solved in polynomial time [GW95], [Nes98], [Zha00] using, e.g., **CVX** [GB11], a package for specifying and solving convex programs, or **SeDuMi** [Stu99] toolboxes. We have derived the SDP problem in (5.6) by dropping the non-convex rank-one constraint in (5.5) and relaxing this constraint to its respective semi-definite counterpart. It is shown [BV04] that, in fact, the resulting problem (5.6) is the Lagrange bidual of the primal problem (5.3). It should be mentioned that bidual problems are frequently used and exploiting them is a powerful tool to convexify original non-convex problems [BV04].

Remark 5.2.1: In general, solving (5.6) results in a solution matrix $\tilde{\mathbf{G}}_{L'+1}^*$ from which we should recover a solution vector $\tilde{\mathbf{g}}_{L'+1}^*$ to the primal optimization problem (5.3). Following from our extensive numerical results, it should be noted that for different types of OSTBCs, real or complex constellations, and the numbers of receive antennas, the rank of the solution matrix $\tilde{\mathbf{G}}_{L'+1}^*$ for (5.6) is in exact agreement with the results presented in Table 3.1, Tables II and III of [Ma07], Table I of [SGM05], and Table I of [VS08a]. These tables summarize numerical or analytical results on the blind channel identifiability for different types of OSTBCs and different number of receive antennas. Therefore, in identifiable cases [VS08a] when non-rotatable OSTBCs [Ma07] are used with $M > 1$ receive antennas, $\tilde{\mathbf{G}}_{L'+1}^*$ is always rank-one. So, converting (5.5) to (5.6) does not involve any approximation and is exact in these cases, and, therefore, $\tilde{\mathbf{g}}_{L'+1}^*$ is the principal component of $\tilde{\mathbf{G}}_{L'+1}^*$.

Remark 5.2.2: If the OSTBC is rotatable or for some non-rotatable OSTBCs in the MISO system configuration, when the rank of $\tilde{\mathbf{G}}_{L'+1}^*$ is higher than one, the weighting

strategies proposed in Section 3 can be implemented to warrant rank-one solution. Moreover, there are several techniques such as odd-even subchannel grouping [CMC08], non-intersecting subspace code generation [Ma07], linear precoding [SGM05], and rate reduction [VS08a] that can be used to cope with non-rank-one solution case. Also, one can exploit randomization techniques [GW95] to obtain $\tilde{\mathbf{g}}_{L'+1}^*$ from $\tilde{\mathbf{G}}_{L'+1}^*$ in this case. The randomization techniques in general use $\tilde{\mathbf{G}}_{L'+1}^*$ to randomly generate a set of candidate vectors from which the best solution is then selected as $\tilde{\mathbf{g}}_{L'+1}^*$; see [SDL06].

Remark 5.2.3: Note that the proposed method in (5.6) suffers from the sign ambiguity. However, such ambiguity is quite common for many blind approaches known so far, e.g., see the method proposed in Chapter 4, and that of [CMC08], [SGM05] and [VSPV09]. To eliminate this type of ambiguity, we refer the reader to Remark 4.3.2 in Chapter 4.

Remark 5.2.4: It should be emphasized that in comparison to the method of (4.22) developed in Chapter 4, the proposed method in (5.6) alleviates the need for per-subcarrier principal eigenvalue calculation, i.e., $\xi_{\lambda_{\max}}$ in (4.2) along with (4.1), and replace it by the need for per-subcarrier CFR vector norm calculation, i.e., $\xi_{\|\mathbf{h}\|}$ in (5.1). Hence, only regarding this issue, the latter approach benefits from slight computational complexity reduction. However, the latter approach, which is based on solving SDP problem, has higher computational cost, and does not offer closed-form solution compared to the former method, that is based on solving eigenvalue problem, and provides closed-form solution. Also, note that the complexity of the approach in (5.6) is typically lower than that of the approach of [CMC08] although both approaches are based on solving SDP problems. To explain this, it should be reminded that the SDP step dominates the complexity of whole algorithm [MVDC06] in the both latter approaches. It is known that the computational cost of SDP problem is $\mathcal{O}(x^{3.5})$ with x stands for the size of problem. In [CMC08], the size of the SDP problem depends both on the size of each data block prior to encoding and the number of subcarriers. For the full OSTBC-OFDM (FOO) algorithm [CMC08], the complexity is $\mathcal{O}((N_0K)^{3.5})$ as we have $x = N_0K$. For the subchannel grouping OSTBC-OFDM (SGOO) scheme [CHMC10], that is developed to reduce the complexity at the cost of performance, (N_0/N_g) separate optimization problems (N_g is the number of subcarriers in each group)

should be solved with the complexity of $\mathcal{O}((N_g K)^{3.5})$ for each. Hence, at best when $N_g = 1$, the complexity is $\mathcal{O}(N_0 K^{3.5})$ and at worst when $N_g = N_0$, the complexity is equal to that of the FOO algorithm. This implies that in both cases, complexity order depends on both K and N_0 which is comparable to the subchannel-wise method of [SGM05] complexity. In contrast to the methods of [CHMC10] and [CMC08], in the proposed approach of (5.6), the size of the SDP problem only depends on the numbers of antennas and the upper bound on number of CIR effective taps, i.e., the time-domain channel parameters, hence, the corresponding complexity is given by $\mathcal{O}(((L' + 1)MN)^{3.5})$. It should be added that in both of the aforementioned SDP-based methods, the number of constraints depends on the number of subcarriers and this is the reason why we only compared the size of the SDP objective functions.

Remark 5.2.5: Last but not the least, when the wireless channel is invariant over several OSTBC-OFDM blocks, that is $P > 1$, any blind detection approach requires to be repeated for each data block. In other words, the approach of [CMC08] needs to solve P separate SDP problems, whereas the proposed method in (5.6) requires to solve only one problem for any value of P . Consequently, the complexity of blind detection approaches such as that of [CMC08] become prohibitively high in the cases when P is large while the proposed approach offers a computationally attractive alternative to the former methods in the quasi-static channel scenarios.

Next, we develop a blind channel estimation technique based on both relaxation of the finite alphabet constraint over the transmitted symbols and aggregate over all subcarriers CFR vector norm constraint instead of per-subcarrier CFR vector norm constraints used in (5.6). As a result, unlike the blind approach of (5.6), the new technique finds the channel estimate in closed form. Also, the latter technique offers remarkable reduced computational complexity compared to the SDR-based method of (5.6) at the cost of performance degradation.

5.3 Relaxed ML-based approach

It is shown in Appendix F that making use of definition (3.4), the blind RML channel estimator at the i th subcarrier reduces to the following estimate for the CFR vector \mathbf{h}_i in the Gaussian noise case

$$\hat{\mathbf{h}}_{i,\text{RML}} = \arg \max_{\|\tilde{\mathbf{h}}_i\|=\|\mathbf{h}_i\|} \tilde{\mathbf{h}}_i^T \hat{\mathcal{X}}_i(\boldsymbol{\gamma}_{\text{RML}}) \tilde{\mathbf{h}}_i, \quad i = 0, \dots, N_0 - 1 \quad (5.7)$$

with $\boldsymbol{\gamma}_{\text{RML}} \triangleq [1, \dots, 1]^T$. Next, to enable coherent processing among different subcarriers of the MIMO-OFDM system, we propose to combine subcarrier covariance matrices $\hat{\mathcal{X}}_i(\boldsymbol{\gamma}_{\text{RML}})$ in (5.7) with equal gains to obtain the following estimate of the true overall CFR vector \mathbf{h}' introduced in (2.33) as

$$\hat{\mathbf{h}}' = \arg \max_{\tilde{\mathbf{h}}} \sum_{i=0}^{N_0-1} \tilde{\mathbf{h}}_i^T \hat{\mathcal{X}}_i(\boldsymbol{\gamma}_{\text{RML}}) \tilde{\mathbf{h}}_i, \quad (5.8)$$

where the norm constraints $\|\tilde{\mathbf{h}}_i\| = \|\mathbf{h}_i\|$, $i = 0, \dots, N_0 - 1$, should be taken into account and $\tilde{\mathbf{h}} \triangleq [\tilde{\mathbf{h}}_0^T, \dots, \tilde{\mathbf{h}}_{N_0-1}^T]^T \in \mathbb{R}^{2MN_0 \times 1}$ stands for the vector of optimization variables in the frequency-domain. This is equivalent to choose uniform normalization scalars $\{\xi_i\}_{i=0}^{N_0-1} = 1$ in (4.1) or

$$\boldsymbol{\xi} = \boldsymbol{\xi}_u \triangleq [1, \dots, 1]^T, \quad (5.9)$$

and to estimate \mathbf{h}' as

$$\hat{\mathbf{h}}' = \arg \max_{\tilde{\mathbf{h}}} \tilde{\mathbf{h}}^T \hat{\mathcal{X}}'(\boldsymbol{\gamma}_{\text{RML}}, \boldsymbol{\xi}_u) \tilde{\mathbf{h}}, \quad (5.10)$$

with the norm constraints $\|\tilde{\mathbf{h}}_i\| = \|\mathbf{h}_i\|$, $i = 0, \dots, N_0 - 1$ due to the block-diagonal structure of $\hat{\mathcal{X}}'(\boldsymbol{\gamma}_{\text{RML}}, \boldsymbol{\xi}_u)$. Since (5.10) is formulated in the frequency-domain, the number of optimization variables increases with the number of subcarriers and, hence, the problem dimension of (5.10) can be extremely large for a large number of subcarriers. To reduce the dimension and the computational cost, it is convenient to exploit the finite delay spread assumption of (2.32), as we did in Section 4.3, and to reformulate (5.10) in the time-domain. Using the linear relationship among the frequency and time-domain variables in (2.30) along with (4.11), (4.12), (4.19)-(4.21), we can rewrite (5.10) in the time-domain as

$$\hat{\mathbf{g}}'_{L'+1} = \arg \max_{\tilde{\mathbf{g}}'_{L'+1}} \tilde{\mathbf{g}}'_{L'+1}{}^T \left(\tilde{\mathcal{F}}'_{L'+1}{}^T \mathcal{F}^T \hat{\mathcal{X}}'(\boldsymbol{\gamma}_{\text{RML}}, \boldsymbol{\xi}_u) \mathcal{F} \tilde{\mathcal{F}}'_{L'+1} \right) \tilde{\mathbf{g}}'_{L'+1}, \quad (5.11)$$

where the norm constraints in (5.10) take the form $\|\mathcal{F}_i \tilde{\mathbf{g}}\| = \|\mathbf{h}_i\|$, $i = 0, \dots, N_0 - 1$ with $\tilde{\mathbf{h}}_i \triangleq \mathcal{F}_i \tilde{\mathbf{g}}$. It can be observed that the problem formulation in (5.11) exploits all available received data within the whole frequency band by performing coherent processing among all subcarriers. Meanwhile, it has advantage of estimating less number of parameters as compared to the problem formulation in (5.10) which is preferable from the performance viewpoint. To come up with a closed-form estimator in contrast to the proposed method in Section 5.2, we relax N_0 individual norm constraints in (5.11) and replace them by one aggregate constraint to approximate the estimator (5.11) as

$$\begin{aligned} \hat{\mathbf{g}}'_{L'+1} = \arg \max_{\tilde{\mathbf{g}}'_{L'+1}} & \tilde{\mathbf{g}}'^T_{L'+1} \left(\tilde{\mathcal{J}}^T_{L'+1} \mathcal{F}^T \mathcal{X}'(\gamma_{\text{RML}}, \boldsymbol{\xi}_{\text{u}}) \mathcal{F} \tilde{\mathcal{J}}_{L'+1} \right) \tilde{\mathbf{g}}'_{L'+1} \\ \text{s.t.} & \quad \|\tilde{\mathbf{g}}'_{L'+1}\| = \|\mathbf{g}'\|, \end{aligned} \quad (5.12)$$

where instead of the original subcarrier norm constraints, corresponding relaxed version $\|\tilde{\mathbf{g}}'_{L'+1}\| = \|\mathbf{g}'\|$ is replaced. It is known that the solution to (5.12) belongs to the subspace spanned by the principal eigenvector of the matrix $\left(\tilde{\mathcal{J}}^T_{L'+1} \mathcal{F}^T \mathcal{X}'(\gamma_{\text{RML}}, \boldsymbol{\xi}_{\text{u}}) \mathcal{F} \tilde{\mathcal{J}}_{L'+1} \right)$ (or several principal eigenvectors in the case of eigenvalue multiplicity). Since the value of objective function in (5.12) can increase arbitrarily if $\|\tilde{\mathbf{g}}'_{L'+1}\| \rightarrow \infty$, we consider norm bounded variable $\tilde{\mathbf{g}}'_{L'+1}$ to avoid such a trivial solution for (5.12). In essence, for any norm bounded variable $\tilde{\mathbf{g}}'_{L'+1}$, the *spatial signature* of the estimated equivalent CIR vector $\hat{\mathbf{g}}'_{L'+1}$ can be obtained from (5.12) which is parallel to the true overall CIR vector in asymptotic scenarios, when $\hat{\mathcal{X}}'(\gamma_{\text{RML}}, \boldsymbol{\xi}_{\text{u}}) = \mathcal{X}'(\gamma_{\text{RML}}, \boldsymbol{\xi}_{\text{u}})$, and, then, a proper scaling factor should be applied to its norm. Hence, the channel can be blindly recovered up to a *real scalar ambiguity* by solving (5.12) for any norm-bounded vector of optimization variable.

Remark 5.3.1: It should be noted that each term in (5.7) contributes to (5.8) with equal gains, i.e., $\boldsymbol{\xi} = \boldsymbol{\xi}_{\text{u}}$. This is in contrast to the methods of (4.22), (5.6), and [VSPV09] which combine subcarrier SOSs with unequal gains. These gains or normalization coefficients are the principal eigenvalue of the virtual snapshots covariance matrix per-subcarrier, i.e., $\boldsymbol{\xi} = \boldsymbol{\xi}_{\lambda_{\text{max}}}$, the subcarrier CFR vector norm, i.e., $\boldsymbol{\xi} = \boldsymbol{\xi}_{\|\mathbf{h}\|}$, and the signal subspace energy at each subcarrier, respectively. As a result, the proposed method of (5.10) alleviates the need and the corresponding computational cost to obtain these normalization coefficients.

However, it is not guaranteed anymore, on the contrary to the method of (4.22), that the property of the subcarrier covariance matrix principal eigenvector is still kept by performing coherent processing among different subcarriers. It can be observed from numerical results in Section 5.5 that although in low SNRs, this equal gain combining together with norm relaxation in (5.12) lead to negligible performance losses, the respective impact is reasonable for high SNRs.

Remark 5.3.2: Since performance of the decoder (2.73) is insensitive to rescaling the channel estimate by any real factor in constant modulus constellation case, there is no need even for the estimation of the overall channel vector norm in (5.12). Therefore, finding the normalized principal eigenvector of $\left(\tilde{\mathcal{J}}_{L'+1}^T \mathcal{F}^T \lambda'(\gamma_{\text{RML}}, \xi_u) \mathcal{F} \tilde{\mathcal{J}}_{L'+1}\right)$ would be sufficient which results in further computation savings.

Remark 5.3.3: The idea of relaxing individual channel norm constraints per-subcarrier and replacing them by aggregated one, that is exploited in (5.12), can be also used along with the approach of Section 5.2 to avoid solving the SDP problem in (5.6). In other words, the subcarrier terms of (F.6) can be normalized by their respective CFR vector norms first, and then, contribute to (5.10). The provided simulation results in Section 5.5 reveal that such unequal-gain combination of the per-subcarrier SOSs generally results in better channel estimation and symbol detection performances.

Remark 5.3.4: Also, we can combine per-subcarrier ECM estimator of (3.41) for all subcarriers and follow the same steps of (5.7)-(5.12) to obtain

$$\begin{aligned} \hat{\mathbf{g}}'_{L'+1, \text{ECM}} = & \arg \max_{\tilde{\mathbf{g}}'_{L'+1}} \tilde{\mathbf{g}}'^T_{L'+1} \left(\tilde{\mathcal{J}}^T_{L'+1} \mathcal{F}^T \hat{\lambda}'(\gamma_{\text{ECM}}, \xi_u) \mathcal{F} \tilde{\mathcal{J}}_{L'+1} \right) \tilde{\mathbf{g}}'_{L'+1} \\ \text{s.t. } & \|\tilde{\mathbf{g}}'_{L'+1}\| = \|\mathbf{g}'\|. \end{aligned} \quad (5.13)$$

In (5.13), the individual norm constraints per-subcarrier are relaxed and replaced by the aggregated one as in (5.12). Repeating the same steps for the subcarrier KCM estimator of (3.48) results in

$$\begin{aligned} \hat{\mathbf{g}}'_{L'+1, \text{KCM}} = & \arg \max_{\tilde{\mathbf{g}}'_{L'+1}} \tilde{\mathbf{g}}'^T_{L'+1} \left(\tilde{\mathcal{J}}^T_{L'+1} \mathcal{F}^T \hat{\lambda}'(\gamma_{\text{KCM}}, \xi_u) \mathcal{F} \tilde{\mathcal{J}}_{L'+1} \right) \tilde{\mathbf{g}}'_{L'+1} \\ \text{s.t. } & \|\tilde{\mathbf{g}}'_{L'+1}\| = \|\mathbf{g}'\|. \end{aligned} \quad (5.14)$$

Both (5.13) and (5.14) can be considered as the generalization of (5.12) if the covariance matrices of the transmitted symbols in different subcarriers differ from a scaled version of the identity matrix due to, for example, power imbalance among different information symbols [VS08b].

Next, we develop a novel blind channel estimator and derive respective optimization problem from different perspective. The resulting approach enjoys from all benefits of the one introduced in Section 5.3 and at the same time exhibits an improved performance at the cost of higher computational complexity.

5.4 Capon-based approach

The key idea is to develop an estimator inspired from the generalized Capon method to obtain the CIR vectors \mathbf{g}_l , $l = 0, \dots, L$, in a blind fashion. To this end, we design a filter at the receiver side which passes the transmitted symbols corresponding to a specific column of the matrix $\mathbf{A}(\tilde{\mathbf{h}}_i)$ without distortion while maximally suppresses all the symbols associated with the other columns of this matrix and noise components at the i th subcarrier. Therefore, we solve the following optimization problem [SGG06]

$$\min_{\mathbf{w}_{k,i}} \mathbf{w}_{k,i}^T \mathbf{R}_i \mathbf{w}_{k,i} \quad \text{s.t.} \quad \mathbf{w}_{k,i}^T \mathbf{a}_k(\tilde{\mathbf{h}}_i) = 1, \quad (5.15)$$

where the solution vector passes the symbols corresponding to $\mathbf{a}_k(\tilde{\mathbf{h}}_i)$ as the k th column of the matrix $\mathbf{A}(\tilde{\mathbf{h}}_i)$ defined in (2.37). It can be shown that the solution to (5.15) is given by [SGG06]

$$\mathbf{w}_{k,i}(\tilde{\mathbf{h}}_i) = \frac{1}{\mathbf{a}_k(\tilde{\mathbf{h}}_i)^T \mathbf{R}_i^{-1} \mathbf{a}_k(\tilde{\mathbf{h}}_i)} \mathbf{R}_i^{-1} \mathbf{a}_k(\tilde{\mathbf{h}}_i), \quad (5.16)$$

where the solution vector depends on the CFR vector at the i th subcarrier, which is explicitly emphasized by adopting the notation $\mathbf{w}_{k,i}(\tilde{\mathbf{h}}_i)$. As a result and according to (5.16), a separate weight vector should be applied for each entry of the transmitted symbol vector $\underline{\mathbf{s}}_i$. Then, we define the Capon spectrum for any CFR vector $\tilde{\mathbf{h}}_i$ and any k th entry of $\underline{\mathbf{s}}_i$ as

$$\mathcal{S}_{k,i}(\tilde{\mathbf{h}}_i) \triangleq \mathbf{w}_{k,i}^T(\tilde{\mathbf{h}}_i) \mathbf{R}_i \mathbf{w}_{k,i}(\tilde{\mathbf{h}}_i) = \frac{1}{\mathbf{a}_k(\tilde{\mathbf{h}}_i)^T \mathbf{R}_i^{-1} \mathbf{a}_k(\tilde{\mathbf{h}}_i)}, \quad (5.17)$$

which indicates the k th Capon receiver output power. If the vector variable $\tilde{\mathbf{h}}_i$, stands for a channel vector at the i th subcarrier, was not norm-bounded, then $\mathcal{S}_{k,i}(\tilde{\mathbf{h}}_i) \rightarrow 0$ when $\|\tilde{\mathbf{h}}_i\| \rightarrow \infty$. However, considering norm constraints $\|\tilde{\mathbf{h}}_i\| = \|\mathbf{h}_i\|$ over the vector variable $\tilde{\mathbf{h}}_i$, as in (F.6), the Capon spectrum of (5.17) has its maximum value at $\tilde{\mathbf{h}}_i = \mathbf{h}_i$.

While we can exploit any of the Capon spectra $\mathcal{S}_{k,i}(\tilde{\mathbf{h}}_i)$, $k = 1, \dots, 2K$, defined in (5.17), to estimate the CFR vector at the i th subcarrier, we combine them to enhance this estimate by using (2.41) and (2.44) as [SGG06]

$$\begin{aligned} \mathcal{T}_i(\tilde{\mathbf{h}}_i) &\triangleq \sum_{k=1}^{2K} \frac{1}{\mathcal{S}_{k,i}(\tilde{\mathbf{h}}_i)} = \sum_{k=1}^{2K} \mathbf{a}_k(\tilde{\mathbf{h}}_i)^T \mathbf{R}_i^{-1} \mathbf{a}_k(\tilde{\mathbf{h}}_i) \\ &= \tilde{\mathbf{h}}_i^T \left(\sum_{k=1}^{2K} \Phi_k^T \mathbf{R}_i^{-1} \Phi_k \right) \tilde{\mathbf{h}}_i \\ &= \tilde{\mathbf{h}}_i^T \Phi^T (\mathbf{I}_{2K} \otimes \mathbf{R}_i^{-1}) \Phi \tilde{\mathbf{h}}_i. \end{aligned} \quad (5.18)$$

Taking into account (4.11) together with $\tilde{\mathbf{h}}_i = \mathcal{F}_i \tilde{\mathbf{g}}$, we can rewrite (5.18) in the time-domain as

$$\mathcal{T}_i(\tilde{\mathbf{g}}) = \tilde{\mathbf{g}}^T \mathcal{F}_i^T \Phi^T (\mathbf{I}_{2K} \otimes \mathbf{R}_i^{-1}) \Phi \mathcal{F}_i \tilde{\mathbf{g}}. \quad (5.19)$$

Using (2.30), (2.31), along with (E.2), (E.5), and (E.8), the subcarrier spectrum expressed in (5.19) can be combined together for all subcarriers to benefit from joint processing as

$$\begin{aligned} \mathcal{T}(\tilde{\mathbf{g}}) &= \sum_{i=0}^{N_0-1} \mathcal{T}_i(\tilde{\mathbf{g}}) = \sum_{i=0}^{N_0-1} \tilde{\mathbf{g}}^T \mathcal{F}_i^T \Phi^T (\mathbf{I}_{2K} \otimes \mathbf{R}_i^{-1}) \Phi \mathcal{F}_i \tilde{\mathbf{g}} \\ &= \tilde{\mathbf{g}}^T \mathcal{F}^T \Psi^T (\mathbf{I}_{2KN_0} \otimes \mathbf{R}^{-1}) \Psi \mathcal{F} \tilde{\mathbf{g}}. \end{aligned} \quad (5.20)$$

Since the Capon spectrum in (5.17) has its maximum value for $\tilde{\mathbf{h}}_i = \mathbf{h}_i$ when norm constraint $\|\tilde{\mathbf{h}}_i\| = \|\mathbf{h}_i\|$ is assumed, $\mathcal{T}_i(\tilde{\mathbf{h}}_i)$ in (5.18) is expected to have its minimum under the same condition and so does $\mathcal{T}(\tilde{\mathbf{g}})$ in (5.20) for $\tilde{\mathbf{g}} = \mathbf{g}'$ with norm constraints $\|\mathcal{F}_i \tilde{\mathbf{g}}\| = \|\mathbf{h}_i\|$, $i = 0, \dots, N_0 - 1$. Next, we consider the finite delay spread assumption of (2.32) to reduce the number of optimization variables and use (4.19) along with (4.20) to rewrite (5.20) as

$$\mathcal{T}(\tilde{\mathbf{g}}_{L'+1}) = \tilde{\mathbf{g}}_{L'+1}^T \left(\tilde{\mathcal{J}}_{L'+1}^T \mathcal{F}^T \Psi^T (\mathbf{I}_{2KN_0} \otimes \mathbf{R}^{-1}) \Psi \mathcal{F} \tilde{\mathcal{J}}_{L'+1} \right) \tilde{\mathbf{g}}_{L'+1}, \quad (5.21)$$

with minimum value for $\tilde{\mathbf{g}}_{L'+1} = [\mathbf{g}_0^T, \dots, \mathbf{g}_{L'}^T]^T$ under the same norm constraints as for (5.20).

To come up with a closed-form estimation approach, we relax the latter individual norm constraints and replace them, as we did before in (5.12), by one aggregate norm constraint. Hence, the proposed Capon-based blind estimator (5.21) can be approximated as

$$\begin{aligned} \hat{\mathbf{g}}'_{L'+1, \text{Capon}} = \arg \min_{\tilde{\mathbf{g}}'_{L'+1}} & \tilde{\mathbf{g}}'^T_{L'+1} \left(\tilde{\mathcal{J}}'^T_{L'+1} \mathcal{F}^T \Psi^T \left(\mathbf{I}_{2KN_0} \otimes \hat{\mathbf{R}}^{-1} \right) \Psi \mathcal{F} \tilde{\mathcal{J}}'_{L'+1} \right) \tilde{\mathbf{g}}'_{L'+1} \\ \text{s.t.} & \quad \|\tilde{\mathbf{g}}'_{L'+1}\| = \|\mathbf{g}'\|, \end{aligned} \quad (5.22)$$

where the sample covariance matrix $\hat{\mathbf{R}}$ is used instead of the true covariance matrix \mathbf{R} . It is known that the solution to (5.22) belongs to the subspace spanned by the *minor* eigenvector (or eigenvectors, in the case of smallest eigenvalue multiplicity) of the matrix $\left(\tilde{\mathcal{J}}'^T_{L'+1} \mathcal{F}^T \Psi^T \left(\mathbf{I}_{2KN_0} \otimes \hat{\mathbf{R}}^{-1} \right) \Psi \mathcal{F} \tilde{\mathcal{J}}'_{L'+1} \right)$.

Remark 5.4.1: Note that each Capon spectra defined in (5.17) or respective combined version introduced in (5.18) can be used to estimate CFR vector per-subcarrier independently. Hence, the proposed approach can be also considered as an alternative candidate for the estimator, introduced in Chapter 3, to perform blind channel estimation in single-carrier scenario.

Remark 5.4.2: It is worth noting that diagonal loaded sample estimate covariance matrix, $\hat{\mathbf{R}}_{dl} \triangleq \hat{\mathbf{R}} + \alpha \mathbf{I}$, in which α is the loading factor, can be used to improve the robustness of estimator (5.22) against the finite sample effect [Van02].

Remark 5.4.3: As compared to the proposed method presented in (5.12), the Capon-based approach of (5.22) exhibits more computational complexity since the inverse of received data covariance matrix has to be calculated. However, simulation results presented in Section 5.5 demonstrate performance advantages of the Capon-based approach.

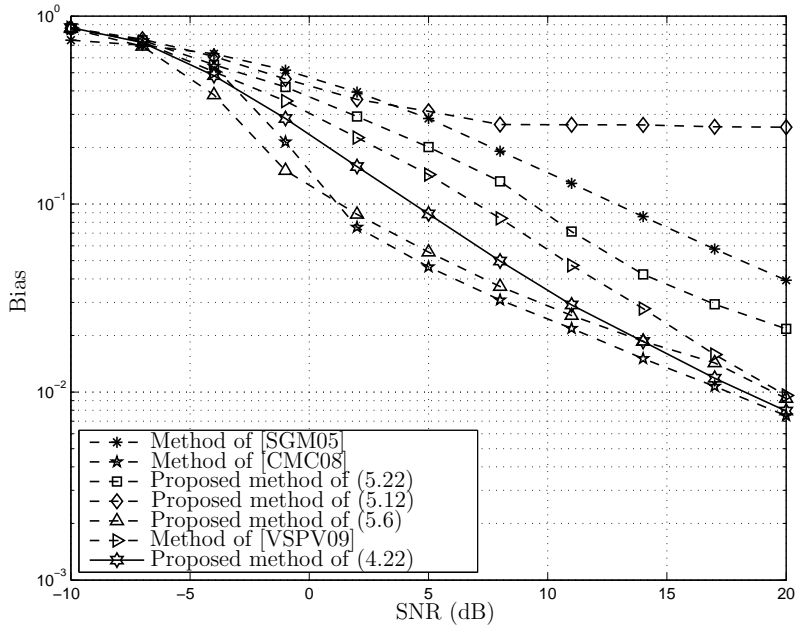
Remark 5.4.4: Note that each subcarrier combined Capon spectra in (5.18) contributes to (5.20) with equal gains. This leads to an extra estimation bias due to the coherent processing among different subcarriers same as for the RML-based method of (5.12) mentioned in Remark 5.3.1. To prevent this, it is also possible to follow the proposed idea of coherent processing introduced in Section 4.2 to combine different Capon spectra in (5.18) for all subcarriers. Since the CFR vector at each subcarrier is the minor eigenvector corresponding to the smallest eigenvalue of $\left(\Phi^T \left(\mathbf{I}_{2K} \otimes \mathbf{R}_i^{-1} \right) \Phi \right)$ according to (5.18), this subcarrier CFR

vector also corresponds to the smallest eigenvalue equal to one in all subcarriers if we utilize proper normalization factor of $\lambda_{\min}(\Phi^T (\mathbf{I}_{2K} \otimes \mathbf{R}_i^{-1}) \Phi)$ as we did in (4.1). Then, it can be guaranteed that the true overall CFR vector in (2.33) can be formed from the subcarrier minor eigenvectors even in the finite sample cases. As a result, the coherent processing among different subcarriers does not introduce extra bias to the estimation of the overall CFR. According to our extensive simulations, following the mentioned idea of normalization by the per-subcarrier smallest eigenvalue, provides us the blind channel estimator with corresponding performance nearly similar to that of the method of (4.22).

Remark 5.4.5: It can be shown that, e.g., in the cases when the OSTBC is rotatable in which (2.64) holds true as discussed in Subsection 2.4.1, the smallest eigenvalue of $(\tilde{\mathcal{F}}_{L'+1}^T \mathcal{F}^T \Psi^T (\mathbf{I}_{2KN_0} \otimes \hat{\mathbf{R}}^{-1}) \Psi \mathcal{F} \tilde{\mathcal{F}}_{L'+1})$ exhibits multiplicity; see [SGG06] for more detail. To resolve such a multiplicity problem, the weighting strategies discussed in Section 3.3 can be implemented. However, when necessary conditions of (3.13) and (3.25) are not satisfied, pilot symbols, if they exist, can be also exploited instead.

5.5 Simulations

In this section, we compare the performance of the proposed blind channel estimators (5.6), (5.12), and (5.22) with that of the method of [CMC08], the subcarrier-wise technique of [SGM05], the method of [VSPV09], and the previously proposed method of (4.22) in the Rayleigh fading frequency-selective channel cases. However, the performance of the last four methods are compared with each other in Section 4.5. We present again their associated performances in this section just to illustrate and compare the performance of the blind channel estimators proposed in this chapter with them. In the presented numerical examples, the channel conditions and all the other simulation parameters are identical to the counterpart examples in Section 4.5. Further, we adopt the same definitions for the SNR, the estimation bias, the estimation RMSE, and SERs or BERs as in Section 4.5. Diagonal loading with the factor of $\alpha = 5\sigma^2$ is used to implement the Capon-based method of (5.22) in all the numerical results; see Remark 5.4.2. Note that in the beamforming community,

Figure 5.1: Bias versus SNR, first example, $P = 2$.

this is quite a popular *ad hoc* choice of the diagonal loading factor [Ger03]. Throughout all numerical examples, subcarrier CFR vector norms are estimated from (4.26). As in this case, equality constraints in (5.6) may make this estimator sensitive to CFR vector norm estimation errors, we have replaced them by inequality constraints, as mentioned in Section 5.2.

Hence, in the first and second examples, the real rate-one OSTBC of (4.31), in which $N = 3$, $K = T = 4$, with BPSK symbols are implemented. Fig. 5.1 and Fig. 5.2 show the estimation bias and RMSE for all the methods tested versus the SNR, respectively. It can be seen from Fig. 5.1 that in this setup, the estimation bias of the SDR-based method of (5.6) is lower than that of all the other methods and nearly similar to that of the method of [CMC08] in high SNRs. Note that this lower estimation bias is achieved at the cost of solving SDP problem with N_0 constraints and no closed-form solution in (5.6). The proposed RML-based method of (5.12) performs quite better compared to the method of [SGM05] in low SNRs while shows highest estimation bias among all the methods tested in high SNRs. This

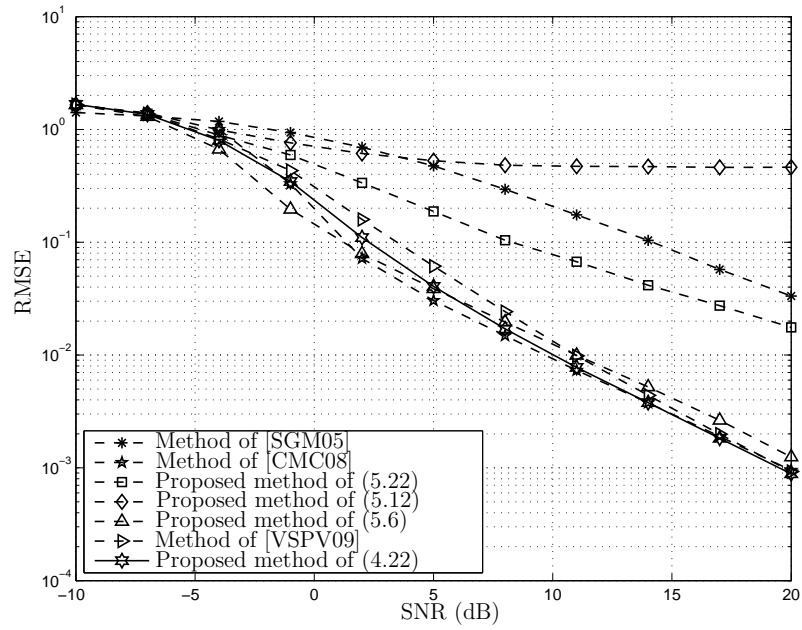


Figure 5.2: RMSE versus SNR, first example, $P = 2$.

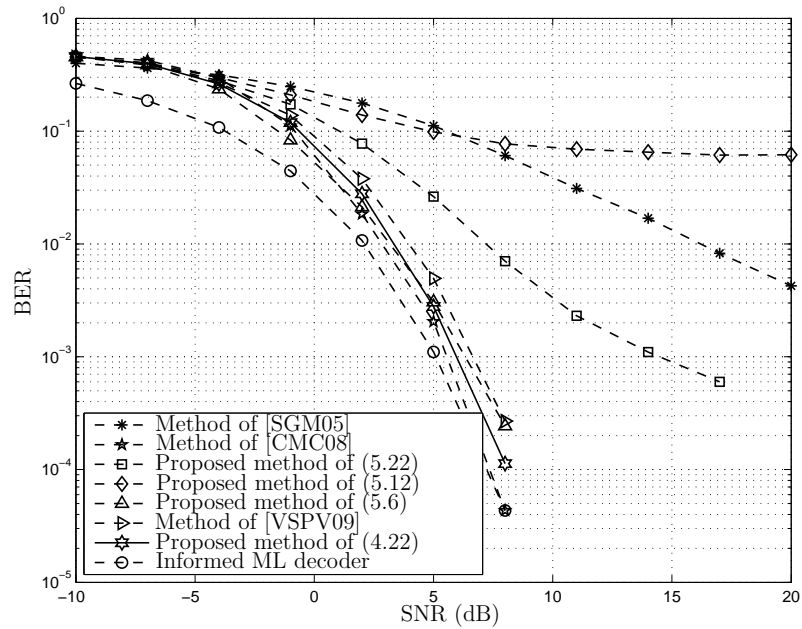
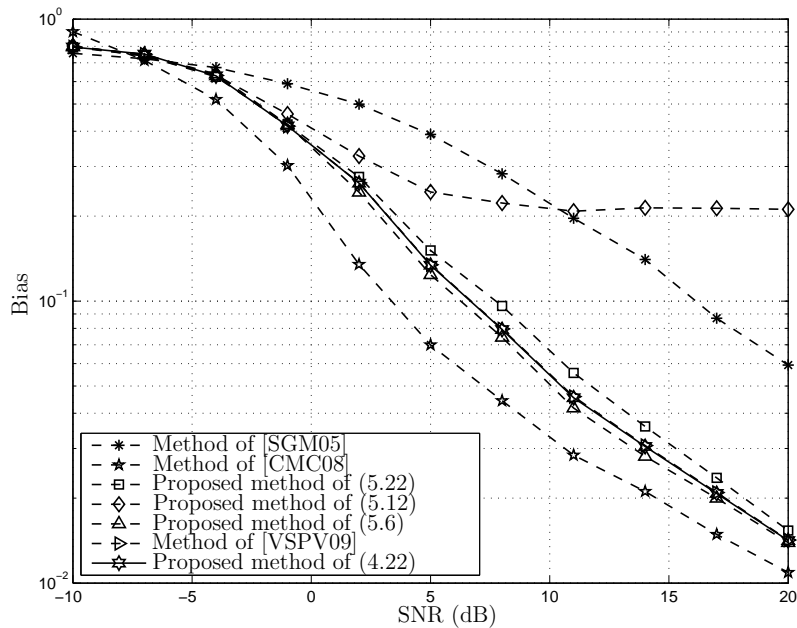


Figure 5.3: BER versus SNR, first example, $P = 2$.

observation verifies well the fact which explained in Remark 5.3.1. Note that as the constant modulus constellation is used in the first and second examples, referring to Remark 5.3.2, there is no need for the estimation of the overall channel vector norm in (5.12). This results in reduced computational cost compared to the methods of (5.6), (4.22), and [VSPV09]. The Capon-based method of (5.22) performs better compared to the RML-based method at the cost of higher computational cost; see Remark 5.4.3. All the proposed estimators in this chapter are capable to benefit from coherent processing over subcarriers to outperform the subcarrier-wise approach of [SGM05]. However, the methods of (5.12) and (5.22), exhibit extra estimation bias in high SNRs referring to Remark 5.3.1 and Remark 5.4.4. We further elaborate this issue in the second setup of the first numerical example. Also note that the performance of the proposed estimators in this thesis substantially improves when the channel can be assumed invariant over many OSTBC-OFDM blocks. The same statement, as mentioned in Section 4.5, also holds true for the methods of [SGM05] and [VSPV09]. Moreover, since the method of [CMC08] originally is proposed in a block-wise manner, it can not benefit from increasing P . However, by increasing P , the computational complexity of the method of [CMC08] dramatically increases compared to all the other methods tested.

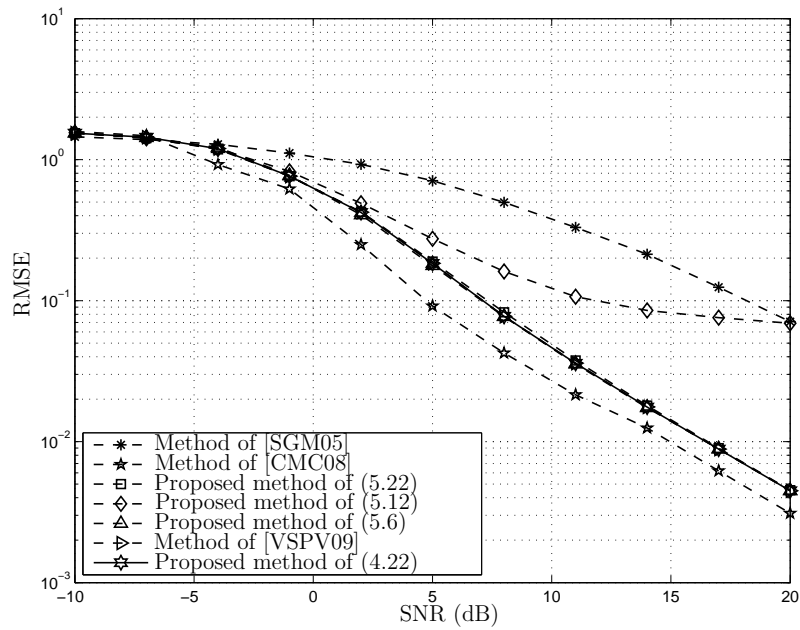
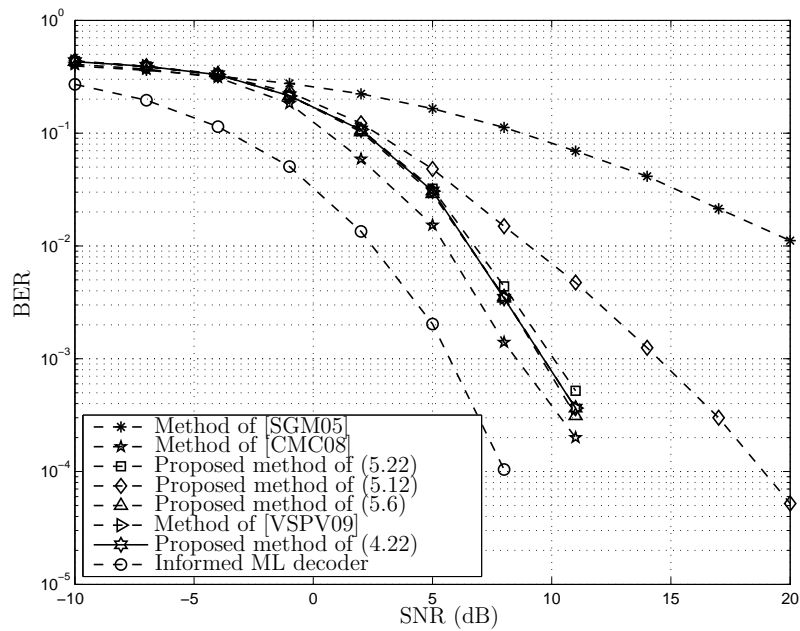
Fig. 5.2 shows the RMSE of all the methods tested versus the SNR. It can be seen that the difference in the estimation RMSE among the proposed method in (5.6) and the methods of (4.22), [CMC08], and [VSPV09] is less pronounced than the corresponding estimation bias in Fig. 5.1. Also, quite similar relationships among the proposed estimators of (5.12) and (5.22) with all the other methods as in Fig. 5.1 for the estimation biases can be noticed.

Fig. 5.3 illustrates BERs of all the methods tested versus the SNR. In Fig. 5.3, to detect the symbols in all the proposed methods of this chapter, the ML decoder of (2.73) is exploited. The informed ML receiver is also included, as a benchmark, in Fig. 5.3. It can be seen that the proposed approach of (5.6) performs considerably better than the method of [SGM05], slightly better than the method of [VSPV09], and quite similar as the methods of (4.22) and [CMC08]. Also, the performance of the method of (5.12) is slightly better than that of the method of [SGM05] in low SNRs while it is the worst among performances of all

Figure 5.4: Bias versus SNR, first example, $P = 1$.

the other methods tested in high SNRs. Further, BERs performance of the Capon-based method of (5.22) is better than that of the both methods of (5.12) and [SGM05], and is worse than that of the others.

It should be added that to reduce the estimation bias resulted from coherent processing especially in the finite sample case and to enhance the performance of the methods of (5.12) and (5.22), the approaches in Remark 5.3.3 and Remark 5.4.4 can be applied. However, this results in higher computational burden corresponding to the calculation of per-subcarrier CFR vector norm or smallest eigenvalue of the modified covariance matrix at each subcarrier, respectively. Furthermore, according to our extensive simulations, applying such modifications does not result in methods which perform better than the method of (4.22). It is noteworthy to mention that from practical viewpoint, there is an interesting scenario in which the extra estimation bias, comes from coherent processing due to equal-gain combination in (5.12) and (5.22), is not significant. This scenario occurs when only one OSTBC-OFDM symbol is available at the receiver to form sample covariance matrix,

Figure 5.5: RMSE versus SNR, first example, $P = 1$.Figure 5.6: BER versus SNR, first example, $P = 1$.

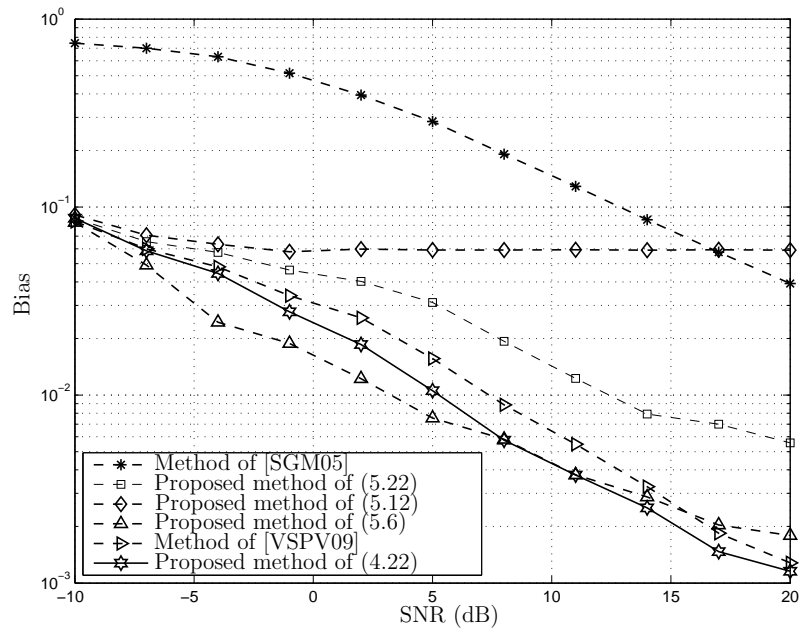


Figure 5.7: Bias versus SNR, second example.

i.e., $P = 1$. In this case, the sample covariance matrix at each subcarrier, i.e., $\hat{\mathbf{R}}_i$, has only one non-zero eigenvalue with associated principal eigenvector (or minor eigenvector of $\hat{\mathbf{R}}_i^{-1}$ in the Capon-based method) that forms one out of N_0 principal eigenvectors of $\hat{\mathbf{R}}$ (or minor eigenvectors of $\hat{\mathbf{R}}^{-1}$ in the Capon-based method) as in (4.3).

To investigate the performance of the proposed methods in this recent scenario, we set $P = 1$ in the first numerical example and keep all the other parameters unchanged. Comparing Figs. 5.4-5.6 with their counterparts Figs. 5.1-5.3 reveals that performance differences among the methods of (5.12) and (5.22) with that of the methods of (4.22), (5.6), [CMC08], and [VSPV09] are substantially decreased. Also, performances of the methods (5.12) and (5.22) experience considerable improvement in comparison with that of the method of [SGM05]. Furthermore, it can be generally observed that all illustrated performance measures in Figs. 5.4-5.6 deteriorate compared to the associated ones in Figs. 5.1-5.3 as P is decreased.

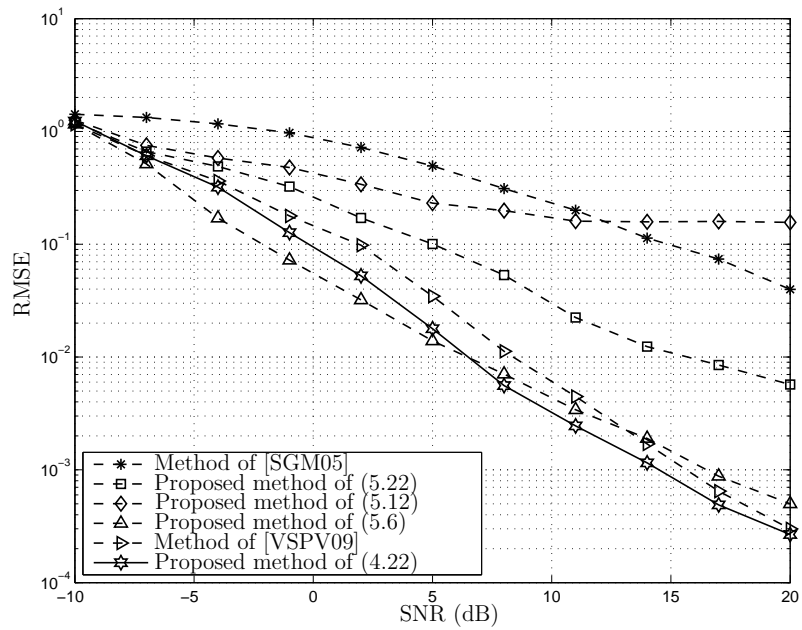


Figure 5.8: RMSE versus SNR, second example.

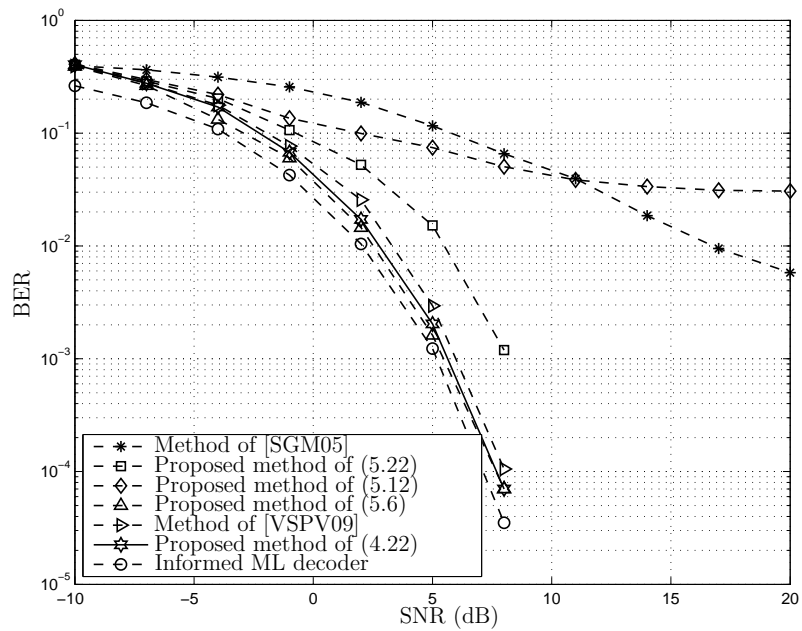


Figure 5.9: BER versus SNR, second example.

Note that all the methods tested, except the subcarrier-wise method of [SGM05], experience performance enhancement by increasing the number of subcarriers. However, quite the same relative performances such as Figs. 5.1-5.3 can be inferred while the enhancements of all methods over the subcarrier-wise method of [SGM05] become more noticeable. To verify this, we set $N_0 = 256$ in the second simulation setup as in Section 4.5. All the other parameters are the same as in the first example. It should be noted again that since the approach of [CMC08] has excessively high computational complexity in this case, it is not included in the second example. Figs. 5.7, 5.8, and 5.9 show, respectively, the channel estimation bias, the channel estimation RMSE, and the BER performances of the proposed methods in this chapter together with that of the ones presented in the second example of Section 4.5 versus the SNR. It can be observed from these figures that according to our expectation, performance of the proposed methods of (5.6), (5.12), and (5.22) are considerably enhanced compared to that of the same estimators in the first example. Also, both blind estimators of (5.12) and (5.22) exhibit performance improvements compared to the subcarrier-wise method of [SGM05]. In particular, performance of the proposed method of (5.6) is much better than that of the method of [SGM05] and is very close to that of the informed ML decoder in Fig. 5.9. Note that obtained BERs performance of the method (5.6) compared to that of the differential schemes [DASC02], [Li05], [MTL05] which suffer from 3 dB performance penalty with respect to the informed ML decoder is promising.

In the third example, same as its counterpart in Section 4.5, we investigate the performance of the proposed methods in this chapter under different OSTBC. So, the 3/4-rate OSTBC of (3.52) with $N = 4, K = 3, T = 4$, and QPSK symbols are used for encoding. All other parameters are the same as in the first example. It should be noted that the blind identifiability of this code under the mentioned setup in Rayleigh fading channels is guaranteed [VS08a]. It can be observed from Fig. 5.10 that the subcarrier-wise approach of [SGM05] exhibits the highest estimation bias and the proposed method of (5.6) shows the lowest estimation bias values for all SNRs. Furthermore, both of the proposed methods of (5.12), and (5.22) perform better than the subcarrier-wise approach of [SGM05] due to the coherent processing ability and worse than the proposed methods of (4.22), and (5.6)

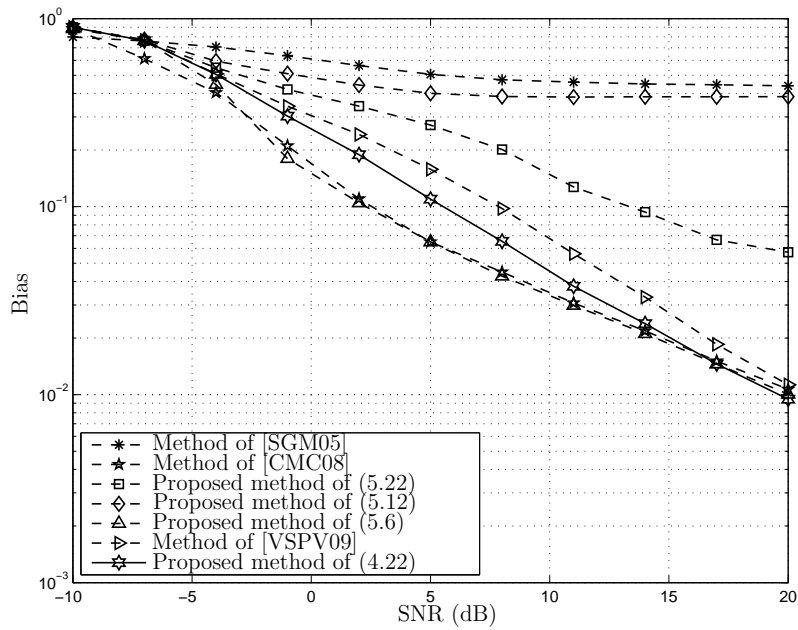


Figure 5.10: Bias versus SNR, third example.

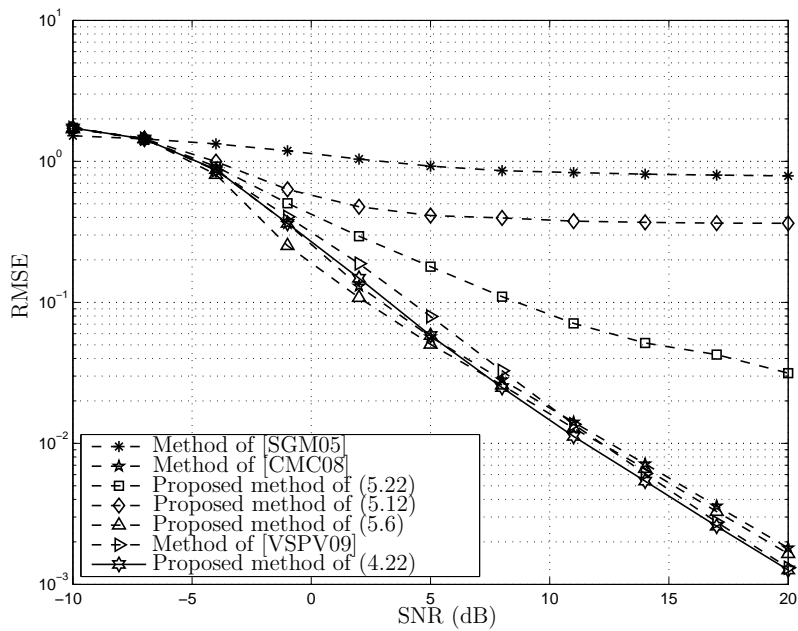


Figure 5.11: RMSE versus SNR, third example.

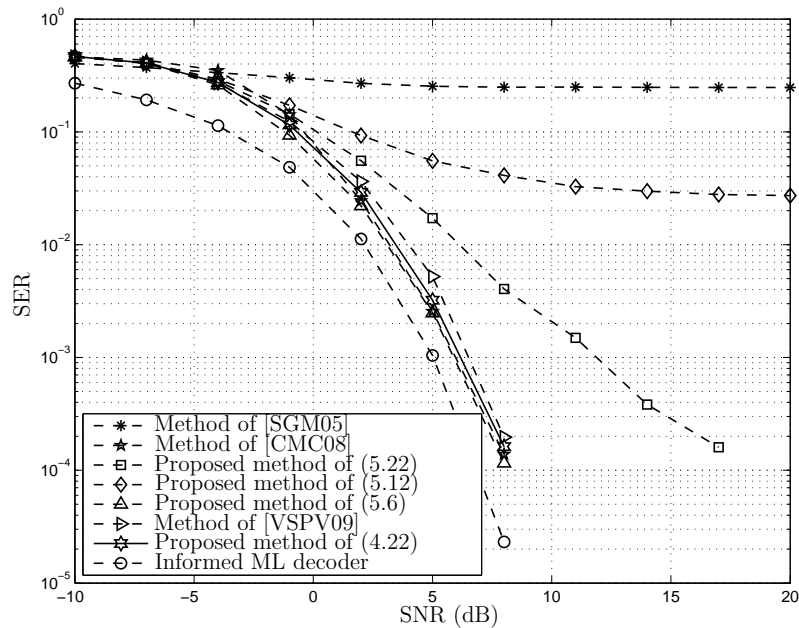
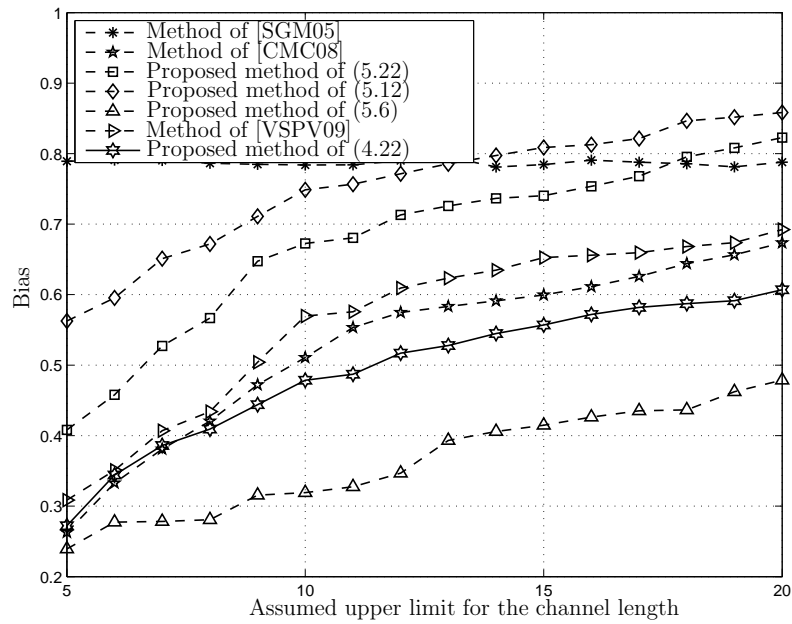
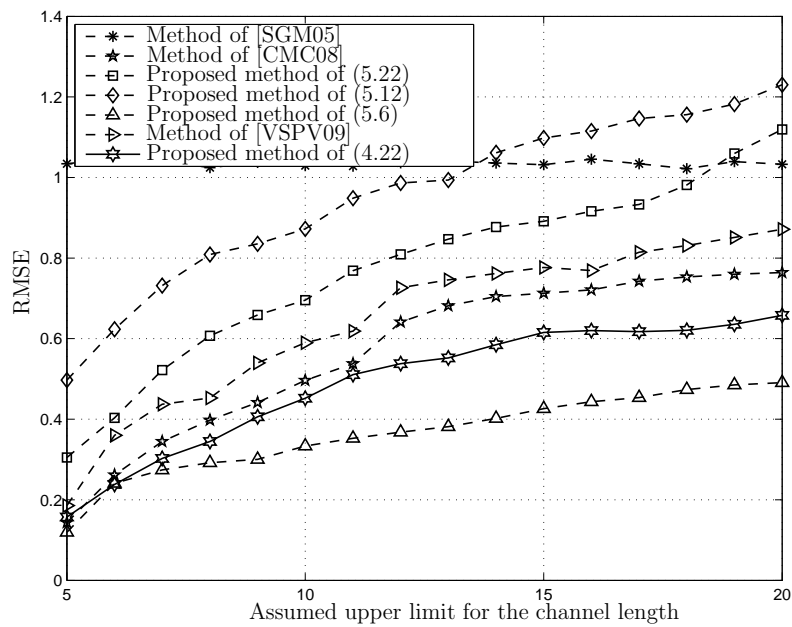


Figure 5.12: SER versus SNR, third example.

because of the extra coherent processing estimation bias corresponding to the equal-gain combination described in Remark 5.3.1 and Remark 5.4.4. A quite similar relationships for the estimation RMSE can be observed among the methods tested in Fig. 5.11 as the estimation bias in Fig. 5.10. Also, it can be observed from Fig. 5.12 that the SER performance of the proposed estimator of (5.6) is the best among all the methods tested. In particular, the SER performance of the proposed estimator of (5.6) is almost same as that of the methods of (4.22) and [CMC08], about 1 dB better than that of the method of [VSPV09] and much better than that of the method of [SGM05].

Same as the corresponding numerical examples in Section 4.5, the SNR and the parameter P are set to 0 dB and 2, respectively, and L' is varied in the fourth and the fifth numerical examples in this section. All other parameters are the same as in the first example. In the fourth example, we set $L = 5$, and in the fifth example, $L = L'$ and is varied from 5 to 20.

Fig. 5.13 and Fig. 5.16 illustrate the estimation bias for all the methods tested versus

Figure 5.13: Bias versus L' , fourth example, $L = 5$.Figure 5.14: RMSE versus L' , fourth example, $L = 5$.

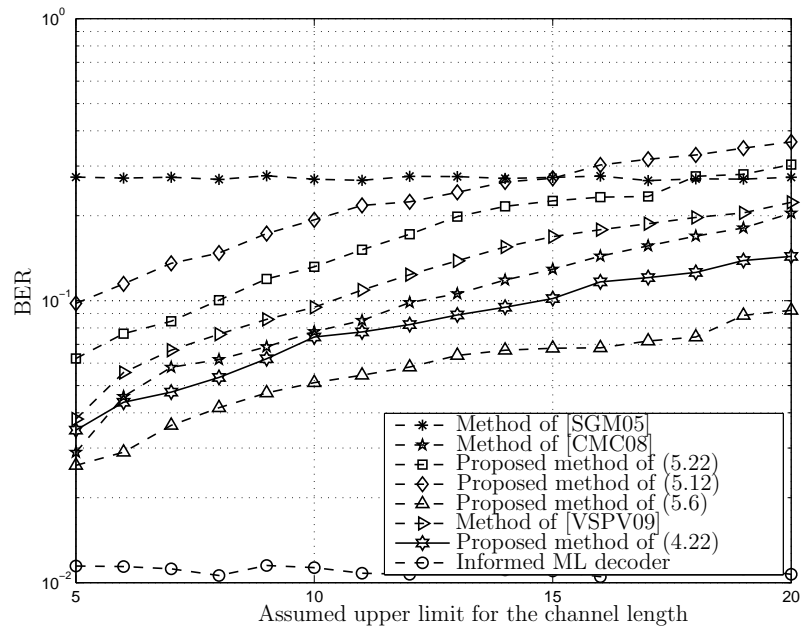


Figure 5.15: BER versus L' , fourth example, $L = 5$.

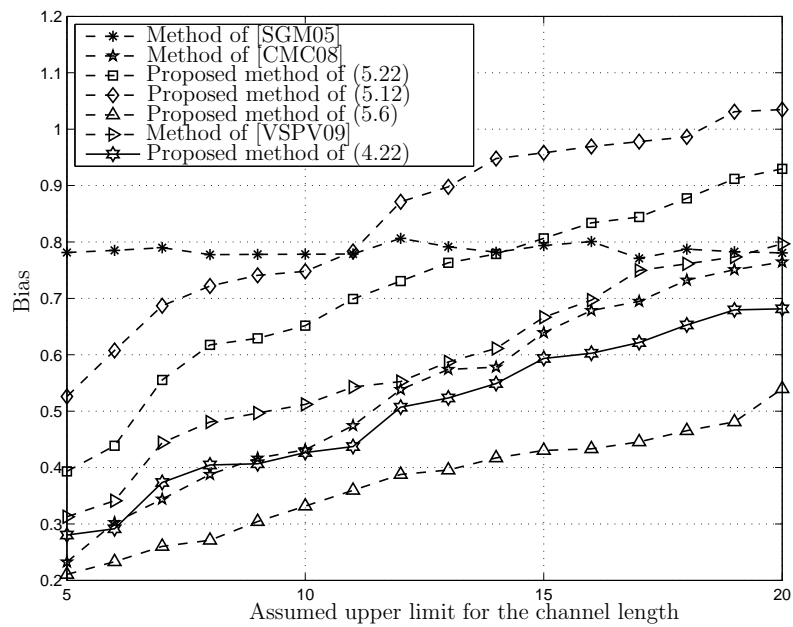


Figure 5.16: Bias versus L' , fifth example, $L = L'$.

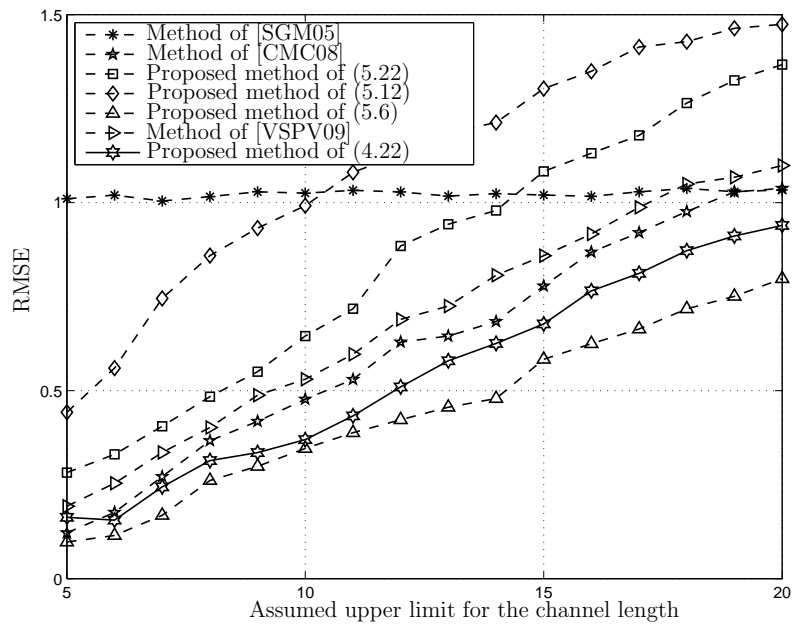


Figure 5.17: RMSE versus L' , fifth example, $L = L'$.

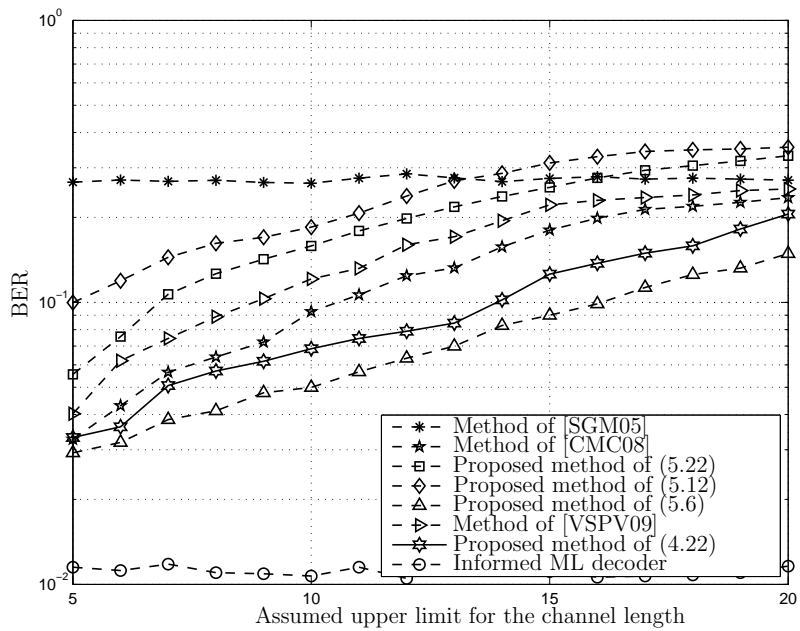


Figure 5.18: BER versus L' , fifth example, $L = L'$.

L' for the the fourth and the fifth numerical examples. It can be seen from Fig. 5.13 and Fig. 5.16 that the proposed method of (5.6) results in the lowest estimation bias compared to the other methods tested. Also, for all values of L' , the proposed method of (5.6) exhibits substantially lower estimation bias compared to the method of [SGM05]. Moreover, both estimators of (5.12) and (5.22) perform better than the method of [SGM05] when L' is close to L , i.e., $L' < 14$ and $L' < 19$, respectively. Furthermore in Fig. 5.13, all methods tested, excluding the subcarrier-wise method of [SGM05], exhibit the best estimation performance for $L = L'$ due to the fact that the number of parameters to be estimated increases with L' . Also, the best performance for all the methods tested, excluding the method of [SGM05], correspond to the case when L is minimum, i.e., $L = 5$. Figs. 5.14 and 5.17 present the channel estimation RMSE performances of the methods tested versus L' . These figures result in quite the same conclusions as Figs. 5.10 and 5.13. Finally, Figs. 5.15 and 5.18 show BERs of the methods tested versus L' . It can be seen from these figures that the performance of the method of [SGM05] and the informed ML receiver are insensitive to L' . Also, the proposed method of (5.6) shows the best BERs performance among all the other methods which deteriorates by increasing L' .

All the methods proposed in this chapter suffer from blind channel non-identifiability either in the case of rotatable codes or the MISO system configuration for most of the OSTBCs; see Table 3.1. To show another benefit of the coherent processing mentioned in Remark 4.3.2 of Section 4.3, we set $M = 1$ in the sixth numerical example. All the other parameters are same as the first example. The principal eigenvalue of $\mathcal{X}_i(\gamma_u)$ exhibits multiplicity of order two for the selected setup according to Table 3.1 for the code index 5. We exploit the non-uniform weighting strategy of (3.26) in the first ten subcarriers and the uniform weighting strategy for all the other subcarriers. Also, the covariance matrices of the transmitted symbols in the first ten subcarriers are chosen as $\{\mathbf{\Lambda}_{\mathbf{s}_i}\}_{i=0}^9 = \frac{K}{6} \text{diag}([3, 1, 1, 1])$ which guarantee $\text{tr}(\mathbf{\Lambda}_{\mathbf{s}_i}) = K$ and fulfill the necessary condition of (3.25). The covariance matrices of the transmitted symbols for the rest of subcarriers are proportional to the identity matrix. The weight vector corresponding to the proposed weighting strategy of (3.26) is selected as $\gamma_n = [2, 1, 1, 1]$ for the first ten subcarriers.

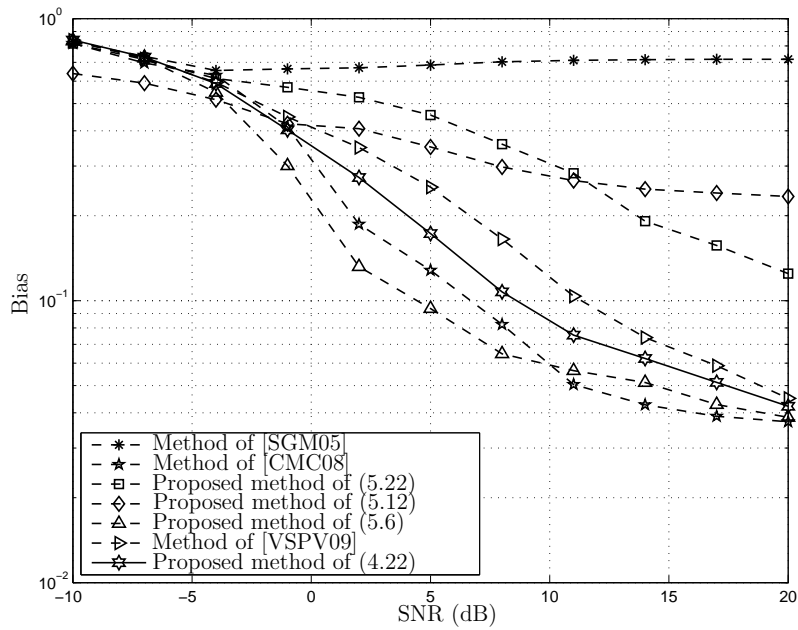


Figure 5.19: Bias versus SNR, sixth example.

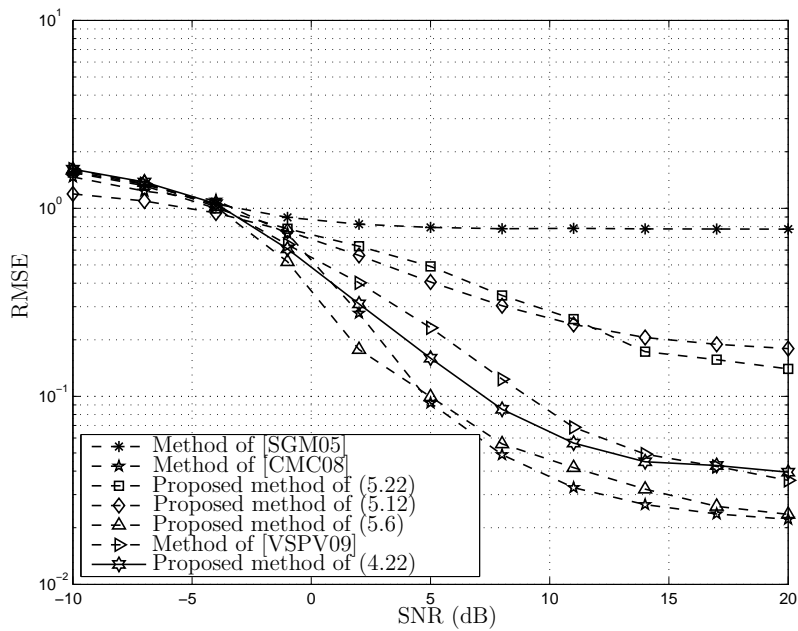


Figure 5.20: RMSE versus SNR, sixth example.

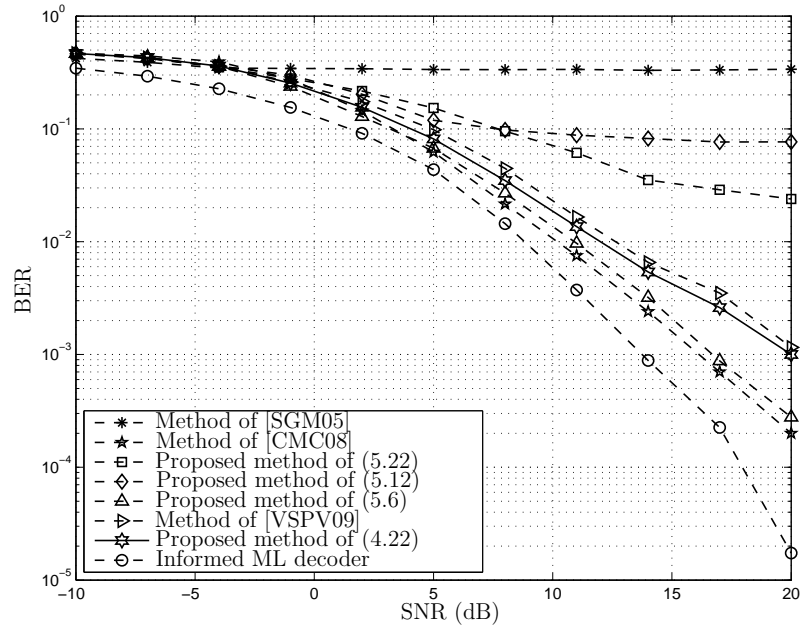


Figure 5.21: BER versus SNR, sixth example.

It can be observed from Figs. 5.19-5.21 that although the method of [SGM05] is not able to resolve non-scalar ambiguities, all the other methods proposed in this chapter have resolved such ambiguities. Among these methods, the SDR-based method of (5.6) shows the best performance which is very close to that of the method of [CMC08] and noticeably better than that of the methods of (4.22) and [VSPV09]. Finally, comparing the symbol decoding performance of all methods tested in Fig. 5.3 and Fig. 5.21, excluding that of the method of [SGM05], reveals that implementing such weighting strategy results in a worse decoding performance.

5.6 Chapter summary

Three new blind channel estimation approach for orthogonally coded MIMO-OFDM wireless communication systems that exhibit different performance-complexity trade-offs have been proposed. The key idea of the presented techniques is to exploit specific properties of

the OSTBCs and the finite delay spread assumption over the wireless channel to estimate the FIR channel parameters in the time-domain jointly for all subcarriers. This has been shown to result in a considerable improved parsimony of the channel parametric model and, hence, lower computational complexity as compared to the direct subcarrier-wise channel estimation methods. This also allows to perform coherent processing across all the subcarriers. First, we developed an optimization problem to estimate the true overall CFR vector that exhibits a close relationship with that of the Chapter 4 for particular choice of normalization vector ξ in (4.1). It has been shown that using the SDR approach, the developed channel estimation problem can be converted to a convex SDP problem which can be solved using modern convex optimization toolboxes. Then, it is shown that relaxing finite alphabet constraint over the transmitted symbols dramatically simplifies the joint blind ML symbol detection and channel estimation problem which provided an opportunity to develop the second estimator. By performing per subcarrier CFR norm relaxation, this RML-based technique is interpreted as a special case of the extended covariance matrix defined in Chapter 4 with uniform normalization coefficients. Finally, we have proposed another estimator based on well-known Capon receiver which corresponding performance outperforms that of the RML-based estimator. We also applied some sort of norm relaxation to devise closed-form version of Capon approach. Provided simulations have demonstrated performance advantages of the proposed methods as compared to several current state-of-the-art blind MIMO-OFDM channel estimation and symbol detection techniques.

Chapter 6

Conclusions and future works

In recent years, the need for high rate reliable transmission over the wireless channels has increased extremely. Multi-antenna and multi-carrier communication systems are known to provide both theoretically attractive and technically feasible solutions that fulfill the aforementioned requirements. However, to achieve the promises of these systems, an accurate channel state information is demanded at the receiver most of the time.

In this thesis, we have proposed several new algorithms for blind channel estimation in orthogonally coded MIMO systems which exhibit different performance-complexity trade-offs. Further, we have studied different respective aspects regarding blind identifiability and uniqueness of estimates taking into account practically notable scenarios.

6.1 Conclusions

In Chapter 2, after presenting signal model considered throughout the thesis and discussing the OSTBCs properties, we studied the special class of the OSTBCs known as the rotatable codes. Then, we went through blind identifiability issue of the wireless channel and proved that in the case of rotatable OSTBCs including well-known Alamouti code, blind channel estimates show non-scalar ambiguity in addition to inherent scalar ambiguity. Finally, we presented the structure of an optimal receiver for orthogonally space-time coded MIMO

systems.

In Chapter 3, we developed a novel virtual snapshot model for orthogonally space-time coded frequency flat MIMO, and, hence, for a single-carrier of orthogonally coded MIMO-OFDM systems. Next, this model was exploited to devise a blind channel estimation method which can be implemented in a single-carrier basis. Further, we proposed two weighting strategies of different virtual snapshots and proved respective abilities to resolve any principal eigenvalue multiplicity of the weighted covariance matrix of the aforementioned virtual snapshots. These weighting strategies correspond to two important practical scenarios: systems involving the rotatable codes like the celebrated Alamouti code that also adopted in the LTE standard and systems involving the single-antenna receivers as in the downlink transmission for mobile handsets. We proved that these two weighting strategies are capable to resolve all non-scalar ambiguities inherent to blind channel estimation if the weighting coefficients and symbol powers satisfy specific conditions. We further showed that the linear precoding method of [SGM05] and the correlation matching method of [VS08b] are special cases of the proposed strategies which particularly satisfy the sufficient part of provided uniqueness conditions. The necessary parts of these conditions have not been introduced before and the latter methods only suggest special cases of appropriate weighting coefficients. Computer simulations verified provided analytical results and showed the performance of devised blind channel estimator along with the proposed weighting strategies.

Next, a novel closed-form blind channel estimation approach for orthogonally space-time coded MIMO-OFDM systems was developed in Chapter 4. We used the virtual snapshot model, devised in Chapter 3, and proposed a new normalization method to retain the desired property of virtual snapshot covariance matrix principal eigenvector for all subcarriers. Then, the finite delay spread assumption of the wireless channel was used to estimate a lower number of parameters in the time-domain rather than the frequency-domain. As a result, the capability of coherent processing among different subcarriers and improved parsimony of the channel parametric model in contrast to the habitual subcarrier-wise channel estimation methods were obtained. These benefits resulted in a considerable reduced computational complexity and improved estimation accuracy. In addition, we derived the

condition which guarantees the uniqueness of the channel estimates. Provided numerical results demonstrated performance advantages of the proposed approach in comparison with other state-of-the-art blind MIMO-OFDM channel estimation or symbol detection methods.

Finally in Chapter 5, three blind MIMO channel estimators for frequency-selective wireless systems, which exploit OSTBCs along with OFDM, were developed. In all these methods, the finite delay spread assumption over the wireless channel together with the properties of the OSTBC were used to estimate the CIR parameters. Like the method presented in Chapter 4, all methods benefit from coherent processing across all the subcarriers which improves estimation quality. For the first approach, we showed that the MIMO-OFDM channel estimation problem exploits a special case of the extended covariance matrix defined in Chapter 4 and can be converted to a convex SDP problem, using the SDR technique, and solved by the aid of current convex optimization toolboxes. In the second approach, we considerably simplified the joint blind ML symbol detection and channel estimation problem by using finite alphabet constraint relaxation over the transmitted symbols. Then, we approximated the corresponding optimization problem by relaxing individual channel norm constraints per-subcarrier and replacing them by one aggregated norm constraint and came up with a closed-form channel estimator. It is also showed that this estimator exploits a special case of the extended covariance matrix defined in Chapter 4. In the third approach, we exploited Capon receiver to develop MIMO-OFDM channel estimator. Coherently combining different subcarrier Capon spectra together with relaxation of the respective CFR norm constraints resulted in another closed-form blind channel estimator with outperformed performance in contrast to that of the RML-based estimator. All of the proposed methods exhibited different performance-complexity trade-offs which were reflected partly in numerical results. Also, computer simulations demonstrated performance advantages of the proposed methods as compared to other current state-of-the-art blind MIMO-OFDM channel estimation and symbol detection techniques.

6.2 Future works

In Chapter 3, we developed a closed-form blind channel estimator based on novel virtual snapshot model and then proposed two weighting strategies which can deal with the problem of non-scalar ambiguities of channel estimates in two important practical scenarios. Since assuming power imbalance among the transmitted symbols (by applying, e.g., linear precoding of [SGM05]), which is necessary to implement the proposed weighting strategies, results in a minimum distance reduction of the symbol constellations, it would be interesting to evaluate the performance losses of these strategies by the help of an experimental setup in addition to computer simulations such as what has been done in [HSGG08]. It would be also attractive to investigate the impact of choosing different weighting sets that satisfy the sufficient conditions of (3.14) and (3.26) on the final symbol decoding performance and to adopt a proper measure, e.g., the SER to derive the optimal weighting coefficients. Moreover, nearly the same idea to that of in Chapter 3 can be exploited to devise a blind symbol detection method for frequency flat extremely fast fading scenarios in which the wireless channel varies even during the transmission of one data block. In this case, by a slight modification of signal model, it can be proved that the vector of the transmitted symbols can be estimated as the principal eigenvector of the *oversampled* received data vector covariance matrix during one data block. Furthermore, although the tensor-based extension of the blind estimator presented in Chapter 3 has been proposed in [RSSHPG11], developing the tensor-based joint estimator for MIMO channel and carrier frequency offset (CFO) is still interesting and deserves further study.

In Chapter 4, we proposed a novel closed-form blind channel estimator for orthogonally space-time coded MIMO-OFDM systems that estimates the subspace which contains the true channel vector irrespective of whether pilots are available or not. Since pilots are already inserted in the data frame structure of modern standards which adopted MIMO-OFDM such as the LTE, how to exploit these pilots in order to further enhance the quality of fully blind channel estimates and to devise a semi-blind estimation method compatible to practical standards can be the subject of a study. One way of doing this is to exploit

available pilots to extract CSI from the subspace attained blindly by the use of the method proposed in Chapter 4. The latter idea and its iterative version have been developed in the sequel of this thesis; see [VSP11a] and [VSP11b], respectively, for more details. The other attractive way which deserves further study could be to use pilots available in the frame structure of standards to obtain a preliminary estimate of the channel vector and then enhance corresponding quality by projecting this estimate onto the blind subspace achieved by the application of the method of Chapter 4. This is subject of an ongoing research project of the thesis author. Also, the tensor-based blind MIMO approach of [RSSHPG11] could be proposed for the frequency-selective fading channel using nearly the same coherent processing idea of Chapter 4.

As we have assumed that the multipath delays, the position of channel taps, are known at the receiver, the performance of the proposed channel estimators in Chapters 4 and 5 could be evaluated in conjunction with any practical method that estimates the multipath delays. Doing this enables us to investigate the robustness of the proposed approaches against multipath delays mismatches.

Further, the key ideas of the proposed methods in this thesis can be extended to the general case of space-time codes, e.g., the quasi-orthogonal space-time codes [Jaf01] or the distributed space-time codes [JH06]. Also, an extension of the proposed channel estimators to orthogonal and quasi-orthogonal designs in one-way or two-way non-regenerative (amplify and forward) wireless relay networks [JJ07] that use OFDM encoding is also interesting and corresponding performance could be investigated. Finally, the proposed approaches can be extended for joint MIMO channel and CFO estimation in such distributed systems.

Chapter 7

Appendices

Appendix A

To prove (2.38), we consider the definition in (2.37) together with (2.40). The (k, l) th entry of the matrix multiplication in (2.38) can be written as $[\mathbf{A}(\mathbf{h}_i)^T \mathbf{A}(\mathbf{h}_i)]_{kl} = \mathbf{a}_k(\mathbf{h}_i)^T \mathbf{a}_l(\mathbf{h}_i)$. This entry can be extended to obtain

$$\mathbf{a}_k(\mathbf{h}_i)^T \mathbf{a}_l(\mathbf{h}_i) = \mathbf{h}_i^T \begin{bmatrix} \operatorname{Re}(\mathbf{I}_M \otimes \mathbf{C}_k^T) & \operatorname{Im}(\mathbf{I}_M \otimes \mathbf{C}_k^T) \\ -\operatorname{Im}(\mathbf{I}_M \otimes \mathbf{C}_k^T) & \operatorname{Re}(\mathbf{I}_M \otimes \mathbf{C}_k^T) \end{bmatrix} \begin{bmatrix} \operatorname{Re}(\mathbf{I}_M \otimes \mathbf{C}_l) & -\operatorname{Im}(\mathbf{I}_M \otimes \mathbf{C}_l) \\ \operatorname{Im}(\mathbf{I}_M \otimes \mathbf{C}_l) & \operatorname{Re}(\mathbf{I}_M \otimes \mathbf{C}_l) \end{bmatrix} \mathbf{h}_i. \quad (\text{A.1})$$

Taking into account that

$$\begin{aligned} \operatorname{Re}(\mathbf{I}_M \otimes \mathbf{C}_k^T) &= \operatorname{Re}(\mathbf{I}_M \otimes \mathbf{C}_k^H), \quad k = 1, \dots, 2K \\ \operatorname{Im}(\mathbf{I}_M \otimes \mathbf{C}_k^T) &= -\operatorname{Im}(\mathbf{I}_M \otimes \mathbf{C}_k^H), \quad k = 1, \dots, 2K \end{aligned} \quad (\text{A.2})$$

expression (A.1) is equal to

$$\mathbf{a}_k(\mathbf{h}_i)^T \mathbf{a}_l(\mathbf{h}_i) = \mathbf{h}_i^T \begin{bmatrix} \operatorname{Re}(\mathbf{I}_M \otimes \mathbf{C}_k^H \mathbf{C}_l) & -\operatorname{Im}(\mathbf{I}_M \otimes \mathbf{C}_k^H \mathbf{C}_l) \\ \operatorname{Im}(\mathbf{I}_M \otimes \mathbf{C}_k^H \mathbf{C}_l) & \operatorname{Re}(\mathbf{I}_M \otimes \mathbf{C}_k^H \mathbf{C}_l) \end{bmatrix} \mathbf{h}_i = \mathbf{h}_i^T \mathbf{C} \mathbf{h}_i, \quad k, l = 1, \dots, 2K \quad (\text{A.3})$$

where

$$\mathbf{C} \triangleq \begin{bmatrix} \operatorname{Re}(\mathbf{I}_M \otimes \mathbf{C}_k^H \mathbf{C}_l) & -\operatorname{Im}(\mathbf{I}_M \otimes \mathbf{C}_k^H \mathbf{C}_l) \\ \operatorname{Im}(\mathbf{I}_M \otimes \mathbf{C}_k^H \mathbf{C}_l) & \operatorname{Re}(\mathbf{I}_M \otimes \mathbf{C}_k^H \mathbf{C}_l) \end{bmatrix}.$$

According to the property of the OSTBCs basis matrices in (2.24), we distinguish two different cases of $k = l$ and $k \neq l$. Since $\mathbf{C}_k^H \mathbf{C}_k = \mathbf{I}_N$, we conclude that

$$\mathbf{a}_k(\mathbf{h}_i)^T \mathbf{a}_k(\mathbf{h}_i) = \mathbf{h}_i^T \begin{bmatrix} \text{Re}(\mathbf{I}_{MN}) & -\text{Im}(\mathbf{I}_{MN}) \\ \text{Im}(\mathbf{I}_{MN}) & \text{Re}(\mathbf{I}_{MN}) \end{bmatrix} \mathbf{h}_i = \mathbf{h}_i^T \mathbf{I}_{2MN} \mathbf{h}_i = \|\mathbf{h}_i\|^2, \quad k = 1, \dots, 2K. \quad (\text{A.4})$$

For the case of $k \neq l$, we exploit the skew-hermitian property of $\mathbf{C}_k^H \mathbf{C}_l = -\mathbf{C}_l^H \mathbf{C}_k$ to show that

$$\mathbf{C} = \begin{bmatrix} \text{Re}(\mathbf{I}_M \otimes \mathbf{C}_k^H \mathbf{C}_l) & -\text{Im}(\mathbf{I}_M \otimes \mathbf{C}_k^H \mathbf{C}_l) \\ \text{Im}(\mathbf{I}_M \otimes \mathbf{C}_k^H \mathbf{C}_l) & \text{Re}(\mathbf{I}_M \otimes \mathbf{C}_k^H \mathbf{C}_l) \end{bmatrix} = \begin{bmatrix} -\text{Re}(\mathbf{I}_M \otimes \mathbf{C}_l^H \mathbf{C}_k) & \text{Im}(\mathbf{I}_M \otimes \mathbf{C}_l^H \mathbf{C}_k) \\ -\text{Im}(\mathbf{I}_M \otimes \mathbf{C}_l^H \mathbf{C}_k) & -\text{Re}(\mathbf{I}_M \otimes \mathbf{C}_l^H \mathbf{C}_k) \end{bmatrix}. \quad (\text{A.5})$$

Using (A.5), we have that $\mathbf{C}^T = -\mathbf{C}$, i.e., \mathbf{C} is skew-symmetric. Therefore, according to (A.3), we obtain

$$\mathbf{a}_k(\mathbf{h}_i)^T \mathbf{a}_l(\mathbf{h}_i) = \mathbf{h}_i^T \mathbf{C} \mathbf{h}_i = \mathbf{h}_i^T \mathbf{C}^T \mathbf{h}_i = -\mathbf{h}_i^T \mathbf{C} \mathbf{h}_i = 0, \quad k \neq l, k = 1, \dots, 2K \quad (\text{A.6})$$

Properties (A.4) and (A.6) complete the proof of (2.38). \square

Appendix B

To prove (2.45) [BSK06], definition (2.37), the orthogonality property (2.38), and expression (2.41) can be used which imply that for any channel vector \mathbf{h}_i , we obtain

$$\mathbf{a}_k(\mathbf{h}_i)^T \mathbf{a}_k(\mathbf{h}_i) = \mathbf{h}_i^T \Phi_k^T \Phi_k \mathbf{h}_i = \mathbf{h}_i^T \mathbf{h}_i. \quad (\text{B.1})$$

As (B.1) holds true for any \mathbf{h}_i and since $(\Phi_k^T \Phi_k)$ is a symmetric matrix, we conclude the first part of (2.45). To prove the second part of (2.45), we use the fact that according to (2.38), different columns of $\mathbf{A}(\mathbf{h}_i)$ are orthogonal to each other and conclude

$$\mathbf{a}_k(\mathbf{h}_i)^T \mathbf{a}_l(\mathbf{h}_i) = \mathbf{h}_i^T \Phi_k^T \Phi_l \mathbf{h}_i = 0 \quad (\text{B.2})$$

$$\mathbf{a}_l(\mathbf{h}_i)^T \mathbf{a}_k(\mathbf{h}_i) = \mathbf{h}_i^T \Phi_l^T \Phi_k \mathbf{h}_i = 0. \quad (\text{B.3})$$

Adding (B.2) and (B.3) side-by-side results

$$\mathbf{h}_i^T (\Phi_k^T \Phi_l + \Phi_l^T \Phi_k) \mathbf{h}_i = 0. \quad (\text{B.4})$$

Since (B.4) holds true for any vector \mathbf{h}_i and as $(\Phi_k^T \Phi_l + \Phi_l^T \Phi_k)$ is a symmetric matrix, we conclude that $(\Phi_k^T \Phi_l + \Phi_l^T \Phi_k) = 0$. This completes the proof of (2.45). It should be stressed that (2.45) can be also deduced from (2.24) together with (2.42).

Appendix C

The result of this appendix, which is based on the following lemma and proposition from linear algebra, is used to prove (3.9) and to conclude property of (3.29) in the thesis.

Lemma C.1: Let matrices $\mathbf{M}, \mathbf{N} \in \mathbb{R}^{2MT \times 2MT}$ be symmetric. Assume that \mathbf{N} is positive semi-definite and $\lambda_n(\cdot)$ shows the n th largest eigenvalue of a matrix. Then [HJ85],

$$\lambda_n(\mathbf{M}) \leq \lambda_n(\mathbf{M} + \mathbf{N}), \quad n = 1, \dots, 2MT.$$

□

Proposition C.1: For any arbitrary matrices \mathbf{M} and \mathbf{N} with conformable dimensions we have

$$\lambda_n(\mathbf{MN}) = \lambda_n(\mathbf{NM}). \quad (\text{C.1})$$

□

Due to the fact that $T \geq N$ for any arbitrary OSTBC and from (2.45), we deduce that $\{\Xi_l\}_{l=1}^{2K} \triangleq \Phi_l \Phi_l^T$ and $\{\mathbf{I} - \Xi_l\}_{l=1}^{2K}$ are all diagonal matrices with ones and zeros on their main diagonal. Let $\boldsymbol{\theta} \triangleq [\theta_1, \dots, \theta_{2K}]^T$ be a vector of non-negative coefficients and $\boldsymbol{\Theta} \triangleq \text{diag}(\boldsymbol{\theta})$. Making use of (2.38), (2.41), (2.45), (3.8), and (C.1) we obtain

$$\begin{aligned} \lambda_n(\mathcal{U}_{il}(\boldsymbol{\theta})) &= \lambda_n \left(\sum_{k=1}^{2K} \theta_k \Phi_l^T \Phi_k \mathbf{h}_i \mathbf{h}_i^T \Phi_k^T \Phi_l \right) = \lambda_n \left(\Phi_l^T \left(\sum_{k=1}^{2K} \theta_k \Phi_k \mathbf{h}_i \mathbf{h}_i^T \Phi_k^T \right) \Phi_l \right) \\ &= \lambda_n \left(\Phi_l^T \mathbf{A}(\mathbf{h}_i) \boldsymbol{\Theta} \mathbf{A}(\mathbf{h}_i)^T \Phi_l \right) = \lambda_n \left(\boldsymbol{\Theta}^{1/2} \mathbf{A}(\mathbf{h}_i)^T \Phi_l \Phi_l^T \mathbf{A}(\mathbf{h}_i) \boldsymbol{\Theta}^{1/2} \right) \\ &= \lambda_n \left(\boldsymbol{\Theta}^{1/2} \mathbf{A}(\mathbf{h}_i)^T \Xi_l \mathbf{A}(\mathbf{h}_i) \boldsymbol{\Theta}^{1/2} \right) \\ &\leq \lambda_n \left(\boldsymbol{\Theta}^{1/2} \mathbf{A}(\mathbf{h}_i)^T \Xi_l \mathbf{A}(\mathbf{h}_i) \boldsymbol{\Theta}^{1/2} + \boldsymbol{\Theta}^{1/2} \mathbf{A}(\mathbf{h}_i)^T (\mathbf{I} - \Xi_l) \mathbf{A}(\mathbf{h}_i) \boldsymbol{\Theta}^{1/2} \right) \\ &= \lambda_n \left(\boldsymbol{\Theta}^{1/2} \mathbf{A}(\mathbf{h}_i)^T \mathbf{A}(\mathbf{h}_i) \boldsymbol{\Theta}^{1/2} \right) = \|\mathbf{h}_i\|^2 \lambda_n(\boldsymbol{\Theta}), \end{aligned} \quad (\text{C.2})$$

in which the inequality in (C.2) follows from Lemma C.1.

Appendix D

If the transmitted symbols covariance matrix $\Lambda_{\underline{s}_i}$ is not diagonal, we apply eigenvalue decomposition to obtain $\Lambda_{\underline{s}_i} = \mathcal{Q} \mathring{\Lambda}_{\underline{s}_i} \mathcal{Q}^T$ where $\mathring{\Lambda}_{\underline{s}_i}$ is a diagonal matrix and $\mathcal{Q}^T \mathcal{Q} = \mathcal{Q} \mathcal{Q}^T = \mathbf{I}_{2K}$. Replacing the previous eigenvalue decomposition in (3.32) yields

$$\mathbf{R}_i = \mathbf{A}(\mathbf{h}_i) \mathcal{Q} \mathring{\Lambda}_{\underline{s}_i} \mathcal{Q}^T \mathbf{A}(\mathbf{h}_i)^T + \frac{\sigma^2}{2} \mathbf{I}_{2MT}. \quad (\text{D.1})$$

Let us define $\mathring{\mathbf{A}}(\mathbf{h}_i) \triangleq \mathbf{A}(\mathbf{h}_i) \mathcal{Q}$ with the property

$$\mathring{\mathbf{A}}(\mathbf{h}_i)^T \mathring{\mathbf{A}}(\mathbf{h}_i) = \mathcal{Q}^T \mathbf{A}(\mathbf{h}_i)^T \mathbf{A}(\mathbf{h}_i) \mathcal{Q} = \|\mathbf{h}_i\|^2.$$

Multiplying (D.1) from the right by the orthonormal matrix $\mathring{\mathbf{A}}(\mathbf{h}_i)/\|\mathbf{h}_i\|$ we obtain

$$\mathbf{R}_i \frac{\mathring{\mathbf{A}}(\mathbf{h}_i)}{\|\mathbf{h}_i\|} = \frac{\mathring{\mathbf{A}}(\mathbf{h}_i)}{\|\mathbf{h}_i\|} \left(\mathring{\Lambda}_{\underline{s}_i} \|\mathbf{h}_i\|^2 + \frac{\sigma^2}{2} \mathbf{I}_{2K} \right). \quad (\text{D.2})$$

As $\mathring{\Lambda}_{\underline{s}_i}$ is a diagonal matrix, (D.2) can be viewed as the characteristic equation for the matrix \mathbf{R}_i and its $2K$ largest eigenvalues depend only on the norm of the CFR vector \mathbf{h}_i and not its respective spatial signature.

Appendix E

In this appendix, making use of a lemma from linear algebra, we derive an optimization problem to estimate the true overall CFR vector for all subcarriers, i.e., \mathbf{h}' , which has a close connection with characteristic equation (4.7) for particular choice of normalization vector $\boldsymbol{\xi}$ used in (4.1). Using (2.33), the multiple input-output relationships (2.36) in the frequency-domain for a certain data block, i.e., fixed index p , can be also represented in the compact form of

$$\mathbf{y}' = \mathcal{A}(\mathbf{h}_0, \dots, \mathbf{h}_{N_0-1}) \mathbf{s}' + \mathbf{v}' = \mathcal{A}(\mathbf{h}') \mathbf{s}' + \mathbf{v}', \quad (\text{E.1})$$

where block-diagonal matrix $\mathcal{A}(\mathbf{h}')$ is defined as

$$\mathcal{A}(\mathbf{h}') \triangleq \begin{bmatrix} \mathbf{A}(\mathbf{h}_0) & \mathbf{0} & \cdots & \mathbf{0} \\ \mathbf{0} & \mathbf{A}(\mathbf{h}_1) & & \mathbf{0} \\ \vdots & & \ddots & \vdots \\ \mathbf{0} & \cdots & \mathbf{0} & \mathbf{A}(\mathbf{h}_{N_0-1}) \end{bmatrix} \in \mathbb{R}^{2MTN_0 \times 2KN_0}, \quad (\text{E.2})$$

and

$$\mathbf{y}' \triangleq \begin{bmatrix} \mathbf{y}_0 \\ \vdots \\ \mathbf{y}_{N_0-1} \end{bmatrix} \in \mathbb{R}^{2MTN_0 \times 1}, \quad \mathbf{s}' \triangleq \begin{bmatrix} \underline{\mathbf{s}}_0 \\ \vdots \\ \underline{\mathbf{s}}_{N_0-1} \end{bmatrix} \in \mathbb{R}^{2KN_0 \times 1}, \quad \mathbf{v}' \triangleq \begin{bmatrix} \mathbf{v}_0 \\ \vdots \\ \mathbf{v}_{N_0-1} \end{bmatrix} \in \mathbb{R}^{2MTN_0 \times 1}, \quad (\text{E.3})$$

as the real-valued vectors which combine the received data, the transmitted data, and the noise, respectively, for all subcarriers. From (2.38), the following generalized version of orthogonality property for $\mathcal{A}(\mathbf{h}')$ can be deduced

$$\mathcal{A}(\mathbf{h}')^T \mathcal{A}(\mathbf{h}') = \mathbf{D}^2, \quad (\text{E.4})$$

with $\mathbf{D} \triangleq \left(\text{diag}([\|\mathbf{h}_0\|, \dots, \|\mathbf{h}_{N_0-1}\|]) \otimes \mathbf{I}_{2K} \right) \in \mathbb{R}^{2KN_0 \times 2KN_0}$. Also, it can be concluded from block-diagonal structure of $\mathcal{A}(\mathbf{h}')$ in (E.2) along with linearity of $\mathbf{A}(\mathbf{h}_i)$ with respect to \mathbf{h}_i , for $i = 0, \dots, N_0 - 1$, according to (2.43) that $\mathcal{A}(\mathbf{h}')$ is linear with respect to \mathbf{h}' and there exist an OSTBC-specific matrix Ψ , such that

$$\text{vec}\{\mathcal{A}(\mathbf{h}')\} = \begin{bmatrix} f_0(\Phi) & \mathbf{0} & \cdots & \mathbf{0} \\ \mathbf{0} & f_1(\Phi) & & \mathbf{0} \\ \vdots & & \ddots & \vdots \\ \mathbf{0} & \cdots & \mathbf{0} & f_{N_0-1}(\Phi) \end{bmatrix} \mathbf{h}' = \Psi \mathbf{h}', \quad (\text{E.5})$$

where each $\{f_i(\Phi)\}_{i=0}^{N_0-1} \in \mathbb{R}^{4KMTN_0 \times 2MN}$. Performing similar steps as in the derivation of (3.32) and (3.33) for the covariance matrix $\mathbf{R} \triangleq \mathbb{E}\{\mathbf{y}'\mathbf{y}'^T\}$ and taking into account (E.1) along with the assumption that the symbol streams and noise are mutually uncorrelated at each subcarrier, we obtain

$$\mathbf{R} = \mathcal{A}(\mathbf{h}')\mathbf{\Lambda}_{\mathbf{s}'}\mathcal{A}(\mathbf{h}')^T + \frac{\sigma^2}{2}\mathbf{I}_{2MTN_0}, \quad (\text{E.6})$$

where $\mathbf{\Lambda}_{\mathbf{s}'} \triangleq \mathbb{E}\{\mathbf{s}'\mathbf{s}'^T\}$. Then, we multiply (E.6), as the generalization of (3.32), from the right by $\mathcal{A}(\mathbf{h}')\mathbf{D}^{-1}$ and apply (E.4) to obtain the generalization of (3.33) as

$$\mathbf{R}\mathcal{A}(\mathbf{h}')\mathbf{D}^{-1} = \mathcal{A}(\mathbf{h}')\mathbf{D}^{-1}\mathbf{\Lambda}, \quad (\text{E.7})$$

with $\mathbf{\Lambda} \triangleq \left(\mathbf{\Lambda}_{\mathbf{s}'}\mathbf{D}^2 + \frac{\sigma^2}{2}\mathbf{I}_{2KN_0} \right)$. Due to the property that the matrix $\mathcal{A}(\mathbf{h}')\mathbf{D}^{-1}$ has orthonormal columns and both \mathbf{D}^2 and $\mathbf{\Lambda}_{\mathbf{s}'}$ (since the entries of \mathbf{s}' are mutually uncorrelated)

are diagonal, (E.7) can be viewed as the characteristic equation for \mathbf{R} . Hence, the diagonal entries of $\mathbf{\Lambda}$ contain the associated $2KN_0$ largest eigenvalues with corresponding eigenvectors equal to the columns of $\mathcal{A}(\mathbf{h}')\mathbf{D}^{-1}$. Further, since the entries of \mathbf{s}' are assumed to be mutually uncorrelated and using (E.2) and (E.6), it can be concluded that \mathbf{R} has the following block-diagonal structure

$$\mathbf{R} = \begin{bmatrix} \mathbf{R}_0 & \mathbf{0} & \cdots & \mathbf{0} \\ \mathbf{0} & \mathbf{R}_1 & & \mathbf{0} \\ \vdots & & \ddots & \vdots \\ \mathbf{0} & \cdots & \mathbf{0} & \mathbf{R}_{N_0-1} \end{bmatrix} \in \mathbb{R}^{2MTN_0 \times 2MTN_0}. \quad (\text{E.8})$$

Next, we present the following lemma [Man02] which is used later to develop our blind channel estimator.

Lemma E.1: Let \mathbf{M} be an $m \times q$ arbitrary real matrix with $q \leq m$. Then, for any $m \times m$ real symmetric matrix \mathbf{N} , the solution to the following optimization problem

$$\begin{aligned} \max_{\mathbf{M}} \quad & \text{tr}(\mathbf{M}^T \mathbf{N} \mathbf{M}) \\ \text{s.t.} \quad & \mathbf{M}^T \mathbf{M} = \mathbf{I}_q, \end{aligned} \quad (\text{E.9})$$

is given by any matrix \mathbf{M}_* whose column space is the same as the subspace spanned by the q principal eigenvectors that correspond to the q largest eigenvalues of \mathbf{N} . For such \mathbf{M}_* , we have

$$\text{tr}(\mathbf{M}_*^T \mathbf{N} \mathbf{M}_*) = \sum_{l=1}^q \nu_l, \quad (\text{E.10})$$

where ν_l 's for $l = 1, \dots, q$ are the q largest eigenvalues of \mathbf{N} . \square

We set $q = 2KN_0$ and replace arbitrary symmetric matrix \mathbf{N} by the covariance matrix \mathbf{R} in (E.9) to obtain the following optimization problem

$$\begin{aligned} \max_{\mathbf{M}} \quad & \text{tr}(\mathbf{M}^T \mathbf{R} \mathbf{M}) \\ \text{s.t.} \quad & \mathbf{M}^T \mathbf{M} = \mathbf{I}_{2KN_0}. \end{aligned} \quad (\text{E.11})$$

Taking into account characteristic equation (E.7) and Lemma E.1, since the diagonal entries of $\mathbf{\Lambda}$ contain the associated $q = 2KN_0$ largest eigenvalues of \mathbf{R} with corresponding

eigenvectors equal to the columns of $\mathcal{A}(\mathbf{h}')$, we conclude that the solution to (E.11) is given by any matrix \mathbf{M}_* which satisfies

$$\begin{aligned} \text{range}\{\mathbf{M}_*\} &= \text{range}\{\mathcal{A}(\mathbf{h}')\}, \\ \text{tr}(\mathbf{M}_*^T \mathbf{R} \mathbf{M}_*) &= \text{tr}(\mathbf{\Lambda}). \end{aligned} \quad (\text{E.12})$$

Then, we use (E.4) and replace the matrix \mathbf{M} in (E.11) by the structured matrix $\mathcal{A}(\tilde{\mathbf{h}})\tilde{\mathbf{D}}^{-1}$ where

$$\tilde{\mathbf{h}} \triangleq [\tilde{\mathbf{h}}_0^T, \dots, \tilde{\mathbf{h}}_{N_0-1}^T]^T, \quad (\text{E.13})$$

stands for the vector of optimization variables in the frequency-domain and

$$\tilde{\mathbf{D}} \triangleq \text{diag}([\|\tilde{\mathbf{h}}_0\|, \dots, \|\tilde{\mathbf{h}}_{N_0-1}\|]) \otimes \mathbf{I}_{2K} \in \mathbb{R}^{2KN_0 \times 2KN_0}, \quad (\text{E.14})$$

to rewrite the corresponding constraint of (E.11) as

$$\mathbf{M}^T \mathbf{M} = \tilde{\mathbf{D}}^{-1} \mathcal{A}(\tilde{\mathbf{h}})^T \mathbf{R} \mathcal{A}(\tilde{\mathbf{h}}) \tilde{\mathbf{D}}^{-1} = \mathbf{I}_{2KN_0}. \quad (\text{E.15})$$

Since the constraint of (E.11), i.e., $\mathbf{M}^T \mathbf{M} = \mathbf{I}_{2KN_0}$, is satisfied for any arbitrary vector $\tilde{\mathbf{h}}$ as can be seen from (E.15), it is redundant and can be dropped. This leads to the following unconstrained optimization problem

$$\max_{\tilde{\mathbf{h}}} \text{tr} \left(\tilde{\mathbf{D}}^{-1} \mathcal{A}(\tilde{\mathbf{h}})^T \mathbf{R} \mathcal{A}(\tilde{\mathbf{h}}) \tilde{\mathbf{D}}^{-1} \right). \quad (\text{E.16})$$

Due to the fact that the matrix \mathbf{M} which is represented by the matrix $\mathcal{A}(\tilde{\mathbf{h}})\tilde{\mathbf{D}}^{-1}$ in (E.16) has a particular structure while it is unstructured in (E.11), these problems are not equivalent to each other. As a result, the sets of optimal matrices \mathbf{M}_* for (E.11) and (E.16) may result in different sets of solutions and the maximum of the objective function in (E.16) can not exceed that of (E.11) in general. Taking into account (E.4) and (E.6), we obtain

$$\text{tr} \left(\tilde{\mathbf{D}}^{-1} \mathcal{A}(\tilde{\mathbf{h}})^T \mathbf{R} \mathcal{A}(\tilde{\mathbf{h}}) \tilde{\mathbf{D}}^{-1} \right) \Big|_{\tilde{\mathbf{h}}=\mathbf{h}'} = \text{tr}(\mathbf{\Lambda}). \quad (\text{E.17})$$

Therefore, the set of solutions to (E.16) is a subset of the set of solutions to (E.11) since the maxima of the objective functions in both problems coincide as can be observed from

comparison of (E.12) and (E.17). Moreover, the true overall CFR vector in the frequency-domain \mathbf{h}' belongs to the subspace spanned by all vectors which maximize (E.16). The objective function in (E.16) can be rewritten as

$$\text{tr} \left(\tilde{\mathbf{D}}^{-1} \mathcal{A}(\tilde{\mathbf{h}})^T \mathbf{R} \mathcal{A}(\tilde{\mathbf{h}}) \tilde{\mathbf{D}}^{-1} \right) = \text{vec} \{ \mathcal{A}(\tilde{\mathbf{h}}) \tilde{\mathbf{D}}^{-1} \}^T (\mathbf{I}_{2KN_0} \otimes \mathbf{R}) \text{vec} \{ \mathcal{A}(\tilde{\mathbf{h}}) \tilde{\mathbf{D}}^{-1} \}. \quad (\text{E.18})$$

Further, using (2.39) and (E.5), we have

$$\text{vec} \{ \mathcal{A}(\tilde{\mathbf{h}}) \tilde{\mathbf{D}}^{-1} \} = \left(\tilde{\mathbf{D}}^{-1} \otimes \mathbf{I}_{2MTN_0} \right) \text{vec} \{ \mathcal{A}(\tilde{\mathbf{h}}) \} = \left(\tilde{\mathbf{D}}^{-1} \otimes \mathbf{I}_{2MTN_0} \right) \boldsymbol{\Psi} \tilde{\mathbf{h}}. \quad (\text{E.19})$$

Inserting (E.19) in (E.18) results in

$$\begin{aligned} \text{tr} \left(\tilde{\mathbf{D}}^{-1} \mathcal{A}(\tilde{\mathbf{h}})^T \mathbf{R} \mathcal{A}(\tilde{\mathbf{h}}) \tilde{\mathbf{D}}^{-1} \right) &= \tilde{\mathbf{h}}^T \boldsymbol{\Psi}^T \left(\tilde{\mathbf{D}}^{-1} \otimes \mathbf{I}_{2MTN_0} \right) (\mathbf{I}_{2KN_0} \otimes \mathbf{R}) \left(\tilde{\mathbf{D}}^{-1} \otimes \mathbf{I}_{2MTN_0} \right) \boldsymbol{\Psi} \tilde{\mathbf{h}} \\ &= \tilde{\mathbf{h}}^T \boldsymbol{\Psi}^T \left(\tilde{\mathbf{D}}^{-2} \otimes \mathbf{R} \right) \boldsymbol{\Psi} \tilde{\mathbf{h}}, \end{aligned}$$

and, therefore, the problem (E.16) is equivalent to

$$\max_{\tilde{\mathbf{h}}} \tilde{\mathbf{h}}^T \boldsymbol{\Psi}^T \left(\tilde{\mathbf{D}}^{-2} \otimes \mathbf{R} \right) \boldsymbol{\Psi} \tilde{\mathbf{h}}. \quad (\text{E.20})$$

Making use of the block-diagonal structures in (E.5) and (E.8) along with the definition (E.14), the optimization problem (E.20) can be reformulated in terms of the variables defined in Chapter 4 as

$$\max_{\tilde{\mathbf{h}}} \tilde{\mathbf{h}}^T \mathcal{X}'(\boldsymbol{\gamma}, \boldsymbol{\xi}_{\|\tilde{\mathbf{h}}\|}) \tilde{\mathbf{h}}, \quad (\text{E.21})$$

where

$$\boldsymbol{\xi} = \boldsymbol{\xi}_{\|\tilde{\mathbf{h}}\|} \triangleq \left[\|\tilde{\mathbf{h}}_0\|^2, \dots, \|\tilde{\mathbf{h}}_{N_0-1}\|^2 \right]. \quad (\text{E.22})$$

Taking into account (E.14), we conclude that $\tilde{\mathbf{D}}^{-2} = (1/\|\tilde{\mathbf{h}}\|^2) \mathbf{I}_{2K}$ in the special case of single-carriers. It is immediate to show that the optimization problem (E.21) reduces to the problem of finding the principal eigenvector of the virtual snapshots covariance matrix $\mathcal{X}_i(\boldsymbol{\gamma})$ introduced in Chapter 3 and that of [SGM05]. Next, we propose a novel approach to solve (E.21) in the multi-carrier case which is able to take advantage of correlations among subcarriers. To this aim, we assume that the CFR vector norm $\|\mathbf{h}_i\|$, $i = 0, \dots, N_0 - 1$, at each subcarrier is known in (E.21), for instance, by the use of (4.24) in Chapter 4. This assumption implies that

$$\boldsymbol{\xi}_{\|\tilde{\mathbf{h}}\|} = \boldsymbol{\xi}_{\|\mathbf{h}\|} \triangleq \left[\|\mathbf{h}_0\|^2, \dots, \|\mathbf{h}_{N_0-1}\|^2 \right], \quad (\text{E.23})$$

or, equivalently,

$$\tilde{\mathbf{h}}^T \mathbf{J}_i \mathbf{J}_i^T \tilde{\mathbf{h}} = \|\mathbf{h}_i\|^2, \quad i = 0, \dots, N_0 - 1 \quad (\text{E.24})$$

where \mathbf{J}_i is the selection matrix defined in (4.15) that obtains the $(i + 1)$ -th optimization vector $\tilde{\mathbf{h}}_i$ as a subvector of the long optimization vector $\tilde{\mathbf{h}}$, i.e., $\tilde{\mathbf{h}}_i = \mathbf{J}_i^T \tilde{\mathbf{h}}$. To integrate the aforementioned assumption in (E.21), we replace $\boldsymbol{\xi}_{\|\tilde{\mathbf{h}}\|}$ by $\boldsymbol{\xi}_{\|\mathbf{h}\|}$ and augment (E.24) as constraint to the resulting problem to obtain

$$\begin{aligned} \max_{\tilde{\mathbf{h}}} \quad & \tilde{\mathbf{h}}^T \boldsymbol{\mathcal{X}}'(\boldsymbol{\gamma}, \boldsymbol{\xi}_{\|\mathbf{h}\|}) \tilde{\mathbf{h}} \\ \text{s.t.} \quad & \tilde{\mathbf{h}}^T \mathbf{J}_i \mathbf{J}_i^T \tilde{\mathbf{h}} = \|\mathbf{h}_i\|^2, \quad i = 0, \dots, N_0 - 1. \end{aligned} \quad (\text{E.25})$$

It is worth noting that replacement of the equality constraints in (E.25) by corresponding inequalities, i.e., $\tilde{\mathbf{h}}^T \mathbf{J}_i \mathbf{J}_i^T \tilde{\mathbf{h}} \leq \|\mathbf{h}_i\|^2$, $i = 0, \dots, N_0 - 1$, does not change the solution of (E.25). This is due to the fact that this inequality constraints are forced to be satisfied with equality by the nature of the objective function in (E.25). This observation, however, can be exploited in practical cases when CFR vector norm is estimated according to (4.26); see Section 5.5. Also as mentioned before in Subsections 3.3.1 or 4.2, in practice, the true covariance matrix $\boldsymbol{\mathcal{X}}'(\boldsymbol{\gamma}, \boldsymbol{\xi}_{\|\mathbf{h}\|})$ is unavailable and, therefore, its corresponding sample estimate $\hat{\boldsymbol{\mathcal{X}}}'(\boldsymbol{\gamma}, \boldsymbol{\xi}_{\|\mathbf{h}\|})$ should be implemented using (4.8). As a result, instead of (E.25), the following optimization problem should be considered

$$\begin{aligned} \max_{\tilde{\mathbf{h}}} \quad & \tilde{\mathbf{h}}^T \hat{\boldsymbol{\mathcal{X}}}'(\boldsymbol{\gamma}, \boldsymbol{\xi}_{\|\mathbf{h}\|}) \tilde{\mathbf{h}} \\ \text{s.t.} \quad & \tilde{\mathbf{h}}^T \mathbf{J}_i \mathbf{J}_i^T \tilde{\mathbf{h}} = \|\mathbf{h}_i\|^2, \quad i = 0, \dots, N_0 - 1. \end{aligned} \quad (\text{E.26})$$

Appendix F

In this appendix, we show that the proposed blind channel estimator in Chapter 3 based on eigenvalue problem can be viewed as the RML channel estimator in the Gaussian noise case. Let us consider again the joint blind RML estimator (2.63) for transmitted symbol vectors $\underline{\mathbf{s}}_i(p)$, for $p = 1, \dots, P$, and the CFR vector \mathbf{h}_i at the i th subcarrier as

$$\left\{ \hat{\mathbf{h}}_{i,\text{RML}}, \hat{\underline{\mathbf{S}}}_{i,\text{RML}} \right\} = \arg \min_{\underline{\mathbf{S}}_i, \tilde{\mathbf{h}}_i} \sum_{p=1}^P \left\| \mathbf{y}_i(p) - \mathbf{A}(\tilde{\mathbf{h}}_i) \underline{\mathbf{s}}_i(p) \right\|^2. \quad (\text{F.1})$$

Considering orthogonality property (2.38), $\mathbf{A}(\tilde{\mathbf{h}}_i)$ has full column rank, and, therefore,

$$\tilde{\mathbf{s}}_i(p) = \left(\mathbf{A}(\tilde{\mathbf{h}}_i)^T \mathbf{A}(\tilde{\mathbf{h}}_i) \right)^{-1} \mathbf{A}(\tilde{\mathbf{h}}_i)^T \mathbf{y}_i(p), \quad (\text{F.2})$$

minimizes each individual term in (F.1). Let us define $\mathbb{Y}_i \triangleq [\mathbf{y}_i(1), \mathbf{y}_i(2), \dots, \mathbf{y}_i(P)]$ that contains all available received data vectors at the i th subcarrier and insert (F.2) into (F.1) and recall that $\text{tr}(\mathbf{X}^T \mathbf{X}) = \|\mathbf{X}\|^2$ for any arbitrary matrix \mathbf{X} . Then, the RML estimator of CFR vector \mathbf{h}_i can be written as

$$\begin{aligned} \hat{\mathbf{h}}_{i,\text{RML}} &= \arg \min_{\tilde{\mathbf{h}}_i} \sum_{p=1}^P \left\| \mathbf{y}_i(p) - \mathbf{A}(\tilde{\mathbf{h}}_i) \left(\mathbf{A}(\tilde{\mathbf{h}}_i)^T \mathbf{A}(\tilde{\mathbf{h}}_i) \right)^{-1} \mathbf{A}(\tilde{\mathbf{h}}_i)^T \mathbf{y}_i(p) \right\|^2 \\ &= \arg \min_{\tilde{\mathbf{h}}_i} \left\| \mathbb{Y}_i - \mathbf{A}(\tilde{\mathbf{h}}_i) \left(\mathbf{A}(\tilde{\mathbf{h}}_i)^T \mathbf{A}(\tilde{\mathbf{h}}_i) \right)^{-1} \mathbf{A}(\tilde{\mathbf{h}}_i)^T \mathbb{Y}_i \right\|^2 \\ &= \arg \min_{\tilde{\mathbf{h}}_i} \text{tr} \left(\mathbb{Y}_i^T \mathbb{Y}_i - \mathbb{Y}_i^T \mathbf{\Pi}_{\mathbf{A}(\tilde{\mathbf{h}}_i)} \mathbb{Y}_i \right) \\ &= \arg \min_{\tilde{\mathbf{h}}_i} \left\{ \|\mathbb{Y}_i\|^2 - \text{tr} \left(\mathbb{Y}_i^T \mathbf{\Pi}_{\mathbf{A}(\tilde{\mathbf{h}}_i)} \mathbb{Y}_i \right) \right\}, \end{aligned} \quad (\text{F.3})$$

where $\mathbf{\Pi}_{\mathbf{A}(\tilde{\mathbf{h}}_i)} \triangleq \mathbf{A}(\tilde{\mathbf{h}}_i) \left(\mathbf{A}(\tilde{\mathbf{h}}_i)^T \mathbf{A}(\tilde{\mathbf{h}}_i) \right)^{-1} \mathbf{A}(\tilde{\mathbf{h}}_i)^T$ stands for the orthogonal projector onto the column space of $\mathbf{A}(\tilde{\mathbf{h}}_i)$ with the property $\mathbf{\Pi}_{\mathbf{A}(\tilde{\mathbf{h}}_i)} \mathbf{\Pi}_{\mathbf{A}(\tilde{\mathbf{h}}_i)} = \mathbf{\Pi}_{\mathbf{A}(\tilde{\mathbf{h}}_i)}$. Dropping the term $(\|\mathbb{Y}_i\|^2)$ in (F.3) which is independent of the optimization variable and considering the identity $\text{tr}(\mathbf{X}\mathbf{Y}) = \text{tr}(\mathbf{Y}\mathbf{X})$ along with (3.34) yields

$$\hat{\mathbf{h}}_{i,\text{RML}} = \arg \max_{\tilde{\mathbf{h}}_i} \text{tr} \left(\mathbb{Y}_i^T \mathbf{\Pi}_{\mathbf{A}(\tilde{\mathbf{h}}_i)} \mathbb{Y}_i \right) = \arg \max_{\tilde{\mathbf{h}}_i} \text{tr} \left(\mathbf{\Pi}_{\mathbf{A}(\tilde{\mathbf{h}}_i)} \hat{\mathbf{R}}_i \right). \quad (\text{F.4})$$

Therefore, this estimator can be considered as a subspace method that maximizes the energy of projection of the received data at the i th subcarrier onto the parameter-dependent signal subspace defined by the equivalent code-channel matrix $\mathbf{A}(\tilde{\mathbf{h}}_i)$. As a result, the criterion in (F.4) is maximized by the true CFR vector \mathbf{h}_i . Using the orthogonality property (2.38) allows us to obtain the following alternative expression for (F.4)

$$\hat{\mathbf{h}}_{i,\text{RML}} = \arg \max_{\tilde{\mathbf{h}}_i} \text{tr} \left(\mathbf{A}(\tilde{\mathbf{h}}_i)^T \hat{\mathbf{R}}_i \mathbf{A}(\tilde{\mathbf{h}}_i) \right) / \|\tilde{\mathbf{h}}_i\|^2. \quad (\text{F.5})$$

It should be again stressed that relaxation of the finite alphabet constraint over the transmitted symbols in (2.60) which in turn is reflected in (F.1) results in the norm ambiguity

associated with channel estimates in (F.5). To avoid this, we consider a norm constraint over the optimization variable in (F.5) to have

$$\hat{\mathbf{h}}_{i,\text{RML}} = \arg \max_{\|\tilde{\mathbf{h}}_i\|=\|\mathbf{h}_i\|} \text{tr} \left(\mathbf{A}(\tilde{\mathbf{h}}_i)^T \hat{\mathbf{R}}_i \mathbf{A}(\tilde{\mathbf{h}}_i) \right). \quad (\text{F.6})$$

This norm constraint is also necessary to preclude the trivial solution of $\|\tilde{\mathbf{h}}_i\| \rightarrow \infty$ for (F.6). Clearly, in practice, the true norm used in (F.6) should be replaced by its estimated version of (4.26). To simplify the objective function in (F.6), we have

$$\text{tr} \left(\mathbf{A}(\tilde{\mathbf{h}}_i)^T \hat{\mathbf{R}}_i \mathbf{A}(\tilde{\mathbf{h}}_i) \right) = \text{vec}\{\mathbf{A}(\tilde{\mathbf{h}}_i)\}^T (\mathbf{I}_{2K} \otimes \hat{\mathbf{R}}_i) \text{vec}\{\mathbf{A}(\tilde{\mathbf{h}}_i)\}. \quad (\text{F.7})$$

Using (2.43) and (F.7), the problem (F.6) becomes equivalent to

$$\hat{\mathbf{h}}_{i,\text{RML}} = \arg \max_{\|\tilde{\mathbf{h}}_i\|=\|\mathbf{h}_i\|} \tilde{\mathbf{h}}_i^T \boldsymbol{\Phi}^T (\mathbf{I}_{2K} \otimes \hat{\mathbf{R}}_i) \boldsymbol{\Phi} \tilde{\mathbf{h}}_i. \quad (\text{F.8})$$

Taking into account the definition (2.44) along with the equations (3.4), and (3.34), we define

$$\begin{aligned} \hat{\mathcal{X}}_i(\boldsymbol{\gamma}_{\text{RML}}) &\triangleq \boldsymbol{\Phi}^T (\mathbf{I}_{2K} \otimes \hat{\mathbf{R}}_i) \boldsymbol{\Phi} \\ &= \sum_{k=1}^{2K} \boldsymbol{\Phi}_k^T \hat{\mathbf{R}}_i \boldsymbol{\Phi}_k = \frac{1}{P} \sum_{k=1}^{2K} \sum_{p=1}^P \tilde{\mathbf{y}}_i(k,p) \tilde{\mathbf{y}}_i(k,p)^T, \end{aligned} \quad (\text{F.9})$$

$$\boldsymbol{\gamma}_{\text{RML}} \triangleq [1, \dots, 1]^T, \quad (\text{F.10})$$

to obtain

$$\hat{\mathbf{h}}_{i,\text{RML}} = \arg \max_{\|\tilde{\mathbf{h}}_i\|=\|\mathbf{h}_i\|} \tilde{\mathbf{h}}_i^T \hat{\mathcal{X}}_i(\boldsymbol{\gamma}_{\text{RML}}) \tilde{\mathbf{h}}_i. \quad (\text{F.11})$$

It is noteworthy to mention that when formulating our proposed approach in Chapter 3, we do not exploit any assumption on the noise pdf, while the RML approach of (F.1) is entirely based on Gaussian noise assumption.

Bibliography

- [ABL09] D. Angelosante, E. Biglieri, and M. Lops, “Sequential estimation of multipath MIMO-OFDM channels,” *IEEE Trans. Signal Process.*, vol. 57, pp. 3167-3181, Aug. 2009.
- [AD06] N. Ammar and Z. Ding, “Channel identifiability under orthogonal space-time coded modulations without training,” *IEEE Trans. Wireless Commun.*, vol. 5, pp. 1003-1013, May 2006.
- [AD07] N. Ammar and Z. Ding, “Blind channel identifiability for generic linear space-time block codes,” *IEEE Trans. Signal Process.*, vol. 55, pp. 202-217, Jan. 2007.
- [AH04] A. Alexiou and M. Haardt, “Smart antenna technologies for future wireless systems: Trends and challenges,” *IEEE Commun. Mag.*, vol. 42, pp. 90-97, Sep. 2004.
- [Ala98] S. M. Alamouti, “A simple transmit diversity technique for wireless communications,” *IEEE J. Sel. Areas Commun.*, vol. 45, pp. 1451-1458, Oct. 1998.
- [BA07] E. Beres and R. Adve, “Blind channel estimation for orthogonal STBC in MISO systems,” *IEEE Trans. Veh. Tech.*, vol. 56, pp. 2042-2050, July 2007.
- [BG06] M. Biguesh and A. B. Gershman, “Training-based MIMO channel estimation: A study of estimator tradeoffs and optimal training signals,” *IEEE Trans. Signal Process.*, vol. 54, pp. 884-893, Mar. 2006.

- [BGP02] H. Bölcskei, D. Gesbert, and A. J. Paulraj, "On the capacity of OFDM-based spatial multiplexing systems," *IEEE Trans. Commun.*, vol. 50, pp. 225-234, Feb. 2002.
- [BHJZ02] W. Bai, C. He, L.-g. Jiang, and H.-w. Zhu, "Blind channel estimation in MIMO-OFDM systems," in *Proc. IEEE GLOBECOM*, Taipei, Taiwan, 2002, pp. 317-321.
- [BHP02] H. Bölcskei, R. W. Heath, and A. J. Paulraj, "Blind channel identification and equalization in OFDM based multiantenna systems," *IEEE Trans. Signal Process.*, vol. 50, pp. 96-109, Jan. 2002.
- [BLM03] I. Barhumi, G. Leus, and M. Moonen, "Optimal training design for MIMO-OFDM systems in mobile wireless channels," *IEEE Trans. Signal Process.*, vol. 51, pp. 1615-1624, June 2003.
- [Bre78] J. W. Brewer, "Kronecker products and matrix calculus in system theory," *IEEE Trans. Circuits Syst.*, vol. 25, pp. 772-781, Sep. 1978.
- [BSK06] B. Balakumar, S. Shahbazpanahi, and T. Kirubarajan, "A Kalman filtering approach to joint MIMO channel tracking and symbol decoding for orthogonal space-time block codes," in *Proc. SAM'06*, Waltham, Massachusetts, USA, 2006, pp. 244-248.
- [BT02] C. Budianu and L. Tong, "Channel estimation for space-time orthogonal block codes," *IEEE Trans. Signal Process.*, vol. 50, pp. 2515-2528, Oct. 2002.
- [BV04] S. Boyd and L. Vandenberghe, *Convex Optimization*, Cambridge Univ. Press, Cambridge, UK, 2004.
- [CB08] M. Coldrey and P. Bohlin, "Training-based MIMO systems: Part II- improvements using detected symbol information," *IEEE Trans. Signal Process.*, vol. 56, pp. 296-303, Jan. 2008.
- [CB11] D. Cescato and H. Bölcskei, "Algorithms for interpolation-based QR decomposition in MIMO-OFDM systems," *IEEE Trans. Signal Process.*, vol. 59, pp. 1719-1733, Apr. 2011.

- [CHMC10] T.-H. Chang, C.-W. Hsin, W.-K. Ma, and C.-Y. Chi, "A linear fractional semidefinite relaxation approach to maximum-likelihood detection of higher-order QAM OSTBC in unknown channels," *IEEE Trans. Signal Process.*, vol. 58, pp. 2315-2326, Apr. 2010.
- [Cla68] R. H. Clarke, "A statistical theory of mobile-radio reception," *Bell Sys. Tech. J.*, vol. 47, pp. 957-1000, 1968.
- [CMC06] T.-H. Chang, W.-K. Ma, and C.-Y. Chi, "Group-wise blind OFDM ML detection for complexity reduction," in *Proc. EUSIPCO'06*, Florence, Italy, 2006, pp. 1-5.
- [CMC08] T.-H. Chang, W.-K. Ma, and C.-Y. Chi, "Maximum-likelihood detection of orthogonal space-time block coded OFDM in unknown block fading channels," *IEEE Trans. Signal Process.*, vol. 56, pp. 1637-1649, Apr. 2008.
- [CMHC09] T.-H. Chang, W.-K. Ma, C.-Y. Huang, and C.-Y. Chi, "On perfect channel identifiability of semiblind ML detection of orthogonal space-time coded OFDM," in *Proc. ICASSP'09*, Taipei, Taiwan, 2009, pp. 2713-2716.
- [CS00] J. Chuang and N. Sollenberger, "Beyond 3G: Wideband wireless data access based on OFDM and dynamic packet assignment," *IEEE Commun. Mag.*, vol. 32, pp. 78-87, July 2000.
- [CT07a] T. Cui and C. Tellambura, "Semiblind channel estimation and data detection for OFDM systems with optimal pilot design," *IEEE Trans. Commun.*, vol. 55, pp. 1053-1062, May 2007.
- [CT07b] T. Cui and C. Tellambura, "Efficient blind receiver design for orthogonal space-time block codes," *IEEE Trans. Wireless Commun.*, vol. 6, pp. 1890-1899, May 2007.
- [CY92] L. Chang and C. C. Yeh, "Performance of DMI and eigenspace-based beamformers," *IEEE Trans. Antennas Propag.*, vol. 40, pp. 1336-1347, Nov. 1992.

- [DASC02] S. N. Diggavi, N. Al-Dhahir, A. Stamoulis, and A. R. Calderbank, "Differential space-time coding for frequency-selective channels," *IEEE Commun. Lett.*, vol. 6, pp. 253-255, June 2002.
- [DASC04] S. N. Diggavi, N. Al-Dhahir, A. Stamoulis, and A. R. Calderbank, "Great expectations: The value of spatial diversity in wireless networks," in *Proc. of the IEEE*, vol. 92, pp. 219-270, Feb. 2004.
- [FG94] D. D. Feldman and L. J. Griffiths, "A projection approach to robust adaptive beamforming," *IEEE Trans. Signal Process.*, vol. 42, pp. 867-876, Apr. 1994.
- [FG98] G. J. Foschini and M. J. Gans, "On limits of wireless communications in a fading environment when using multiple antennas," *Wireless Pers. Commun.*, vol. 6, pp. 311-335, Mar. 1998.
- [GB11] M. Grant and S. Boyd, "CVX: Matlab software for disciplined convex programming," available at <http://cvxr.com/cvx/>, V.1.21, Apr. 2011.
- [Ger03] A. B. Gershman, "Robustness issues in adaptive beamforming and high-resolution direction finding," in *High-Resolution and Robust Signal Processing*, Y. Hua, A. B. Gershman, and Q. Cheng, Eds., Marcel Dekker, New York, USA, 2003, ch. 2.
- [GG05] M. Gharavi-Alkhansari and A. B. Gershman, "Constellation space invariance of orthogonal space-time block codes," *IEEE Trans. Inf. Theory*, vol. 51, pp. 331-334, Jan. 2005.
- [GN07] F. Gao and A. Nallanathan, "Blind channel estimation for MIMO OFDM systems via nonredundant linear precoding," *IEEE Trans. Signal Process.*, vol. 55, pp. 784-789, Feb. 2007.
- [GN08] F. Gao and A. Nallanathan, "Resolving multidimensional ambiguity in blind channel estimation of MIMO-FIR systems via block precoding," *IEEE Trans. Veh. Tech.*, vol. 57, pp. 11-21, Jan. 2008.

- [GS01] G. Ganesan and P. Stoica, "Space-time block codes: A maximum SNR approach," *IEEE Trans. Inf. Theory*, vol. 47, pp. 1650-1656, May 2001.
- [GS02] G. Ganesan and P. Stoica, "Differential modulation using space-time block codes," *IEEE Signal Process. Lett.*, vol. 9, pp. 57-60, Feb. 2002.
- [GS05] A. B. Gershman and N. D. Sidiropoulos, Eds., *Space-Time Processing for MIMO Communications*, John Wiley & Sons, Chichester, UK, 2005.
- [GSSSN03] D. Gesbert, M. Shafi, D. Shiu, P. J. Smith, and A. Naguib, "From theory to practice: An overview of MIMO space-time coded wireless systems," *IEEE J. Sel. Areas Commun.*, vol. 21, pp. 281-302, Apr. 2003.
- [GW95] M. X. Goemans and D. P. Williamson, "Improved approximation algorithms for maximum cut and satisfiability problem using semi-definite programming," *J. ACM*, vol. 42, pp. 1115-1145, 1995.
- [GZNN08] F. Gao, Y. Zeng, A. Nallanathan, and T. S. Ng, "Robust subspace blind channel estimation for cyclic prefixed MIMO OFDM systems: Algorithm, identifiability and performance analysis," *IEEE J. Sel. Areas Commun.*, vol. 26, pp. 378-388, Feb. 2008.
- [HH02] B. Hassibi and B. M. Hochwald, "High-rate codes that are linear in space and time," *IEEE Trans. Inf. Theory*, vol. 48, pp. 1804-1824, July 2002.
- [HH03] B. Hassibi and B. M. Hochwald, "How much training is needed in multiple-antenna wireless links?," *IEEE Trans. Inf. Theory*, vol. 49, pp. 951-963, Apr. 2003.
- [HJ85] R. A. Horn and C. R. Johnson, *Matrix Analysis*, Cambridge Univ. Press, 1985.
- [HM00] B. M. Hochwald and T. L. Marzetta, "Unitary space-time modulation for multiple-antenna communications in Rayleigh flat fading," *IEEE Trans. Inf. Theory*, vol. 46, pp. 543-564, Mar. 2000.

- [HMRSU00] B. M. Hochwald, T. L. Marzetta, T. J. Richardson, W. Sweldens, and R. Urbanke, "Systematic design of unitary space-time constellations," *IEEE Trans. Inf. Theory*, vol. 46, pp. 1962-1973, Sep. 2000.
- [HS00] B. M. Hochwald and W. Sweldens, "Differential unitary space-time modulation," *IEEE Trans. Commun.*, vol. 48, pp. 2041-2052, Dec. 2000.
- [HSGG08] V. Havary-Nassab, S. Shahbazpanahi, A. Gerami, and A. B. Gershman, "Experimental performance evaluation of blind channel estimation for orthogonal space-time block codes," in *Proc. SAM'08*, Darmstadt, Germany, 2008, pp. 45-48.
- [Hug00] B. L. Hughes, "Differential space-time modulation," *IEEE Trans. Inf. Theory*, vol. 46, pp. 2567-2578, Nov. 2000.
- [Jaf88] A. G. Jaffer, "Maximum likelihood direction finding of stochastic sources: A separable solution," in *Proc. ICASSP'88*, New York, New York, USA, 1988, pp. 2893-2896.
- [Jaf01] H. Jafarkhani, "A quasi-orthogonal space-time block code," *IEEE Trans. Commun.*, vol. 49, pp. 1-4, Jan. 2001.
- [Jaf05] H. Jafarkhani, *Space-Time Coding: Theory and Practice*, Cambridge Univ. Press, New York, USA, 2005.
- [JH06] Y. Jing and B. Hassibi, "Distributed space-time coding in wireless relay networks," *IEEE Trans. Wireless Commun.*, vol. 5, pp. 3524-3536, Dec. 2006.
- [JJ07] Y. Jing and H. Jafarkhani, "Using orthogonal and quasi-orthogonal designs in wireless relay networks," *IEEE Trans. Inf. Theory*, vol. 53, pp. 4106-4118, Nov. 2007.
- [JT01] H. Jafarkhani and V. Tarokh, "Multiple transmit antenna differential detection from generalized orthogonal design," *IEEE Trans. Inf. Theory*, vol. 47, pp. 2626-2631, Sep. 2001.

- [LGBS01] Z. Liu, G. B. Giannakis, S. Barbarossa, and A. Scaglione, "Transmit-antennae space-time block coding for generalized OFDM in the presence of unknown multipath," *IEEE J. Sel. Areas Commun.*, vol. 19, pp. 1352-1364, July 2001.
- [Li02] Y. Li, "Simplified channel estimation for OFDM systems with multiple transmit antennas," *IEEE Trans. Wireless. Commun.*, vol. 1, pp. 67-75, Jan. 2002.
- [Li05] H. Li, "Differential space-time modulation over frequency-selective channels," *IEEE Trans. Signal Process.*, vol. 53, pp. 2228-2242, June 2005.
- [LMSYZ10] Z.-Q. Luo, W.-K. Ma, A. M.-C. So, Y. Ye, and S. Zhang, "Semidefinite relaxation of quadratic optimization problems: From its practical deployments and scope of applicability to key theoretical results," *IEEE Signal Process. Mag.*, vol. 27, pp. 20-34, May 2010.
- [LPMY07] M.-T. Le, V.-S. Pham, L. Mai, and G. Yoon, "Efficient algorithm for blind detection of orthogonal space-time block codes," *IEEE Signal Process. Lett.*, vol. 14, pp. 301-304, May 2007.
- [LS03] E. G. Larsson and P. Stoica, *Space-Time Block Coding for Wireless Communications*, Cambridge Univ. Press, Cambridge, UK, 2003.
- [LSA98] Y. Li, N. Seshadri, and S. Ariyavisitakul, "Transmitter diversity of OFDM systems with mobile wireless channels," in *Proc. IEEE GLOBECOM*, Sydney, Australia, 1998, pp. 968-973.
- [LSA99] Y. Li, N. Seshadri, and S. Ariyavisitakul, "Channel estimation for OFDM systems with transmitter diversity in mobile wireless channels," *IEEE J. Sel. Areas Commun.*, vol. 17, pp. 461-471, Mar. 1999.
- [LSL02] E. G. Larsson, P. Stoica, and J. Li, "On maximum-likelihood detection and decoding for space-time coding systems," *IEEE Trans. Signal Process.*, vol. 50, pp. 937-944, Apr. 2002.

- [LSL03] E. G. Larsson, P. Stoica, and J. Li, "Orthogonal space-time block codes: Maximum likelihood detection for unknown channels and unstructured interferences," *IEEE Trans. Signal Process.*, vol. 51, pp. 362-372, Feb. 2003.
- [Ma07] W.-K. Ma, "Blind ML detection of orthogonal space-time block codes: Identifiability and code construction," *IEEE Trans. Signal Process.*, vol. 55, pp. 3312-3324, July 2007.
- [Man02] J. H. Manton, "Optimization algorithms exploiting unitary constraints," *IEEE Trans. Signal Process.*, vol. 50, pp. 635-650, Mar. 2002.
- [Mey00] C. D. Meyer, *Matrix Analysis and Applied Linear Algebra*, SIAM, 2000.
- [MTL05] Q. Ma, C. Tepedelenlioglu, and Z. Liu, "Differential space-time-frequency coded OFDM with maximum multipath diversity," *IEEE Trans. Wireless Commun.*, vol. 4, pp. 2232-2243, Sep. 2005.
- [MVDC06] W.-K. Ma, B.-N. Vo, T. N. Davidson, and P.-C. Ching, "Blind ML detection of orthogonal space-time block codes: Efficient high-performance implementations," *IEEE Trans. Signal Process.*, vol. 54, pp. 738-751, Feb. 2006.
- [MYG05] X. Ma, L. Yang, and G. B. Giannakis, "Optimal training for MIMO frequency-selective fading channels," *IEEE Trans. Wireless Commun.*, vol. 4, pp. 453-466, Mar. 2005.
- [Nes98] Y. E. Nesterov, "Semidefinite relaxation and nonconvex quadratic optimization," *Optimiz. Meth. Software*, vol. 9, pp. 140-160, Sep. 1998.
- [Oss64] J. Jr. Ossana, "A model for mobile radio fading due to building reflections: Theoretical and experimental fading waveform power spectra," *Bell Sys. Tech. J.*, vol. 43, pp. 2935-2971, 1964.
- [PGNB04] A. J. Paulraj, D. A. Gore, R. U. Nabar, and H. Bölcskei, "An overview of MIMO communications-A key to gigabit wireless," in *Proc. of the IEEE*, vol. 92, pp. 198-218, Feb. 2004.

- [PK10] D. S. Papailiopoulos and G. N. Karystinos, "Maximum-likelihood noncoherent OSTBC detection with polynomial complexity," *IEEE Trans. Wireless Commun.*, vol. 9, pp. 1935-1945, June 2010.
- [PNG03] A. J. Paulraj, R. U. Nabar, and D. A. Gore, *Introduction to Space-Time Wireless Communications*, Cambridge Univ. Press, Cambridge, UK, 2003.
- [PP97] A. J. Paulraj and C. B. Papadias, "Space-time processing for wireless communications," *IEEE Signal Process. Mag.*, vol. 14, pp. 49-83, Nov. 1997.
- [Rap02] T. S. Rappaport, *Wireless Communications: Principles and Practice*, (2nd Ed.) Prentice Hall, Inc., 2002.
- [RSSHPG11] F. Römer, N. Sarmadi, B. Song, M. Haardt, M. Pesavento, and A. B. Gershman, "Tensor-based semi-blind channel estimation for MIMO OSTBC-coded systems," in *Proc. Asilomar conference on signals, systems and computers*, Pacific Grove, California, USA, 2011.
- [SA00] M. K. Simon and M.-S. Alouini, *Digital Communications over Fading Channels: A Unified Approach to Performance Analysis*, John Wiley & Sons, New York, NY, 2000.
- [SDL06] N. D. Sidiropoulos, T. N. Davidson, and Z.-Q. Luo, "Transmit beamforming for physical-layer multicasting," *IEEE Trans. Signal Process.*, vol. 54, pp. 2239-2251, June 2006.
- [SDWL06] D. Shen, Z. Diao, K.-K. Wong, and V. O. K. Li, "Analysis of pilot-assisted channel estimators for OFDM systems with transmit diversity," *IEEE Trans. Broadcast.*, vol. 52, pp. 193-202, June 2006.
- [SG03] P. Stoica and G. Ganesan, "Space-time block codes: Trained, blind, and semi-blind detection," *Digital Signal Process.*, vol. 13, pp. 93-105, Jan. 2003.
- [SGG06] S. Shahbazpanahi, A. B. Gershman, and G. B. Giannakis, "Semiblind multiuser MIMO channel estimation using Capon and MUSIC techniques," *IEEE Trans. Signal Process.*, vol. 54, pp. 3581-3591, Sep. 2006.

- [SGG08] S. Shahbazpanahi, A. B. Gershman, and G. B. Giannakis, "Blind and semiblind channel and carrier frequency-offset estimation in orthogonally space-time block coded MIMO systems," *IEEE Trans. Signal Processing*, vol. 56, pp. 702-711, Feb. 2008.
- [SGM05] S. Shahbazpanahi, A. B. Gershman, and J. H. Manton, "Closed-form blind MIMO channel estimation for orthogonal space-time block codes," *IEEE Trans. Signal Process.*, vol. 53, pp. 4506-4517, Dec. 2005.
- [SGS10] N. Sarmadi, A. B. Gershman, and S. Shahbazpanahi, "Closed-form blind channel estimation in orthogonally coded MIMO-OFDM systems," in *Proc. ICASSP'10*, Dallas, Texas, USA, 2010, pp. 3306-3309.
- [SHP07] C. Shin, R. W. Heath, and E. J. Powers, "Blind channel estimation for MIMO-OFDM systems," *IEEE Trans. Veh. Tech.*, vol. 56, pp. 670-685, Mar. 2007.
- [SHP08] C. Shin, R. W. Heath, and E. J. Powers, "Non-redundant precoding-based blind and semi-blind channel estimation for MIMO block transmission with a cyclic prefix," *IEEE Trans. Signal Process.*, vol. 56, pp. 2509-2523, June 2008.
- [SL02] A. L. Swindlehurst and G. Leus, "Blind and semi-blind equalization for generalized space-time block codes," *IEEE Trans. Signal Process.*, vol. 50, pp. 2489-2498, Oct. 2002.
- [SLL04] M. Shin, H. Lee, and C. Lee, "Enhanced channel-estimation technique for MIMO-OFDM systems," *IEEE Trans. Veh. Tech.*, vol. 53, pp. 261-265, Jan. 2004.
- [SOZ11] A. Sibille, C. Oestges, and A. Zanella, Eds., *MIMO: From Theory to Implementation*, Elsevier Academic Press, USA, 2011.
- [SP11a] N. Sarmadi and M. Pesavento, "Closed-form blind channel estimation in orthogonally coded MIMO-OFDM systems: A simple strategy to resolve non-scalar ambiguities," in *Proc. SPAWC'11*, San Francisco, CA, USA, 2011, pp. 301-305.

- [SP11b] N. Sarmadi and M. Pesavento, "Closed-form blind MIMO channel estimation for OSTBCs: Resolving ambiguities in rotatable codes," in *Proc. EUSIPCO'11*, Barcelona, Spain, 2011, pp. 644-648.
- [SPG11] N. Sarmadi, M. Pesavento, and A. B. Gershman, "Closed-form blind channel estimation for orthogonally coded MIMO-OFDM systems: An algorithm and uniqueness study," in *Proc. WSA '11*, Aachen, Germany, 2011, pp. 1-6.
- [SRHFG11] E. P. Simon, L. Ros, H. Hijazi, J. Fand, D. P. Gaillot, and M. Berbineau, "Joint carrier frequency offset and fast time-varying channel estimation for MIMO-OFDM systems," *IEEE Trans. Veh. Tech.*, vol. 60, pp. 955-965, Mar. 2011.
- [SS89] T. Söderström and P. Stoica, *System Identification*, Prentice Hall International, Hemel Hempstead, U.K., 1989.
- [SSG09] N. Sarmadi, S. Shahbazpanahi, and A. B. Gershman, "Blind channel estimation in orthogonally coded MIMO-OFDM systems: A semidefinite relaxation approach," *IEEE Trans. Signal Process.*, vol. 57, pp. 2354-2364, June 2009.
- [STTEP02] H. Sampath, S. Talwar, J. Tellado, V. Erceg, and A. J. Paulraj, "A fourth generation MIMO-OFDM broadband wireless system: Design, performance, and field trial results," *IEEE Commun. Mag.*, vol. 40, pp. 143-149, Sep. 2002.
- [Stu99] J. F. Sturm, "Using SEDUMI 1.02, A Matlab toolbox for optimizations over symmetric cones," *Optim. Meth. Soft.*, vol. 11-12, pp. 625-653, 1999.
- [Stü01] G. Stüber, *Principles of Mobile Communications*, Kluwer Academic Publishers, 2001.
- [TC10] C.-C. Tu and B. Champagne, "Subspace-based blind channel estimation for MIMO-OFDM systems with reduced time averaging," *IEEE Trans. Veh. Tech.*, vol. 59, pp. 1539-1544, Mar. 2010.
- [Tel99] E. Telatar, "Capacity of multi-antenna Gaussian channels," *European Trans. Telecommun.*, vol. 10, pp. 585-595, Nov./Dec. 1999.

- [TJ00] V. Tarokh and H. Jafarkhani, "A differential detection scheme for transmit diversity," *IEEE J. Sel. Areas Commun.*, vol. 18, pp. 1169-1174, July 2000.
- [TJC99] V. Tarokh, H. Jafarkhani, and A. R. Calderbank, "Space-time block codes from orthogonal designs," *IEEE Trans. Inf. Theory*, vol. 45, pp. 1456-1467, July 1999.
- [TSC98] V. Tarokh, N. Seshadri, and A. R. Calderbank, "Space-time codes for high data rates wireless communication: Performance criterion and code construction," *IEEE Trans. Inf. Theory*, vol. 44, pp. 744-765, Mar. 1998.
- [TV05] D. Tse and P. Viswanath, *Fundamentals of Wireless Communication*, Cambridge Univ. Press, Cambridge, UK, 2005.
- [TVP96] S. Talwar, M. Viberg, and A. Paulraj, "Blind separation of synchronous co-channel digital signals using an antenna array-Part I: Algorithms," *IEEE Trans. Signal Process.*, vol. 44, pp. 1184-1197, 1996.
- [UAG01] M. Uysal, N. Al-Dhahir, and C. N. Georghiades, "A space-time block coded OFDM scheme for unknown frequency-selective fading channels," *IEEE Commun. Lett.*, vol. 5, pp. 393-395, Oct. 2001.
- [Van02] H. L. Van Trees, *Optimum Array Processing*, Wiley, New York, 2002.
- [VS08a] J. Vía and I. Santamaría, "On the blind identifiability of orthogonal space-time block codes from second-order statistics," *IEEE Trans. Inf. Theory*, vol. 54, pp. 709-722, Feb. 2008.
- [VS08b] J. Vía and I. Santamaría, "Correlation matching approaches for blind OSTBC channel estimation," *IEEE Trans. Signal Process.*, vol. 56, pp. 5950-5961, Dec. 2008.
- [VSP11a] J. Vinogradova, N. Sarmadi, and M. Pesavento, "Subspace-based semiblind channel estimation method for fast fading orthogonally coded MIMO-OFDM systems," in *Proc. CAMSAP2011*, San Juan, Puerto Rico, 2011, pp. 149-152.

- [VSP11b] J. Vinogradova, N. Sarmadi, and M. Pesavento, "Iterative semiblind channel estimation method for fast fading orthogonally coded MIMO-OFDM systems," to be submitted.
- [VSPV09] J. Vía, I. Santamaría, J. Pérez, and L. Vielva, "A new subspace method for blind estimation of selective MIMO-STBC channels," *Wirel. Commun. Mob. Comput.*, Wiley InterScience, pp. 1-15, Aug. 2009.
- [VTP97] A. J. Van der veen, S. Talwar, and A. J. Paulraj, "A subspace approach to blind space-time signal processing for wireless communication systems," *IEEE Trans. Signal Process.*, vol. 45, pp. 173-190, Jan. 1997.
- [WG00] Z. Wang and G. B. Giannakis, "Wireless multicarrier communications: Where Fourier meets Shannon," *IEEE Signal Process. Mag.*, vol. 17, pp. 29-48, May 2000.
- [WZS08] F. Wan, W.-P. Zhu, and M. N. S. Swamy, "A semiblind channel estimation approach for MIMO-OFDM systems," *IEEE Trans. Signal Process.*, vol. 56, pp. 2821-2834, July 2008.
- [WZS11] F. Wan, W.-P. Zhu, and M. N. S. Swamy, "Semiblind sparse channel estimation for MIMO-OFDM systems," *IEEE Trans. Veh. Tech.*, vol. 60, pp. 2569-2582, July 2011.
- [Yan05] H. Yang, "A road to future broadband wireless access: MIMO-OFDM-based air interface," *IEEE Commun. Mag.*, vol. 43, pp. 53-60, Jan. 2005.
- [ZD10] M. Zia and Z. Ding, "A linear programming receiver for blind detection of full rate space-time block codes," *IEEE Trans. Signal Process.*, vol. 58, pp. 5819-5834, Nov. 2010.
- [Zha00] S. Zhang, "Quadratic maximization and semidefinite relaxation," *Math. Program.*, vol. 87, pp. 453-465, 2000.

- [ZLN06] Y. Zeng, W. H. Lam, and T. S. Ng, "Semiblind channel estimation and equalization for MIMO space-time coded OFDM," *IEEE Trans. Circuits Syst. I, Reg.*, vol. 53, pp. 463-474, Feb. 2006.
- [ZM05] T. Zemen and C. F. Mecklenbräuker, "Time-variant channel estimation using discrete prolate spheroidal sequences," *IEEE Trans. Signal Process.*, vol. 53, pp. 3597-3607, Sep. 2005.
- [ZMG02] S. Zhou, B. Muquet, and G. B. Giannakis, "Subspace-based (semi-) blind channel estimation for block precoded space-time OFDM," *IEEE Trans. Signal Process.*, vol. 50, pp. 1215-1228, May 2002.

Curriculum vitae

Education

- **Ph.D. (2012), Electrical Engineering Communications, Darmstadt University of Technology, Darmstadt, Germany**
Advisors: Prof. Alex B. Gershman and Prof. Marius Pesavento
Thesis title: “*Advanced blind signal processing for MIMO communications*”
- **M.Sc. (2001), Electrical Engineering Control, K. N. Toosi University of Technology, Tehran, Iran**
Advisor: Prof. M. Teshnelab
Thesis title: “*Time series forecasting using neuro-fuzzy and cerebellar model arithmetic computer (CMAC) approach*”
- **B.Sc. (1998), Electrical Engineering Control, University of Tehran, Tehran, Iran**

Publications

1. N. Sarmadi, M. Pesavento, and A. B. Gershman, “Closed-form blind channel estimation in orthogonally coded MIMO-OFDM systems,” in preparation.
2. N. Sarmadi, S. Shahbazpanahi, and A. B. Gershman, “Blind channel estimation in orthogonally coded MIMO-OFDM systems: A semidefinite relaxation approach,” *IEEE Trans. Signal Process.*, vol. 57, pp. 2354-2364, June 2009.
3. J. Vinogradova, N. Sarmadi, and M. Pesavento, “Iterative semiblind channel estimation method for fast fading orthogonally coded MIMO-OFDM systems,” to be submitted.
4. J. Vinogradova, N. Sarmadi, and M. Pesavento, “Subspace-based semiblind channel estimation method for fast fading orthogonally coded MIMO-OFDM systems,” in *Proc. International Workshop on Computational Advances in Multi-Sensor Adaptive Processing (CAMSAP)*, San Juan, Puerto Rico, 2011, pp. 149-152.
5. F. Römer, N. Sarmadi, B. Song, M. Haardt, M. Pesavento, and A. B. Gershman, “Tensor-based semi-blind channel estimation for MIMO OSTBC-coded systems,” in *Proc. Asilomar Conference on Signals, Systems and Computers*, Pacific Grove, California, USA, 2011.

6. N. Sarmadi and M. Pesavento, "Closed-form blind MIMO channel estimation for OS-TBCs: Resolving ambiguities in rotatable codes," in *Proc. European Signal Processing Conference (EUSIPCO)*, Barcelona, Spain, 2011, pp. 644-648.
7. N. Sarmadi and M. Pesavento, "Closed-form blind channel estimation in orthogonally coded MIMO-OFDM systems: A simple strategy to resolve non-scalar ambiguities," in *Proc. IEEE International Workshop on Signal Processing Advances in Wireless Communications (SPAWC)*, San Francisco, California, USA, 2011, pp. 301-305.
8. N. Sarmadi, M. Pesavento, and A. B. Gershman, "Closed-form blind channel estimation for orthogonally coded MIMO-OFDM systems: An algorithm and uniqueness study," in *Proc. International ITG Workshop on Smart Antennas (WSA)*, Aachen, Germany, 2011, pp. 1-6.
9. N. Sarmadi, A. B. Gershman, and S. Shahbazpanahi, "Closed-form blind channel estimation in orthogonally coded MIMO-OFDM systems," in *Proc. IEEE International Conference on Acoustics, Speech, and Signal Processing (ICASSP)*, Dallas, Texas, USA, 2010, pp. 3306-3309.
10. N. Sarmadi, A. B. Gershman, and S. Shahbazpanahi, "Blind channel estimation in MIMO-OFDM systems using semi-definite relaxation," in *Proc. IEEE International Conference on Acoustics, Speech, and Signal Processing (ICASSP)*, Las Vegas, Nevada, USA, 2008, pp. 2381-2384.
11. N. Sarmadi, and M. Teshnelab, "Short-term weather forecasting using neuro-fuzzy approach," in *Proc. IASTED International Multi-Conference on Modeling, Identification and Control (MIC)*, Innsbruck, Austria, 2002.
12. N. Sarmadi, and M. Teshnelab, "Short-term weather forecasting using CMAC structure," in *Proc. IASTED International Multi-Conference on Applied Informatics (AI)*, Innsbruck, Austria, 2002.

Erklärung laut §9 der Promotionsordnung

Ich versichere hiermit, dass ich die vorliegende Dissertation allein und nur unter Verwendung der angegebenen Literatur verfasst habe. Die Arbeit hat bisher noch nicht zu Prüfungszwecken gedient.

Darmstadt, 2. Februar 2012,